The chemistry of new fluorescent and amino acid-appended phosphorus-based ligands

The Chemistry of New Fluorescent and Amino Acid Appended Phosphorus Based Ligands

by

Jade K. M. Markham

A Doctoral Thesis

Submitted in partial fulfilment of the requirements

for the award of Doctor of Philosophy of

Loughborough University

Department of Chemistry

Loughborough University

Loughborough

Leicestershire

LE11 3TU

I dedicate this thesis to the people I love; Jasmine, Lukas, Liam, Zeb and my parents, Sue and Steve.

Abstract

This thesis describes the use of the phosphorus analogous Mannich based condensation reaction, a procedure well established within our research group, to synthesise a number of phosphine containing ligands and their associated coordination complexes which may have potential for medicinal applications.

The first research and discussion (R&D) chapter of this thesis (Chapter 2) utilises the well-established route of adding substituents, in this case PPh_2CH_2- groups, through a hydrazide moiety on a naphthalimide substructure, affording PCNCP ligands **2.16** - **2.19** in yields of 76 – 94%. Synthesised phosphine containing naphthalimide ligand's coordination capabilities were explored utilising late transition metal precursors $PtCl_2$(cod), $PdCl_2$(cod), Au(tht)Cl and $AgBF_4$. Preliminary fluorescence measurements were conducted on two naphthalimide ligands (**2.18** and **2.19**) and their associated coordination complexes, excluding silver(I) complexes which could not be explored due to solubility issues. Fluorescence was quenched on coordination to platinum(II) and palladium(II); this may allow the phosphine containing naphthalimides synthesised to be used as a "turn-off" sensor for these species.

Chapter 3 explores another class of phosphine containing fluorescent compounds. Naphthalimide fluorophores were substituted for fluorescein ($C_{20}H_{12}O_5$) and rhodamine ($C_{28}H_{30}N_2O_3$) derivatives. In a similar approach to Chapter 2, a hydrazide group was introduced to the fluorophore to allow the subsequent monoaddition of a PPh_2CH_2-group, yielding monophosphine (PCN) ligands **3.5** and **3.6**. Fluoresceinamine isomer I ($C_{20}H_{13}NO_5$) was also investigated as a precursor; fluoresceinamine isomer I does not require the addition of the hydrazide functionality since it already possesses an amine moiety which can undergo addition of PPh_2CH_2- groups. This provided access to a *bis*functionalised (PCNCP) fluorescein derivative **3.18** and allowed for exploration of the effect the position of the PPh_2CH_2- groups has on photophysical properties. Phosphine ligands **3.5**, **3.6** and **3.18** were coordinated to dichloroplatinum(II), dichloropalladium(II) and chlorogold(I) species and preliminary fluorescence measurements were conducted on all ligands synthesised and their associated coordination complexes.

Similarly to the phosphine functionalised fluorescein ligand (**3.5**) synthesised, the fluoresceinamine derivative (**3.13**) fluorescence was quenched on coordination to the metal centres explored. The rhodamine derivative (**3.6**) preliminarily explored however displayed an additional UV absorption and fluorescence emission band when coordinated to Pt(II) and Pd(II); this may suggest that the rhodamine ligand synthesised could be used as a sensor for the detection of Pt(II) and Pd(II) species.

The final R&D chapter of this thesis (Chapter 4) is a continuation of work studied both by the Smith group and in the literature; synthesising aminomethylphosphine ligands with amino acid backbones. The work described explores expanding the number of amino

acids, natural and unnatural, and dipeptides, with PPh_2CH_2- substituents. Examples of $(Ph_2PCH_2)_2NX$ ligands synthesised include: where X = $CH_2CONHCH(CH_3)CO_2H$ (**4.8)**, $NHCO_2CH_2CH_3$ (**4.11**) and $CH(CH_2Ph)CO_2CH_3$ (**4.20**). Like Chapter 2 and 3, phosphine moieties were introduced *via* the phosphorus analogous Mannich based condensation reaction.

The coordination capabilities of synthesised aminomethylphosphine ligands, both novel and known, were investigated using $PtCl_2(cod)$, $[Ru(\eta^6\text{-}p\text{-cymene})Cl_2]_2$ and Au(tht)Cl precursors, as well as Group 11 metals [Cu(I), Ag(I), Au(I)] which are widely known to exhibit medicinal properties. All compounds synthesised as part of this thesis were analysed through standard spectroscopic techniques, such as ^{1}H NMR, $^{31}P\{^1H\}$ NMR, FT-IR, ESI-MS and CHN analysis, with some compounds also studied by single crystal X-ray crystallography. A preliminary study of the antibacterial properties of silver(I) complexes, **4.71** – **4.77**, synthesised here as part of Chapter 4 is also included and demonstrates silver(I) complexes synthesised showed antibacterial activity against *E. Coli* and *S. Aureus.*

Acknowledgements

I would like to thank Loughborough University for providing the 'Loughborough experience' in both my undergraduate and postgraduate degrees, the Graduate school for providing the scholarship allowing me to undertake my PhD, and my supervisors Dr Martin Smith and Dr Marc Kimber for their guidance in this project.

I would also like to acknowledge the following people for their various contributions to this thesis: Mr Oliver Scaife, Miss Cecelia Yan, Mrs Pauline King, Mr Simon Sharp, Dr Mark Edgar, Mr Edward Simpson, Dr Mark Elsegood, Dr David Worrall, Mr Craig Buck, Dr Thomas Noble and Dr Sweta Ladwa.

Abbreviations and Symbols

Å	Angström unit (10^{-10}m)
AAS	Atomic absorption spectrometry
ATSM	Diacetyl *bis*(N^4-methylthiosemicarbazate)
Bodipy	Boron-dipyrromethene
Cbz	Carboxybenzyl
$CDCl_3$	Deuterated chloroform
CHN	Carbon, Hydrogen, Nitrogen, elemental analysis
cm^{-1}	Wavenumber
cod	Cycloocta–1,5–diene
conc	Concentration
CSD	Cambridge Structural Database
CT	X-ray Computer Tomography
Cy	Cyclohexyl
d^6	Deuterated
DCM	Dichloromethane, CH_2Cl_2
DHMPE	1,2-*bis*(dihydroxymethylphosphino)ethane
DME	Dimethyl ether
DMSO	Dimethyl sulfoxide, $OS(CH_3)_2$
dppFc	1,1'-bis(diphenylphosphino)ferrocene
EC	Electron capture
E.Coli	Escherichia Coli
eq./equiv	Molar equivalent
ESI-MS	Electron Spray Ionisation Mass Spectrometry
Et_2O	Diethyl ether $(CH_3CH_2)_2O$
FR–IR	Fourier Transform Infrared Spectroscopy

FMISO	Fluoromisonidazole
Fmoc-	Fluorenylmethyloxycarbonyl-
g	Grams
h	Hours
HOMO	Highest Occupied Molecular Orbital
Hz	Hertz
I	Spin
IT	Internal transfer
J	Coupling constant, Hz
Leu	Leucine
LUMO	Lowest Unoccupied Molecular Orbital
LMCT	Ligand-to-Metal Charge Transfer
^{m}	Metastable
MeOH	Methanol, CH_3OH
mg	Milligrams
min	Minutes
µl	Microliter
mL	Millilitre
MLCT	Metal-to-Ligand Charge Transfer
mm	Millimetre
MMCT	Metal-to-Metal Charge Transfer
mol	Mole
mmol	Millimole ($x10^{-3}$ mol)
MRI	Nuclear Magnetic Resonance Imaging
MS	Mass spectrometry
m/z	Mass to charge ratio

NMR	Nuclear Magnetic Resonance
PET	Positron Emission Tomography
PeT	Photoelectron transfer
Ph	Phenyl, $–C_6H_5$
Phe	Phenylalanine
PPh_2CH_2OH	Hydroxymethyldiphenylphosphine
PPh_2Cl	Chlorodiphenylphosphine
ppm	Parts per million
PTA	1,3,5–triaza–7–phosphaadamantane
rt	Room Temperature
S.aureus	Staphylococcus aureus
Ser	Serine
SPECT	Single Photon Emission Computed Tomography
THF	Tetrahydrofuran
THP	Tris(hydroxymethyl)phosphine
tht	Tetrahydrothiophene
Trp	Tryptophan
Tyr	Tyrosine
Val	Valine
VOC	Volatile organic compound
°	Degrees
°C	Degrees Celcius
ε	Molar absorption coefficient
δ	Chemical shift
υ	Frequency
λ	Wavelength (nm)

$\Delta\nu_{st}$	Stokes shift
λ_{em}	Emission wavelength (nm)
λ_{ex}	Excitation wavelength (nm)
$\{^1H\}$	Proton decoupled
%	Percentage
Φ_F	Quantum yield (photons emitted/photons absorbed)

Key for XP Diagrams

Au

O

C

P

Cl

Pd

H

Pt

N

Ru

Table of Contents

Chapter 1 - Introduction

1.1 Overview

Phosphine ligands and their associated metal complexes are well-known to exhibit medicinal properties and have been investigated for applications towards anti-cancer, anti-bacterial and imaging agents, to name just a few.[1–3] This introduction will begin with a description of tertiary phosphines and will discuss the mechanism of an important reaction in phosphine chemistry, the Mannich based condensation reaction. This will lead into the synthesis of phosphine functionalised amino acids, which feature greatly in the research and development chapters of this thesis.

A brief description of radiopharmaceutical techniques, PET (positron emission tomography) and SPECT (single photon emission computed tomography), will follow. Radiopharmaceuticals are a growing area of chemistry, in which phosphine ligands have not been exploited extensively. Although synthesised phosphine ligands, described in this thesis have not been complexed here with radionuclides, the ligands synthesised have potential to be used in this area; this is supported by the exploration of analogous compounds in literature for use in radiopharmaceuticals.[3,4] For that reason, a discussion of radiopharmaceuticals will feature in this introduction.

The coordination chemistry and medicinal properties of six transition metals will be discussed to highlight why these metals have been investigated in the research and development chapters of this thesis. Luminescence will be described, followed by a discussion to highlight some of the research conducted on a number of fluorophores of interest. This will then lead into the applications of luminescence, *i.e.* cellular imaging agents and the emerging area of bimodal fluorescence microscopy radiopharmaceuticals. Again, this area is highlighted in the introduction of this thesis, as although synthesised compounds in Chapter 2 are in the early stages of design they may be investigated for this application at a later date.

1.2 Tertiary Phosphine Chemistry

The chemistry of tertiary phosphines is largely based on the lone pair the phosphine possesses, which enables the phosphine to coordinate to transition metals. Unlike analogous nitrogen compounds, which undergo rapid inversion of their pyramidal geometry at room temperature, phosphine inversion is slow and therefore phosphines can be said to have a fixed pyramidal geometry. This difference in geometry leads to differences observed in the coordination chemistry of amines and phosphines.[5]

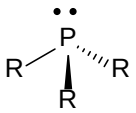

(1.1)

Figure 1.1 Pyramidal geometry of a tertiary phosphine.

Interest in tertiary phosphines stem from the control modifying the organic substituents (R) on the phosphine have on steric and electronic properties of a metal complex when coordinated. The organic substituents on the phosphine also allow solubility of the ligand to be modified; increased water solubility can be achieved through the introduction of polar functional groups, such as hydroxyl groups, which is important for biological purposes.[6] In the case of ditertiary phosphines, the backbone linking the phosphine moieties may be modified to further enhance the properties of these compounds. The ease by which properties of phosphine compounds can be influenced, coupled with phosphine's affinity for stabilising electron deficient metal centres has led to the exploration of phosphine coordination chemistry towards a number of applications including medicines and catalysis.[6,7]

A variety of different substituents on a central phosphine atom have been reported in the literature including aminocarboxylic acids, alcohols, alkyl, and aromatics.[6] Chiral substituents are of interest as chiral phosphines are especially attractive in asymmetric catalysis providing a pathway for the synthesis of a single isomeric product. Amino acids are readily available and, excluding glycine, all natural amino acids have a chiral backbone. Phosphine functionalised amino acids have received attention as catalysts themselves and also as building blocks for more complex peptides, which can form helical or turn structures.[8] It is hoped that through using a biological approach enzyme-like catalysts can be synthesised providing control over chemo-, regio-, enantio- and substrate selectivities.[6]

Kellner *et al.* were the first to functionalise the terminal amine on a number of amino acids with *bis*(diphenylphosphinomethyl) moieties utilising the phosphorus analogous Mannich condensation.[9] Since the phosphorus based Mannich condensation features greatly in this thesis, this reaction will now be discussed in detail, with reference to the work of Kellner *et al.*[9]

1.2.1 Phosphorus analogous Mannich condensation

The phosphorus analogous Mannich condensation is a commonly used method for the synthesis of aminomethylphosphine ligands, both by the Smith group and others.[4,10,11]

Here, a hydroxymethyl functionalised phosphine and an amine, or as a "one pot" reaction, a secondary phosphine, aldehyde and an amine, primary or secondary, can form aminomethylphosphines, as shown in Scheme 1.1. This reaction has numerous advantages; many of the resulting aminomethylphosphines synthesised are air-stable which is a rarity for phosphine ligands, no protection groups are needed and the facile chemistry can be performed in one pot.[10] The ability to vary the substituents on the amine and phosphine and also vary the alcohol is very enticing as it allows for a broad range of compounds to be synthesised; however only primary amines can react with aryl substituted phosphines. The presence of phosphine and nitrogen, both of which have a lone pair available for coordination, allow for multidentate coordination. Amino groups within phosphine ligands give basicity in the secondary coordination sphere activating small molecule substrates such as Lewis acids and bases.[12]

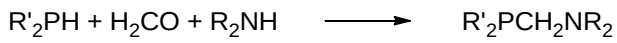

Scheme 1.1 Phosphorus analogous Mannich condensation.

Swor *et al.* investigated the mechanism of the phosphorus based Mannich condensation in 2011.[12] To do this they investigated, *via in situ* NMR, the reaction of hydroxymethyldiphenylphosphine and DHMPE [1,2-*bis*(dihydroxymethylphosphino)ethane] with diethylamine and the phosphine-borane derivatives of hydroxymethyldiphenylphosphine and DHMPE with diethylamine. As summarised in Scheme 1.2, while the uncoordinated hydroxymethyldiphenylphosphine and DHMPE reacted with the amine to give the expected products, the coordinated phosphine-boranes did not react with the amine.[12]

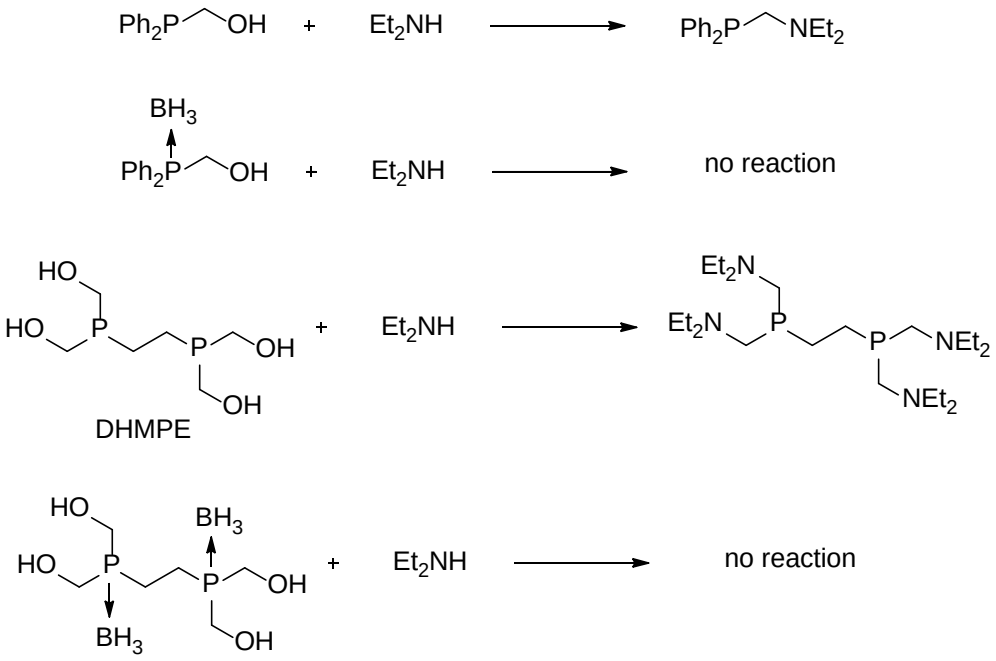

Scheme 1.2 Reactions conducted by Swor *et al.* to investigate the mechanism of the phosphorus analogous Mannich condensation.[12]

These reactions demonstrated that the phosphine lone pair is essential for the reaction to proceed and disproved the previously suggested mechanism, which assumed the reaction to proceed *via* a typical Mannich pathway.[13] Swor *et al.* subsequently proposed a revised mechanism, shown in Figure 1.2.[12]

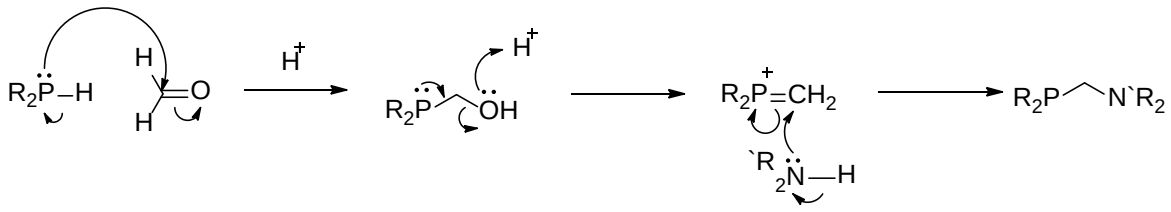

Figure 1.2 Mechanism for the phosphorus analogous Mannich-type reaction as suggested by Swor *et al.*[12]

The hydroxymethylphosphine eliminates the hydroxide ion, OH^-, forming an electrophilic methylenephosphonium ion, which attacks the amine. The phosphorus lone pair is

required to form a phosphorus-carbon pi bond, therefore template reactions are not likely to work as the phosphines coordinate bonds would have to be cleaved from the metal for the mechanism to occur.[12]

1.2.2 Phosphine functionalised amino acids

Kellner *et al.* were the first to utilise the phosphorus analogous Mannich condensation to functionalise amino acids, for the purpose of synthesising chiral catalysts.[9] Initially, using glycine, alanine, valine, phenylalanine and serine in individual reactions with formaldehyde and diphenylphosphine, viscous oils or resins were collected and recrystallised to obtain pure samples of ligands **1.2** – **1.6**.[1]

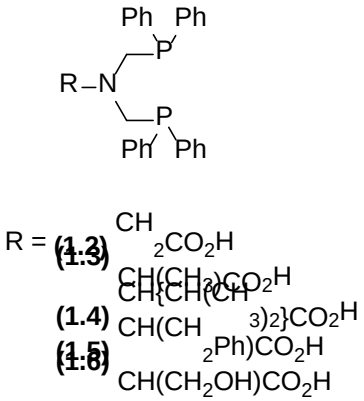

Figure 1.3 Chemical structures of a number of *bis*(phosphinomethyl) functionalised amino acids as synthesised by Kellner *et al.*[9]

Kellner *et al.* further investigated the reaction of diphenylphosphine with esters and sodium salts of a number of amino acids, followed by the coordination of these *bis*(phosphinomethyl) ligands with rhodium(I). Subsequent catalytic studies were performed on the rhodium(I) complexes synthesised, however only a maximum optical purity of 29% for enantioselective hydrogenation under the conditions trialled was obtained.[9,14]

Kellner and coworkers were not the only researchers to investigate coordination complexes using phosphine functionalised amino acids. Markel *et al.* synthesised molybdenum complexes with the formulae $[Mo(CO)_4P\hat{}P]$, where P^P is *bis*(phosphinomethyl) functionalised leucine or alanine methyl esters.[15] Hoye and colleagues also studied similar *bis(*phosphinomethyl) ligands complexed to Pt(II) and Rh(I) centres, investigating their potential as hydrogenation and hydroformylation catalysts.[16]

It was found that in many cases the chiral -CH group of the amino acids was too far from the phosphine active sites to be feasibly used in asymmetric catalysis.[17]

Zhang *et al.* showed *bis*(phosphinomethyl) amino acid systems synthesised *via* the phosphorus analogous Mannich condensation can be used to form pre-chelate radiopharmaceuticals, which involves the coordination to a radiometal before attachment to a protein targeting vector *via* a functional group on the amino acid component of the ditertiary phosphine ligand.[3] The *bis*(phosphinomethyl) functionalised amine is central in the PCNCP backbone and therefore when the targeting vector is attached to the central amine, steric interactions between the coordination sphere and the targeting vector are at a minimum.

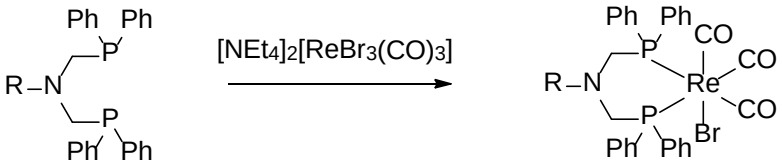

R = **(1.7)** $CH_2CH_2CO_2H$
(1.8) CH_2CO_2H
(1.9) $CH_2CONHCH_2CO_2H$

R = **(1.10)** $CH_2CH_2CO_2H$
(1.11) CH_2CO_2H
(1.12) $CH_2CONHCH_2CO_2H$

Scheme 1.3 Coordination reaction between ligands **1.7 – 1.9**, synthesised by the phosphorus analogous Mannich condensation, with rhenium.[3]

As shown in Scheme 1.3, after synthesising *bis*(phosphinomethyl) β-alanine, glycine and glycylglycine, the ditertiary phosphine ligands were coordinated to a tricarbonylrhenium(I) metal centre. ESI-MS (electron spray ionisation mass spectrometry) investigations of acidic, basic and neutral solutions of the complexes showed the phosphine-rhenium chelate was stable in varying pH. The complexes synthesised also showed cytotoxic activity against several murine and human cancer cell lines, which may suggest ^{186}Re or ^{188}Re complexes can be used as chemo- and radiotheraputic agents.[3]

Forthcoming chapters in this thesis will utilise the phosphorus based Mannich condensation to expand the library of *bis*(phosphinomethyl) amino acids known. Synthesised ligands will undergo complexation to metal centres with previously known medicinal properties and those with potential in radiopharmaceuticals. Phosphines of this type have been shown to have applications in imaging and the aim is to expand the library of ligands allowing the introduction of different functional groups and different coordination chemistry to be explored.[3] This literature review will now describe some of

the alternative methods for the synthesis of phosphine functionalised amino acids, before discussing radiopharmaceuticals in Section 1.3.

1.2.3 Alternative methods for the synthesis of phosphine functionalised amino acids

Alternative methods for the synthesis of phosphine functionalised amino acids described in the literature focused on addition of phosphine moieties to amino acids at the chiral centre. The original method to yield this type of amino acid was *via* Evans chiral oxazolidone chemistry.[8,18–20] The initial steps in this procedure were the addition of diphenylphosphine to acrylic acid using tetramethylammonium hydroxide as a base.[21] The phosphine is converted to the phosphine sulphide using sodium thiosulphide to prevent phosphine oxidation during the subsequent steps in the method.[22] The overall scheme leads to the formation of Fmoc-protected amino acid **1.15**. A variety of other amino acids were also synthesised using this methodology, all in high yields with high optical purity. However, the method is limited by the number of steps and chromatographic purification required.[8]

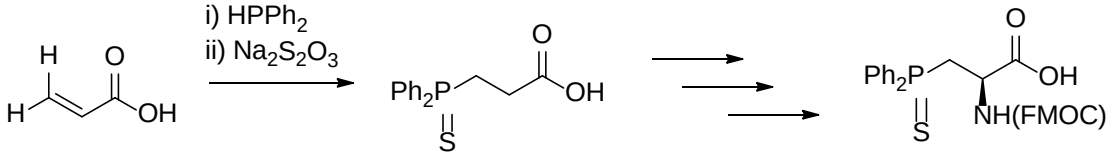

(1.13) **(1.14)** **(1.15)**

Scheme 1.4 Synthesis of phosphine functionalised amino acid as described by Evans *et al.*[8]

A different technique uses commercially available iodo-amino acid **1.16**, which is converted to the desired product **1.17** using chlorodiphenylphosphine, PPh_2Cl. Starting material **1.16** is reacted with ZnI_2 and stoichiometric amounts of $CuCN{\cdot}2LiCl$ to form an unknown zinc/copper reactive intermediate, which is then reacted with PPh_2Cl. Again, the phosphine is protected as a phosphine sulphide, though on this occasion the reagent used is elemental sulphur. This method has also been used to synthesize a number of amino acids, with different dichlorophosphines used including both aromatic and alkyl.[8,23]

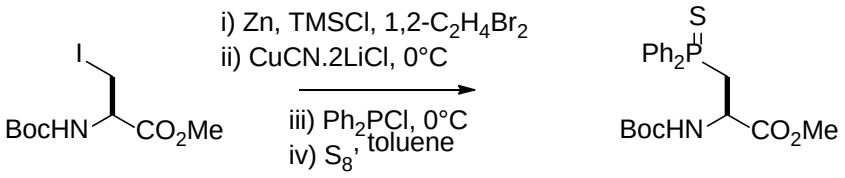

(1.16) **(1.17)**

Scheme 1.5 Synthesis of phosphine functionalised amino acid as described by Agarkov *et al.*[8]

Agarkov *et al.* discussed the incorporation of amino acids described above into peptide chains with helical and beta-turn secondary structures.[8] Once synthesized the phosphine sulphide can be reduced to the free phosphine and coordinated to rhodium metal centres.[8] Catalytic capabilities of synthesised compounds were then investigated; the results will not be discussed here since it lies outside the remit of this thesis.

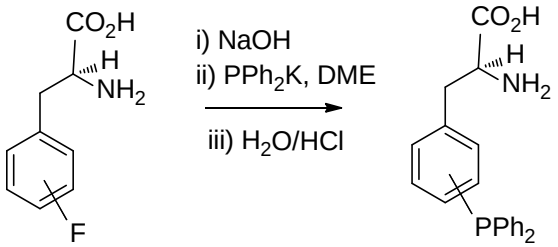

(1.18) **(1.19)**

Scheme 1.6 Synthesis of (*ortho*- and *para*-) phosphine functionalised amino acid, **1.19**, as described by Brauer *et al.*[24]

Research concerning alternative pathways for accessing phosphine functionalised amino acids is not limited to the application of catalysis only. Brauer and coworkers employed nucleophilic phosphination of starting fluoroaromatic tagged amino acids to synthesis 2- and 4-diphenylphosphino derivatives of phenylalanine and glycine (as shown in Scheme 1.6).[24] This was inspired by compounds **1.20**, **1.21** and **1.22**, shown in Figure 1.4, which have been investigated for their potential as building blocks in new peptidomimetric drugs.[24]

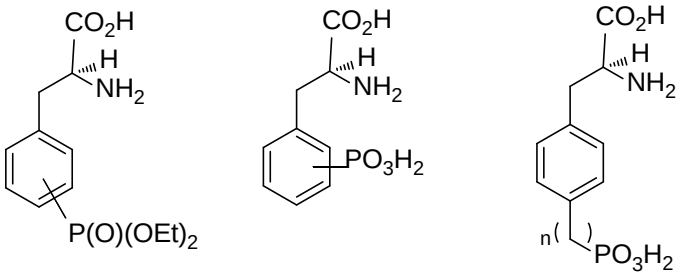

(1.20) **(1.21)** **(1.22)**

Figure 1.4 Compounds **1.20**, **1.21** and **1.22**.[24]

By utilising a phosphorus(III) moiety in **1.19**, as opposed to the phosphorus(V) oxidation states in compounds **1.20 – 1.22**, the available lone pair on **1.19** can be used for coordination to a metal centre opening up the potential for **1.19** and derivatives to be used in medical imaging or homogenous catalysis.[24]

This section has covered only a few examples in the literature concerning the addition of phosphine moieties to amino acids, though it is hoped this emphasises the multiple ways in which phosphine can be added to amino acids and also the potential for phosphine containing amino acids in a number of applications, including medicinal purposes. Medical imaging is a fast growing area of interest to inorganic chemists and will be discussed briefly in the following section.

1.3 Medical Imaging

Medical imaging is a highly beneficial method in medicine which allows biological processes to be monitored in a non-destructive and often non-invasive manner. There are a number of techniques available for medical diagnostics including MRI (nuclear magnetic resonance imaging), CT (X-ray computed tomography) and radiopharmaceutical techniques, SPECT (single-photon emission computed tomography) and PET (positron emission tomography). The sensitivity and specificity capabilities of each system differ depending on the physical properties of the individual technique. This thesis will describe radiopharmaceutical processes SPECT and PET.

1.3.1 PET

PET imaging requires a patient to intake a pharmaceutical, usually intravenously, within which a positron emitting radionuclide is incorporated. On decay of the radionuclide, a

position is emitted. The emitted positron travels through tissue until its kinetic energy is exhausted, at which time the positron is annihilated by its antiparticle, an electron. This reaction results in the emission of two gamma rays of equal energy, 511 KeV, in opposite directions, 180° apart. These gamma rays are measured using coincidence detectors, a signal is sent to a photomultiplier tube which converts the signal so it can be recorded by a computer.[25]

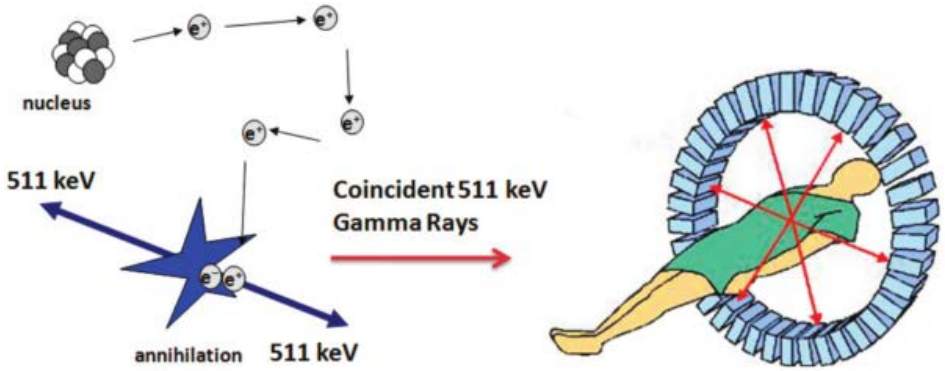

Figure 1.5 Schematic of PET imaging, taken from a paper by Anderson *et al.*[26]

Radiopharmaceuticals containing non-metallic nuclides, such as ^{11}C and ^{18}F, are much more commonly used clinically than metallic counterparts. The biological pathways of an amino acid, sugar, steroid *etc* can be studied through substitution of an atom with a radioactive isotope of itself. This is advantageous as the radiopharmaceutical is a structural duplicate of the inactive structure providing 'true' imaging of the biological processes the molecule undergoes.

Fluorine and carbon are the most commonly used non-metallic nuclides; however nitrogen and oxygen are also used. Although fluorine is not a common component of bioorganic molecules, it is a good isostere of hydrogen and provides a desirable half-life, which is longer than most other non-metallic radioisotope half-lives.

Table 1.1 Four commonly used non-metallic isotopes and half-lives.

Radionuclide	Half-life (mins)	Positron Yield (%)
^{18}F	110.00	96.9
^{11}C	20.40	>99
^{13}N	9.96	>99
^{15}O	2.04	>99

A radionuclide half-life needs to be comparable to the biological half-life of the compound which will ensure the radiopharmaceutical accumulates in the desired region for imaging. Therefore non-metallic nuclides are limited to imaging simple molecules; simple molecules with biological half-lives between minutes and a few hours, similar to the half-lives of the isotopes listed in Table 1.1.

There are also many PET active metallic radionuclides available from across the periodic table, providing a range of physical and chemical properties which can be exploited. Metallic nuclides are attractive as they have longer half-lives than non-metallic nuclides which allows for biological processes with longer biological half-lives (hours versus minutes) to be investigated.

Table 1.2 Half-lives of common metallic nuclides.

Radionuclides	**Half-life (h)**	**Positron yield (%)**
^{52}Fe	8.2	57
^{55}Co	18.0	77
^{61}Cu	3.4	62
^{64}Cu	12.7	19
^{66}Ga	9.5	57
^{68}Ga	1.1	89

Some elements have several isotopes which are PET active, such as copper. This allows for radiopharmaceutical research to be performed on a longer lived isotope and once refined a shorter lived isotope can be used if the half-life is more comparable to the pharmaceuticals biological half-life.

Thernostics describes a pharmaceutical which can be used for both therapy and diagnostics by altering only the radionuclide used, maintaining the chemical behaviour of the pharmaceutical but altering the decay mode. This can be done through the swapping of one isotope for a sister isotope, i.e. a PET active copper isotope could be switched for ^{67}Cu; however this is not limited to isotopes of the same element.[27]

There are two methods for the delivery of a metallic radiopharmaceutical. The first is termed ‘metal-essential’, here, the radiopharmaceutical is a simple coordination complex which relies on the combination of the metal and ligand(s) to localise the complex *in vivo*. The second is termed ‘metal-tagged’. In ‘metal-tagged’ compounds the radionuclide is incorporated into a biologically active molecule which targets a specific site of accumulation, therefore providing more selective imaging than metal-essential pharmaceuticals. These methods of delivery are also used in SPECT imaging; examples of both methods of delivery can be found in Section 1.3.2.

1.3.2 SPECT

The advantages of SPECT imaging over PET include the cost of SPECT detectors and the use of longer lived radionuclides, which provides additional time for transport and radiosynthesis, and therefore removes the need for an on-site cyclotron reducing cost further. The use of longer lived radionuclides also allows for bigger targeting vectors to be utilised, such as antibodies, as biodistribution requires a longer amount of time. Commonly used gamma emitting nuclides are included in Table 1.3.

Table 1.3 Four common isotopes for SPECT.

Isotope	Half-Life (hours)	Mode of decay
^{99m}Tc	6.04	IT (100%)
^{67}Ga	78.3	EC (100%)
^{123}I	13.2	EC (100%)
^{111}In	67.9	EC (100%)

IT (internal transfer), EC (electron capture)

^{99m}Tc is a commonly used radionuclide for SPECT, being described as 'the workhorse for diagnostic nuclear medicine'.[28] ^{99m}Tc imaging also benefits from low cost ^{99}Mo/^{99m}Tc generators, which produce ^{99m}Tc-pertechnetate but which can be reduced to the +5 oxidation state *via* stannous ions in commercially available kits. Myoview, or ^{99m}Tc-Tetrofosmin is a well-known ^{99m}Tc-phosphine complex used clinically for myocardial perfusion scans (Figure 1.6).[29]

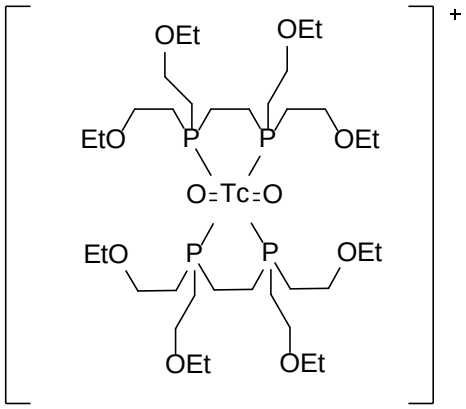

(1.23)

Figure 1.6 Chemical structure of ^{99m}Tc-Tetrofosmin, **1.23**.

This type of technetium compound is termed 'technetium-essential' as the biodistribution is dependent on the properties, such as size, charge, lipophilicity, *etc*, of the complex itself.[28] In the case of Myoview, previously synthesised phosphine-^{99m}Tc

complexes with aryl substituents on the phosphine displayed poor clearance from non-target tissue, while the ether functionalised phosphine groups in Myoview allow for the pharmaceutical to diffuse into the tissue and not be retained in the blood.[29]

Alternatively, technetium complexes may be conjugated to a targeting vector with biodistribution determined solely by the targeting vector and independent of the presence of technetium, such complexes are termed 'technetium-tagged'.[28]

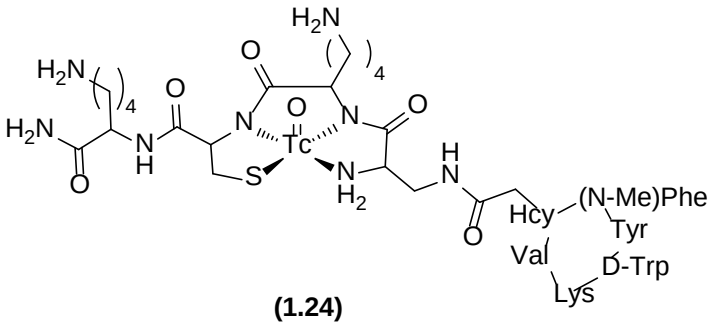

(1.24)

Figure 1.7 Chemical structure of Neotact.

Neotect, otherwise known as ^{99m}Tc-Depreotide, shown in Figure 1.7 is an example of a 'technetium-tagged' radiopharmaceutical. The targeting vector, depreotide is a cyclic hexapeptide, which shows high affinity for somatostatin receptors which are upregulated in some cancers. Depreotide is bound via an amide bond to a tetrapeptide which coordinates to the technetium metal centre in a N_3S fashion. Neotect is currently used clinically for the diagnostics of lung cancers.[30,31]

Despite the use of SPECT clinically and the cost effectiveness of the procedure in comparison to PET, PET offers many advantages over SPECT. PET is more sensitive than SPECT and offers higher resolution images (resolution of SPECT is typically in the range of 6-8mm, while 2-3mm is achieved using PET).[25]

1.4 Metal phosphine complexes

Metal phosphine complexes, with and without attached amino acid moieties, are well known for their medicinal properties, and have been applied to many areas including, but not limited to, medical imaging, antibacterial and cytotoxic applications.[2,32,33] This literature review will focus on a select number of metals, starting with Group 11, which are of interest to this thesis.

1.4.1 Copper

Copper is the third most naturally abundant trace metal in the body. Diseases, such as Alzheimer's, Wilkinson's and Menkes' disease are known to be copper related, and the mechanisms of such diseases have to be studied using ^{64}Cu.[32,34] Copper is a first row transition metal and has three common oxidation states, excluding Cu(0), which are Cu(I), Cu(II) and Cu(III), however Cu(III) is rare. Cu(II) dominates copper chemistry as it is the preferred oxidation state in aqueous solution. Cu(II) has an electron configuration of [Ar] $3d^9$, is paramagnetic and is often arranged in a tetrahedral or Jahn Teller tetragonally distorted octahedral geometry.

Table 1.4 Copper radioisotopes available for PET and radionuclide therapy.[34]

Isotope	β^- (%), E_{ave}	β^+ (%), E_{ave}	Other	Half-life
^{60}Cu		93%, 0.87 MeV	EC	24 min
^{61}Cu		62%, 0.53 MeV	EC	3.33 h
^{62}Cu		98%, 1.32 MeV	EC	9.75 min
^{64}Cu	39%, 0.19 MeV	18%, 0.28 MeV	EC	12.7 h
^{67}Cu	100%, 0.12 MeV		γ, 93 keV, 52%	62 h

(EC = Electron Capture)

There are a number of copper isotopes with diagnostic or therapeutic potential. ^{60}Cu, ^{61}Cu, ^{62}Cu and ^{64}Cu are positron emitters, with varying half-lives as shown in Table 1.4. ^{64}Cu and ^{67}Cu are potential theranostic agents; ^{64}Cu is a beta and auger electron emitter, as well as a positron emitter and ^{67}Cu is a beta and imageable gamma emitter. ^{64}Cu is the most widely used copper isotope due to its long half-life which allows for transportation from the cyclotron where it is produced, conversion to the desired radiopharmaceutical and for applications longer imaging times permit.[34,35] To prevent the labile Cu(II) radionuclide dissociating from the PET ligand, donor atoms such as nitrogen or sulphur are often used in the form of a macrocycle or porphyrin.[32,36,26]

A key disadvantage of using Cu(II) is the potential for reduction to Cu(I) in the biological environment, which may result in the breakdown of the radiopharmaceutical.[37] This can be managed through the type of ligand donor used; if a 'softer' donor is used to coordinate to the metal this will facilitate reduction, whereas the use of a 'harder' donor will prevent reduction. However, in some cases such as [Cu(ATSM)] (copper(II) diacetyl bis(N^4-methylthiosemicarbazate), reduction can be utilised.

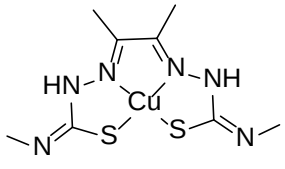

(1.25)

Figure 1.8 Chemical structure of Cu(ATSM).

Lipophilic Cu(II) bis(thiosemicarbazones) diffuse into cells where they are reduced to Cu(I) by intracellular reducing agents. These complexes then dissociate either quickly or slowly, like [Cu(ATSM)]. [^{64}Cu(ATSM)] is used in hypoxia mapping; Cu(II) is reduced and trapped irreversibly in hypoxic regions but not non-hypoxic regions. [^{64}Cu(ATSM)] provides superior pharmokinetics to ^{18}F-FMISO (fluoromisonidazole), which was previously used, due to the slow dissociation of the ATSM ligand which allows for oxidation of Cu(I) back to Cu(II) by molecular oxygen in the non-hypoxic cells and therefore the complex can escape out of the cell.[26,34,38,39]

Cu(I) is diamagnetic, has an electronic configuration of [Ar] $3d^{10}$ and is commonly observed as tetrahedral, square planar, pyramidal, and linear shaped complexes with 4, 3 and 2 donor atoms respectively. Cu(I) chemistry has not been exploited for the application of PET to the extent of Cu(II). As a research group Cu(I) chemistry is of interest since it has a high affinity for phosphine ligands. Many copper(I)-phosphine complexes previously reported have been shown to be cytotoxic and antitumour agents.[40] Tertiary phosphines are good reducing agents, which can stabilise low oxidation state metals through the formation of phosphine oxide or *via* pi-backbonding. Alidori and colleagues synthesised some of the first ^{64}Cu-phosphine complexes, as shown in Figure 1.9.[40]

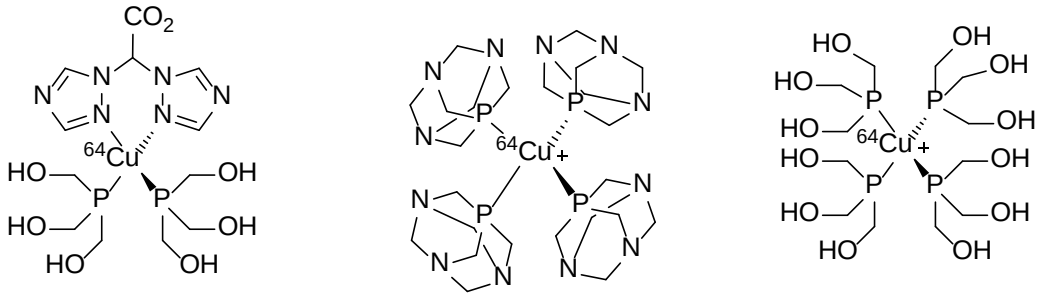

(1.26) **(1.27)** **(1.28)**

Figure 1.9 ^{64}Cu-phosphine complexes synthesised by Alidori *et al.*[40]

Phosphine ligands, THP [tris(hydroxymethyl)phosphine] and TPA (1,3,5-triaza-7-phosphaadamantane), were used to synthesise water-soluble and hydrophilic complexes **1.26**, **1.27** and **1.28**. The syntheses of these complexes were rapid and therefore ideal for radiopharmaceutical applications. Toxicity studies in MCF-7 mammary carcinoma cell and tumour lines showed promising toxicity levels in comparison to cisplatin, therefore illustrating their potential as therapeutic agents. Copper has a high affinity for serum, a copper transport protein, which is often a cause for decomposition of copper radiopharmaceuticals *in vivo*. Serum stability studies of complexes **1.26** to **1.28** showed radio-copper partially bound to serum proteins, which indicates poor kinetic stability *in vivo*. The least stable complex of the series was complex **1.28**, the smallest and least hydrophobic ligand, this suggests that protection from decomposition of the copper complex is related to the steric hindrance of the associated ligand or due to the inhibition of dissociation of more hydrophobic ligands in the aqueous medium.[40] In addition, the complexes showed little lipophilicity resulting in poor cellular uptake.

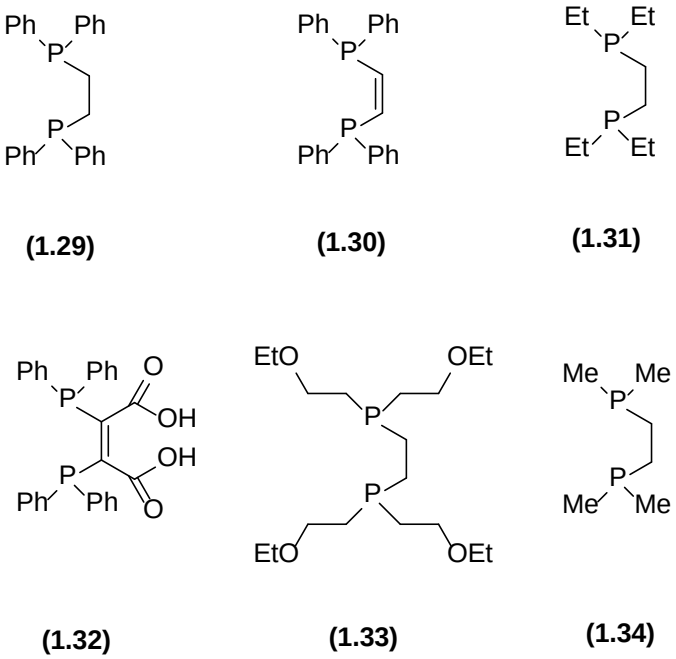

Figure 1.10 Bidentate phosphine ligands investigated for copper coordination.

To improve stability bidentate phosphine ligands have been investigated for copper complexation, some of which are shown in Figure 1.10.[1,43–47] Bidentate phosphine ligands offer a number of advantages including quick and easy synthesis, *in vivo* stability, the ability to control biodistribution through modification of the phosphine substituents and bioconjugate formation.[41] Desirable rapid synthesis also allows for coordination to short lived radio-copper, such as ^{62}Cu(I).[45]

1.4.2 Silver

Ag(I), Ag(II) and Ag(III) oxidation states are all known, however Ag(I) is the most common. Ag(I) has an electronic configuration of [Kr] $4d^{10}$, is diamagnetic and can be observed in a number of geometries with different ligands. Silver complexes are known for their antimicrobial properties and are utilised in medical devices such as intravascular catheters or wound dressings. The mode of action is believed to be the slow release of silver which may inhibit cell growth.[46]

With the known antitumour properties of gold-phosphine complexes, as discussed in the following gold section, Berners-Price and co-workers investigated the antifungal, antibacterial and antitumour activities of analogous silver complexes, as shown in Figure 1.11.[2]

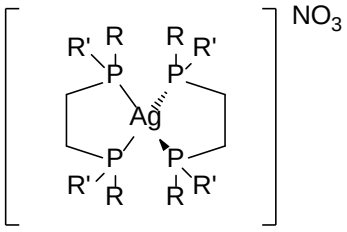

(1.35) R = Ph, R' = Ph
(1.36) R = Et, R' = Et
(1.37) R = Ph, R' = Et

Figure 1.11 Silver complexes investigated by Berners-Price *et al.*[2]

Interestingly, unlike monodentate phosphine-silver complexes, *bis*phosphine chelated silver complexes showed clearly resolved silver coupling (^{107}Ag/^{109}Ag) observed in the $^{31}P\{^{1}H\}$ NMR spectra, illustrating slow ligand exchange. This stability allows the bisphosphine chelating silver complexes to reach their target site *in vivo*, but the ligands are also labile enough to ring open at the target site. Alkyl phosphine complex **1.36** is less cytotoxic than **1.35**, $[Ag(dppe)_2]NO_3$, this is a result of the higher reactivity of alkyl phosphine complexes to oxidation reactions *in vivo*, reducing the amount of complex which reaches the target site.[2] Although complexes **1.35 – 1.37** showed antifungal, antibacterial and antitumour activity, this was coupled with high toxicity which limits the potential of complexes **1.35 – 1.37** for *in vivo* applications.

Radioisotope ^{111}Ag is a high beta emitter (1.05MeV) with potential for radiotherapeutic applications; however ^{111}Ag is also a gamma emitter with energy too high for use in imaging and will therefore damage non-target tissue. Additionally, the labile nature of silver will limit its use. Nevertheless, silver complexes have shown to have antitumour, antibacterial and antifungal properties and continue to be investigated.[47–49]

1.4.3 Gold

Gold can exist in one of two oxidation states *in vivo*. Au(I), the most common oxidation state, has an electronic configuration of [Xe] $4f^{14}$ $5d^{10}$ and is therefore diamagnetic. Au(I) complexes form linear, trigonal or tetrahedral geometries, with 2, 3 or 4 ligands respectively and since Au(I) is a soft acid, soft ligands such as cyanide, thiolate or phosphines are preferred.[50] Au(III) has an electronic configuration of [Xe] $4f^{14}$ $5d^{8}$, is isoelectronic to Pt(II) and similarly to Pt(II), Au(III) complexes prefer a square planar orientation. Many simple Au(III) complexes can be reduced to Au(I) by donors such as thiol or thioesters, functional groups in amino acids cysteine and methionine, therefore its chemistry *in vivo* is hard to predict. However, Au(I) can also undergo oxidation to Au(III) *in vivo*.[50]

Gold compounds have been used for their medicinal properties for thousands of years.[51] In 1929, Jacques Forestier became the first to use a gold complex, in this case $Na[Au(CN)_2]$, for the treatment of rheumatoid arthritis.[51] Research in this area progressed and in the 1980's a breakthrough discovery was made by Sutton in his orally administered antiarthritic drug auranofin.[7] Auranofin is clinically used to treat rheumatoid arthritis.

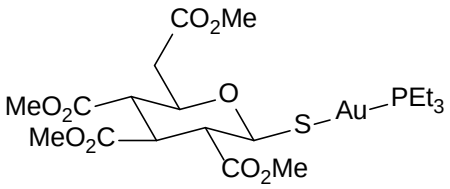

(1.38)

Figure 1.12 Chemical structure of auranofin.

As well as having antiarthritic properties, auranofin and derivatives were found to effectively kill cancerous cells in cell cultures. During research into the synthesis of new gold-phosphine complexes with cytotoxic properties, $[Au(dppe)_2]Cl$ was found to have a cytotoxic effect on a larger number of tumours than auranofin. Berners-Price studied the thermodynamic and kinetic stability of $[Au(dppe)_2]Cl$ using $^{31}P\{^{1}H\}$ NMR, which showed the bulky phenyl substituents are key for stability *in vivo* and biodistribution.[52,1,53] The phenyl groups prevent nucleophiles, such as thiols, from attacking the Au(I) metal centre as well as masking the cationic charge of the Au(I) allowing for diffusion through the lipid bilayer of the cell membrane.[47,52,53]

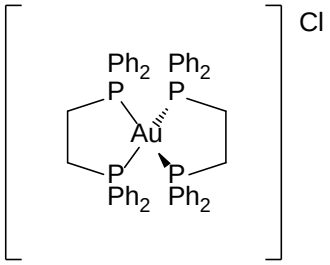

(1.39)

Figure 1.13 Chemical structure of $[Au(dppe)_2]Cl$.

As well as its chemotherapeutic properties gold also has potential for radiotherapy using ^{199}Au, a beta and gamma emitter; although there are no ^{199}Au radiopharmaceuticals currently used clinically. The potential for ^{199}Au as a radiopharmaceutical is often not studied due to the instability of known gold complexes *in vivo*. However, Katti *et al.* investigated the *in vivo* and *in vitro* properties of three radioactive gold complexes shown in Figure 1.14.[54]

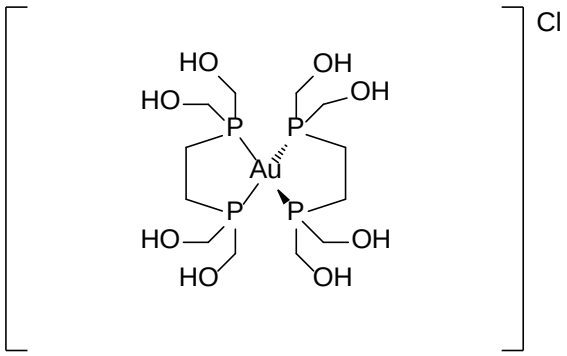

(1.40)

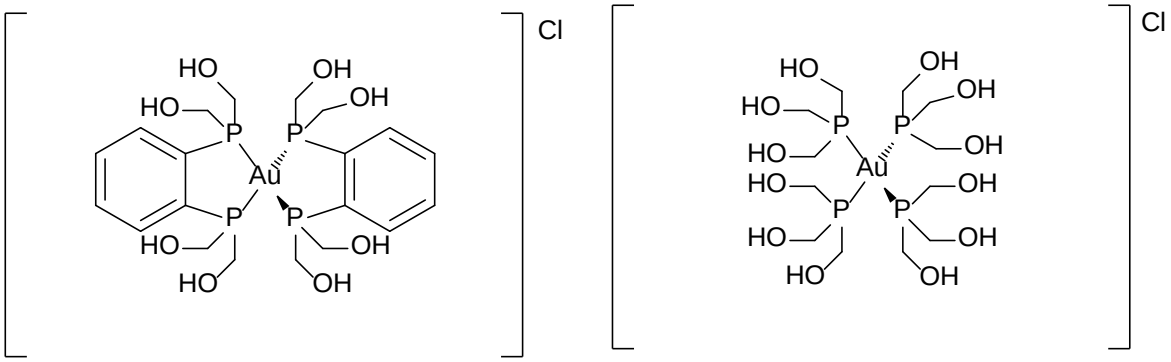

(1.41) **(1.42)**

Figure 1.14 Chemical structure of compounds **1.40**, **1.41** and **1.42** synthesised by Katti *et al.* [54]

Taking inspiration from $[Au(dppe)_2]Cl$, Katti and colleagues synthesised radioactive ^{198}Au compounds of **1.40**, **1.41** and **1.42**. Hydroxyl substituents were used on the phosphine moieties rather than phenyl groups like $[Au(dppe)_2]Cl$ were used in order to aid water solubility. Compounds **1.40** and **1.42** showed little *in vivo* and *in vitro* stability, with **1.42** showing the least stability; this was attributed to the use of monodentate ligands. **1.41**, in contrast, showed good stability stemming from the use of a rigid bidentate ligand large enough to shield the gold metal centre from potential nucleophiles.[54]

1.4.4 Platinum

Rosenberg's discovery of the anticancer properties of cisplatin, $PtCl_2(NH_3)_2$, the first metallodrug to be clinically used worldwide for the treatment of cancer, has driven the study of platinum coordination complexes ever since.[55] Platinum is a group 10 metal and can exist in one of two oxidation states, excluding Pt(0), Pt(II) and Pt(IV). Pt(II) has an electronic configuration of [Xe] $4f^{14}$ $5d^8$, is diamagnetic and forms a square planar geometry with coordination ligands. Cisplatin and related metallodrugs typically contain two labile ligands which are displaced *in vivo* allowing for coordination of the platinum centre to DNA or a protein. Cisplatin, while still used clinically, is used much less due to the toxicity to healthy tissue which limits dose. Research has focused on synthesising less toxic derivatives of cisplatin such as carboplatin and oxaliplatin, shown in Figure 1.15.[50]

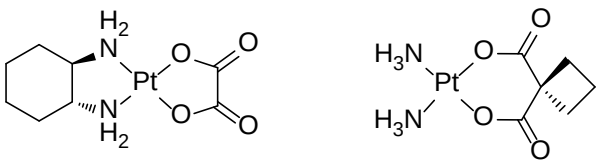

(1.43) **(1.44)**

Figure 1.15 Chemical structure of oxaliplatin and carboplatin.

Carboplatin, **1.44**, was designed with a dicarboxylate ligand which due to the chelation effect stabilises the metal complex, therefore making carboplatin less reactive than cisplatin. Although toxicity is reduced, carboplatin is still toxic, reducing the white cell count of patients exposing them to infection. Carboplatin is used clinically by itself and in combination with other drugs. Oxaliplatin, **1.43**, is also used clinically in the treatment of cancers, however there are also some side effects associated with this pharmaceutical. Despite its toxicity cisplatin is seen as the 'gold' standard to which all new metallodrugs are compared. [50]

Pt(IV) ions have an electronic configuration of [Xe] $4f^{14}$ $5d^{6}$, are diamagnetic and prefer octahedral geometry. Pt(IV) metal centres have also been explored for the synthesis of metallodrugs. Satraplatin, shown in Figure 1.16, is an example and is currently the only orally administrated Pt(IV) pharmaceutical being studied in clinical trials.[50] Similarly to other Pt(IV) metallodrugs, satraplatin is reduced in the bloodstream by metal containing redox proteins into the respective Pt(II) complex, which then interacts with DNA or proteins.[46]

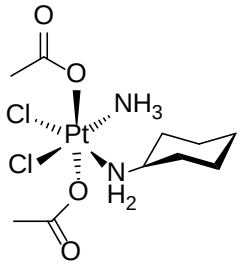

(1.45)

Figure 1.16 Chemical structure of satraplatin.

^{195m}Pt is a reactor produced radionuclide emitting low abundance gamma photons (γ, 85%, $t_{0.5}$ = 4d). ^{195m}Pt is already used for biodistribution and pharmacokinetic studies of platinum containing metallodrugs, as well as being investigated for radiotherapy due to accompanying Auger electron emissions.[34]

1.4.5 Palladium

Interest in the medicinal properties of palladium originate from the structural and thermodynamic analogy of Pt(II) and Pd(II) complexes. Graham and coworkers were one of the first groups to investigate the anticancer properties of palladium complexes; since then many other research groups have explored this area.[56,57] The difficulty with the use of palladium drugs lies in the rate of ligand exchange; Pd(II) complexes hydrolysis 10^5 times faster than Pt(II) complexes. To slow down the rate of exchange, a number of techniques have been trialled; these including the use of bulky monodentate ligands, bidentate and tridentate ligands, and the use of cyclopalladated compounds.[57]

Trans-isomers have been found to have greater cytotoxicity than their *cis*-configured counterparts.[57] An early example of a *trans*-palladium compound investigated for its anticancer properties is **1.46**, shown in Figure 1.17, which was synthesised by Tusek-Bozic *et al*.[58] Compound **1.46** features diethyl phosphonate moieties which aid the solubility of the complex. A monoethyl phosphonate analogue of **1.46** was also investigated, however **1.46** was found to have greater cytotoxic potential.[57,58]

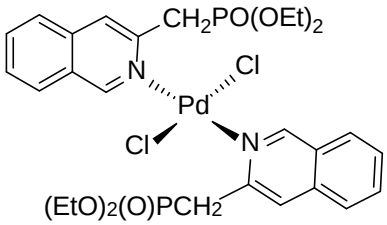

(1.46)

Figure 1.17 Chemical structure of *trans*-palladium *bis*(quinonyl-phosphonate).

Due to their well-known medicinal properties, *bis*-phosphine ligands have also been explored for the synthesis of potential anticancer palladium complexes. Travassos and colleagues investigated the use of *bis*phosphine ligands with cyclopalladated phosphine complexes.[59] *In vitro* and *in vivo* studies were conducted against murine melanoma cells subcutaneously implanted into mice. Results showed compounds **1.48** and **1.49** exhibited the highest antitumour activity.[59,57]

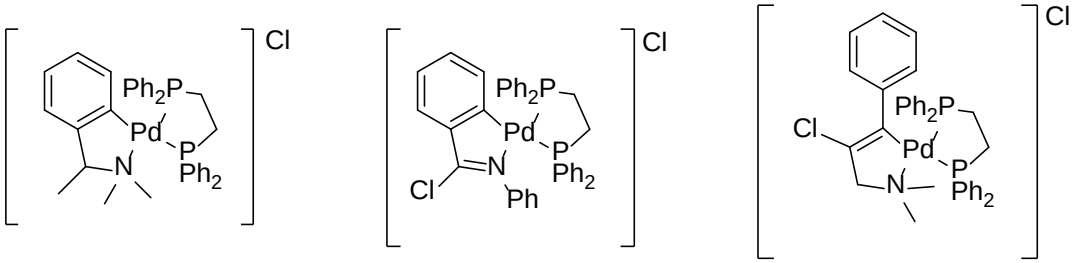

(1.47) **(1.48)** **(1.49)**

Figure 1.18 Chemical structures of example complexes investigated by Travassos *et al.*[59]

Overall, further investigation into the use of palladium complexes as potential metallodrugs and their mode of action is required. Stability of complexes through the use of chelating ligands or cyclopalladated complexes is important to ensure complexes are stable enough to reach their biological target. Palladium compounds have been shown to be more soluble and have similar, and on occasion better, antitumour activity than their platinum counterparts.[57]

1.4.6 Ruthenium

Ruthenium compounds have also been explored for the treatment of cancers. Ruthenium can adopt of number of oxidation states *in vivo*, these being Ru(II), Ru(III) and Ru(IV) (electronic configuration of [Kr] $4d^6$, [Kr] $4d^5$ and [Kr] $4d^4$, respectively). Due to the low

energy barrier between oxidation states, redox chemistry is possible on the metal centre inside the cell. Ruthenium metal centres prefer an octahedral geometry; therefore chemists have an additional two ligands in comparison to platinum metallodrugs that can be exploited for modification of the chemical properties of a complex.[60]

KP1019 and NAMI-A, as shown in Figure 1.19, are the first ruthenium metallodrugs to enter clinical trials. Although chemically similar, KP1019 and NAMI-A have been shown to have anticancer effects on different types of cancers, with KP1019 targeting primary tumours and NAMI-A reducing secondary cancers. Both KP1019 and NAMI-A likely undergo structural changes *in vivo* since they contain ligands which may hydrolyse (Cl, DMSO).[46,60,61]

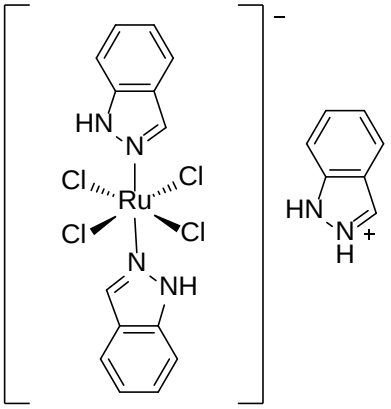

(1.50)

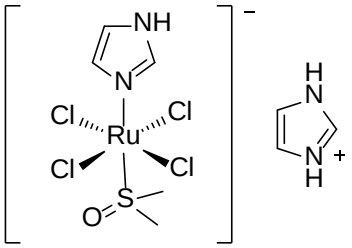

(1.51)

Figure 1.19 Chemical structures of KP1019 (**1.50**) and NAMI-A (**1.51**).[61]

Organometallic ruthenium compounds have also been shown to have some anticancer activity; this couples well with other known properties of organometallic ruthenium compounds such as high water solubility and air stability. RAPTA, displayed in Figure 1.20, is an example. Despite the difference in oxidation state, geometry, ligands and charge, RAPTA shows similar anticancer activity to NAMI-A.[61]

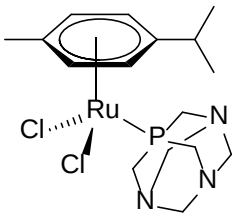

(1.52)

Figure 1.20 Chemical structure of RAPTA.

PTA (1,3,5-triaza-7-phosphaadamantane), which among other things, aids water solubility of the complexes it is coordinated to, has been utilised in a number of applications.[62] RAPTA exhibits pH-dependent DNA damage which is attributed to the PTA ligand. In hypoxic tumour cells the low pH allows the protonation of PTA, which is the active agent that causes DNA damage. In healthy cells, PTA is not protonated in normal physiological pH and therefore little or no damage in done to healthy tissue.[61,63]

Although ruthenium has a radionuclide namely ^{97}Ru (γ, 85%, $t_{0.5}$ = 2.9d), which has attractive gamma photon emission and a half-life suitable for the study of pharmaceuticals with slow pharmacokinetics, ^{97}Ru is produced *via* high proton bombardment which limits its potential preventing clinical applications.[34]

1.5 Luminescence

The emission of photons from a substance in an electronically excited state is termed luminescence. Fluorescence is the emission of light from the first singlet excited state to the singlet ground state ($S_1 \rightarrow S_0$). Fluorescence is not the only mode of de-excitation, competing with processes such as internal conversion, intersystem crossing, non-radiative pathways and radiative process, phosphorescence. Fluorescence is a spin allowed process allowing for rapid emission to singlet ground state. Typical emission lifetimes are in the nanosecond and sub-nanosecond timescale.[64]

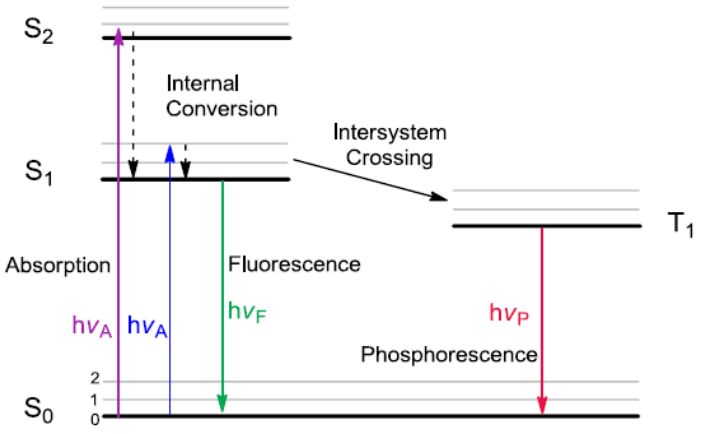

Figure 1.21 Jablonski diagram.[65]

As shown in the Jablonski diagram above, each electronic energy level is comprised of vibrational energy levels. When light is absorbed by a species, the fluorophore is usually excited to a higher vibrational level than the lowest available vibrational level in the electronic energy level. The fluorophore undergoes internal conversion to populate the

lowest vibrational level before fluorescing to the electronic ground state. As a result of this the fluorescence spectra is at a lower energy (higher wavelength) than that of the absorption spectra. The difference between the positions of the energy maximum for the absorption spectra and the energy maximum of the fluorescence spectra is termed the Stokes shift, Δv_{st}.[65]

Species in the first excited singlet electronic state can undergo intersystem crossing to the first triplet electronic excited state. Emission of light from the triplet state, T_1, is called phosphorescence. The lowest vibrational energy for the singlet state is higher than the lowest vibrational energy of the triplet state and therefore phosphorescence is observed at a higher wavelength than fluorescence. The radiative rate constant for phosphorescence is low, leading to long lifetimes, usually in the milliseconds range. This is a result of a change in spin multiplicity from the triplet state to the singlet ground state ($T_1 \rightarrow S_0$) and therefore the emission is forbidden.[65]

Quenching is the term used to describe a reduction in fluorescence. Quenching can occur in a number of ways. Intersystem crossing, as mentioned above, reduces fluorescence through the population of isoenergetic vibrational levels of the triplet state ($S_1 \rightarrow T_1$). In the presence of heavy atoms intersystem crossing is enhanced. Solutions prepared for fluorescence are purged with an inert gas before measurement to prevent quenching by dioxygen and concentrations of solutions are low to avoid the formation of excimers, which are electronically excited dimers formed from the collision of an excited molecule with an identical unexcited molecule, and the formation of exciplexes, which are electronically excited complexes formed from the collision of an excited molecule and an non-identical unexcited molecule; all of which reduce fluorescence. Temperature can also cause quenching as de-excitation via non-radiative pathways increase with an increase in temperature.[64]

1.5.1 Photoinduced Electron Transfer

Photoinduced electron transfer, or PeT, can be divided into two subgroups: reductive PeT and oxidative PeT. Oxidative PeT occurs through the donation of electrons from the excited state of the fluorophore to the non-planar substituent's LUMO (lowest unoccupied molecular orbital), reducing fluorescence. This is often a result of electron-withdrawing substituents on the fluorophore, such as nitrile, nitro and ester substituents.[64]

For reductive PeT, the fluorophore acts as an acceptor as the non-planar substituent donates electrons from its LUMO to the fluorophore HOMO (highest molecular orbital). This process is promoted by electron donating substituents on the fluorophore, such as aryl amines or alcohols.[64] Overall, PeT is enhanced in the prescence of nitro, amine and

heavy atom substituents, but only when the orbital energies of the substituents and fluorophore are of similar energy to allow interaction.

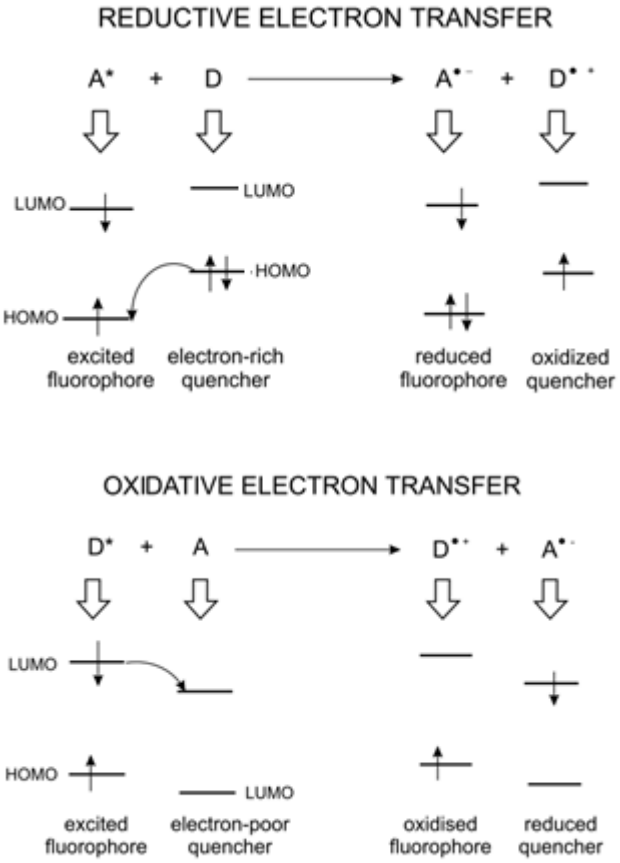

Figure 1.22 Diagram illustrating PeT.[64]

1.5.2 Metal to ligand charge transfer

Upon coordination of ligands to a metal, in many cases, the metal *d* orbitals are split and there is a change in electron distribution giving rise to charge transfer bands. There are different types of charge transfer associated with metal complexes. When an electron is promoted within the *d* orbitals, and is confined to the metal centre, this is termed metal centred transition (MC). MLCT (metal to ligand charge transfer) occurs when a metal is reducing and the coordinated ligand provides an empty orbital of low energy for electron transfer. Similarly ligand-to-metal charge transfer (LMCT) can occur when the ligand is reducing and the metal is oxidising, and therefore electron transfer occurs from the ligand pi system to the metal centred orbitial. MMCT or metal-to-metal charge transfer occurs in a bi- or polynuclear complex, typically where two identical metals in different oxidation states are bridged by a ligand(s).[66]

1.5.3 Internal charge transfer

Promotion of an electron to an orbital separated in space from the initial ground state orbital causes an instantaneous change in dipole moment of the fluorophore on electronic transition. If the fluorophore contains electron donating groups conjugated to electron withdrawing groups, the increase in dipole moment can be large. If the solvent is polar then the dipole is stabilised and the lower energy CT state can be accessed, with an accompanying bathochromic shift in emission. Fluorescent sensing probes using ICT work through the binding of the species being sensed to either the electron withdrawing or electron donating group, therefore making the CT state inaccessible and restoring the locally excited state (LE) wavelength.[64,65]

1.5.4 1, 10-Phenanthroline and derivatives

1,10-Phenanthroline (phen), shown in Figure 1.23, is a heterocyclic system with two inward pointing nitrogen atoms in juxtaposition which can be utilised for bidentate coordination to a metal centre. Phen is planar, hydrophobic and has a rigid structure; these structural features allow phen to intercalate and groove bind to DNA and RNA.[67] $[Cu(phen)_2]^{2+}$ is one example of a commonly used DNA cleaving agent.[68] Phen derivatives also have applications in molecular recognition, molecular self-assembly and photoswitchable molecular devices, amongst others.[69–72]

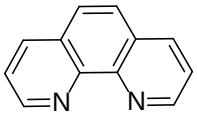

(1.53)

Figure 1.23 Chemical structure of 1,10-phenanthroline.

Phen, itself, is a weak fluorescence emissive, with a quantum fluorescence yield of 0.0087 and a short lifetime (τ <1ns). However, when coordinated to a metal centre some complexes exhibit very desirable fluorescence properties. Phen is electron deficient and has low lying π^* antibonding orbitals making phen a good electron acceptor. When coordinated to a reducing metal, low energy MLCT electronic states are available and fluorescence is observed.[67,69]

Copper(I)-phen complexes display MLCT fluorescence.[69] Attention now focuses on copper(I)-phen complexes with the formula, $[Cu(N^N)(P^P)]^+$, where N^N is a diimine and P^P is a *bis*phosphine ligand, since these complexes exhibit enhanced fluorescence in

comparison to copper(I) complexes with the formula $[Cu(N^N)_2]^+$.[73] Complexes with the formula $[Cu(N^N)(P^P)]^+$ were first synthesised by McMillian *et al.* and exhibit enhanced fluorescence due to higher energy MLCT electronic states which disfavour non-radiative decay.[74,75]

In 2013 Kaesar *et al.* reviewed the formation of heteroleptic copper(I) complexes with various *bis*phosphine and phenanthroline ligands.[76] The ligands explored are listed in Figure 1.24. The study found when using 2,9-unsubstituted-1,10-phenantholine derivatives, phen and Bphen, only heteroleptic complexes were obtained independent of the *bis*phosphine used, excluding dppm. On coordination of dppm in a bidentate fashion a four membered chelate ring is formed which is unstable due to strain and therefore dppm can act only as a monodentate or bridging ligand.[76]

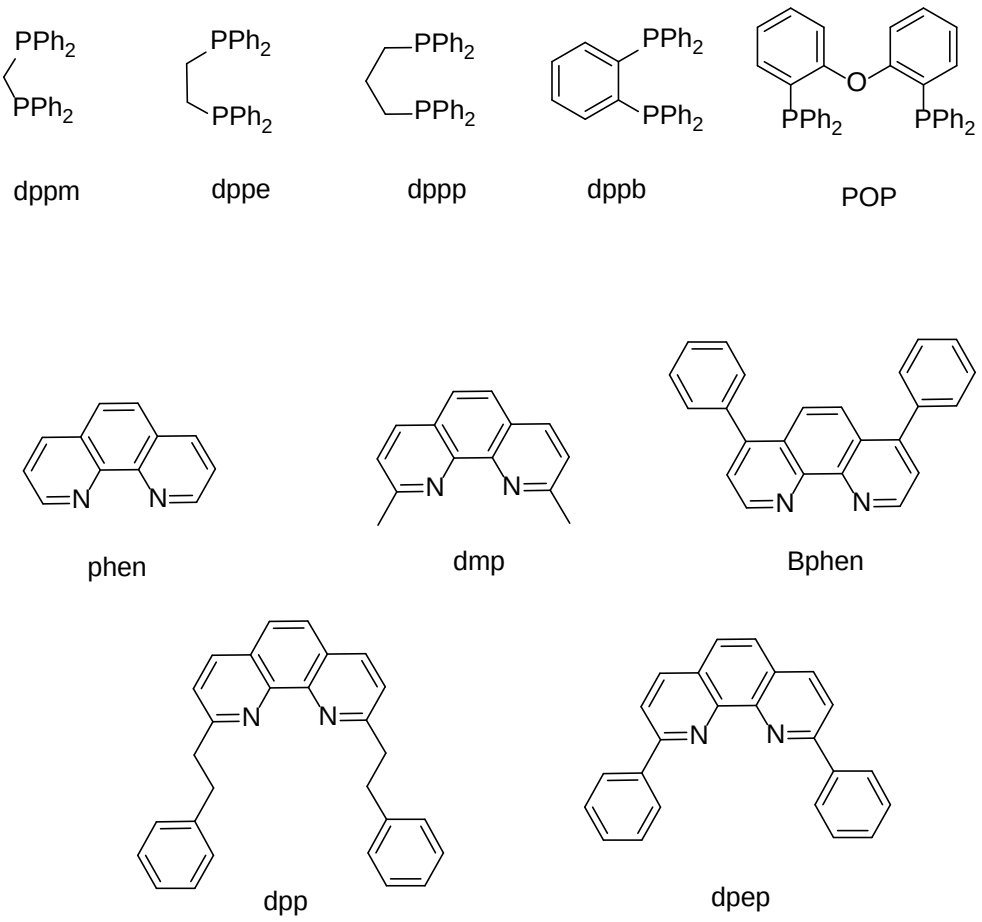

Figure 1.24 Library of NN and PP ligands used for the preparation of heteroleptic $[Cu(N^N)(P^P)]^+$ and $[Ag(N^N)(P^P)]^+$ complexes.[76,77]

For 2,9-substituted-1, 10-phenanthroline ligands, dmp, dpp and dpep, on reaction with copper(I) and equimolar amounts of *bis*phosphine ligand, a mixture of homoleptic and

heteroleptic complexes were formed. This is due to destabilisation caused by the bulky substituents in the 2- and 9- positions. The ratio of homoleptic and heteroleptic complexes is not solely dependent on the sterics of the 2,9-substituents, but is also dependant on the *bis*phosphine bite angle. dppFc (1,1'-bis(diphenylphosphino)ferrocene) and POP heteroleptic complexes were obtained in higher yields than analogous dppe, dppp and dppb complexes. *Bis*phosphines, dppe, dppp and dppb can form thermodynamically stable homoleptic complexes, however a small copper(I) cation cannot accommodate two bulky ligands dppFc and POP and therefore $[Cu(N\text{^}N)(P\text{^}P)]^+$ is more thermodynamically favourable in this case then $[Cu(P\text{^}P)_2]^+$.[76]

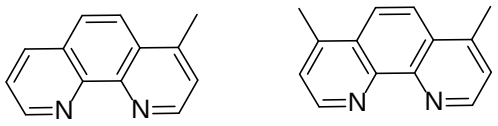

Mephen diMephen

Figure 1.25 Additional NN ligands used for the preparation of heteroleptic $[Ag(N\text{^}N)(P\text{^}P)]^+$ complexes.[77]

Kaesar *et al.* also reviewed silver(I) complexes with various *bis*phosphine ligands and phenanthroline derivatives, shown in Figure 1.24 and 1.25.[77] While POP and phen gave desired complex of the formula, $[Ag(N\text{^}N)(P\text{^}P)]^+$, dppm and dppp formed dinuclear complexes, illustrated in Figure 1.26, with a small amount of mononuclear complex present only in the dppp reaction NMR. Even with excess *bis*phosphine, dppp acts as a bridging ligand rather than chelating.[77]

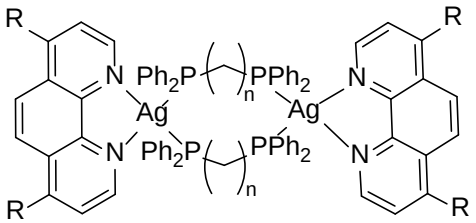

(1.54) R = H, n = 1
(1.55) R = H, n = 3
(1.56) R = Me, n = 1
(1.57) R = Me, n = 3

Figure 1.26 Monobridged species synthesised by Kaesar *et al.*[77]

*Bis*phosphine, dppe, formed only a monobridged complex, as presented in Figure 1.26, with reagents in stoichiometric ratios of 2:2:2 or 2:2:1 for phen:Ag:dppe. Kaesar *et al*.

also synthesised monobridged complexes with *bis*phosphines, dppm and dppp, and phenanthroline derivatives using stoichiometric ratios 2:2:1 (N^N: Ag: P^P) to demonstrate for some *bis*phosphines the formation of mono- or dibridged species could be controlled.[77]

Silver(I) can form a number of luminescent complexes, many of which are polynuclear. Silver(I) has an electronic configuration of [Kr] $4d^{10}$ and is redox inert. Coupled with electron accepting phen, no low lying MLCT electronic states are available, therefore many silver-phen complexes decay by phosphorescence *via* the heavy atom effect.[69,73]

1.5.5 1,8-Naphthalimide and derivatives

A broad range of 1,8-naphthalimide derivatives can be synthesised through the reaction of 1,8-naphthalic anhydride with a number of amines; additional functionalisation is available via substitution at the 3, 4, 5 or 6 position. 1,8-naphthalimide derivatives often strongly fluoresce and exhibit a strong stokes shift, with emission in the green part of the electromagnetic spectrum.[78] The addition of substituents to the aromatic system causes a shift in fluorescence emission in the electromagnetic spectrum; for example, amino substituents in the 3-, 4-, 5- or 6- position cause absorption and emission to shift to the visible region due to internal charge transfer transitions (ICT).[79–81] The influence in chemical, electronic and physical properties of compounds through functionalisation make 1,8-naphthalimide derivatives an attractive prospect for fluorescence confocal microscopy.

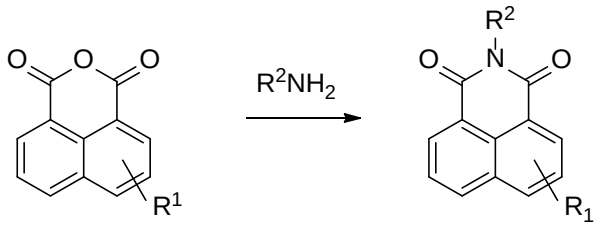

(1.58) **(1.59)**

Scheme 1.7 Reaction of 1,8-naphthalic anhydride with a primary amine.[78]

As well as showing potential as laser dyes,[82,83] solar energy collectors[84,85] and for application in supramolecular chemistry, 1,8-naphthalimide derivatives have been investigated for medicinal purposes, both as antitumour agents[86] and antiviral agents.[87] Braña and co-workers synthesised a family of 1,8-naphthalimide derivatives, including amonafide (3-amino-1,8-naphthalimide) shown in Figure 1.27. Amonafide is a DNA binding agent and shows high antitumour activity. Amonafide induces DNA breakages and protein DNA crosslinking in cultured mammalian cells. Quinamed®, a dihydrochloride

salt of amonafide has been investigated for its use against prostate cancer. However, during metabolism amonafide can be converted into a number of toxic metabolites which differ in quantity from person to person. Therefore research into developing derivatives with reduced side effects is of interest.[88]

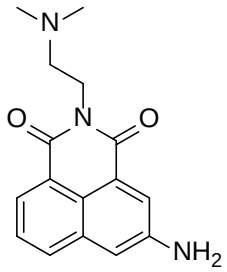

(1.60)

Figure 1.27 Chemical structure of amonafide.[88]

In the search for further derivatives, a number of *bis*-naphthalimides were synthesised. Gunnlaugsson and colleagues synthesised some *bis*-naphthalimide derivatives with Tröger's base separating the two, continuing work started by Deprez *et al*. [80,89–91] Carl Tröger first synthesised Tröger's base in 1887, with Spielman determining it's structure in 1935.[92,93] Tröger's base is a chiral, rigid, v-shape molecule with a C_2 axis of symmetry provided by the central diazocine ring. Tröger's base derivatives are synthesised by the reaction of an aromatic amide with formaldehyde in the presence of acid to yield a racemic mixture of *R,R* and *S,S* enantiomers. The cavity created by the fixed geometry of Tröger's base derivatives allows some derivatives to interact with DNA, as the cavity can intercalate with DNA enabling conformationally selective binding. [94,95]

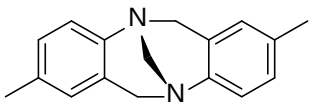

(1.61)

Figure 1.28 Chemical structure of Tröger's base.

Examples of the synthetic work performed by Gunnlaugsson and colleagues are shown in Figure 1.29.[78,89,90] Compounds **1.62** and **1.63** were shown to protonate in biological pH, allowing for stronger binding to the negatively charged phosphate DNA backbone and

increased solubility in aqueous media. Affinity for DNA was enhanced by the presence of the diazocine ring. It was also found compounds **1.62** and **1.63** on addition to cancer cell lines were taken up by the cell and localised in the nucleus, causing cell death.[89] Related compounds exhibited similar results and underwent cellular imaging via fluorescence confocal microscopy.[78]

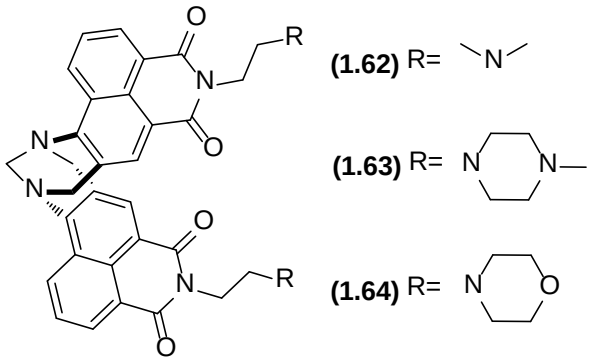

Figure 1.29 Example of Tröger's base and naphthalimides.[78,89,90]

Metal complexes with 1,8-naphthalimide derivatives have also been synthesised for their application as metallo-drugs. Gold is of interest as a metal for metallo-drug applications; the properties of gold are discussed in more detail in Section 1.43. Ott and colleagues synthesised complex **1.65** using a mercapto-functionalised naphthalimide coordinated to a gold-phosphine generating S-Au-P type bonding similar to auranofin. The 1,8-naphthalimide again was chosen for fluorescence properties and ability to intercalate to DNA, with a protonable nitrogen to strengthen electrostatic interactions. Fluorescence of complex **1.65** was substantial in chloroform, but decreased significantly in highly polar solvents due to PeT between the nitrogen on the side chain and heterocyclic system.[96]

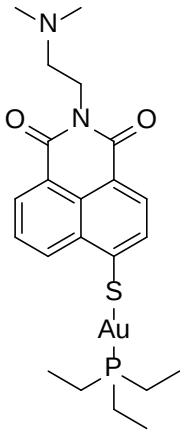

(1.65)

Figure 1.30 Chemical structure of **1.65** synthesised by Ott *et al.*[96]

Due to the solvent polarity effects on fluorescence, fluorescence microscopy studies of the complex in colon carcinoma (HT-29) and breast cancer cells (MCF-7) imaged only some compartments of the cell which are apolar or of medium polarity, for example the apolar cell membranes. Further work used AAS (atomic absorption spectrometry) to determine cell uptake in complex **1.65** and in $Au(PEt_3)Cl$ allowing for a comparison to be drawn. Complex **1.65** uptake was five times greater than the uptake of $Au(PEt_3)Cl$ in HT-29 cells and uptake was 25 times higher than $Au(PEt_3)Cl$ in MCF-7 cells. Therefore the naphthalimide can act as a targeting vector transporting the gold into nuclei. The antiproliferative effects of the complex on the cancerous cells were also studied showing similar activity of auranofin.[96]

Ott *et al.* found cellular uptake and biodistribution of chloro auric phosphine complexes benefited from larger, lipophilic substituents on the phosphine centre.[97] Therefore with this in mind Ott *et al.* synthesised derivatives of complex **1.65** with different substituents on the phosphine; these being methyl, ethyl, *tert*-butyl and phenyl substituents. Although no enhanced bioactivity was observed by changing the substituents on the phosphine, all complexes showed cellular uptake was higher than chloro analogues, [RS-Au-Cl].[98]

Dyson *et al.* synthesised two series of ruthenium complexes with naphthalimide derivatives conjugated via a linker to coordinating ligand η^6-*p*-cymene.[99] Both series are presented in Figure 1.31. There is potential for the chlorides to be hydrolysed allowing for reaction to biological targets. Series 1 is similar to $[Ru(\eta^6\text{-}p\text{-cymene})(PTA)Cl_2]$, a known complex with medicinal properties.[100] The PTA ligand has been used for medicinal purposes in the past and provides solubility in organic and aqueous solvents aiding biodistribution.[61,63] For series one the naphthalimide is conjugated to the arene via an aliphatic chain and for series 2 an imidazole linker is used. Naphthalimide derivatives are again attractive for their targeting properties for DNA and their photophysical potential.[99]

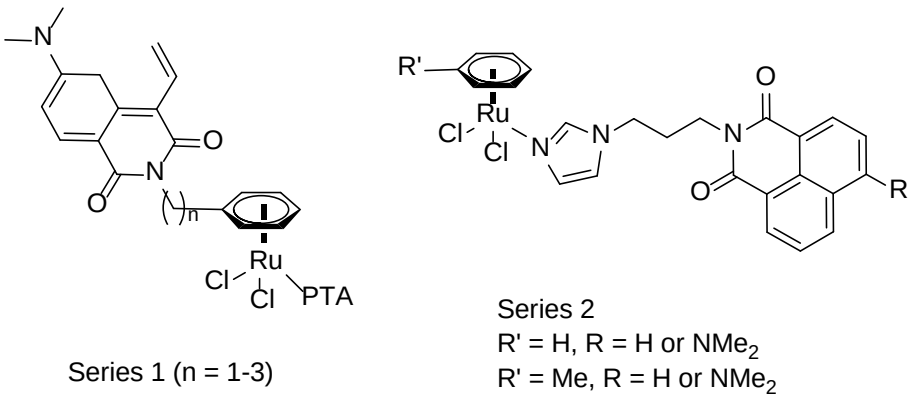

Figure 1.31 Two ruthenium(II) series as synthesised by Dyson *et al.* [99]

Both series showed enhanced cytotoxicity activity in comparison to $[Ru(\eta^6\text{-}p\text{-cymene})(PTA)Cl_2]$, possibly due to two modes of targeting; the first, through the

intercalation of DNA by naphthalimide and the second, through binding of proteins by the Ru-arene unit. Series 1 showed the greatest selectivity toward cancer cells and were active against cisplatin resistant cells.[99]

1.5.6 Fluorescein and Rhodamine

Fluorescein and the derivatives, rhodamine, are highly fluorescent molecules which have been used widely due to their high fluorescent quantum yield, photostability and absorption and emission wavelengths which lie in the visible region. Both fluorescein and rhodamine can exist in a non-fluorescent, colourless, spirolactam form or in a fluorescent, pink, ring open form.[101, 102] Fluorescein, rhodamine and their derivatives have been investigated for the fluorescence sensing of VOCs (volatile organic compounds), ozone, hydrogen sulphide, to name just a few.[103–105]

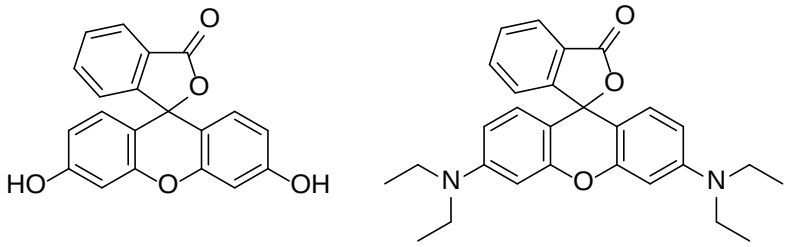

(1.66) **(1.67)**

Figure 1.32 Chemical structure of fluorescein, **1.66**, and rhodamine, **1.67**, based spirolactams.

Palladium complexes are involved in many chemical transformations and are used as catalysts for the synthesis of a number of compounds including pharmaceuticals; however this can lead to the presence of harmful palladium residues. There are a number of fluorescein derivatives described in the literature for the sensing of palladium.[102,106,107] Zhang *et al.* designed **1.69**, a fluorescent probe for fluorescent detection of palladium based on Rhodamine B.[101] Compound **1.69** was synthesised through the addition of 9-anthraldehyde to rhodamine b hydrazide, as shown in Scheme 1.8.

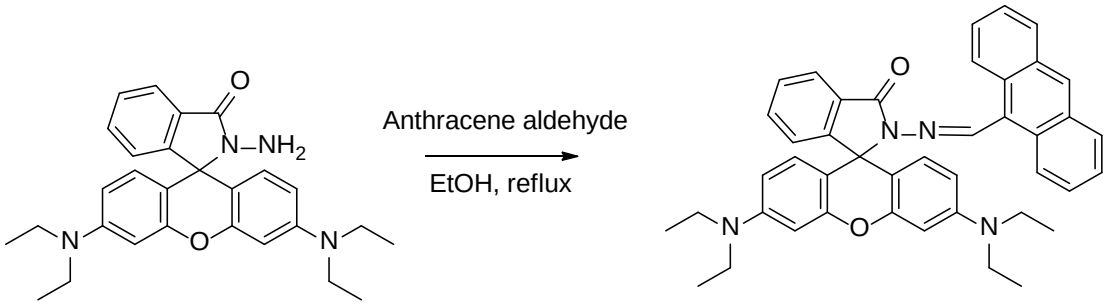

(1.68) **(1.69)**

Scheme 1.8 Addition of 9-anthraldehyde to rhodamine b hydrazide.[101]

The UV absorption spectra of **1.69** with a variety of metals were performed. These experiments showed a large increase in absorption after the addition of Pd(II) metal ions to **1.69**, but little or no increase in absorption with a variety of other metals including Pt(II) and Cu(II). Furthermore, on addition of Pd(II) ions to the solution of **1.69**, a change in colour from colourless to pink was observed; again this did not occur on the addition of any other metal ions trialled and therefore would suggest **1.69** could be used as a 'naked eye' detector for Pd(II) ions. Fluorescence microscopy of Arabidopsis guard cells incubated with **1.69** were imaged before and after addition of Pd(II). Results showed probe **1.69** could penetrate cell membranes and had potential for the use of sensing Pd(II) in cells.[101]

Li *et al.* also synthesised a fluorescent chemosensor, **1.70**, for the detection of palladium.[108] On addition of Pd(II) ions to a colourless solution of **1.70**, a pink colour is observed; this is due to the opening of the spirolactam ring. Probe **1.70** coordinates to a Pd(II) ion in a tridentate manner, chelating through the lone pair on the phosphine, through the nitrogen and the oxygen.

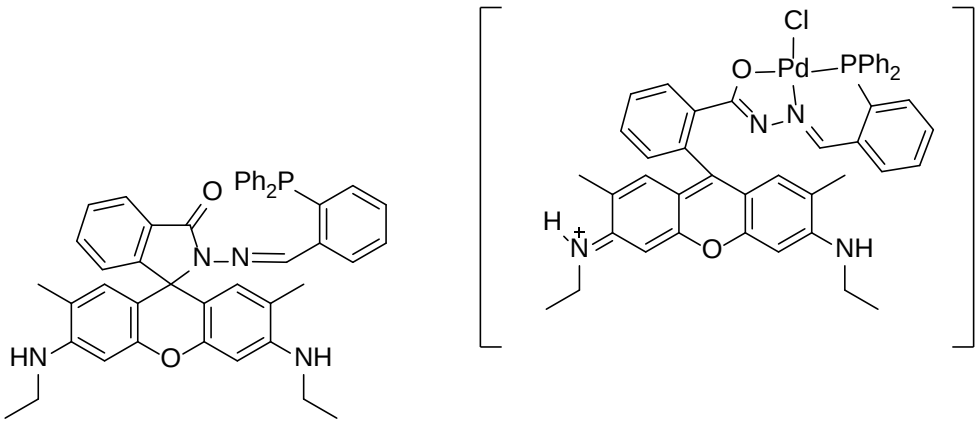

(1.70)

Figure 1.33 Fluorescent chemosensor synthesised by Li *et al.*[108]

Competition studies were performed which showed probe **1.70** to be selective for Pd(II) ions over other metals. Additionally, coordination experiments of probe **1.70** to Pd(0) species were investigated; differences in the rates of reaction observed may suggest probe **1.70** could be used to selectively discriminate between the two oxidation states.[108]

HNO-releasing drugs are potential candidates in the treatment of congestive heart failure. To understand the process of HNO (nitroxyl) production in the body and for the design of new drugs, a detection method for HNO is required. Miao *et al.* synthesised probe **1.71** through the addition of 1-(diphenylphosphino)benzoic acid with fluorescein methyl ether, for the sensing of HNO.[109]

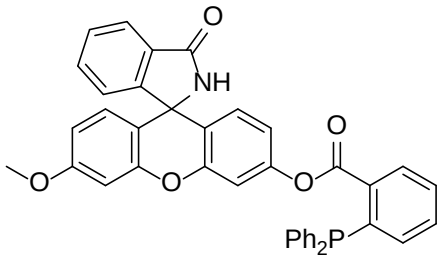

(1.71)

Figure 1.34 Chemical structure of probe **1.71**.[109]

Organophosphines react with HNO rapidly based on their documented Staudinger ligation reaction and show limited reactivity with other nitrogen oxides such as nitrite, nitrate and peroxynitrite. Non-fluorescent probe **1.71** reacts in a 2:1 ratio (probe to HNO, respectively) to yield fluorescein monomethyl ether, which is fluorescent and can therefore be detected. Miao and coworkers showed in their study that probe **1.71** is highly sensitive and selectively reacts with HNO, and confirmed the mechanism of the reaction between HNO and **1.71** through the use of mass spectrometry.[109]

1.5.7 Cellular Imaging Agents

The biological mechanisms of many metallodrugs is not always fully understood and as a result new therapeutics cannot be rationally designed. The cellular uptake of metallodrugs and their intracellular distribution can be investigated through analytical methods to allow elemental isotopic composition to be mapped or through the use of fluorescent tags on metal complexes compatible with fluorescence microscopy.[110]

In the design of a fluorescent imaging agent, the following photophysical properties are desired:[111,112]

- Large Stokes shift, to prevent self-quenching
- Long luminescence lifetimes (100 ns to ms) to prevent interference by autofluorescence
- Photostability, to reduce photobleaching
- High quantum yield, for brighter images at lower concentrations
- Wavelengths for emission and excitation which can be transmitted through tissue allowing imaging and avoiding tissue damage

As well as photophysical properties, fluorescent probes must also be stable *in vivo* and accumulate in the area of interest. The probe should be kinetically stable, to avoid degradation by other biomolecules *in vivo*, and should be soluble in solvents suitable for

administration to a patient. The probe must also have high cellular uptake accumulating in the area of interest, and display low toxicity.[113,111]

Pope and colleagues designed an alkynyl-naphthalimide fluorophore for investigating gold based metallodrugs.[110] Gold-based compounds have been successfully utilised in the treatment of diseases such as rheumatoid arthritis, but the toxicity of many gold compounds and the unclear mechanism of these drugs detract from the medicinal benefits. After synthesising ligands **1.72 – 1.78**, the ligands were coordinated to gold through the reaction of $AuCl(PPh_3)$ in EtOH in the presence of KO^tBu yielding complexes **1.79** - **1.85**.

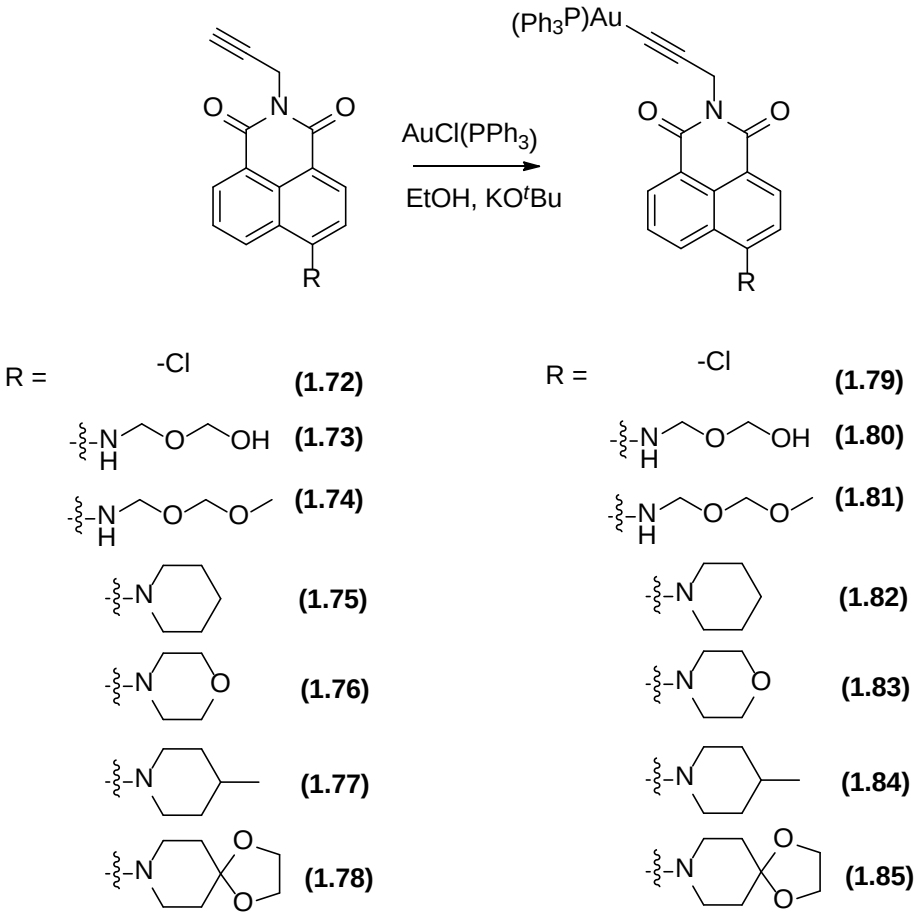

Scheme 1.9 Synthesis of complexes **1.79 – 1.85**.[110]

Photophysical properties were dictated by ligand centred ICT dominated transitions that provide visible absorption and emission characteristics. Lifetimes were approx. 10ns and quantum yields in excess of 50%. Cellular imaging studies were performed on HEK cells and *Spironucleus vortens,* a protistan fish parasite*.* **1.83** demonstrated quick uptake in HEK cells with imaged cells showing staining of the filapdia, glycogen vacuoles and various organelles. In contrast **1.83** had limited uptake in *S. vortens* cell, with **1.85**

showing good uptake and imaging. Overall uptake and localisation depended on the nature of the structure, with more lipophilic fluorophores localising in subcellular environments such as mitochondria.[110]

1.5.8 Bimodal Fluorescent Imaging and Radio-imaging Pharmaceuticals

The combining of techniques to provide superior imaging is a popular idea.[37,114,115] The combination of fluorescence imaging and radio-imaging can provide a well-rounded procedure, since PET/SPECT and fluorescent imaging have different advantages and disadvantages. PET/SPECT benefit from the ability to image the whole body, however PET is limited to imaging in the millimetre resolution range and cannot be imaged at the cellular level. *In vitro* fluorescence microscopy provides high resolution in the nanometre range, allowing for subcellular imaging, but is unsuitable to full body imaging.[116]

Synthesising a compound suitable for both fluorescent microscopy and radio-imaging is of interest as it replaces the need to use two separate pharmaceuticals, which may not localise in the same area and will not give a true representation of the mechanisms of the radiopharmaceutical. A dual imaging agent may consist of several parts; these being (i) a radiometal, (ii) a chelator to hold the radiometal to the radiopharmaceutical, (iii) a targeting vector and (iv) a fluorescent probe to provide *in vitro* fluorescence microscopy. Having clear components of the pharmaceutical allows for easy modification of components to develop a family of related agents.[116]

The Re/^{99m}Tc-acridine complexes, shown in Figure 1.35, were synthesised by Santos *et al.*[117] In these examples the fluorescent component, in this case, acridine is also the targeting vector, intercalating to DNA in melanoma cells. The acridine probe is linked *via* a short chain to a ^{99m}Tc/Re metal centre through a pair of pyrazoyl-diamine chelating units.[117] As well as gamma emissions for SPECT imaging, ^{99m}Tc has therapeutic properties; more specifically ^{99m}Tc emits four Auger or Coster-Kronig electrons, which if in close proximity to DNA can cause breakages, as previously shown by Alberto *et al*.[118]

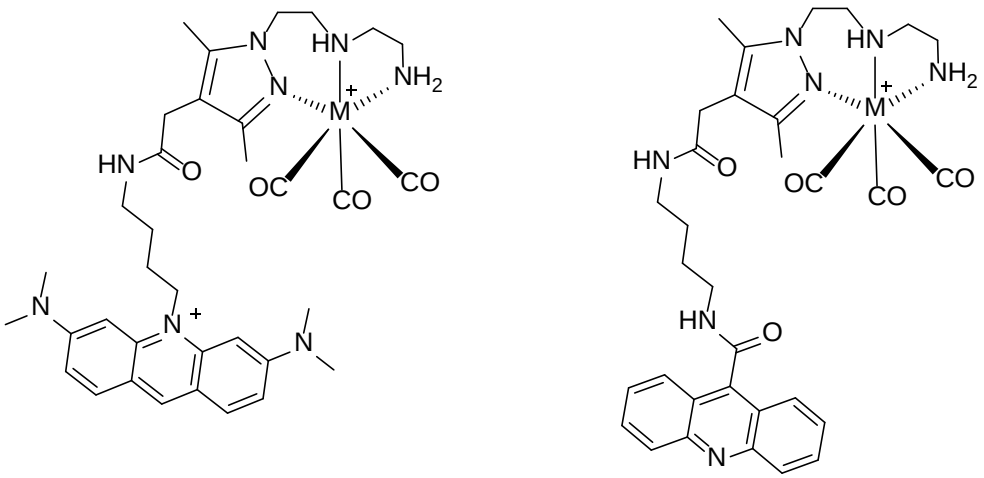

M^+ = ^{99m}Tc **(1.86)**
= Re **(1.87)**

M^+ = ^{99m}Tc **(1.88)**
= Re **(1.89)**

Figure 1.35 Re/^{99m}Tc-acridine complexes synthesised by Santos *et al.*[117]

Fluorescence microscopy of the above rhenium complexes showed **1.86** and **1.87** had higher affinity for DNA than **1.88** and **1.89**, with complexes **1.86** and **1.87** retained in the nucleus of melanoma cells. The study also showed evidence of DNA damage when using a ^{99m}Tc metal centre, but studies will continue to investigate if therapeutic effects are increased when a shorter linker is used, reducing the distance between the DNA-acridine intercalation and the ^{99m}Tc complex.[117]

Alberto *et al.* synthesised pyrene based fluorescent probes **1.90** – **1.91**. Probe **1.90** was used to observe the nucleus targeting properties of the radiopharmaceutical by *in vitro* fluorescent microscopy and the ^{99m}Tc analogue was designed for its cytotoxic properties, damaging DNA in melanoma cells.[119] In contrast to complexes **1.86** – **1.89**, radiopharmaceutical **1.90** – **1.91** fluorescent probes are not the targeting vector, a nonapeptide linked to the backbone of the chelator determines biodistribution. Without the peptide, there is no accumulation in melanoma cell nuclei. Although the study showed the radiopharmaceutical accumulates in cancerous cells and damages DNA, the uptake of ^{99m}Tc was too slow or too small to be a useful therapeutic drug.[119]

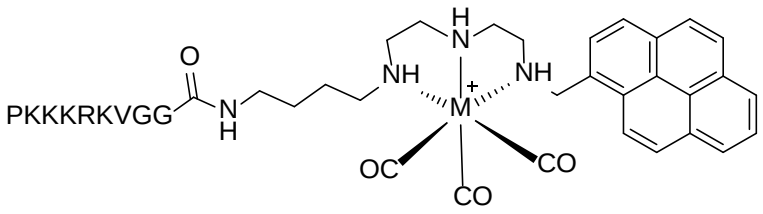

M^+ = ^{99m}Tc **(1.90)**
= Re **(1.91)**

Figure 1.36 Radiopharmaceuticals synthesised by Alberto *et al.*[119] (P = Proline; K = Lysine; R = Arginine; V = Valine; G = Glycine)

Another example of a bimodal radiopharmaceutical is presented in Figure 1.37 and was designed by Valliant *et al.*[120] Unlike the previous two examples, here, the fluorophore is intrinsic to the metal core. The bimodal imaging agent is based around the chelating tridentate quinoline ligand, which provides kinetic stability to the radiometal and MLCT *in vitro* fluorescence. The protected lysine conjugated to the chelator provides the opportunity to add a variety of peptide based targeting vectors using solid phase peptide synthesis. Valliant *et al.* extended the lysine to a pentapeptide with affinity for formyl peptide receptors expressed on neutrophilis allowing the imaging of leukocyte cells.[120]

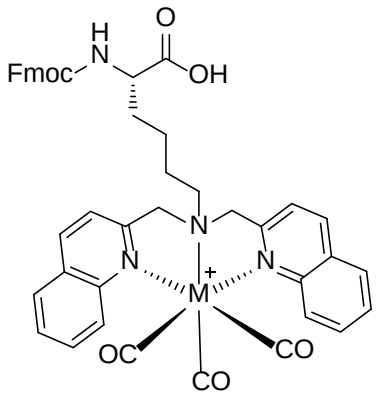

M^+ = ^{99m}Tc **(1.92)**
= Re **(1.93)**

Figure 1.37 Multifunctional pharmaceutical synthesised by Valliant *et al.*[120]

Although **1.93** has a desirable large Stokes shift, the fluorescent agent **1.93** showed varying lifetimes in the presence of varying amounts of oxygen indicating that quenching by photobleaching may be occurring. Additionally quantum yields were low and the resolution of fluorescent microscopic images was low.[120] Fluorescent agent **1.93** has nevertheless been a base for the development of covalent nitrogen systems.[121–126]

1.5.9 Phosphine-functionalised Fluorescent Imaging and Radio-imaging Pharmaceuticals

Higham *et al*. recently synthesised a phosphine-functionalised bodipy derivative, illustrated in Figure 1.38, complexing this to Re/^{99m}Tc metal centres.[127] Bodipy derivative, **1.94**, was reacted with *mer*-$ReCl(CO)_3(PPh_3)_2$ to give one stereoisomeric product. The ^{99m}Tc counterpart was prepared with Isolink®.[127]

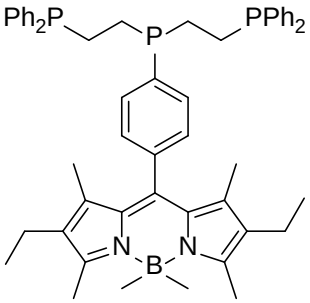

(1.94)

Figure 1.38 Bodipy probe synthesised by Higham *et al.*[127]

The coordinated compounds exhibited little change in energy maxima than that of **1.94**. The quantum yield of fluorescence, Φ_F, was slightly lower than that of **1.94** for all complexes as a result of the 'heavy atom effect' promoting intersystem crossing, however the quantum yield of fluorescence is higher than complex **1.92**/**1.93**.[120] Complexes also underwent competition studies with two amino acids found *in vivo* and were found to be stable. Technetium-phosphine coordination bonds have been shown to be inert.[127] Preliminary epifluorescence of rhenium complexed with **1.94** showed good imaging.[127]

Similarly, Higham *et al.* also synthesised four bodipy (boron-dipyrromethene) monodentate tertiary phosphines as shown in Figure 1.39.[33] These ligands were complexed with group 11 monovalent metals, gold, silver and copper. These metals have shown medicinal applications, presenting antitumour and cytotoxic properties and have radioisotopes suitable for PET imaging or therapeutics, as previously discussed in Section 1.4.

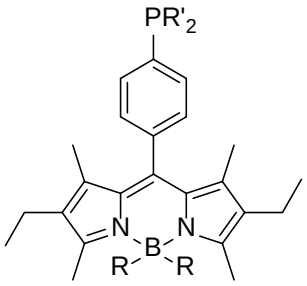

(1.95) R = Ph, R' = Ph
(1.96) R = Me, R' = Ph
(1.97) R = Ph, R' = Cy
(1.98) R = Me, R' = Cy

Figure 1.39 Four bodipy monodentate tertiary phosphines synthesised by Higham *et al.*[33]

In comparison to the bodipy precursor, the phosphine functionalised bodipy ligands **1.95** and **1.96** showed little quenching in fluorescent properties, while for ligands **1.97** and **1.98** the fluorescence was slightly enhanced. Similarly once coordinated to gold, silver and copper, the respective complexes were not significantly quenched. Therefore, the synthesised complexes with ligands **1.95 – 1.98** show potential applications for radio-imaging and cell imaging.[33]

1.5.10 Mixed ligand [2+1] bimodal radiopharmaceuticals

Covalently linked multifunctional radiopharmaceuticals can be unfavourable due to long synthesis times. Alberto *et al.* presented the mixed ligand [2+1] method, where a bidentate ligand and a monodentate ligand are coordinated to the metal centre with the fluorophore and the targeting vector conjugated to separate ligands.[128] Through utilising separate ligands, families of related structures can be formed with ease by substituting functional groups on either ligand. However, the monodentate ligand may be less stable than a chelating ligand *in vivo* and purification of [2+1] complexes will be required, leading to longer reaction times and smaller yields.

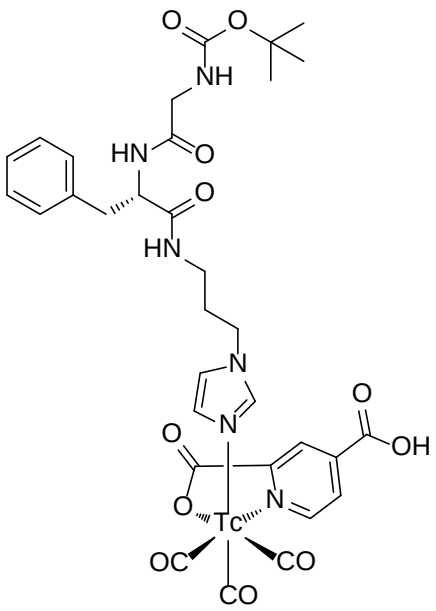

(1.99)

Figure 1.40 The [2+1] mixed ligand radiopharmaceutical synthesised by Alberto *et al.*[128]

1.6 Aims of this thesis

The aims of this thesis are as follows:

1) To functionalise naphthalimide derivatives with methylenediphenylphosphine moieties, CH_2PPh_2, *via* the phosphorus analogous Mannich condensation. Exploring the absorption and fluorescent properties of both the *bis*phosphine ligands and subsequent coordination complexes with Pt(II), Pd(II) and Au(I).

2) To investigate the changes in absorption and fluorescence of ligands and coordination complexes, when altering the fluorophore and the position of the PCN on the fluorophore, using fluorescein and derivatives.

3) Expanding the library of PCN framework functionalised amino acids, again synthesised *via* the phosphorus analogous Mannich condensation. Utilising these ligands to investigate the coordination chemistries of six metals of interest in different stoichiometric ratios.

4) Performing initial antibacterial studies of silver(I) complexes with *bis*phosphine functionalised amino acids.

Chapter 2 - Synthesis, coordination and characterisation of fluorescent naphthalimides with PCN moieties

2.1 Fluorescent phosphine containing naphthalimides

Naphthalimides have been investigated for their antitumour, antiviral and medicinal imaging properties, as they can localise in cells, have DNA binding capabilities and strong fluorescent properties; examples are discussed in Section 1.55.[86–88] There are a variety of naphthalimide derivatives, including metal complexes which have been investigated as metallodrugs. Research into naphthalimide metal complexes have included coordination to Au(I) and Ru(II) centres, as described in Section 1.55, and have also featured phosphine ligands.[96–98] Phosphine ligands benefit from the ability to manipulate physical properties, such as the electronic, steric and solubility capabilities of the metal complex they coordinate to through the addition of different substituents on the phosphine moiety and the ability to stabilise low oxidation state metals.[6,7]

The following research, discussed in this chapter, utilises the well-established route of adding substituents through a hydrazide moiety in the 4- position of the naphthalimide ring, but novelly introduces phosphine substituents through the phosphorus analogous Mannich based condensation reaction.[129] The coordination chemistries of the ligands synthesised here have been studied with a number of metal centres, and a preliminary investigation of their photophysical properties has also been performed. The synthesis of fluorescent phosphine ligands for medicinal imaging purposes is an area of great interest, with a number of papers published in recent years on this topic.[33,127]

2.2 Synthesis of phosphine containing naphthalimides

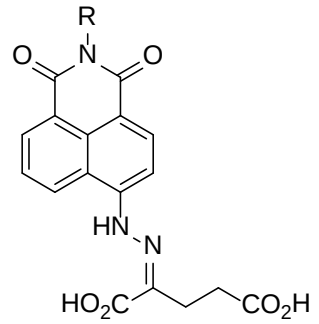

R = **(2.1)** $(CH_2)_3CH_3$
(2.2) $(CH_2)_{11}CH_3$
(2.3) $(CH_2)_2O(CH_2)_2OH$

Figure 2.1 Chemical structures of chemosensors synthesised by Zhu *et al*. for the detection of alpha-ketoglutaric acid.[129]

When designing the naphthalimide probes inspiration was taken from Zhu *et al.* whom synthesised three naphthalimide probes for utilisation as turn-on chemosensors for alpha-ketoglutaric acid.[129] The general chemical structure of Zhu and colleagues design was attractive for synthesising new phosphine containing compounds as fluorescent sensors as it possessed the naphthalimde fluorophore which is fluorescent and chemically stable, the imido group which can be altered for refinement of chemical properties, while the hydrazino moiety facilitates the addition of phosphine moieties for coordination to metals of interest.

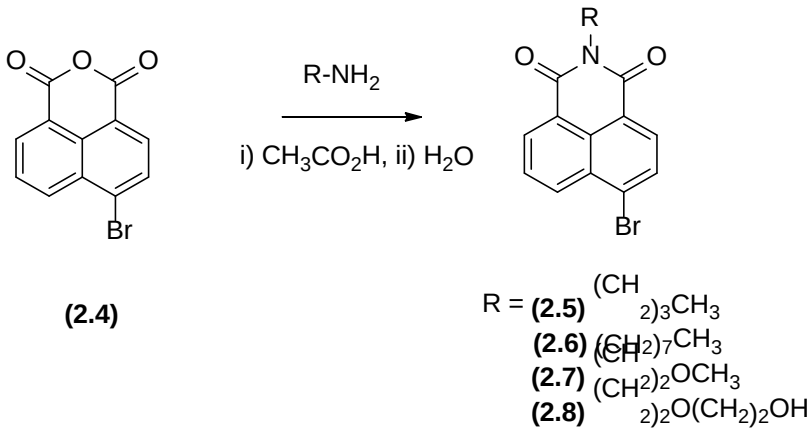

Scheme 2.1 Addition of four different primary amines to 4-bromo-1,8-naphthalic anhydride.

To begin with, the procedure taken from Zhu *et al.* was used to replicate the addition of n-butylamine and 2-ethoxyethylamine to 4-bromo-1,8-naphthalic anhydride to form **2.5** and **2.8**.[129] A further two amines, n-octylamine and 2-methoxyethylamine, were also reacted with 4-bromo-1,8-naphthalic anhydride under identical conditions to afford light brown powders of **2.6** and **2.7**. The yields of the imido-naphthalimides ranged between 80 - 90%, slightly higher than literature values. Collected analyses of **2.5** and **2.8** agreed with data recorded by Zhu and coworkers.[129] Compounds **2.6** and **2.7** are also known in the literature and analysis collected was comparable to that previously recorded.[130,131] In the ^{1}H NMR spectra, the triplet resonance at *ca.* 4.0 - 4.5 ppm is characteristic of the N-CH_2 proton signal, with coupling constants of $^{3}J_{HH}$ = 5.9-7.6 Hz.

2.2.1 Molecular structure of compound 2.5

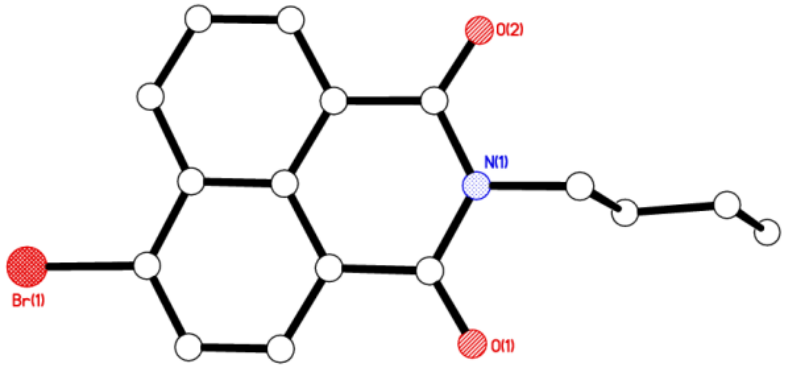

Figure 2.2 Molecular structure of **2.5**. All hydrogen atoms have been removed for clarity.

Colourless rods of **2.5** suitable for single crystal X-ray diffraction, were grown *via* slow evaporation of the ethanolic filtrate of **2.5** and the molecular structure determined (Figure 2.2). No solvent of crystallisation was present. Compound **2.5** is well known in the literature, however a search of the CSD[132] shows the X-ray structure of **2.5** has not been studied previously. The X-ray structures of similar compounds, **2.9** – **2.11** have previously been reported.[133–136] Bond lengths and angles of the naphthalimide moiety for compound **2.5** are comparable to that recorded in the literature for related structures **2.9** – **2.11**.[133–136] Due to the differing nature of the R groups in compound **2.5** and literature examples **2.9** – **2.11**, packing is different in each case.

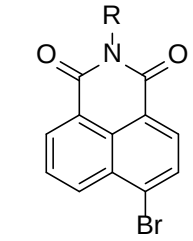

R = **(2.9)** OH
(2.10) $CH_2(C_4H_3S)$
(2.11) $N(CH_2CCH)_2$

Figure 2.3 Chemical structures of **2.9** - **2.11**.[133–136]

Molecules of **2.5** stack in columns with spirals of C–H···Br H-bonds along the *b* direction. There are also pi-pi stacking interactions with shortest contacts of *ca.* 3.298 Å. The rings do not fully overlap, as shown in Figure 2.4. In addition hydrogen bonding is observed between C=O and a hydrogen (C-H) on the ^{n}butyl chain. There may be some Br···Br

interaction since the distance between stacked molecules is 3.773 Å and the van der Waals radii for symmetrical halogen interactions for Br···Br is 3.70 Å.[137]

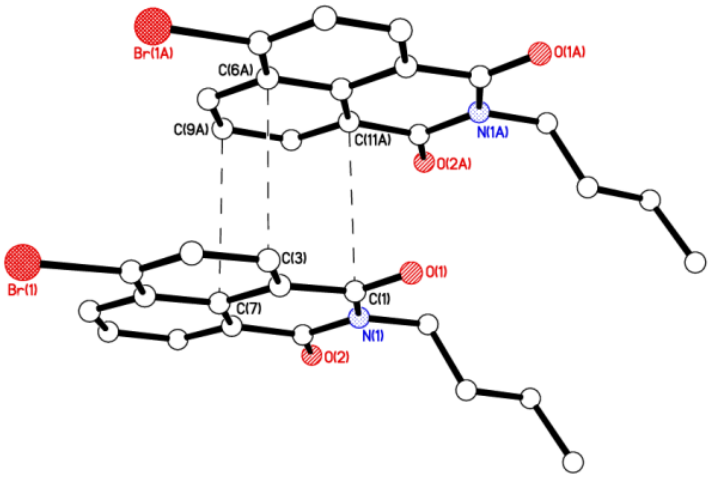

Figure 2.4 Packing structure of **2.5** highlighting pi-pi stacking interactions present. All hydrogen atoms have been omitted for clarity.

2.2.2 Synthesis of hydrazides 2.12 – 2.15

Compounds **2.12** – **2.15** were synthesised by reacting compounds **2.5** – **2.8** with hydrazine monohydrate, in a nucleophilic substitution reaction to replace the bromine with a hydrazino (NH-NH_2) group at the 4-position on the naphthalimide ring. This was performed according to a literature procedure, as described by Zhu *et al.*[6] While this method, describing the synthesis of **2.12** and **2.15**, was successfully extended to the methoxyethanol derivative, **2.14**, octylamine derivative, **2.13**, required longer reflux times and the addition of water to precipitate product **2.13**.

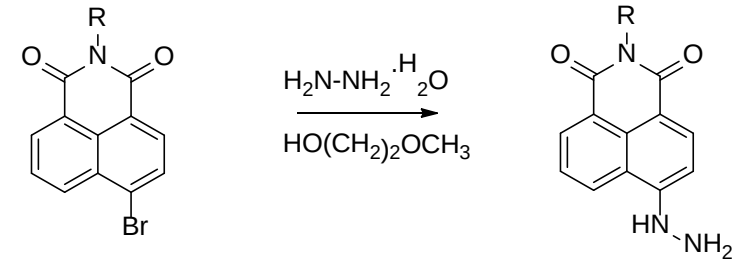

R = **(2.5)** $(CH_2)_3CH_3$
(2.6) $(CH_2)_7CH_3$
(2.7) $(CH_2)_2OCH_3$
(2.8) $(CH_2)_2O(CH_2)_2OH$

R = **(2.12)** $(CH_2)_3CH_3$
(2.13) $(CH_2)_7CH_3$
(2.14) $(CH_2)_2OCH_3$
(2.15) $(CH_2)_2O(CH_2)_2OH$

Scheme 2.2 Addition of hydrazine monohydrate to compounds **2.5** – **2.8**.

The characterising data collected for compounds **2.12**, **2.13** and **2.15** were in agreement with analysis recorded in the literature, described by Zhu *et al*. and Cao *et al*.[129,138] The synthesis and characterisation of methyoxyethanol derivative, **2.14**, however has not been previously recorded in literature, according to the Scifinder database and therefore a direct comparison cannot be drawn. Compounds **2.12** – **2.15** were synthesised in yields of 51-76%. The broad singlet peak at *ca.* 9.1 ppm is characteristic of the secondary amine hydrogen signal in the ^{1}H NMR for compounds **2.12** – **2.15**, with the primary amine hydrogens found at *ca.* 4.6 ppm. Analyses of novel hydrazide **2.14** were comparable to analogous compounds **2.12**, **2.13** and **2.15**. Mass spectra confirmed the synthesis of compound **2.14**, with a $[M + H]^{+}$ fragment found at *m/z* 286.1180 ppm. Elemental analysis was also in agreement with the empirical formula calculated for compound **2.14**. Despite numerous attempts crystals suitable for X-ray crystallography were not grown during synthesis of **2.12** – **2.15**.

2.2.3 Mannich based condensation reaction

Using a well-established procedure, *bis*phosphine compounds **2.16** – **2.19** were synthesised.[139,140] Compounds **2.12** to **2.14** underwent addition of two equivalents of Ph_2PCH_2OH *via* phosphorus analogous Mannich based condensations to yield yellow solids **2.16** to **2.18**. Initially, reaction conditions consisted of a 2h reflux in methanol followed by stirring at room temperature (*ca.* 72h), before filtration of precipitated products **2.16** – **2.18**. Reflux allowed the dissolution of hydrazides **2.12** – **2.14**, while stirring at r.t. for several hours was conducted to increase the reaction yield. Stirring was proven to improve the overall yield as **2.14** was synthesised both with and without room temperature stirring after reflux, affording a yield of 84 and 81% respectively. Overall through a combination of reflux and room temperature stirring compounds **2.16** – **2.18** were synthesised with a yield between 76 – 86%.

For **2.19**, the hydroxyl moiety on the imido functionality increased solubility and therefore **2.19** was soluble in methanol. To encourage precipitation of product **2.19** the volume was reduced, however no solid was apparent and the solution was reduced to dryness to yield an orange solid. Through optimising reaction conditions a 5h reflux followed by stirring for *ca.* 72h afforded a 94% conversion to the *bis*phosphine as determined by $^{31}P\{^{1}H\}$ NMR. Furthermore, ligand **2.19** was purified by recrystallisation *via* slow evaporation of the methanolic mother liquor.

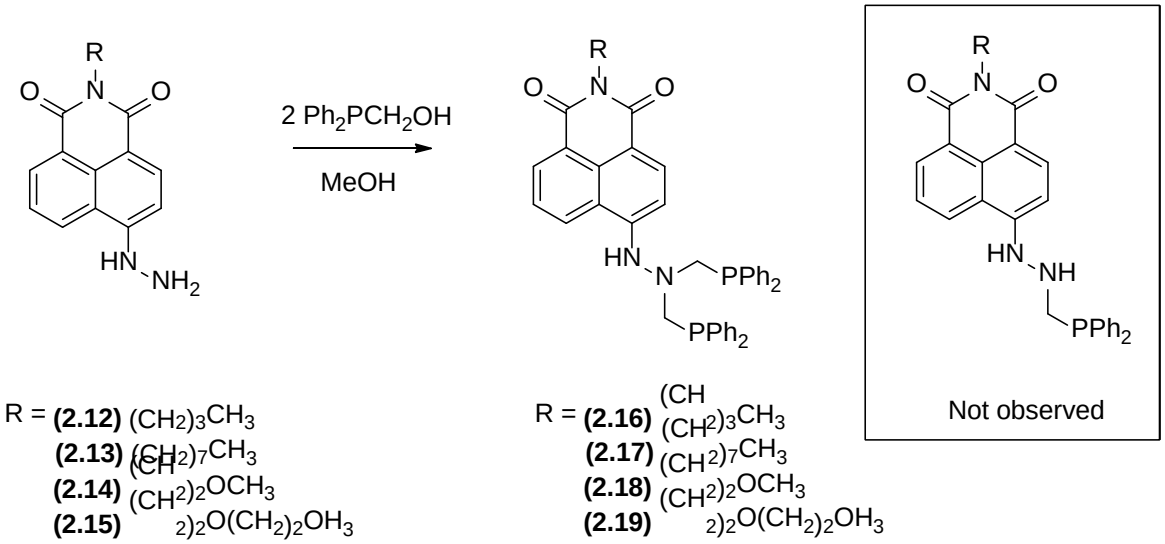

R = **(2.12)** $(CH_2)_3CH_3$
(2.13) $(CH_2)_7CH_3$
(2.14) $(CH_2)_2OCH_3$
(2.15) $(CH_2)_2O(CH_2)_2OH_3$

R = **(2.16)** $(CH_2)_3CH_3$
(2.17) $(CH_2)_7CH_3$
(2.18) $(CH_2)_2OCH_3$
(2.19) $(CH_2)_2O(CH_2)_2OH_3$

Scheme 2.3 Addition of Ph_2PCH_2OH to compounds **2.12** – **2.15**.

$^{31}P\{^1H\}$ NMR spectra of compounds **2.16** – **2.19** all displayed a single resonance at approx. -28 ppm, in the region expected for PCNCP ligands as displayed in Chapter 4 of this thesis and in the literature.[140] The $^{31}P\{^1H\}$ NMR spectra showed no additional resonances indicating there were no phosphorus containing starting materials, phosphine oxides or monosubstituted PCN compounds present. The CH_2P protons resonanated at 4.00ppm in the ^1H NMR for all products as a broad single peak and no $^2J_{PH}$ splitting was observed. The aromatic hydrogens from the phenyl groups on the phosphine appeared as a multiplet between 7.53 and 7.23 ppm. The disappearance of the hydrazide NH_2 group at *ca.* 4.64 ppm in the ^1H NMR confirmed starting materials **2.12** – **2.15** were fully converted to *bis*phosphines **2.16** - **2.19**. Elemental analyses were in agreement with the calculated empirical formulae for desired products **2.16** – **2.19**. Mass spectra further confirmed the synthesis of **2.16** – **2.19**, displaying $[M+H]^+$ fragments for **2.16** – **2.19** as summarised in Table 2.1.

Table 2.1 Selected $^{31}P\{^1H\}$ NMR, ^1H NMR and ESI-MS data for complexes **2.16** to **2.19**.[a]

Compound	δ(P)	δ(CH_2P)	*m/z* $[M-H]^+$ found (ppm difference)
2.16	28.4	4.00	680.2579 (1.6 ppm)
2.17	28.3	4.00	736.3226 (0.9 ppm)
2.18	28.3	4.00	682.2383 (0.1 ppm)
2.19	28.3	4.00	712.2484 (0.6 ppm)

[a]All NMRs were recorded in $CDCl_3$ (in ppm).

2.2.4 Molecular structure of aminomethylphosphine ligands 2.16, 2.18 and 2.19

Crystals of ligands **2.16**, **2.18** and **2.19**, suitable for single crystal X-ray diffraction studies, were grown *via* slow evaporation of respective methanolic filtrates of **2.16**, **2.18** and **2.19**. The crystal structures of these compounds are shown in Figure 2.6. Known naphthalimide compounds containing phosphorus appendages are shown in Figure 2.5, as determined by the CSD database.[132] Since compounds **2.20** – **2.23** are all phosphorus(V) compounds, aminomethylphosphines directly linked to a naphthalimide moiety are the first of this type [phosphorus(III)] to be synthesised and therefore cannot be directly compared to literature examples.[132,141–144]

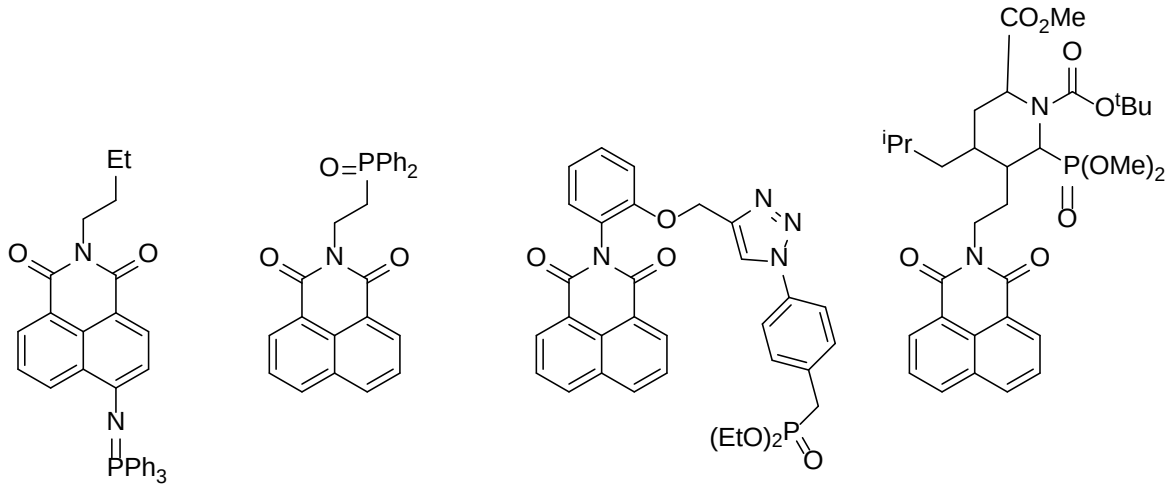

(2.20) **(2.21)** **(2.22)** **(2.23)**

Figure 2.5 Chemical structures of related literature examples.[141–144]

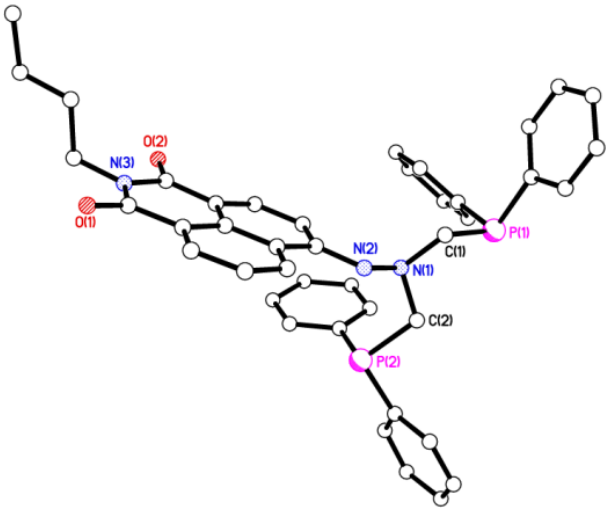

a)

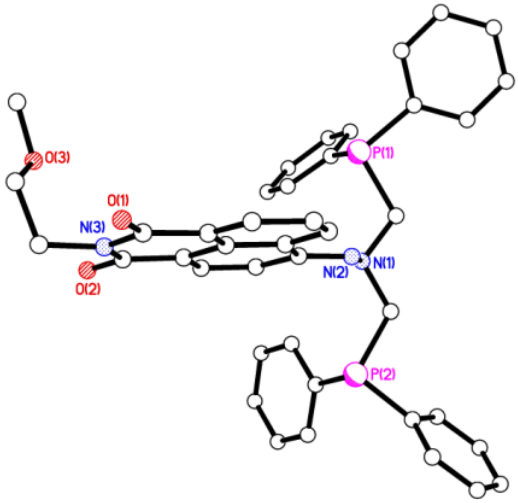

b)

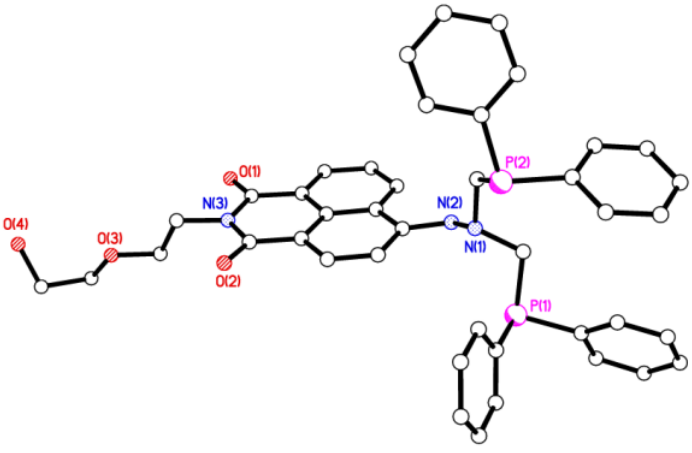

c)

Figure 2.6 X-ray structures of a) **2.18**, b) **2.16**, and c) **2.19**. All hydrogen atoms and MeOH solvent for **2.19** have been removed for clarity.

For compounds **2.16** and **2.18**, molecules pack in columns along the *b* axis, in a head-to-tail zig-zag type formation held by hydrogen bonding from the carbonyl moiety on the naphthalimide group with the methyl hydrogens and neighbouring amine hydrogens on the hydrazine end of the second naphthalimide: for ligand **2.16** [C(2)–H(2A)···O(2) 3.256(3) Å, N(2)–H(2)···O(2) 2.862(3) Å] and for ligand **2.18** [C(2)–H(2A)···O(2) 3.243(2) Å, N(2)–H(2C)···O(2) 2.967(2) Å]. The $–PPh_2$ rings are perpendicular to the plane the naphthalimide substructure lies within extending out into the spaces between columns. Compound **2.18** exhibits an additional weak intermolecular interaction between a hydrogen on a phenyl ring and the carbonyl group on the second naphthalimide which is layered above/below the first.

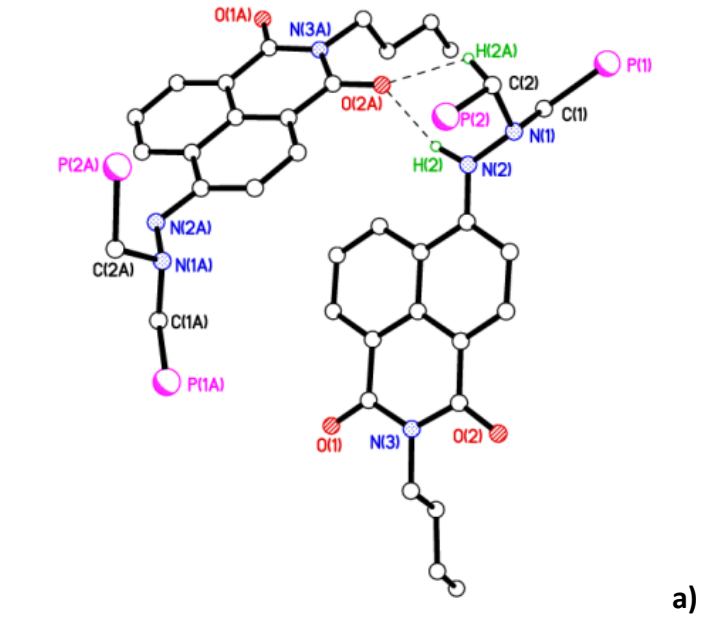

a)

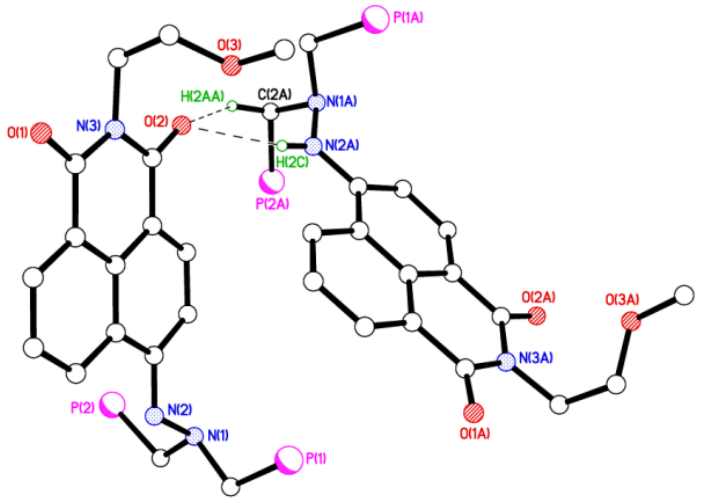

b)

Figure 2.7 Packing structure of a) **2.16**, and b) **2.18** to highlight the head-to-tail zig-zag formation. The phenyl rings and all hydrogen atoms, except H(2A) and H(2) in **2.16** and H(2AA) and H(2C) in **2.18** have been removed for clarity. Symmetry operator for equivalent molecule A: x, -y+1/2, z+1/2 (**2.18**), x+1/2, y, -z+1/2 (**2.16**).

Unlike compounds **2.16** and **2.18**, ligand **2.19** does not exhibit zig-zag type packing; this is due to the presence of a methanol solvate which prevents hydrogen bonding in a similar fashion to compounds **2.16** and **2.18**. Instead the methanol hydrogen bonds to the amine groups on the hydrazine and 'a methylene hydrogen' on the PCNCP moiety. For compound **2.19** the naphthalimides are stacked parallel to each other in a head-to-tail arrangement, with some pi-pi interactions occurring (shortest contact length 3.357Å).

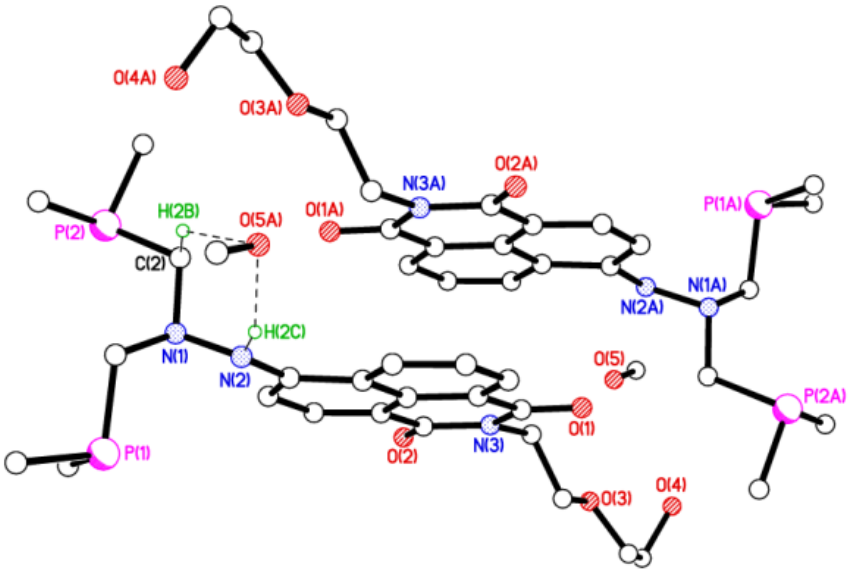

Figure 2.8 Packing structure of **2.19** to highlight the stacking. All hydrogen atoms except H(2B) and H(2C) have been removed for clarity. Symmetry operator for equivalent molecule A: -x+1, -y+1, -z+1.

The presence of the hydroxyl moiety on compound **2.19** allows for additional interactions not observed in ligands **2.16** and **2.18**; for compound **2.19** the hydroxyl moiety allows for the formation of hydrogen bonded dimers, as shown in Figure 2.9, between two naphthalimide molecules in the same plane. Since the molecules lie in a head-to-tail conformation, every other molecule interacts with one of its neighbouring columns of stacked molecules. This results in the formation of a 20-membered ring, as shown in Figure 2.9.

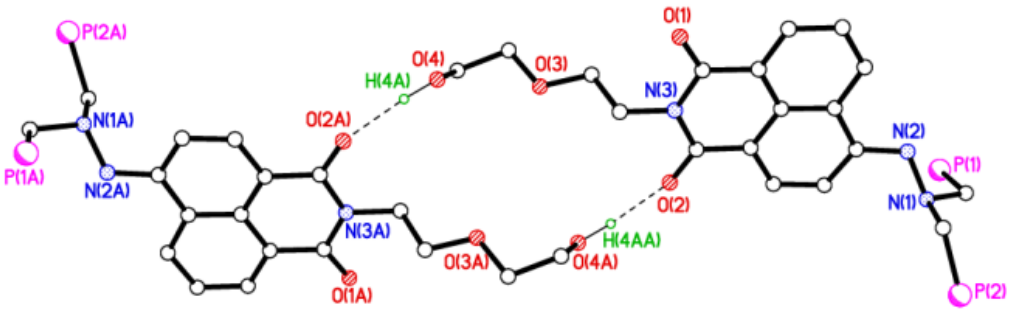

Figure 2.9 Packing structure of **2.19** to highlight hydrogen bonded dimers. All hydrogen atoms except H(4A) and H(4AA) have been removed for clarity. Symmetry operator for equivalent molecule A: -x+2, -y+2, -z+1.

Table 2.2 Selected bond lengths (Å) and angles (°) for compounds **2.16, 2.18** and **2.19**.

	2.19	**2.16**	**2.18**
P1—C9	1.8418 (17)	1.834 (3)	1.846 (2)
P1—C3	1.8448 (17)	1.828 (3)	1.836 (2)
P1—C1	1.8511 (16)	1.858 (2)	1.861 (2)
C1—N1	1.463 (2)	1.467 (3)	1.479 (2)
N1—N2	1.4303 (17)	1.421 (3)	1.418 (2)
N1—C2	1.478 (2)	1.467 (3)	1.484 (2)
C2—P2	1.8632 (15)	1.857 (2)	1.861 (2)
P2—C15	1.8333 (17)	1.824 (3)	1.837 (2)
P2—C21	1.8345 (17)	1.832 (2)	1.842 (2)
C9—P1—C3	99.86 (7)	105.07 (12)	102.21 (9)
C9—P1—C1	102.49 (8)	95.39 (11)	99.30 (9)
C3—P1—C1	98.82 (7)	101.74 (11)	100.14 (9)
N2—N1—C1	109.79 (12)	107.38 (17)	107.85 (15)
N2—N1—C2	108.90 (11)	110.28 (18)	110.83 (15)
C1—N1—C2	114.53 (12)	112.24 (18)	108.68 (15)
C15—P2—C21	104.09 (8)	102.72 (11)	100.46 (9)
C15—P2—C2	97.30 (7)	101.00 (11)	101.50 (9)
C21—P2—C2	102.18 (8)	97.97 (10)	95.99 (9)

2.2.5 Complexation studies with platinum(II)

The coordination chemistries of ligands **2.16** – **2.19** were explored initially through the synthesis of platinum(II) complexes **2.24** – **2.27**, which were accessed *via* the ligand substitution of cod from the metal precursor, $PtCl_2$(cod). This is a well-known

methodology for accessing platinum phosphine coordination compounds.[140] After stirring the metal precursor and respective ligand at r.t. in CH_2Cl_2 for 1h, the solution was reduced in volume and precipitation using diethyl ether afforded orange solids **2.24** – **2.27** in yields of 80-92%.

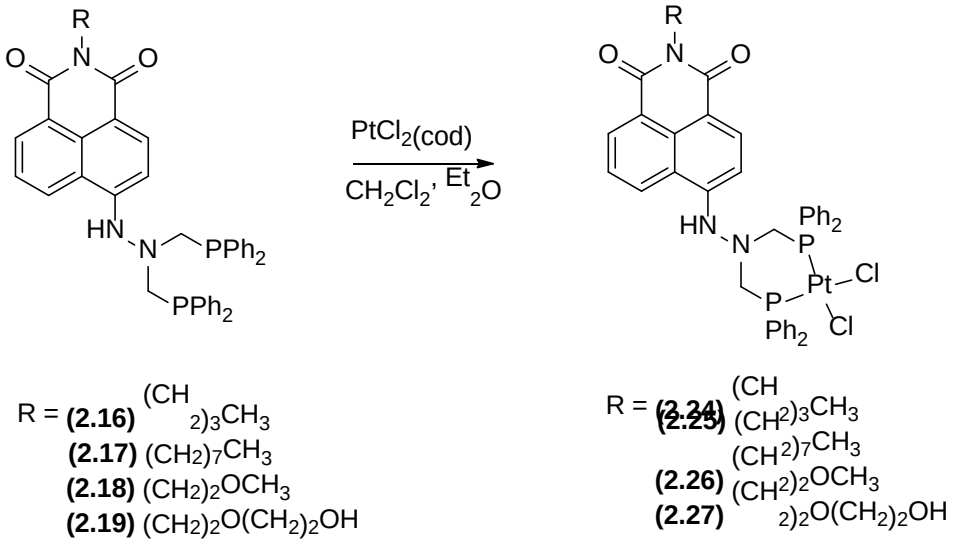

Scheme 2.4 Coordination of ligands **2.16** – **2.19** to a Pt(II) metal centre.

Analysis of dichloroplatinum(II) species **2.24** – **2.27** by $^{31}P\{^1H\}$ NMR showed a single resonance for each of the species at *ca.* 0 ppm, a downfield shift of approx. 28 ppm from the parent phosphines **2.16** – **2.19**. This is a similar shift to that observed in the formation of PCNCP dichloroplatinum complexes **4.35** – **4.41** in Chapter 4 and in the literature.[145] The ^{195}Pt satellites, in all four cases, display $^1J_{PtP}$ coupling constants of *ca.* 3450Hz indicative of the species adopting a *cis* conformation; this is further confirmed by the presence of two vPtCl stretches in the IR spectrum for **2.24**, as summarised in Table 2.3.[146] For complexes **2.25** – **2.27** only one vPtCl could be identified. *Trans* complexes with the formula PtL_2Cl_2 typically depict one stretch at *ca.* 339 cm^{-1}; as a signal was not observed here, it is likely a second vibration is present in the IR spectra but cannot be identified clearly from the background.[146]

Table 2.3 - Summary of NMR and IR data for complexes **2.24** – **2.27**.[a]

Complex	δ(P)	^1J(PtP)	ν_{PtCl}
2.24	0.1	3449	296, 318
2.25	0.1	3456	312
2.26	0.1	3460	311
2.27	0.1	3455	311

[a]All NMR data recorded in d^6-DMSO (in ppm). All IR spectra recorded as KBr discs (in cm^{-1}).

In the ^{1}H NMR spectra for complexes **2.24** – **2.27**, a change in splitting for the PCH_2 methylene protons was observed; in the starting phosphine material a singlet is observed at δ 4.0 ppm for all compounds (**2.16** – **2.19**), however when coordinated to the Pt(II) metal centre the four hydrogens from the two PCH_2 groups are split into two separate multiplet peaks. This is due to coordination leading to a fixed arrangement in the PCNCP moiety. In the fixed arrangement the energy of one hydrogen on the PCH_2 group is not the same as the other, and so a difference in shift is observed. The observed splitting is also due to the fixed arrangement, with one hydrogen on the PCH_2 moiety interacting with the other hydrogen on the same carbon and also the hydrogen on the neighbouring NH moiety. Support for the preparation of **2.24** – **2.27** was also obtained from ESI-MS results which revealed $[M\text{-}Cl]^+$ fragments for **2.24** – **2.27** at *m/z* 909.1836, 965.2469, 911.1629 and 941.1732 respectively. Elemental analyses also reinforced the proposed empirical formulae of species **2.24** – **2.27**.

2.2.6 Molecular structure of platinum species 2.24 and 2.27

Brown blocks of **2.24** were grown by slow evaporation of a $MeOH/CHCl_3$ solution of **2.24** and its molecular structure was determined, as shown in Figure 2.10. Yellow plates were also grown of the related compound **2.27** *via* vapour diffusion of Et_2O into a $(CH_3)_2SO/CH_2Cl_2$ solution of **2.27** and its molecular structure was determined, as also shown in Figure 2.10. Since no naphthalimides functionalised with PCNCP moieties have been previously studied, platinum coordinated PCNCP naphthalimides **2.24** and **2.27** are the first X-ray structures of this type, as confirmed by the CSD.[132] Selected bond lengths and angles of **2.24** and **2.27** are given in Table 2.4**.**

X-ray crystallography analysis of compound **2.24** showed one molecule of **2.24** per asymmetric unit, with one methanol solvent molecule of crystallisation present. Chloroform was also present but was disordered over an inversion centre so contributed half weight. The asymmetric unit of **2.27** featured one molecule of **2.27**, one DMSO solvent of crystallisation and a disordered solvent molecule that was part CH_2Cl_2, part DMSO. Each complex adopted a pseudo square planar geometry with respect to the Pt(II) centre [compound **2.24**: P(1)–Pt(1)–Cl(2) 173.97(12)° and P(2)–Pt(1)–Cl(1) 174.47(12)°; compound **2.27**: P(1)–Pt(1)–Cl(2) 171.79(3)° and P(2)–Pt(1)–Cl(1) 176.54(4)°] with phosphorus (III) centres adopting a distorted square planar geometry in all cases [displayed *via* the relevant Pt–P–C bond angles]. Pt–P bond lengths are consistent with *cis* dichloro *bis*phosphorus compounds found in the literature.[147,148]

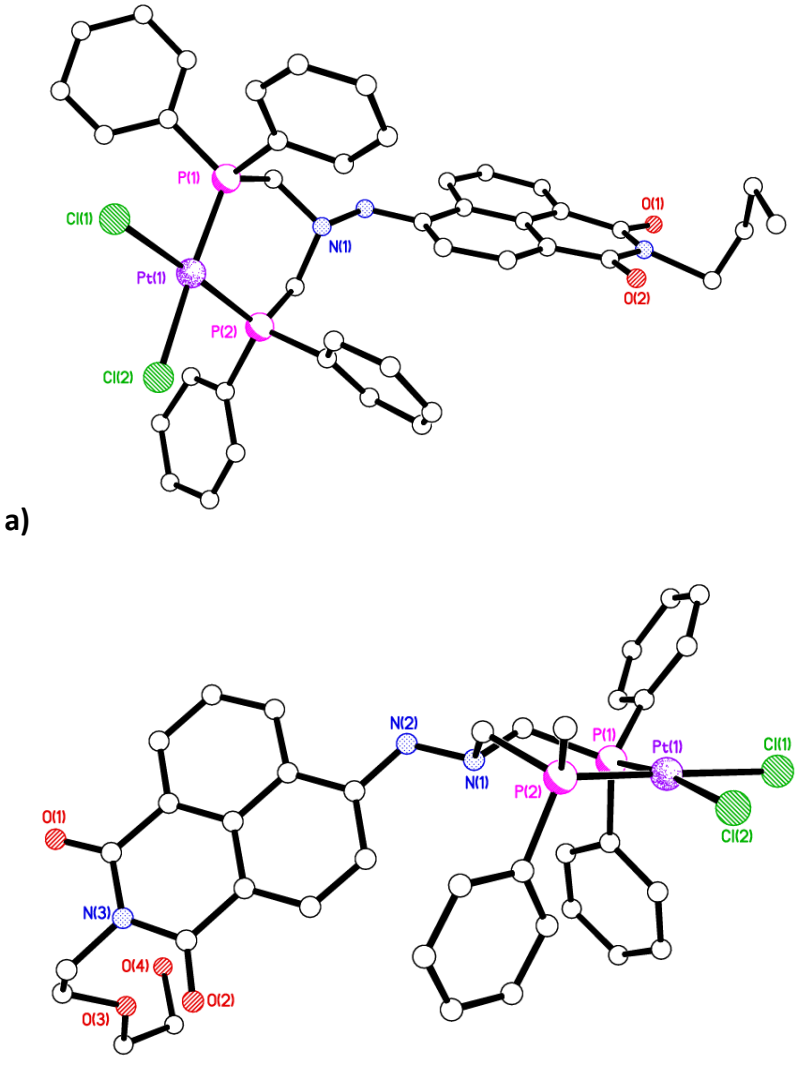

Figure 2.10 Molecular structure of a) **2.24** and b) **2.27**. All hydrogen atoms, solvent molecules of crystallisation have been omitted for clarity. One phenyl ring on b) **2.27** has also been omitted for clarity.

Crystal packing structures for both complex **2.24** and **2.27** display dimer pairs linked *via* head-to-tail hydrogen bonding, with the large naphthalimide aromatic systems sitting face-to-face. Analysis of the crystal structures showed intermolecular π–π interactions *via* cofacial naphthalimide overlap. The C(38)–C(29A) distance in this case is 3.448 Å, which is only slightly longer than the accepted value of 3.35 Å for graphite, which would suggest that a strong interaction exists.[149] However, the mean inter–phenyl ring centroid distance of 4.094 Å demonstrates that this interaction is weaker than first thought, although inter–ring distances of 3.9 – 4.4 Å have previously been recorded. This confirms that indeed, a valid interaction is found.[149]

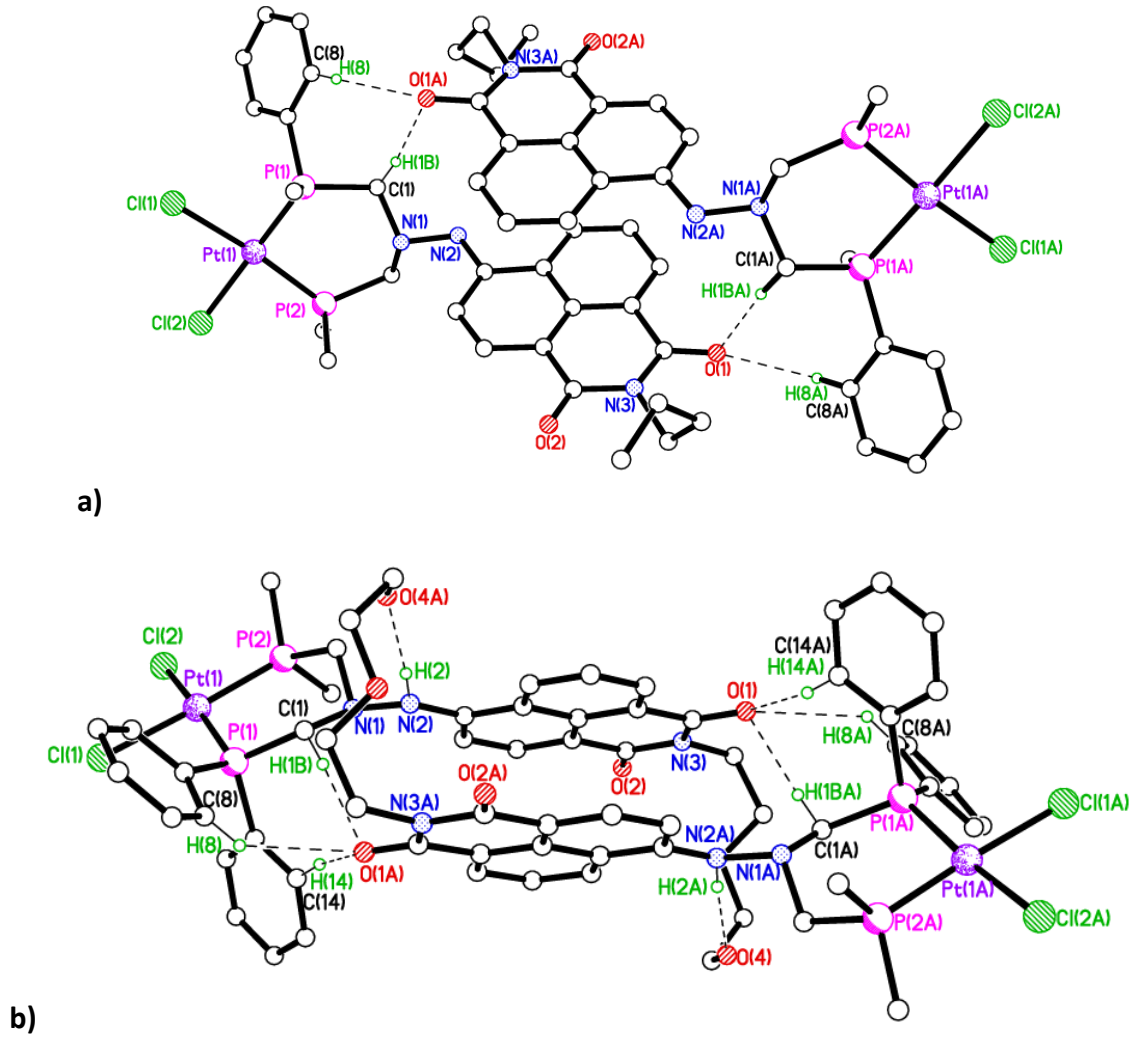

Figure 2.11 Packing structure of a) **2.24**, and b) **2.27**. All hydrogen atoms, except H(1B), H(1BA), H(8) and H(8A) in **2.24** and H(1B), H(1BA), H(2), H(2A), H(8), H(8A), H(14) and H(14A) in **2.27** have been removed for clarity. Symmetry operator for equivalent molecule A: -x+1, -y+1, -z+1 (**2.24**), -x+1, -y+1, -z+1 (**2.27**).

2.2.7 Coordination studies with palladium(II)

In order to synthesise analogous palladium(II) square planar complexes with **2.16** – **2.19**, the palladium analogue of $PtCl_2$(cod) was used in an identical procedure to that of **2.24** – **2.27**. Again, this is a well-known method for the synthesis of palladium phosphine complexes.[140,150] The reaction of equimolar amounts of $PdCl_2$(cod) and ligands **2.16** – **2.19** generated yellow complexes **2.28** – **2.31** in isolated yields of 50-90%.

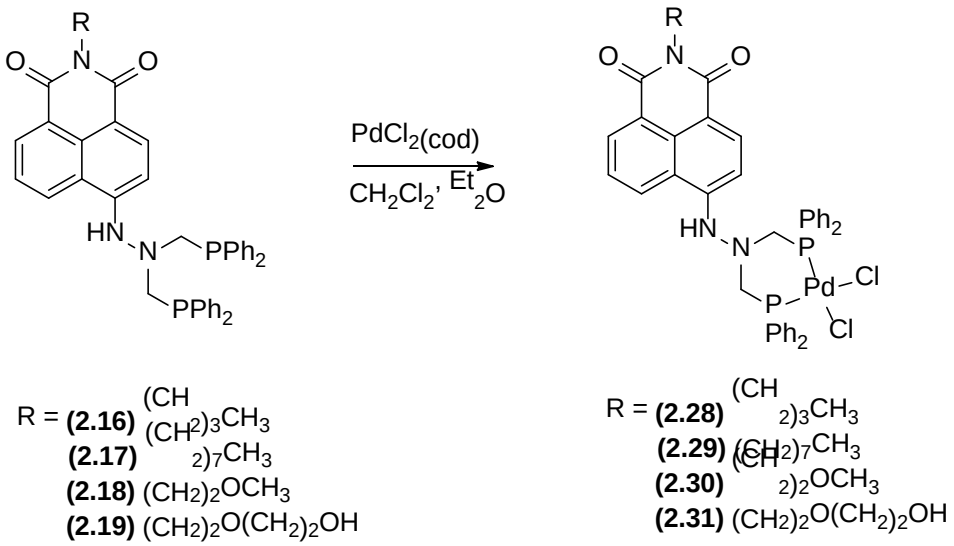

Scheme 2.5 Coordination of ligands **2.16** – **2.19** to a Pd(II) metal centre.

The $^{31}P\{^{1}H\}$ NMR spectra for complexes **2.28** – **2.31** each displayed a sharp singlet at *ca.* 17 ppm, approx. 45 ppm downfield from free ligands **2.16** – **2.19**. This downfield shift is comparable with similar palladium(II) complexes also synthesised by the Smith group and others.[140,150] Similarly to platinum(II) complexes **2.24 – 2.27**, the PCH_2 hydrogens in the ^{1}H NMR spectra of analogous palladium(II) compounds **2.28** – **2.31** are also observed as two multiplets.

ESI-MS data displayed fragments representative of $[M\text{-}Cl]^+$ for each complex (at *m/z* 820.1217, 876.1860, 822.1013 and 852.1115). The proposed empirical formulae of **2.28** – **2.31** were also in agreement with elemental analyses. For **2.25**, two vPdCl IR stretches were observed in the FTIR at 334 and 315 cm^{-1}. Like the analogous platinum(II) compounds two IR stretches are expected for *cis* configured palladium(II) compounds.

2.2.8 Molecular structure of palladium species 2.28

Yellow plates of complex **2.28**, suitable for single crystal X-ray diffraction, were obtained by slow evaporation of a CH_2Cl_2:MeOH mother liquor and its molecular structure determined (Figure 2.12). Selected bond lengths and angles of **2.28** are given in Table 2.4, with selected bond lengths and angles of related platinum complexes **2.24** and **2.27.**

The crystal structure of complex **2.28** exhibits two PCNCP functionalised naphthalimide molecules along with three molecules of MeOH and one molecule of CH_2Cl_2 in the asymmetric unit. The dichloropalladium(II) species both show a distorted square planar geometry with respect to the Pd(II) metal centres [P(1)—Pd(1)—Cl(2) 177.86(5)°, P(2)—Pd(1)—Cl(1) 177.17(4)°, P(3)—Pd(2)—Cl(4) 177.28(4)°, P(4)—Pd(2)—Cl(3) 174.01(4)°]

with the bidentate **2.16** ligand coordinating to the Pd(II) centre in *cis* conformation. Similarly to related platinum complexes **2.24** and **2.27**, the phosphorus atoms in all four cases have a distorted tetrahedral geometry (illustrated by the relevant bond angles), with the neighbouring nitrogen atom, also part of the PCNCP moiety, displaying a distorted pyramidal geometry (illustrated by the relevant bond angles).

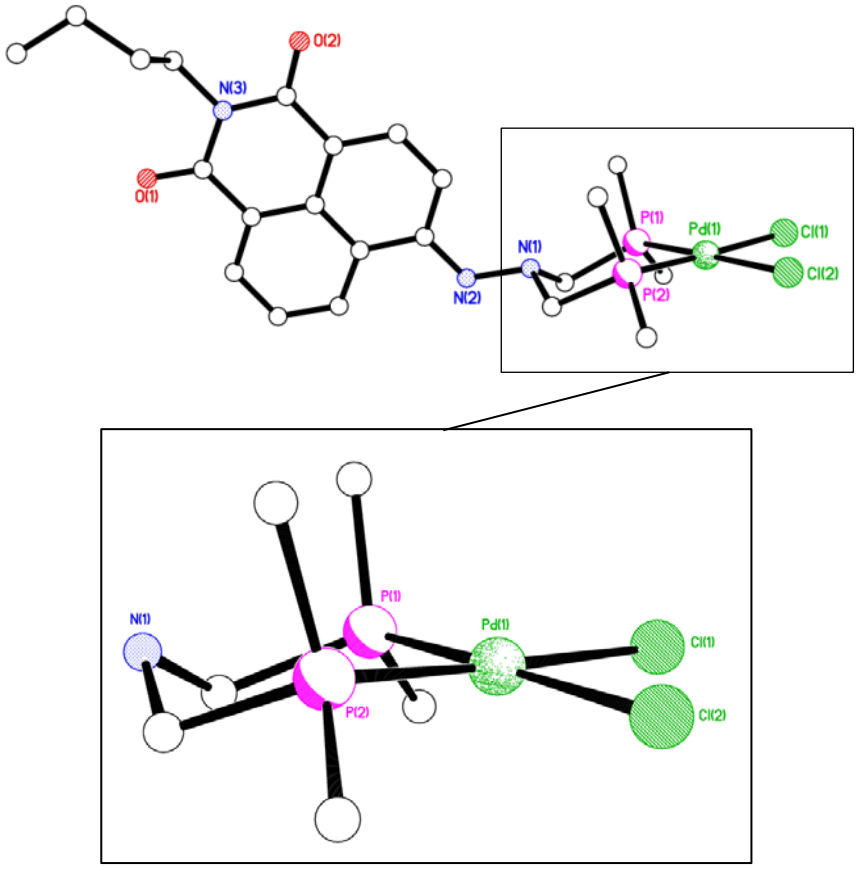

Figure 2.12 Molecular structure of **2.28**. All hydrogen atoms, three molecules of MeOH and a molecule of CH_2Cl_2 of crystallisation and the phenyl rings have been omitted for clarity. 'Zoomed in' component illustrates the chair conformation of the Pd-P-C-N-C-P ring.

The two naphthalimide molecules in the asymmetric unit lie head-to-tail with their naphthalimide backbones in parallel planes to each other with only the ^{n}butyl chain and $N(CO)_2$ groups overlapping with the molecule above/below itself. The PCNCP moiety is orientated in the plane perpendicular to the plane the naphthalimide substructure lies within. Two MeOH and one CH_2Cl_2 solvent molecules reside close (2.735 – 3.297 Å) to the overlapping ^{n}butyl chains, resulting in intermolecular interactions between the solvent residues and the individual naphthalimide molecules.

Intermolecular interactions are observed with other naphthalimides in the crystal structure which lie in the same plane; these are weak intermolecular hydrogen bonds between amine groups and corresponding chloride ligands and methylene hydrogens on

the PCNCP moiety and corresponding chloride ligands. A summary of intermolecular hydrogen bonding observed is listed in Table 2.5. Intramolecular interactions between phenyl hydrogens and chloride ligands were also observed [C(1)—H(1B)···Cl(2) 3.449(4) Å, C(2)—H(2A)···Cl(1) 3.536(4) Å].

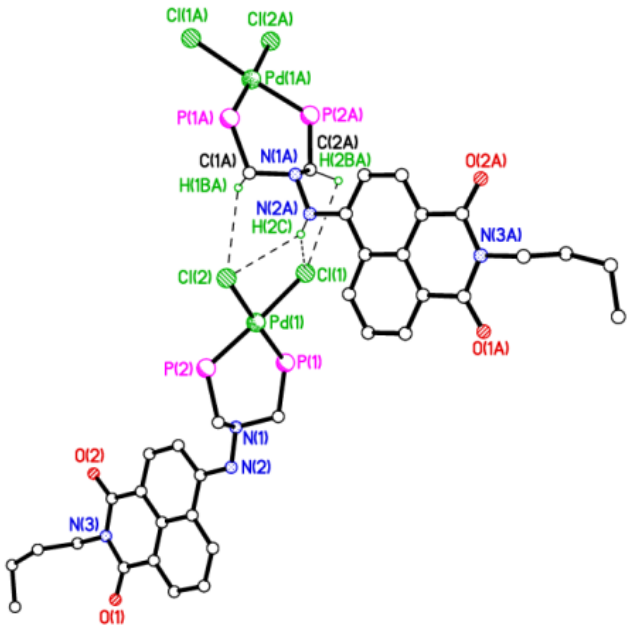

Figure 2.13 Packing structure of **2.28** highlighting the intermolecular interactions present between amine groups and methylene groups on one PCNCP moiety with the chloride groups of the neighboring PCNCP moiety. All phenyl rings and hydrogen atoms except those on C(1A), N(2A) and C(2A) have been omitted for clarity. Symmetry operator for equivalent molecule A: -x+2, y+1/2, -z+1/2.

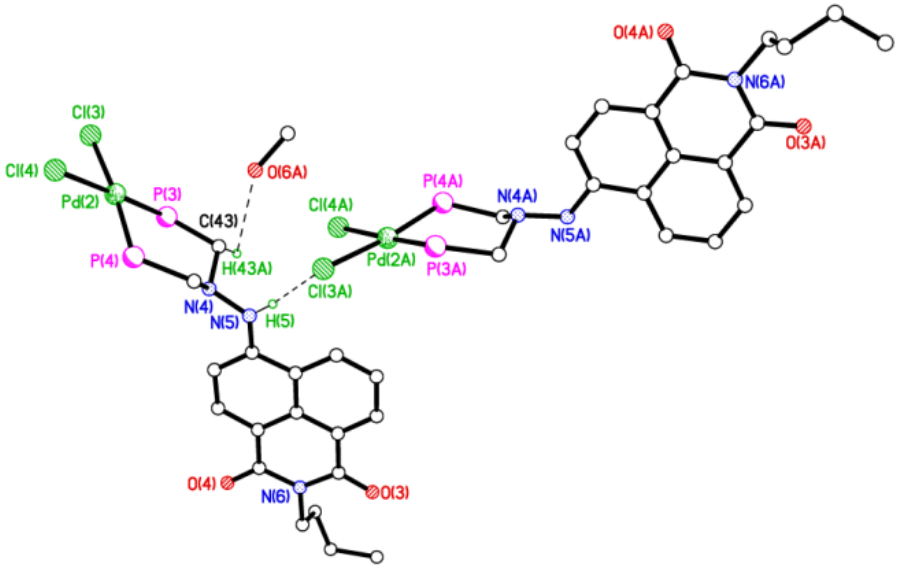

Figure 2.14 Packing structure of **2.28** highlighting the intermolecular interactions present between the two naphthalimide compounds in the asymmetric unit. All hydrogen atoms except those on C(43) and N(5) have been omitted for clarity. Symmetry operator for equivalent molecule A: -x+1, y-1/2, -z+1/2.

Table 2.4 Selected bond lengths (Å) and angles (°) for the palladium(II) complex **2.28** and platinum(II) complexes **2.24** and **2.27**.

	2.28 (M1 = Pd)	**2.24** (M1 = Pt)	**2.27** (M1 = Pt)		**2.28** (M1 = Pd)	**2.24** (M1 = Pt)	**2.27** (M1 = Pt)
M1—P1	2.2434 (11)	2.221 (3)	2.2248 (10)	P2—M1—Cl1	177.17 (4)	174.47 (12)	176.54 (4)
M1—P2	2.2473 (11)	2.230 (3)	2.2251 (10)	Cl2—M1—Cl1	89.65 (4)	89.33 (11)	89.30 (4)
M1—Cl2	2.3403 (11)	2.371 (3)	2.3499 (10)	C9—P1—C3	109.5 (2)	106.8 (5)	107.61 (17)
M1—Cl1	2.3581 (11)	2.349 (3)	2.3569 (10)	C9—P1—C1	99.27 (19)	105.2 (5)	107.13 (17)
P1—C9	1.813 (4)	1.830 (10)	1.824 (3)	C3—P1—C1	106.5 (2)	99.7 (5)	95.37 (17)
P1—C3	1.816 (4)	1.837 (12)	1.826 (4)	C9—P1—M1	111.18 (14)	107.1 (4)	108.86 (13)
P1—C1	1.833 (4)	1.847 (10)	1.836 (4)	C3—P1—M1	113.50 (14)	118.5 (3)	119.11 (13)
C1—N1	1.460 (5)	1.489 (13)	1.456 (5)	C1—P1—M1	115.87 (14)	118.3 (4)	117.54 (13)
N1—N2	1.430 (5)	1.428 (11)	1.422 (4)	N2—N1—C1	109.6 (3)	107.2 (8)	106.6 (3)
N1—C2	1.471 (5)	1.479 (13)	1.477 (5)	N2—N1—C2	110.3 (3)	110.0 (8)	110.1 (3)
C2—P2	1.841 (4)	1.844 (10)	1.832 (4)	C1—N1—C2	111.6 (3)	112.6 (8)	111.5 (3)
P2—C15	1.815 (4)	1.818 (12)	1.819 (4)	C15—P2—C21	110.7 (2)	107.3 (5)	108.14 (18)
P2—C21	1.816 (4)	1.820 (10)	1.814 (4)	C15—P2—C2	101.19 (19)	104.4 (5)	102.45 (18)
P1—M1—P2	92.48 (4)	94.55 (10)	93.82 (4)	C21—P2—C2	99.12 (19)	100.5 (5)	100.91 (17)
P1—M1—Cl2	177.86 (5)	173.97 (12)	171.79 (3)	C15—P2—M1	111.73 (14)	110.3 (4)	112.73 (13)
P2—M1—Cl2	88.97 (4)	86.29 (11)	87.30 (4)	C21—P2—M1	115.30 (14)	114.2 (3)	114.48 (13)
P1—M1—Cl1	88.96 (4)	89.45 (11)	89.64 (4)	C2—P2—M1	117.42 (15)	119.0 (4)	116.81 (14)

Table 2.5 Specified intermolecular hydrogen bond lengths (Å) and angles (°) for **2.28**.

D—H···*A*	*D*—H	H···*A*	*D*···*A*	*D*—H···*A*
C1—H1*B*···Cl2^{i}	0.99	2.96	3.449 (4)	112
C2—H2*A*···Cl1^{i}	0.99	2.94	3.536 (4)	120
N2—H2···Cl1^{i}	0.91 (5)	2.68 (5)	3.498 (4)	150 (4)
N2—H2···Cl2^{i}	0.91 (5)	2.77 (5)	3.456 (4)	133 (4)
C43—H43*B*···O6^{ii}	0.99	2.64	3.568 (6)	156
N5—H5···Cl3^{ii}	0.81 (5)	2.69 (5)	3.419 (4)	151 (4)
O5—H5*B*···O2	1.00 (7)	1.75 (7)	2.735 (5)	167 (6)
O6—H6···Cl3	0.84	2.56	3.399 (4)	173
O7—H7···O3	1.08 (6)	1.69 (7)	2.754 (5)	168 (5)
C88—H88*A*···O2	0.99	2.41	3.297 (7)	148
C88—H88*B*···O5	0.99	2.48	3.080 (7)	118

2.2.9 Coordination studies with gold(I)

Due to the interesting luminescent properties of gold(I) phosphine complexes documented in the literature, ligands **2.16** – **2.19** were coordinated to gold(I) metal centres as described in the following section.[73] The binuclear aspect of the gold(I) complexes synthesised should be highlighted as this may influence the luminescence properties of complexes synthesised through aurophilicity. Weak interactions between neighbouring gold metal centres may be related to low energy emission bands in the respective complexes.[151,152]

Four binuclear gold complexes were synthesised *via* ligand displacement of tht (tetrahydrothiophene) from Au(tht)Cl by phosphine ligands **2.16** – **2.19** in a 2:1 stoichiometry respectively. Similarly to **2.24** – **2.31**, the metal precursor and ligands **2.16** – **2.19** were stirred in dichloromethane, before reduction in volume and precipitation with diethyl ether. This generated yellow solids of **2.32** – **2.35** in the region of 66-84% isolated yield.

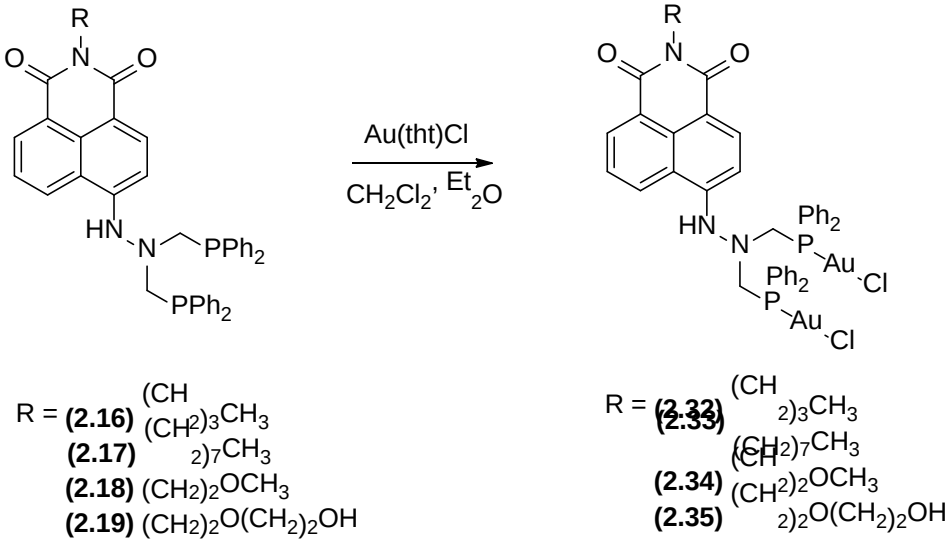

Scheme 2.6 Synthesis of binuclear compounds **2.32** – **2.35**.

$^{31}P\{^{1}H\}$ NMR data showed a single resonance at approx. 26 ppm, some 53 ppm downfield from the parent ligands **2.16** – **2.19**. This shift is indicative of linear P-Au-Cl complexes with PCNCP ligands, as further confirmed in Chapter 4 of this thesis. In the ^{1}H NMR spectra, the PCH_2 hydrogens were observed as two peaks; a double doublet at *ca.* 5.0 and a doublet at *ca.* 4.6 ppm. The expected empirical formulae for compounds **2.32** – **2.35** were in agreement with elemental analyses, supporting the successful synthesis of compounds **2.32** – **2.35**. IR analyses showed vAuCl stretches in the expected region, 315 – 330 cm^{-1}, for all compounds.[145] Predicted $[M–Cl]^+$ fragments for compounds **2.32** – **2.35** were found in their respective spectra with less than 1.5 ppm mass difference to the fragments observed. Numerous attempts were made to obtain X-ray quality crystals of complexes **2.32** – **2.35** without success affording only powdered material. No additional analysis was performed on the powdered material afforded.

2.2.10 Coordination studies with silver(I)

Although silver is not known for its photophysical properties, ligands **2.16** – **2.19** were reacted with $AgBF_4$ in a 2:1 reaction respectively to generate complexes **2.36** – **2.39**, as shown in Scheme 2.7. These di-ligated silver(I) complexes were synthesised for potential as antibacterial agents. As well as silver's known antibacterial and antimicrobial properties, naphthalimides have also been investigated for their antibacterial properties.[87,96,98] The combination of naphthalimide and silver phosphine moieties could potentially result in the synthesis of more selective antibacterial

agents. With this in mind and with ample amounts of naphthalimide phosphine ligands **2.16** – **2.19** available, complexes **2.36** – **2.39** were investigated.

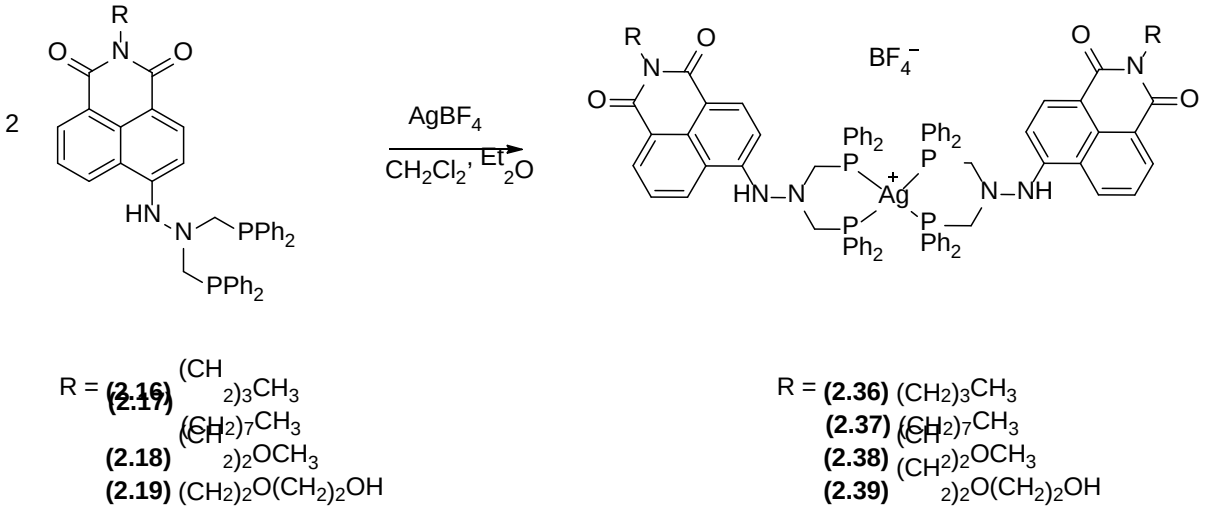

Scheme 2.7 Coordination of ligands **2.16** – **2.19** to a Ag(I) metal centre.

Ligands **2.16** – **2.19** and $AgBF_4$ were dissolved in CH_2Cl_2 and stirred for 1h. During this time, bright yellow solids precipitated. The mixture was reduced in volume and diethyl ether was added. Bright yellow solids of **2.36** – **2.39** were collected by filtration in yields of 52 - 63%. Complexes **2.36** – **2.39** dissolved partially in d^6-DMSO. NMR characterisation on complex **2.39** was attempted through centrifuging a saturated solution of **2.39** in d^6-DMSO, removing the liquid and analysing the sample using NMR over 24 hours. However the $^{31}P\{^1H\}$ NMR spectra obtained displayed only a broad peak and no analysable information could be gathered from the ^1H NMR spectra obtained due to broadening. Analysis by solid state NMR was considered but not pursued as solid state NMR would not reduce broadening sufficiently to gain analysable information.

Complexes **2.36** – **2.39** were analysed by FT-IR and ESI-MS, which showed molecular ion fragments for all complexes. Most crucially elemental analyses were in agreement which the expected formulae of complexes **2.36** – **2.39**. Due to solubility issues, no attempts were made to crystallise material (**2.36** – **2.39**) for single crystal X-ray crystallography purposes. Antibacterial studies of complexes **2.36** – **2.39** were also not performed due to poor solubility issues.

2.3 Preliminary Study of Photophysical Properties

The naphthalimide compounds synthesised here (**2.16** – **2.19**, **2.24** – **2.35**) are brightly coloured and appear to be highly fluorescent, however there is a concern regarding whether fluorescence is quenched by the presence of the phosphine and amine groups through PeT.[33,153] An initial check for luminescence using a black light, also referred to as a UV-A light, was performed on ligand **2.18** and its respective metal complexes, the results of which are shown in Figure 2.15. Since there appears to be luminescence for the metal complexes, especially the gold derivative, but less so for ligand, **2.18**, an investigation into the luminescent properties of all four compounds was performed.

It was decided that due to the similar chemical structures of the ligands synthesised as part of this study, two ligands and their corresponding complexes would be chosen for a preliminary investigation into their respective photophysical properties. The ligands chosen were **2.18** and **2.19**. Samples of **2.18** and **2.19** were dissolved in DMSO (99+%) and investigated by UV absorbance for their excitation maxima, λ_{ex}, and concentration at which the sample has 0.1 absorbance at said maxima. Using the 0.1 absorbance concentrations, fluorescence measurements were performed to find the emission maxima, λ_{em}. The DMSO solutions of all compounds were purged with nitrogen before measurements in order to prevent the formation of phosphine oxide and to limit quenching by photobleaching (excited oxygen).

A

B

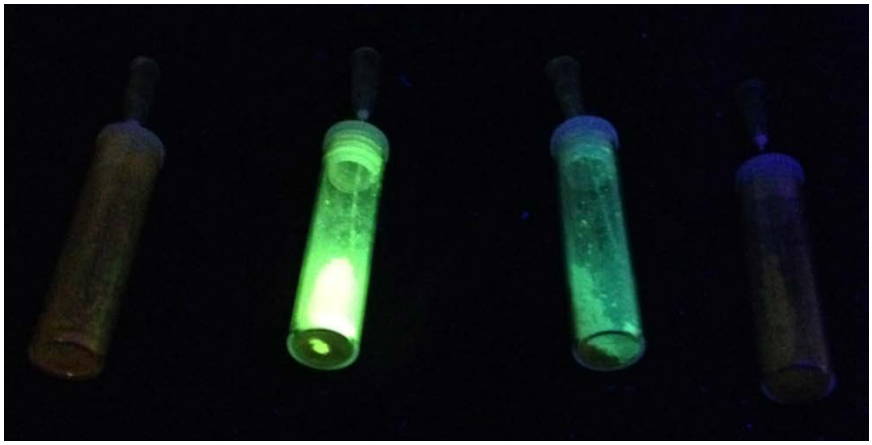

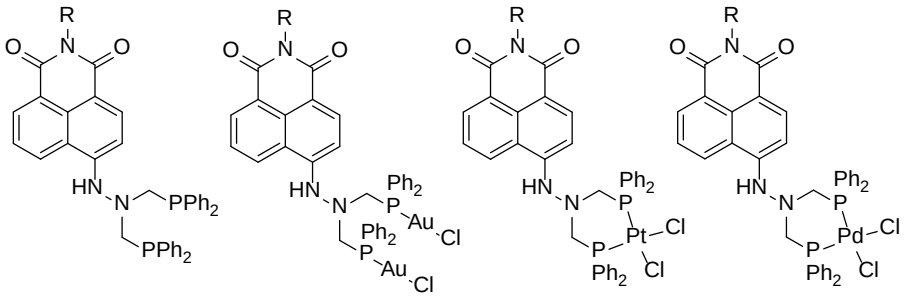

R = **(2.18)** $(CH_2)_2OCH_3$ **(2.19)** $(CH_2)_2O(CH_2)_2OH$ R = **(2.34)** $(CH_2)_2OCH_3$ **(2.35)** $(CH_2)_2O(CH_2)_2OH$ R = **(2.26)** $(CH_2)_2OCH_3$ **(2.27)** $(CH_2)_2O(CH_2)_2OH$ R = **(2.30)** $(CH_2)_2OCH_3$ **(2.31)** $(CH_2)_2O(CH_2)_2OH$

C

Figure 2.15 Top image (**A**) shows the samples in natural light, middle image (**B**) shows samples under black light in order to illustrate the luminescent properties of the samples, bottom image (**C**) shows order and chemical structure of samples in the above two images [R = $(CH_2)_2OCH_3$].

Table 2.6 Summary of UV and fluorescence data for both **2.18** and **2.19**, and their respective complexes.

Compound	0.1 abs. conc at λ_{ex} (x10^{-6} mol dm^{-3})	λ_{ex} (nm)	λ_{em} (nm)	$\Delta\nu_{st}$ (nm)	ε (M cm^{-1})
2.18[a]	6.36	445	518	73	15100
2.26[b]	6.79	431	529	98	14950
2.30[c]	6.78	431	525	94	15900
2.34[d]	7.59	434	504	70	15250
2.19[a]	6.76	433	520	87	14550
2.27[b]	6.76	431	520	89	14962
2.31[c]	6.53	432	519	87	17300
2.35[d]	6.71	433	507	74	15550

[a] free ligand, [b]Pt(II) complex, [c]Pd(II) complex, [d]Au(I) complex

The absorbance maxima, λ_{ex}, for **2.18** and **2.19** are different at 445 and 433 nm respectively; both absorbance maxima are attributed to intramolecular charge transfer character (ICT) arising from the electron donating character of the substituents and the electron withdrawing properties of the naphthalimide core. This difference in absorbance maxima is interesting and may be attributed to the change in substituent in the imido position. This difference results in **2.19** having a similar absorbance maxima to its corresponding metal complexes, therefore leading ligand **2.19** to have a similar Stokes shift to **2.27** and **2.31**, but not the gold complex, **2.35**. Ligand **2.18** has a slightly longer wavelength absorbance maximum than **2.19** resulting in differences in Stokes shift in comparison with platinum/palladium complexes **2.26** and **2.30**, but a close Stokes shift value for gold complex **2.34**. Interestingly ligand **2.18** showed greater fluorescence intensity than the corresponding platinum/palladium complexes **2.26** and **2.30** in contrast to the conclusion drawn from the initial test with a black light. The molar absorption coefficients (ε) are in keeping with previous findings for naphthalimide compounds.[80]

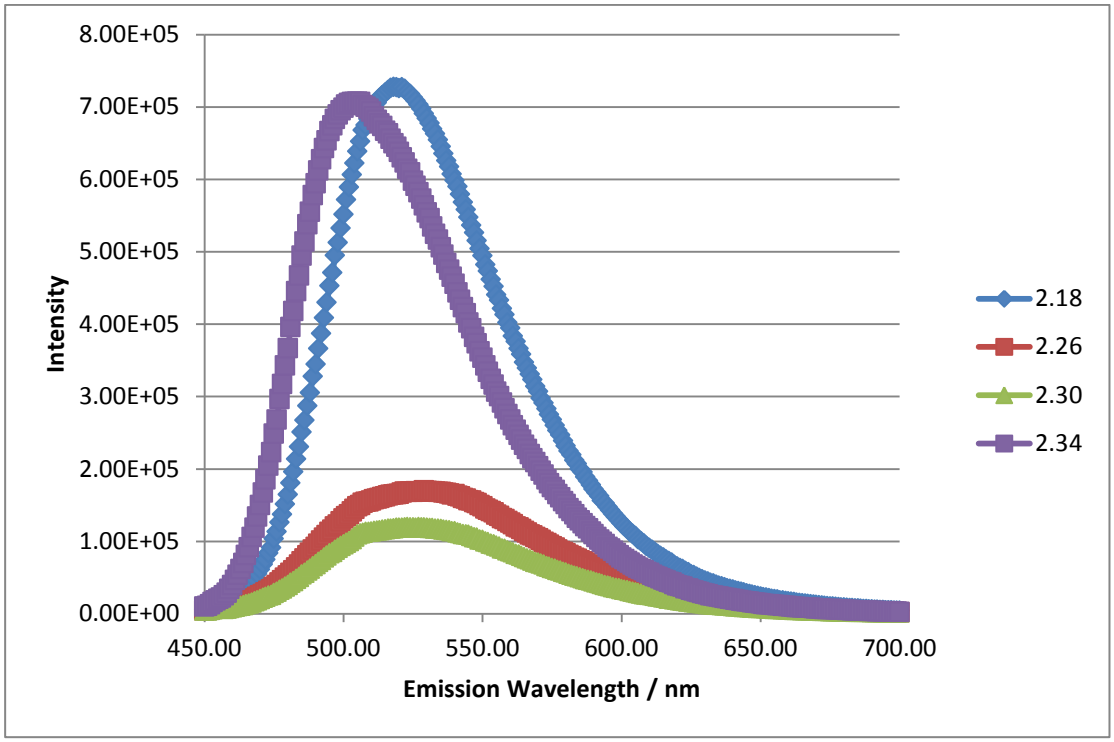

Figure 2.16 Emission profile of phosphine **2.18** and respective complexes **2.26**, **2.30** and **2.34**. Recorded in DMSO (99+%) at r. t., with an excitation wavelength of 440 nm.

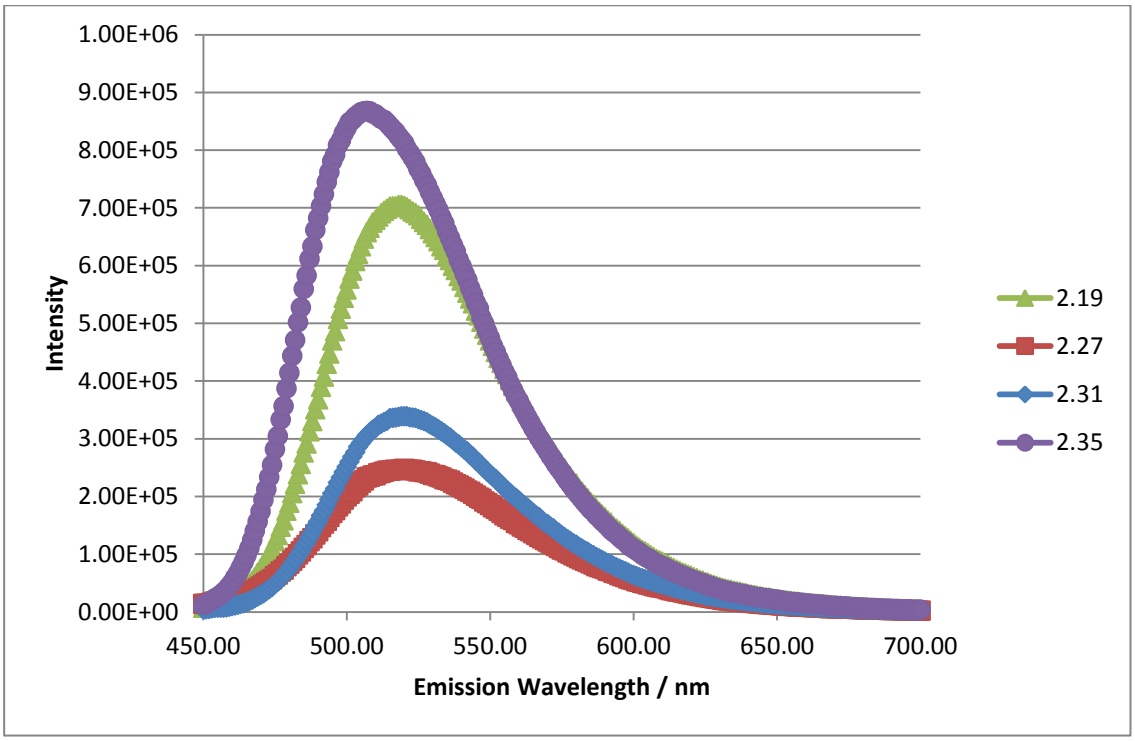

Figure 2.17 Emission profile of phosphine **2.19** and respective complexes **2.27**, **2.31** and **2.35**. Recorded in DMSO (99+%) at r. t., with an excitation wavelength of 440 nm.

As shown in the emission profiles of **2.18** and **2.19**, coordination of the phosphine to a platinum(II) or palladium(II) centre results in quenching of fluorescent intensity in the region of the orders of magnitude of 2-3. This is due to MLCT transitions into the vacant *d* orbitals of the group 10 metals. Interestingly there is no reduction in fluorescence on coordination with gold(I). For **2.16** there is an increase in fluorescent intensity, while for **2.18** there is little change in intensity. However for both **2.18** and **2.19**, the Stokes shift is lowest when coordinated to gold(I). The difference in Stokes shift in comparison to group 10 metals may be attributed to the differences in geometry at the metal-ligand centre.

In addition to the measurement of emission spectra, lifetimes measurements were also performed on **2.18**, **2.19** and all respective coordination compounds to elucidate the mechanism of quenching. The recorded lifetimes of all ligands and complexes are short, in the region of 10 ns. All compounds exhibit a biexpontial lifetime decay, as recorded in Table 2.7. Although the lifetimes of the phosphine ligands and their respective coordination compounds are not drastically different, the lifetime decay profiles as shown in Figure 2.18 and 2.19 show that the phosphine decays slowest, with the palladium(II) and platinum(II) decaying at a similar rate and finally, gold(I) complexes decaying quickest. The minimal changes in lifetime suggest fluorescent quenching observed on complexation of group 10 metals is static quenching.

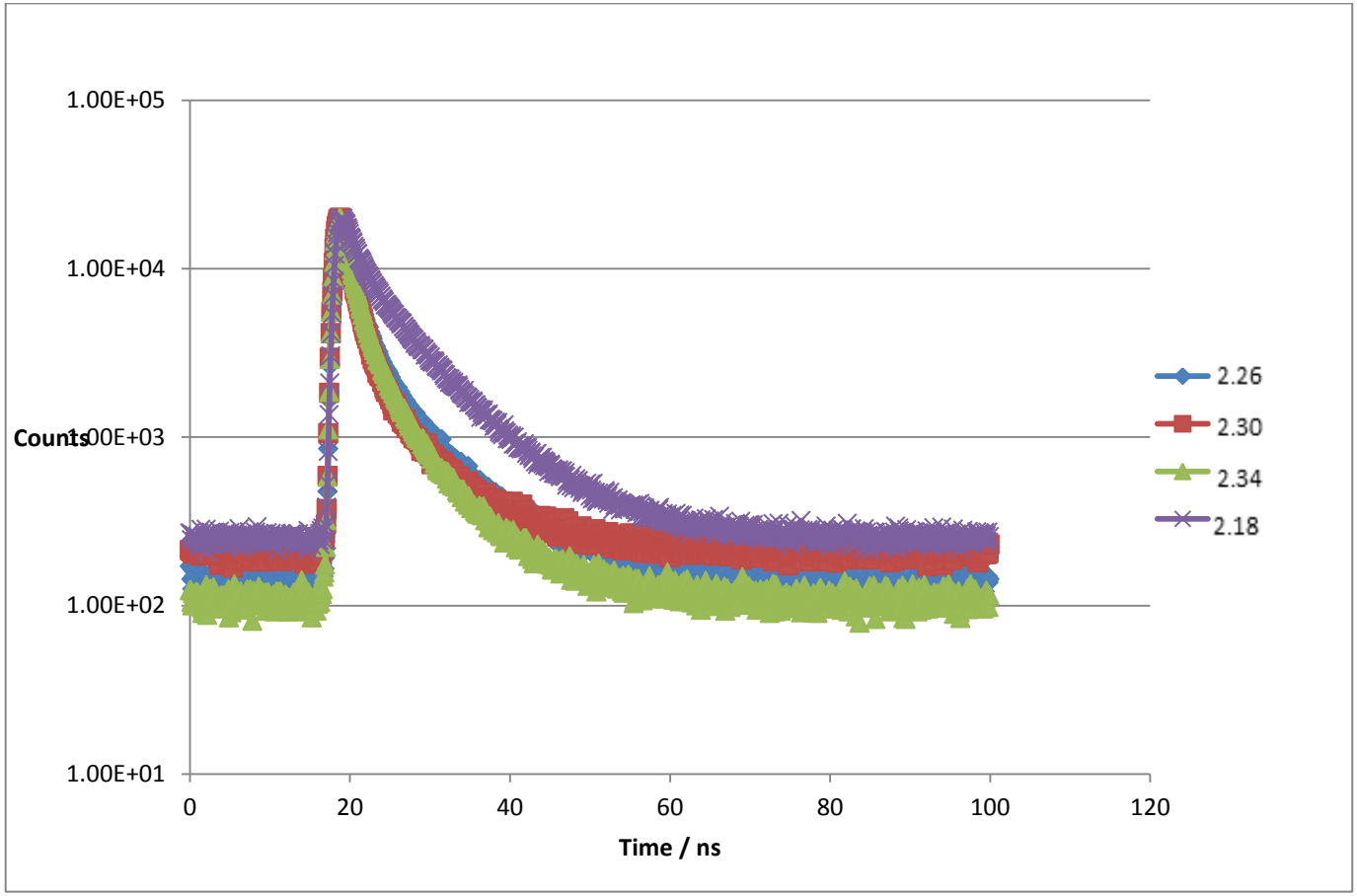

Figure 2.18 Lifetime decay profile of phosphine **2.18** and respective complexes **2.26**, **2.30** and **2.34**. Recorded in DMSO (99+%) at r. t., with an excitation wavelength of 375 nm.

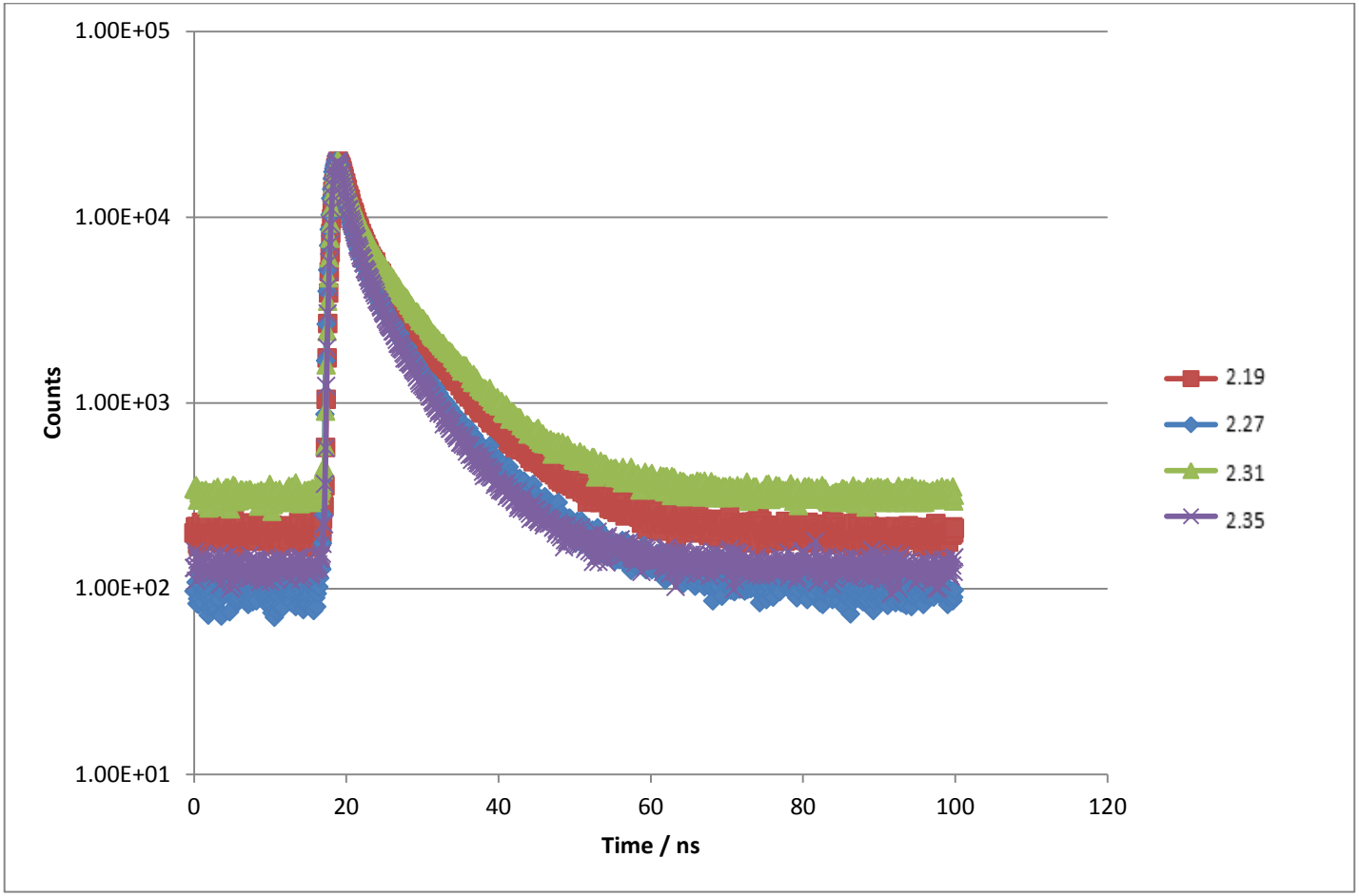

Figure 2.19 Lifetime decay profile of phosphine **2.19** and respective complexes **2.27**, **2.31**, and **2.35**. Recorded in DMSO (99+%) at r. t., with an excitation wavelength of 375 nm

Table 2.7 Lifetime constants for investigated compounds.

Compound	τ_1 (ns)	τ_2 (ns)	B1 (Rel. %)	B2 (Rel. %)	X^2
2.18	2.0220	7.9874	10348.974(19.93)	10523.413(80.07)	1.200
2.26	1.5602	7.537	11492.595(39.37)	3663.139(60.63)	1.360
2.30	1.4571	7.2781	17325.697(56.33)	2688.960(43.67)	1.242
2.34	1.6989	6.4936	7946.432(39.60)	3170.629(60.40)	1.315
2.19	1.6993	7.7669	10763.124(22.32)	8193.772(77.68)	1.212
2.27	1.9313	7.8254	7077.228(26.78)	4775.095(73.22)	1.288
2.31	1.7629	7.7962	7954.428(15.97)	9466.803(84.03)	0.979
2.35	1.1682	6.447	7394.995(26.32)	5399.81(73.68)	1.214

τ is the lifetime component (ns), B is the contribution to that component, X^2 is the exponential fit

2.4 Further work

Naphthalimides are versatile fluorophores which can be formed through the addition of different amino containing moieties to the acid anhydride group of naphthalic anhydrides and can subsequently undergo addition in the 3-, 4-, 5- and 6- positions of the resulting naphthalimide. Although this thesis focuses on the formation of PCNCP moieties on hydrazino groups, the work described here also explored initial reactions investigating the addition of a diamine to 4-bromo-1,8-naphthalic anhydride, which could later undergo the phosphorus analogous Mannich based condensation reaction with Ph_2PCH_2OH. This concerned the reaction between diamine, **2.40**, to 4-bromo-1,8-naphthalic anhydride, as shown in Scheme 2.8.

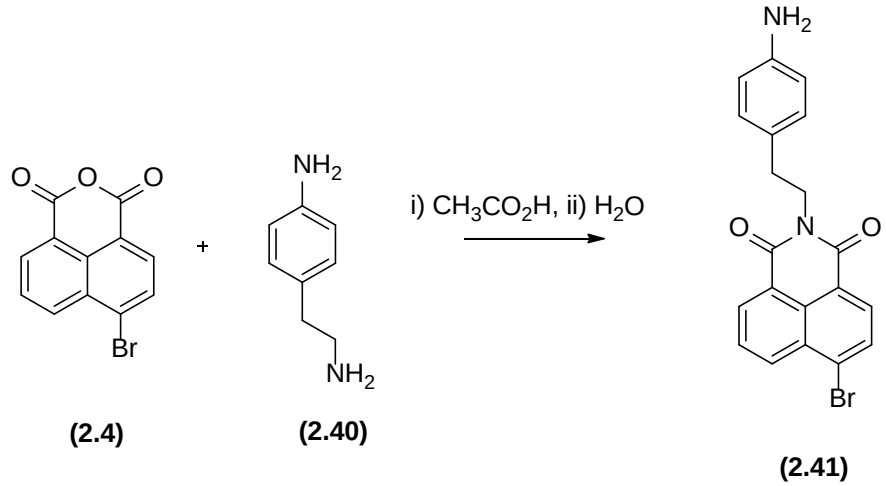

Scheme 2.8 Addition of diamine, **2.40**, to 4-bromo-1,8-naphthalic anhydride.

Compound **2.41** was formed through identical conditions to **2.5** – **2.8**. The ^{1}H NMR spectrum of **2.41** showed the CH_2 groups of the 4-(2-aminoethyl)aniline moiety shifted from 2.80 and 2.55 ppm in the starting material, **2.40**, to 3.58 and 2.90 ppm respectively in the product. The hydrogens on the naphthalic anhydride group also shifted indicating a change in chemical structure. Analysis by ESI-MS and IR further confirmed the synthesis of compound **2.41**.

The addition of two equivs. of Ph_2PCH_2OH to **2.41** was investigated under varying conditions. Initially, conditions trialled were identical to that used in the synthesis of **2.16** – **2.19**, however after stirring, the precipitated solid was examined by NMR and found to be starting diamine, **2.41**, while the filtrate contained only the starting phosphine material. Reflux overnight in MeOH was then trialled, however similar results were obtained.

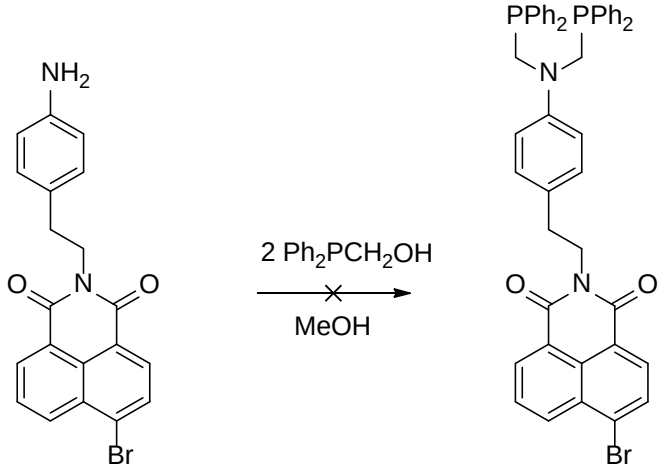

(2.41) **(2.42)**

Scheme 2.9 Addition of Ph_2PCH_2OH to compound **2.41**.

Concerned solubility may play a role in the lack of reaction, an *in situ* $^{31}P\{^{1}H\}$ NMR was ran of the two starting materials after 2h and again after 24h, the $^{31}P\{^{1}H\}$ NMR showed only a single resonance representing starting material, Ph_2PCH_2OH. The Smith group continues to conduct this work, with an undergraduate project student having synthesised a number of derivatives, including **2.41**, and exploration of the addition of Ph_2PCH_2- groups.

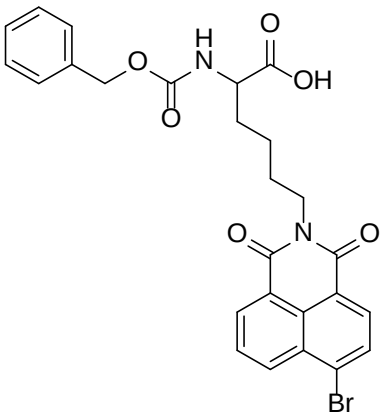

(2.43)

Figure 2.17 Chemical structure of **2.43**.

The addition of a lysine moiety in the imido position has also briefly been studied. Although naphthalimides are known to localise in the body, lysine would allow conjugation to a peptide based targeting vector through the free amine or carboxylic acid moiety.[96,99] The targeting vector would aid target specific accumulation of the compound *in vivo*. Addition of N_{α}-Cbz-L-lysine to 4-bromo-1,8-naphthalic anhydride using the same method utilised for the formation of **2.5** – **2.8** was performed, however initial attempts to form compound **2.43** produced only poor yields of a mixture containing starting material and product. Exploration of different conditions or through utilising known procedures in literature for the synthesis of **2.43** continues to be conducted by the Smith group.

2.5 Summary

In conclusion, four fluorescent probes containing PCNCP moieties have been successfully synthesised *via* the phosphorus analogous Mannich based condensation reaction, characterised and their molecular structures explored *via* single crystal X-ray diffraction studies. This method can be replicated with a range of naphthalimides by changing the position of the hydrazino group on the naphthalimide or altering the substituent in the imido position. The coordination chemistries of probes **2.16** – **2.19** were extensively studied using four metal precursors, demonstrating the versatility of coordination abilities of ligands **2.16** – **2.19**.

Preliminary studies were conducted to investigate the photophysical properties of phosphine ligands **2.18** and **2.19**. On coordination to platinum(II) and palladium(II) metal centres, fluorescence was quenched, however no quenching is observed when

complexed to gold(I). This could allow platinum and palladium species to be detected through a “turn-off” fluorescence method. Further photophysical tests are required to allow for a deeper understanding of the mechanisms behind the fluorescence of these synthesised compounds. Ligands **2.16** and **2.17** should be investigated by UV absorbance to determine if the length of the hydrocarbon chain on the imido functionality influences λ_{em}. Studies of further naphthalimde compounds with ether and alcohol moieties on the imido functionality may explain the difference observed in **2.18** and **2.19** λ_{em}. Photophysical characterisation of ligands **2.18** and **2.19** and their respective complexes could also be repeated to authenticate the data presented here.

Naphthalimide derivatives have been shown to facilitate cellular imaging, therefore novel ligands **2.16 – 2.19** and their subsequent complexes have potential for applications in medicinal imaging.[78,96] Furthermore the metals chosen here have shown cytotoxic properties, as described in Section 1.4, therefore the compounds synthesised will be investigated in future work for use in diagnostic imaging and therapy.

Chapter 3 - Synthesis, coordination and characterisation of fluorescent fluorescein and rhodamine derivatives with PCN moieties

3.1 Fluorescent fluorescein and rhodamine derivatives

Chapter 2 of this thesis explored the synthesis of fluorescent naphthalimide compounds with PCN moieties, subsequent complexation of synthesised ligands to a number of metals and a preliminary study of their photophysical properties. In the following chapter, the naphthalimide fluorophore has been substituted for fluorescein and rhodamine derivatives. Fluorescein and rhodamine derivatives are attractive fluorophores as they are highly fluorescent, have high fluorescent quantum yields and high photostability. This has resulted in a large number of papers exploring fluorescein and derivatives as fluorescent sensors; some examples are described in Section 1.5.6. For this reason, fluorophores with aminomethylphosphine moieties were expanded to include fluorescein and rhodamine derivatives. PCN moieties have been added to the fluorophore *via* the phosphorus analogous Mannich condensation reaction to the fluorophores corresponding hydrazides, in a similar fashion to Chapter 2. Later, fluoresceinamine isomer I was used to investigate the influence of the position of the aminomethylphosphine group, with respect to the fluorophore, has on the photophysical properties of the synthesised ligand. The coordination chemistries of ligands synthesised were studied with Pt(II), Pd(II) and Au(I) metal centres, and preliminary studies of their photophysical properties were also examined and compared to that of their corresponding PCN ligand.

3.2 Synthesis of PCN containing fluorescein and rhodamine derivatives

In order to facilitate the addition of phosphine moieties to the fluorescein/rhodamine fluorophore *via* the Mannich based condensation reaction, the introduction of an amine group was required. This was conducted *via* the amidation of fluorescein/rhodamine using hydrazine monohydrate to give the corresponding hyrazides, as shown in Scheme 3.1, following a procedure described by Shen *et al*.[154]

Although Shen and coworkers describe a recrystallization step for **3.3**, the ^{1}H NMR and ESI-MS data collected for the unrecrystallised yellow precipitate of **3.3** matched that reported and was suitably pure for further reaction.[154] Small peaks in the ^{1}H NMR spectrum alluded to the presence of residual ethanol. Water was also observed in the ^{1}H NMR spectrum, though this may be attributed to the d^{6}-DMSO used to make up the NMR sample. Due to the omission of the recrystallisation step an improvement in yield was observed from 54%, as recorded by Shen and coworkers, to 81%.[154]

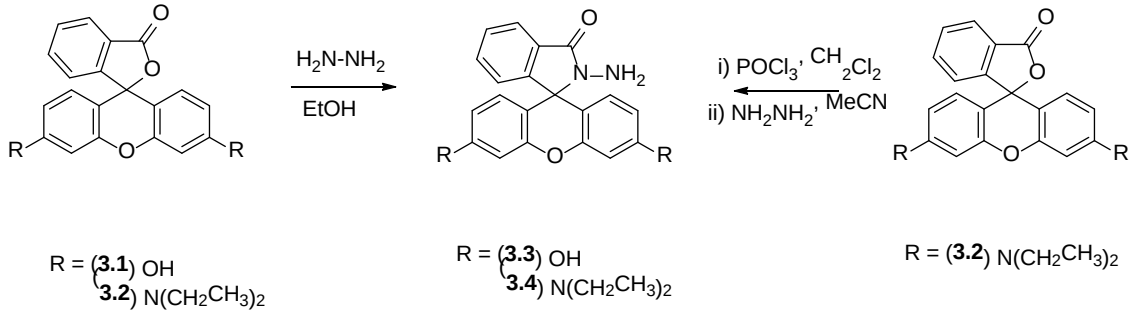

Scheme 3.1 Amidation of **3.1** and **3.2** using hydrazine monohydrate and formation of **3.4** using a method described by Dujols *et al.*[155]

Shen *et al.* did not describe the synthesis of **3.4** along with the synthesis of **3.3**, however identical conditions were utilised in the preparation of **3.4**.[154] A separate publication by Dujols and colleagues elucidates the synthesis of **3.4** using a two-step method involving the formation of an acid chloride using phosphorus oxychloride followed by nucleophilic substitution with hydrazine, as shown in Scheme 3.1, provided recorded analysis in which data collected for **3.4** could be compared.[155] As with **3.3** ^{1}H NMR and ESI-MS data collected correlated to that observed in the literature.[101]

To begin the investigation of the reactions between hydrazides **3.3** and **3.4** with PPh_2CH_2OH it was decided to first attempt the addition of one equiv. of PPh_2CH_2OH with hydrazide **3.3**. Formation of a monofunctionalised phosphine is highly desirable as it allows exploration of an intermediate between a *bis*phosphine and hydrazide; something which could not be achieved with the phosphine naphthalimide probes, described in Chapter 2, which preferred to form *bis*phosphines. The conditions used were similar to those used for the synthesis of phosphine functionalised naphthalimide probes **2.13** - **2.16**, a 4h reflux in methanol followed by stirring at room temperature for approximately 65h. After cooling, filtration of the white precipitate gave product **3.5** with a maximum yield of 90% observed. These conditions were found to be the best for optimising the yield. When trialled here, longer refluxing times, i.e. overnight, did not improve the yield while the absence of any r.t. stirring slightly reduced the yield of **3.5**.

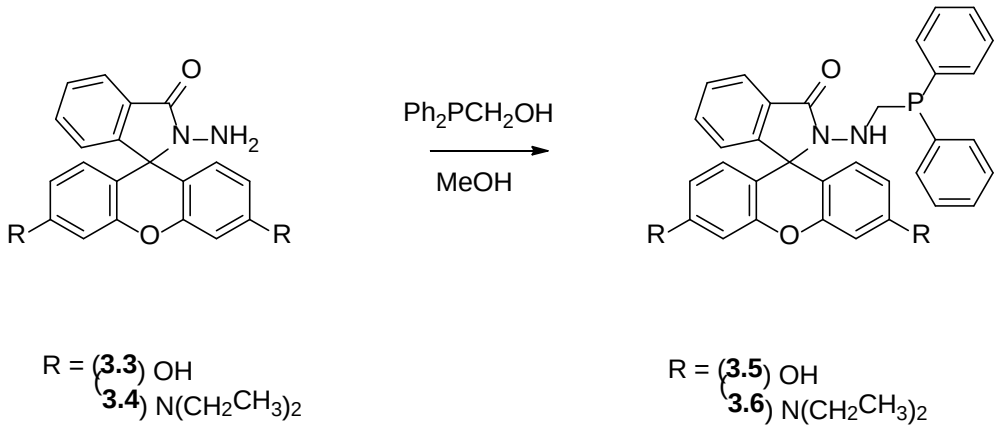

Scheme 3.2 Addition of a phosphine moiety to **3.3** and **3.4** respectively.

Initial conditions utilised in an attempt to form the desired monophosphine **3.6** consisted of a 3h reflux in methanol followed by a 33h stir at r.t., conditions comparable to those utilised successfully for analogous product **3.5**. Due to the absence of a precipitate during the r.t. stir, the solution was evacuated to dryness and a sample taken for NMR analysis. $^{31}P\{^{1}H\}$ NMR showed only 56% of phosphorus species present was the desired compound **3.6**. Degassed methanol was reintroduced to the reaction mixture and the solution was refluxed for 19h, followed by r.t. stir for a further 23h. An aliquot of the reaction mixture was again taken for NMR analysis. $^{31}P\{^{1}H\}$ NMR showed no increase in desired product **3.6**, however the presence of a new peak in the region expected for a *bis*phosphine product was observed (8%). To prevent synthesis of the *bis*phosphine, an extra 20% rhodamine hydrazide, **3.4**, was added and again the reaction mixture was refluxed for 24h, followed by 24h r.t. stir. On this occasion a white precipitate formed; this was filtered under suction and NMR showed **3.6** to be present in 97% purity as determined by $^{31}P\{^{1}H\}$ NMR analysis. Subsequent reactions consisted of 1.2 equivalent **3.4** to one equivalent Ph_2PCH_2OH refluxed in methanol over 22h, followed by stirring at r.t. over 72h to generate white solid **3.6** in a yield of approximately 72%.

Figure 3.1 $^{31}P\{^{1}H\}$ NMR (in d_6-DMSO) of ligand **3.5**. Chemical shifts in ppm/δP.

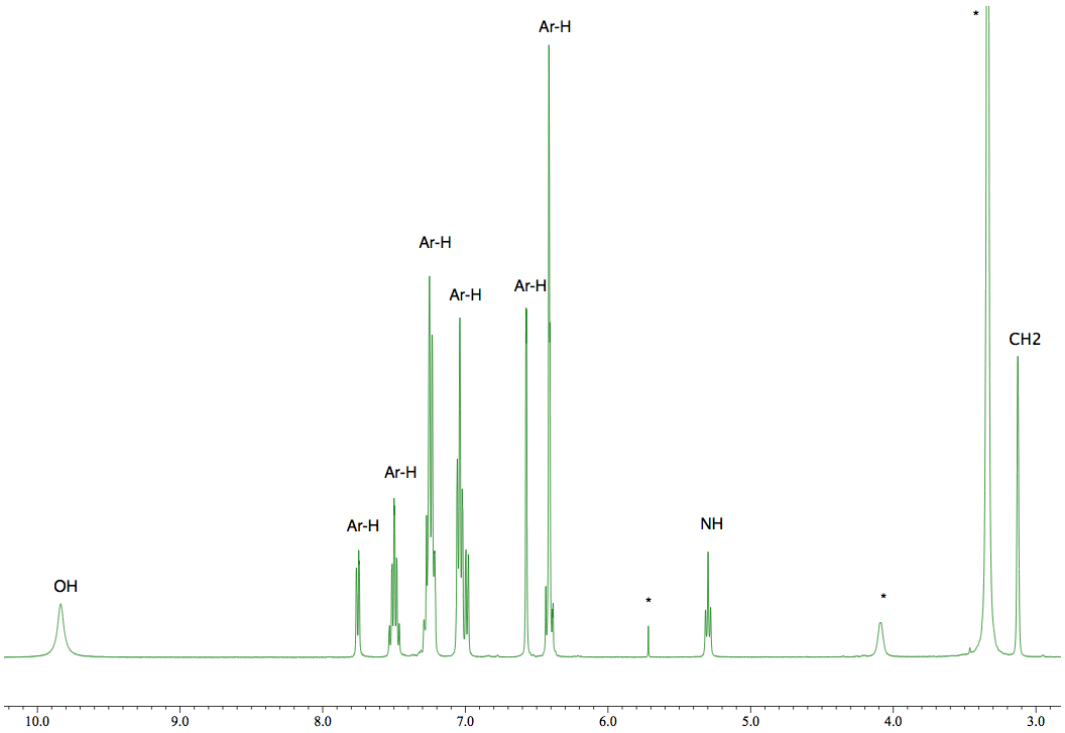

Figure 3.2 ^{1}H NMR of ligand **3.5**, recorded in d_6-DMSO (* denotes residual solvent). Chemical shifts in ppm/δP.

The $^{31}P\{^{1}H\}$ NMR of ligands **3.5** and **3.6** both showed single resonances residing at -22.8 and -23.4 ppm respectively; these lie within the range indicative of monosubstituted PCN ligands.[156] In the ^{1}H NMR spectra of **3.5** the broad singlet observed for the NH_2 group in **3.3** at 4.35 ppm is no longer present and a downfield triplet peak at 5.29 ppm is observed for the NH moiety. This coincides with the presence of the neighbouring CH_2 group observed as a doublet at 3.13 ppm. Similarly in the ^{1}H NMR spectrum of ligand **3.6**, a broad NH_2 singlet peak at 3.64 ppm is replaced by a triplet NH peak at 5.16 ppm, with the PCH_2 peak residing at 3.27 ppm.

Further characterisation supporting the preparation of ligands **3.5** and **3.6** were obtained from ESI-MS results which showed $[M+H]^+$ fragments at *m/z* 545.1619 and 655.3206 for ligands **3.5** and **3.6** respectively. IR analysis showed two NH peaks in the starting materials **3.3** and **3.4**, and one NH vibration after addition of the phosphine moiety. Elemental analysis was also in agreement with calculated values for the empirical formulae of products **3.5** and **3.6**.

3.2.1 Molecular structure of ligand 3.5

X-ray quality crystals of ligand **3.5** were grown *via* vapour diffusion of Et_2O into a DMSO/CH_2Cl_2 solution of ligand **3.5**. The molecular structure of ligand **3.5** is displayed in Figure 3.3. A fluorescein derivative incorporating the PCN scaffold has not been previously studied using X-ray crystallography, however the precursor to ligand **3.5**, compound **3.3** has been studied.[157] The comparable bond lengths and angles of **3.3** agree with those recorded for ligand **3.5**.[157]

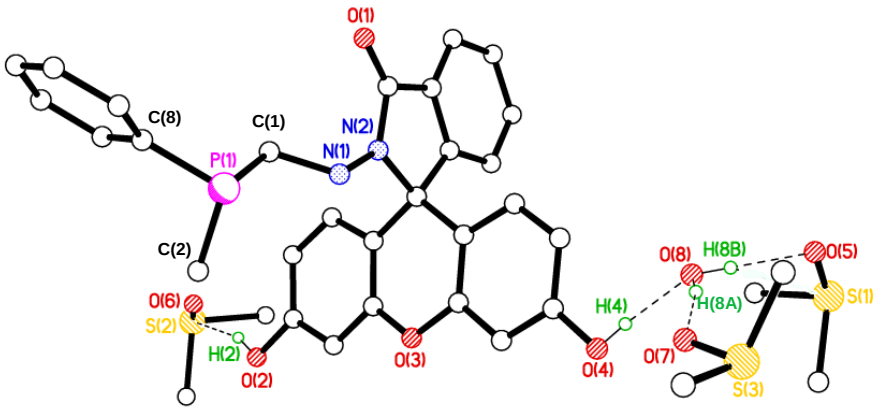

Figure 3.3 Molecular structures of **3.5**, one H_2O and three DMSO solvent of crystallisation molecules. One phenyl ring on the phosphine and all hydrogen atoms, except H(2), H(4), H(8A) and H(8B), were omitted for clarity.

The phosphorus centre shows a distorted tetrahedral geometry [C(8)-P(1)-C(2) 101.87; C(8)-P(1)-C(1) 101.38; C(2)-P(1)-C(1) 101.96], with angles smaller than the idealised angle of 109.5° for tetrahedral geometries; smaller angles for free PCN ligands have been previously observed in literature.[156] Three DMSO and one water solvent of crystallisation was also present in the asymmetric unit along with one molecule of **3.5**. The complex packs in columns perpendicular to the *a* axis. Rows of molecules laying parallel to the *a* axis are hydrogen bonded through solvent of crystallisation molecules sat in the voids between the molecules. Intermolecular bonding was also observed between the amine group on one molecule and the carbonyl group of the neighbouring molecule, as shown in Figure 3.4.

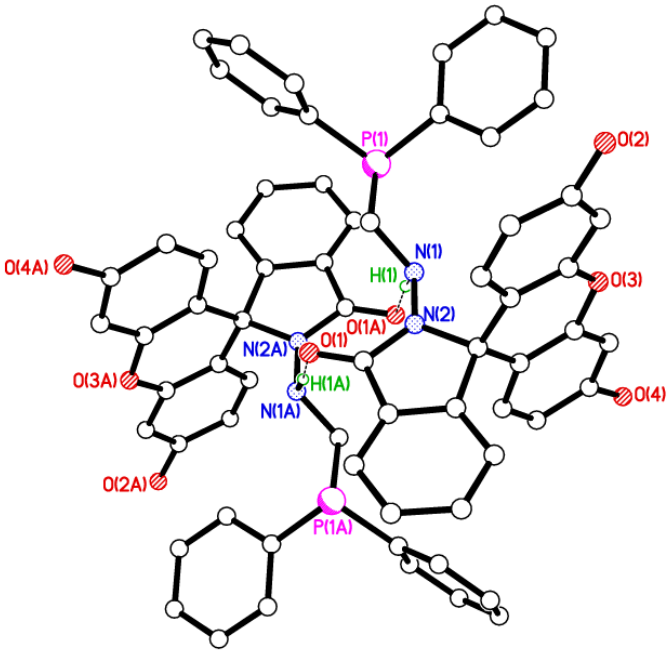

Figure 3.4 Packing structure of **3.5** highlighting some of the intermolecular interactions present. All hydrogen atoms except those on N(1) and N(1A) have been omitted for clarity. Symmetry operator for equivalent molecule A: -x+2, -y+1, -z+1.

3.2.2 Attempted synthesis of *bis*phosphine ligands

In an attempt to form *bis*phosphine **3.7**, two equivs. of Ph_2PCH_2OH were reacted with one equivalent **3.3** in a 2h reflux followed by a 72h r.t. stir. However only the monofunctionalised phosphine **3.5** was yielded, with the filtrate containing only unreacted Ph_2PCH_2OH as determined by $^{31}P\{^1H\}$ NMR. Reaction times were increased

to an 18h reflux in methanol, but these conditions did not promote the reaction to proceed past the monofunctionalised phosphine **3.5**. Therefore a 65h reflux in toluene and methanol (3:1) was trialled. Again, under the conditions examined, desired product **3.7** could not be obtained.

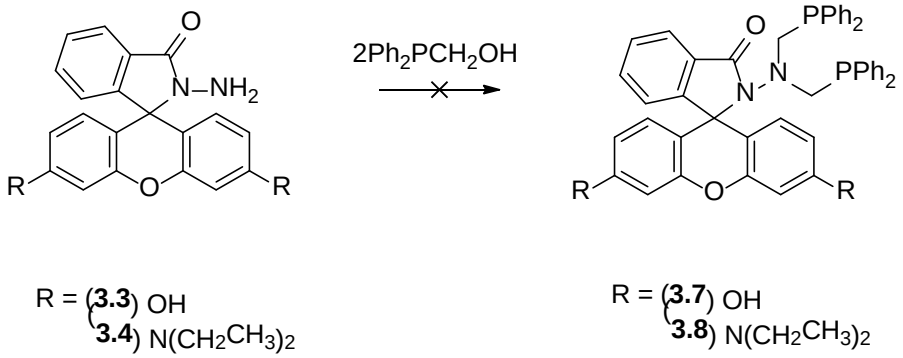

Scheme 3.3 Attempted synthesis of **3.7** and **3.8**.

Finally, monofunctionalised phosphine **3.5** was reacted with one equivalent of Ph_2PCH_2OH in methanol, refluxing for 22h followed by a 48h r.t. stir. $^{31}P\{^1H\}$ NMR analysis of the precipitate showed a single resonance at -23 ppm, representing starting material phosphine **3.5**. The filtrate contained only unreacted Ph_2PCH_2OH phosphorus species, as determined by $^{31}P\{^1H\}$ NMR. Failure to produce the desired product **3.7** under the conditions trialled may be due to steric hindrance preventing the second bulky methyldiphenylphosphine group from undergoing addition, or perhaps after the formation of the first PCN bond, the NH is deactivated.

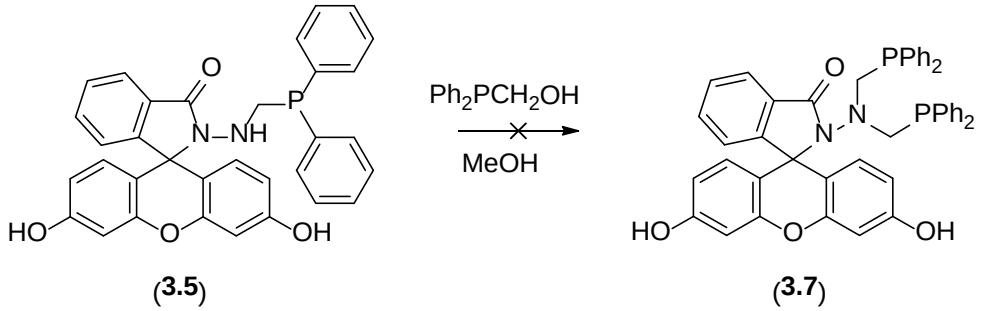

Scheme 3.4 Attempted synthesis of **3.7**.

Due to the prescence of 8% impurity observed in the $^{31}P\{^1H\}$ NMR in the region associated with *bis*phosphines during the initial experiments to form **3.6**, the reaction of 2 equivs. Ph_2PCH_2OH to **3.4** was also trialled. Refluxing over 18h in methanol followed by 48h r.t. was trialled; however no *bis*phosphine could be reproduced under the conditions used.

3.2.3 Coordination studies with platinum(II)

Monodentate phosphine ligands **3.5** and **3.6** underwent coordination to platinum(II) *via* the reaction of two equivalents of ligand to one equivalent of the dichloroplatinum(II) species, $PtCl_2$(cod), to yield a white solid **3.9** and bright pink-purple powder **3.10** in a yield of 85 and 62% respectively. Whilst **3.9** precipitates fully with diethyl ether, more soluble **3.10** required hexane as well as ether to precipitate out fully.

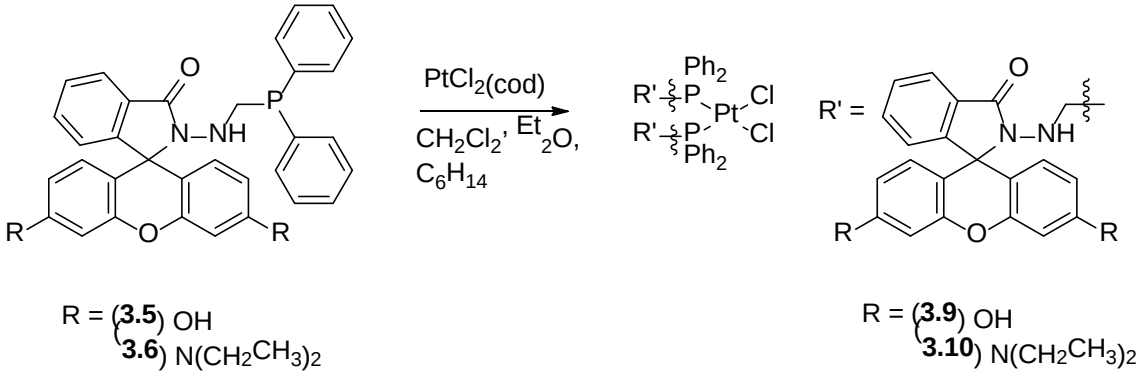

Scheme 3.5 Coordination of ligands **3.5** and **3.6** to a platinum(II) metal centre.

Formation of only the *cis*-isomer was evident from the $^{31}P\{^1H\}$ NMR spectra of both **3.9** and **3.10**, as a singlet peak at 1.8 and 1.2 ppm were observed with associated satellites displaying $^1J_{PtP}$ coupling constants of 3644 and 3646 Hz, in the range indicative of *cis* configuration Pt-P coupling.[158] To ensure no *trans* isomer had formed during the reaction, the filtrate was reduced and examined by NMR. No phosphorus containing species were present in the filtrate as determined by $^{31}P\{^1H\}$ NMR. FT-IR analysis of both products exhibited two vPt-Cl bands in the region expected for *cis*-configured Pt-Cl complexes.[146]

Confirmation of the formation of complexes **3.9** and **3.10** were further supplied by CHN and ESI-MS results. Elemental analyses confirmed the empirical formulae for **3.9** and **3.10**, though **3.10** had some CH_2Cl_2 present, as also seen in the ^1H NMR, which were taken into account. ESI-MS gave $[M\text{-}Cl]^+$ fragments for **3.9** and **3.10** at *m/z* 1318.2416 and 1538.5566 respectively. Despite numerous attempts to crystallise both **3.9** and **3.10**, X-ray quality crystals were not obtained.

3.2.4 Coordination studies with palladium(II)

Under identical conditions to that used in the formation of complexes **3.9** and **3.10**, palladium(II) complexes **3.11** and **3.12** were yielded through the ligand substitution of cod from $PdCl_2$(cod) with two equivalents of **3.5** or **3.6**. Coordination with **3.5** gave a yellow precipitate in a yield of 86%, while complexation with **3.6** generated a purple powder in a yield of 62%.

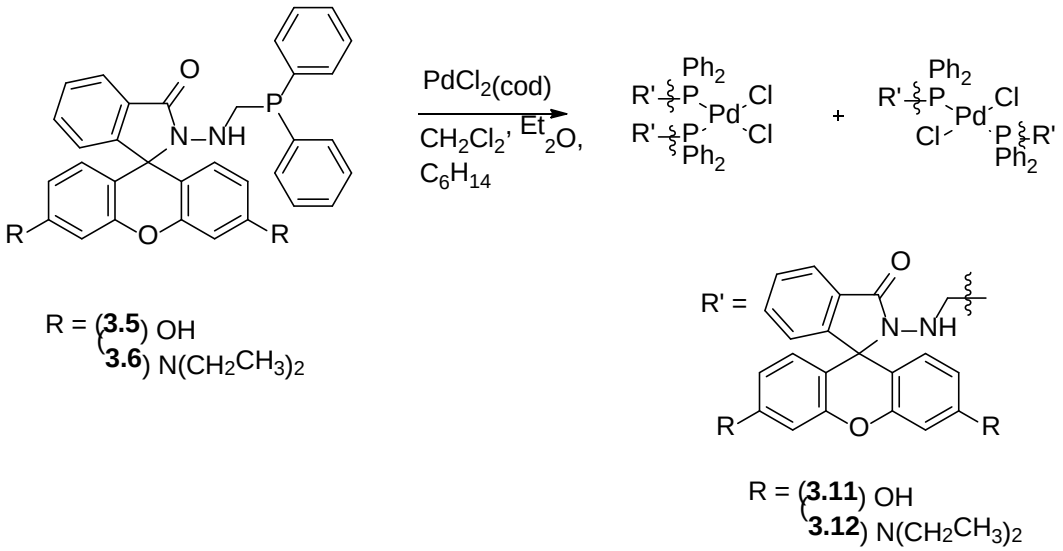

Scheme 3.6 Coordination of ligands **3.5** and **3.6** to a palladium(II) metal centre.

Unlike analogous platinum(II) compounds **3.9** and **3.10**, when coordinated to a palladium(II) centre, complexes **3.11** and **3.12** form both *cis* and *trans* isomers. This is a result of complex thermodynamic and kinetic energetics.[189] Both isomers are clearly observed in the $^{31}P\{^{1}H\}$ NMR spectra which depicts two peaks in each of the spectra; **3.11** exhibits peaks at 10.9 and 21.5 ppm, whereas **3.12** displays resonances at 10.1 and 20.9 ppm.

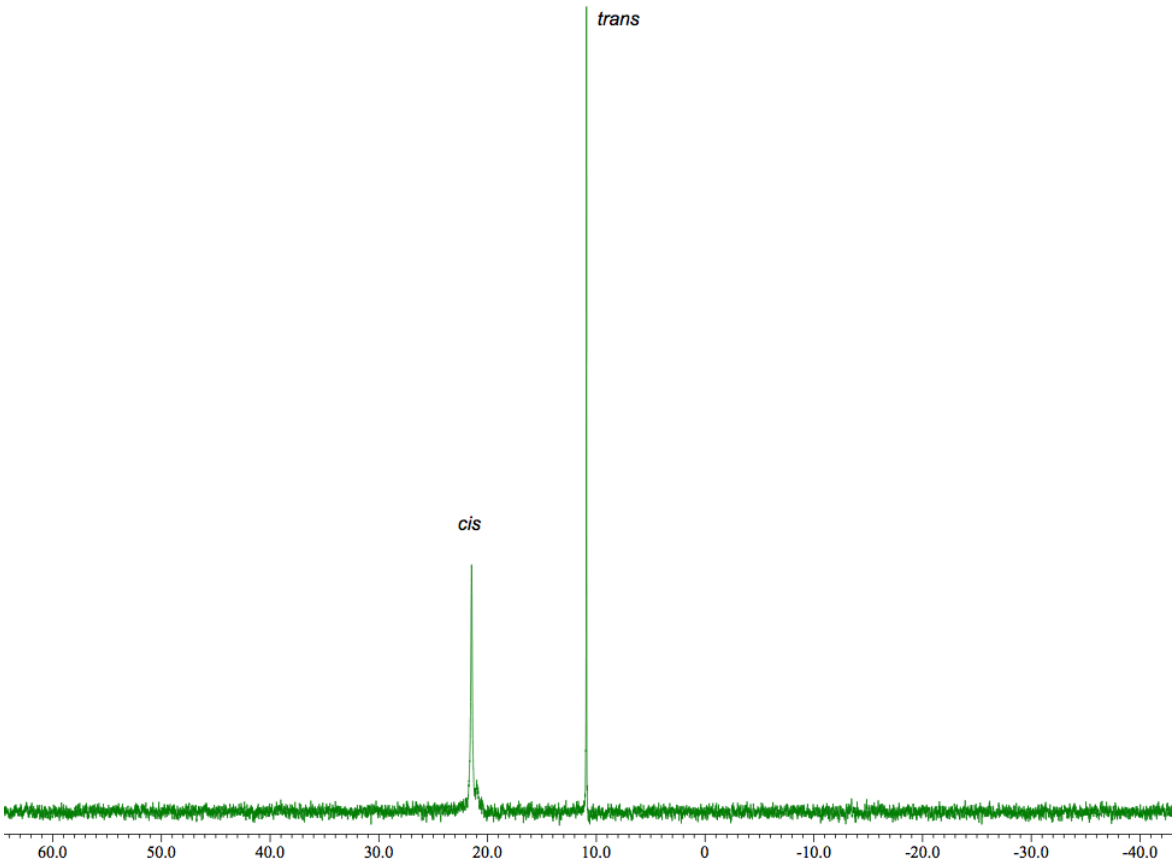

Figure 3.5 $^{31}P\{^{1}H\}$ NMR of palladium complex, **3.11**. Chemical shifts in ppm/δP.

Peaks at 21.5 and 20.9 ppm, in complexes **3.11** and **3.12** respectively, represent the *cis*-configured isomer, as a downfield shift of this magnitude is indicative of *cis* isomers.[145,156] In complex **3.11** the ratio by $^{31}P\{^{1}H\}$ NMR between *cis* and *trans* isomers is 58:42, and therefore *cis* configuration is slightly more favourable than *trans*. In the case of **3.12** the ratio of *cis* to *trans* isomer is 70:30 and therefore *cis* configuration is more favourable. The filtrate of **3.11** was analysed by $^{31}P\{^{1}H\}$ NMR, but no phosphorus containing species were present.

The ^{1}H NMR spectra of both products show two isomers present. Some peaks have been identified through their relative integrations and a number of NMR techniques, including HMQC and COSY, while some peaks, most notably the aromatic hydrogens of both products formed, cannot be distinguished from each other. FT-IR data also shows the presence of both isomers through the presence of typical vPd-Cl *trans* stretches at approx. 350 cm^{-1} and two further vPd-Cl *cis* stretches in the region 330-300 cm^{-1}.[146]

As both the *cis* and *trans* isomers of compounds **3.11** and **3.12** have the same empirical formulae, elemental analyses of both products (**3.11** and **3.12**) gave results

concordant with the expected formulae. ESI-MS analysis also displayed expected [M-Cl]$^+$ fragments at *m/z* 1229.1835 and 1449.4982 for **3.11** and **3.12** respectively.

3.2.5 Molecular structure of palladium(II) complex 3.11

Orange blades of complex **3.11**, suitable for single crystal X-ray diffraction, were obtained by vapour diffusion of Et_2O into a CH_2Cl_2 mother liqueur of **3.11** and its molecular structure determined (Figure 3.6). The crystal contained *trans* isomers of **3.11** exclusively.

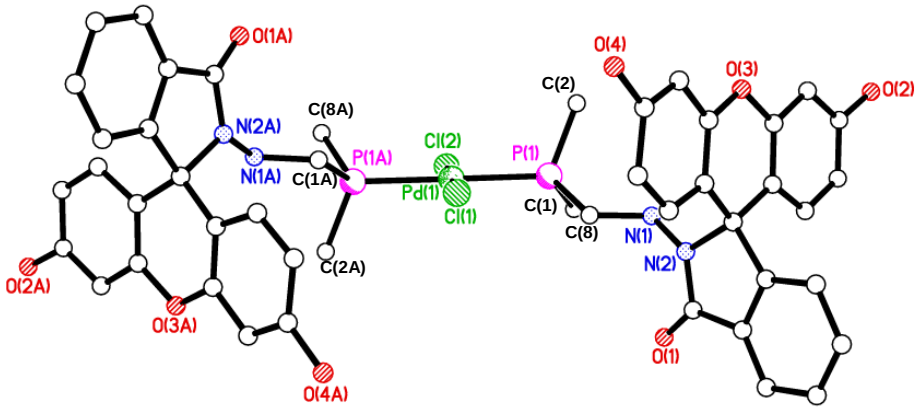

Figure 3.6 Molecular structure of **3.11**. All hydrogen atoms, solvent of crystallisation and phenyl rings, except the ipso carbons, have been omitted for clarity.

Two molecules of solvent crystallisation (Et_2O) were present per Pd(II) complex, with a further two molecules of Et_2O modelled as diffuse areas of electron density by Platon squeeze. The palladium(II) metal complex depicts a square planar geometry with respect to the palladium metal centre [P(1A)—Pd(1)—P(1) 178.04 (5)°, Cl(2)—Pd(1)—Cl(1) 180.0°]; this is in contrast to *cis*palladium(II) complex **3.13** described in Section 3.2.7 which depicts a distorted square planar geometry at the palladium centre. Both complexes **3.11** and **3.13** feature phosphorus in a distorted tetrahedral geometry [**3.11**: C(2)—P(1)—C(8) 107.08(19)°; C(2)—P(1)—C(1) 101.9(2)°; C(1)—P(1)—C(8) 106.6(2)°, **3.13**: C(2)—P(1)—C(8) 105.4(3)°; C(2)—P(1)—C(1) 105.4(2)°; C(1)—P(1)—C(8) 97.1(2)°].

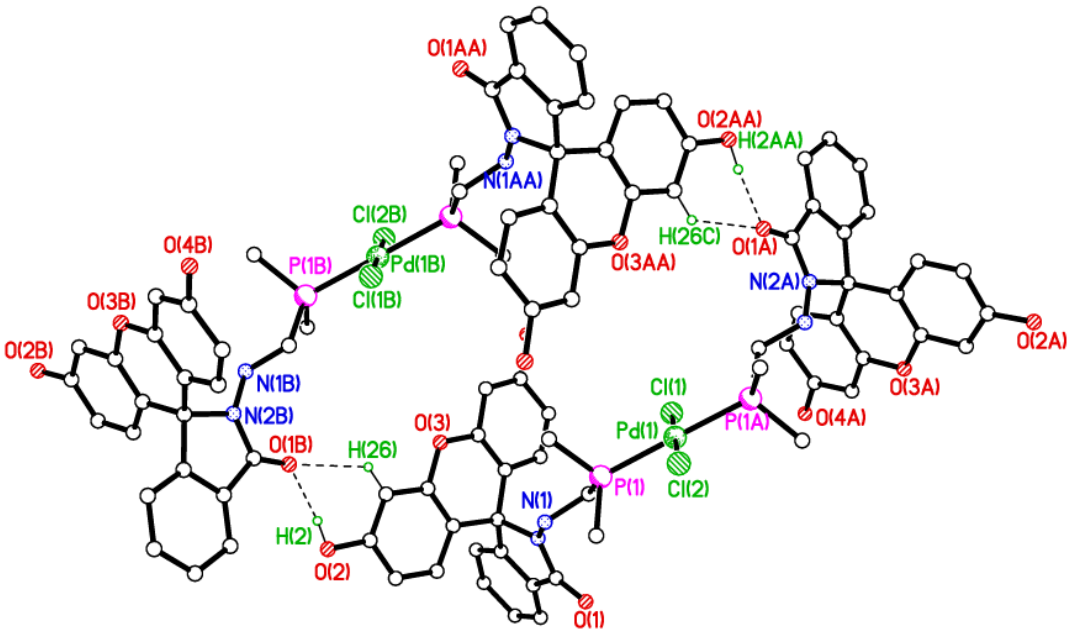

Figure 3.7 Packing structure of **3.11** highlighting some of the intermolecular interactions present. All hydrogen atoms except for H(2), H(2AA), H(26) and H(26C) have been omitted for clarity. All solvent molecules and phenyl rings, except the ipso carbons, on the phosphine moieties have also been removed for clarity. Symmetry operator for equivalent molecule A: x, -y+1, z-1/2.

The complex packs in columns parallel to the *c* axis, with the dichloropalladium(II) moiety stacking above and below one another. Intramolecular bonding is observed between aromatic hydrogens on the phosphine moiety and neighbouring chloro- and amine groups. Intermolecular bonding is observed between the carbonyl group of one molecule and the hydroxyl moiety of the fluorescein group of a neighbouring complex [O(2)—H(2)···O(1B) 2.669(5) Å], as shown in Figure 3.7.

3.2.6 Further coordination studies using palladium(II)

As described in Section 1.4.5, cyclopalladated compounds are of interest as anticancer agents, in order to improve stability of metallodrugs and ensure they reach their biological target.[59,57] It was noted that on complexation of **3.5** with $PdCl_2$(cod) to form **3.11** a yellow precipitate was generated which was visibly yellow in solution unlike the phosphine itself or the respective Pt(II) and Au(I) complexes. Colour can indicate fluorescence in some cases; for this reason it was decided to investigate the coordination of **3.5** with two further palladium centres and their subsequent properties.

Firstly, to a stirred CH_2Cl_2 solution of di-μ-chlorobis[2-[(dimethylamino)methyl]phenyl-C,N]dipalladium(II), two equivalents of **3.5** were added. Following stirring for 1h, the solution was reduced in volume to 1-2 mL and diethyl ether added resulting in the formation of white precipitate **3.13** with a yield of 65%.

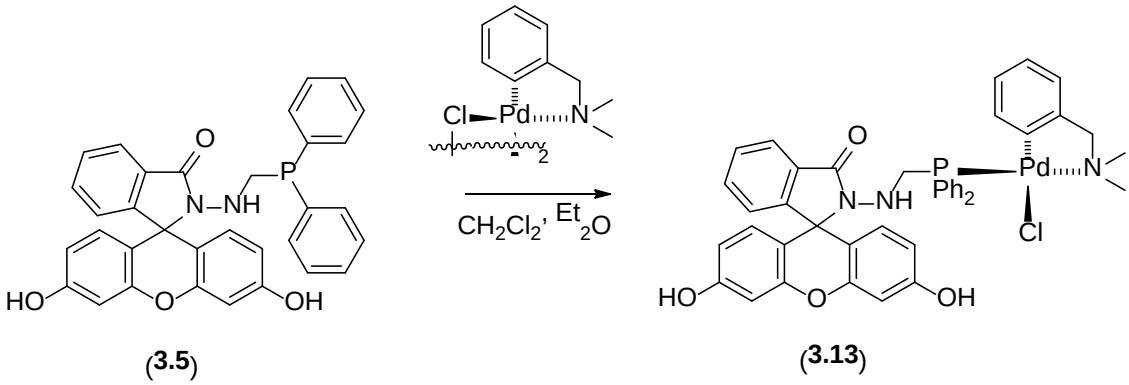

(**3.5**) (**3.13**)

Scheme 3.7 Synthesis of **3.13**.

A single resonance was observed in the $^{31}P\{^1H\}$ NMR spectrum at 29.4 ppm for complex **3.13**, a shift of *ca.* 52 ppm from ligand **3.5**. The ^1H NMR spectrum for compound **3.13** showed a shift in the peak representing PCH_2, from a doublet at 3.13 ppm in starting ligand **3.5** to a double doublet at 3.74 ppm in complex **3.13**, supporting coordination. Peaks were also observed for the cyclopalladated ligand in stoichiometric amounts supporting formation of complex **3.13**; these included a singlet peak at 2.47 ppm representing $2CH_3$ moieties. Confirmation of the formation of complex **3.13** was further supplied by the CHN and ESI-MS results. Elemental analyses confirmed the empirical formulae for **3.13**, though **3.13** had some water present, as also seen in the ^1H NMR, which was taken into account. ESI-MS gave $[M\text{-}Cl]^+$ fragment for **3.13** at *m/z* 784.1560.

3.2.7 Molecular structure of 3.13

Colourless plates of **3.13** were grown by slow diffusion of Et_2O into a $(CH_3)_2SO/CH_2Cl_2$ solution of **3.13** and its molecular structure was determined, as shown in Figure 3.8. Since ligand **3.5** is a novel ligand itself, any respective complexes have not been previously studied by X-ray crystallography. In addition the cyclopalladated metal motif ($PdC_9H_{12}NCl$) with a coordinated PCN ligand has not been determined by X-ray crystallography, as determined by a CSD search.[132]

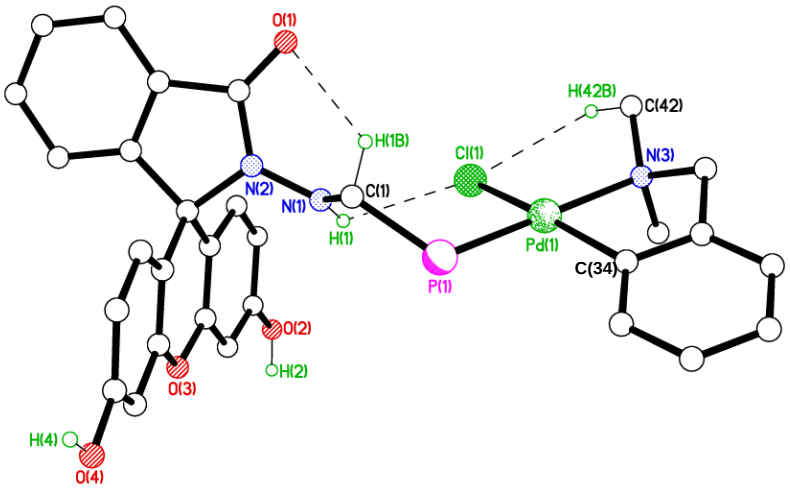

Figure 3.8 Molecular structure of **3.13** highlighting the intramolecular interactions present. All hydrogen atoms except those on O(1), O(2), O(4), C(1), N(1) and C(42) have been omitted for clarity.

The crystal structure of **3.13** exhibits one molecule of **3.13** and one molecule of Et_2O in the asymmetric unit. There are two voids present per unit cell (*Z*=4) with two disordered $CHCl_3$ molecules in each void. Platon squeeze modelled one $CHCl_3$ molecule per asymmetric unit. The palladium(II) metal complex depicts a distorted square planar geometry with respect to the palladium metal centre [N(3)—Pd(1)—P(1) 177.39(13)°, C(34)—Pd(1)—Cl(1) 167.43(14)°]. In comparison to *trans*-palladium(II) complex **3.11**, Pd-P bond length was shortened from 2.311Å to 2.248Å, showing the weaker *trans* effect of N compared to P; this is a phenomenon also observed in literature.[159]

Molecules of **3.13** stack in columns along the *a* direction with hydrogen bonding between O(2A)—H(2A)···O(1) holding the stacked molecules together, as shown in Figure 3.9. This intermolecular bonding has contacts of *ca.* 2.749 Å. Intramolecular interactions were also observed between C(1)—H(1B)···O(1), N(1)—H(1)···Cl(1) and C(42)—H(42B)···Cl(1) with contact lengths of 3.189, 3.133 and 3.278 Å respectively.

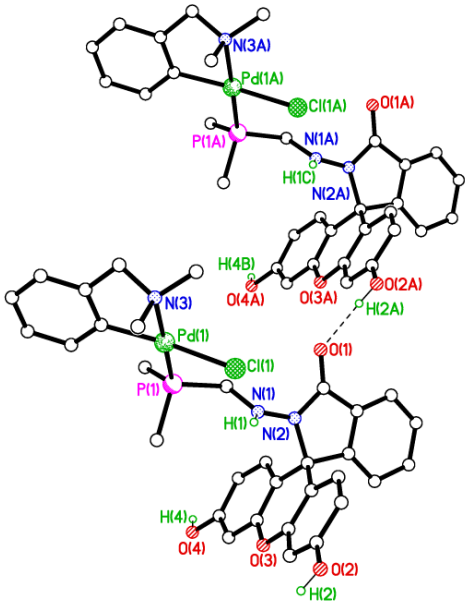

Figure 3.9 Packing structure of **3.13** highlighting the intermolecular interactions present. All hydrogen atoms except those on O(2A), O(2) and O(4) have been omitted for clarity. Symmetry operator for equivalent molecule A: x-1, y, z.

Similarly, the palladium dimer $[Pd(\mu\text{-}Cl)(C_{12}H_{12}N)]_2$ was reacted in a 1:2 ratio with **3.5** under identical conditions to **3.13** generating a white solid, **3.14**, with a yield of 47%; the yield of **3.14** afforded was less than that afforded for comparable complex **3.13** (65%). The $^{31}P\{^{1}H\}$ NMR spectrum for **3.14** comprised of a single resonance at 3.35 ppm, *ca.* 26 ppm downfield from starting material **3.5**.

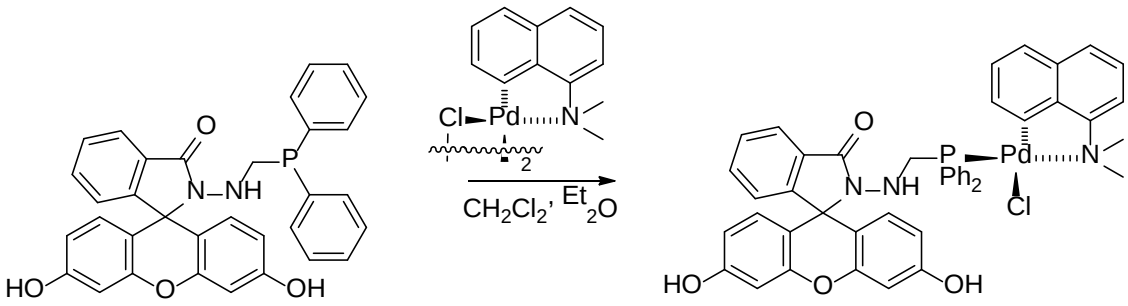

(**3.5**) (**3.14**)

Scheme 3.8 Synthesis of **3.14**.

Similar to complex **3.13**, the ^{1}H NMR spectrum for compound **3.14** showed a double doublet peak at 3.85 ppm for the PCH_2 moiety, a downfield shift from uncoordinated PCH_2 group in ligand **3.5**, which is observed as a doublet at 3.13 ppm. FT-IR spectrum of **3.14** showed two νPdCl stretches at 331 and 316 cm^{-1}. Analysis of **3.14** *via* ESI-MS revealed predictable fragment at: {*m/z* 820.1548 $[M\text{-}Cl]^+$}. The empirical formula for complex **3.14** was supported by elemental analysis data. Despite numerous attempts X-ray quality crystals of **3.14** were not obtained.

3.2.8 Coordination studies with gold(I)

In combination with the utilisation of Pt(II) and Pd(II), Au(I) metal centres were also employed to investigate the coordination chemistry of ligands **3.5** and **3.6**. Probes **3.5** and **3.6** underwent complexation with Au(tht)Cl in a 1:1 ratio to form white powder **3.15** and lilac solid **3.16** with a yield of 70 and 72%.

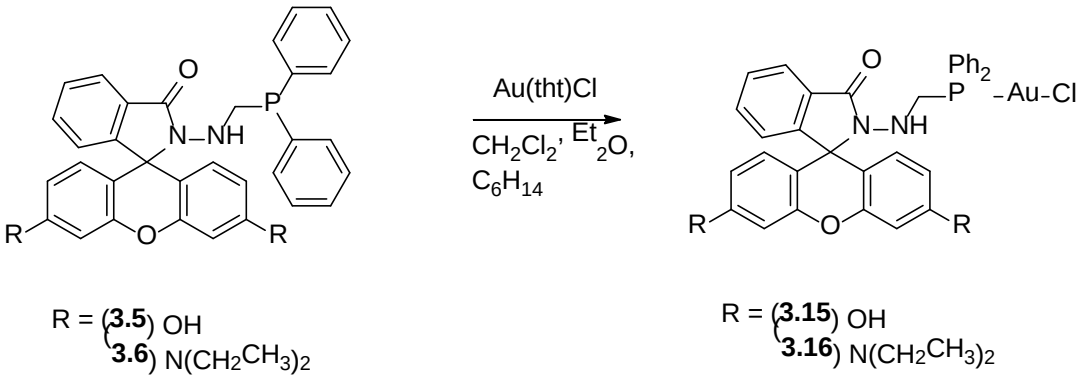

Scheme 3.9 Coordination of ligands **3.5** and **3.6** to a gold metal centre.

In the $^{31}P\{^{1}H\}$ NMR spectra for compounds **3.15** and **3.16** a singlet resonance is observed appearing at 20.2 and 24.2 ppm, with a downfield shift of 43.0 and 47.5 ppm from the parent ligands **3.5** and **3.6** respectively. This shift is typical for the coordination of a monodentate PCN ligand to a AuCl moiety, as observed in the literature and in Chapter 4.[145]

FT-IR data displayed Au-Cl stretches at ν 327 and 319 cm^{-1} for **3.15** and **3.16** respectively. Analysis of **3.15** and **3.16** *via* ESI-MS revealed predictable fragments at: {*m/z* 777.0979 $[M+H]^+$ and {*m/z* 851.2784} $[M\text{-}Cl]^+$ respectively. The empirical formulae for these complexes (**3.15** and **3.16**) are supported by elemental analysis data. Despite

numerous attempts, X-ray quality crystals for compounds **3.15** and **3.16** were not obtained.

3.3 Preliminary study of photophysical properties

An initial check for luminescence using a black light was performed on ligands **3.5** and **3.6** and respective complexes **3.9** – **3.12**, **3.15** and **3.16**, the results of which are shown in Figure 3.10 and Figure 3.11, respectively. Under black light the samples do not luminesce significantly, however a preliminary study into their UV and fluorescent properties was undertaken.

Figure 3.10 Image in daylight, on left, and image of compounds under a black light, on the right. Compounds ordered **3.5**, **3.9**, **3.11** and **3.15**, from left to right, in both images.

Figure 3.11 Image in daylight, on left, and image of compounds under a black light, on the right. Compounds ordered **3.6**, **3.10**, **3.12** and **3.16**, from left to right, in both images.

Ligands **3.5** and **3.6** and respective complexes were dissolved in DMSO (99+%) and investigated by UV absorbance for their excitation maxima, λ_{ex}, and concentration at which the sample has 0.1 absorbance at said maxima. Ligand **3.5** and complexes **3.9**,

3.11 and **3.15** all showed an absorbance maxima at *ca.* 280 nm. Palladium(II) complex, **3.11**, also had a peak at 340 nm which was not observed for related compounds **3.5**, **3.9** and **3.15**. Fluorescein derivatives often have an excitation maximum at *ca.* 516 nm however this is not the case for compounds **3.5**, **3.9**, **3.11** and **3.15**, which may be a result of their spirolactam conformation.[154,160]

Using the 0.1 absorbance concentrations, fluorescence measurements were performed to find the emission maxima, λ_{em}, when exciting at 280 nm. The DMSO solutions of all compounds were purged with nitrogen before measurements in order to prevent the formation of phosphine oxide and to limit quenching by photobleaching (excited oxygen). The emission spectra for **3.5**, **3.9**, **3.11** and **3.15** when excited at 280 nm are shown in Figure 3.12.

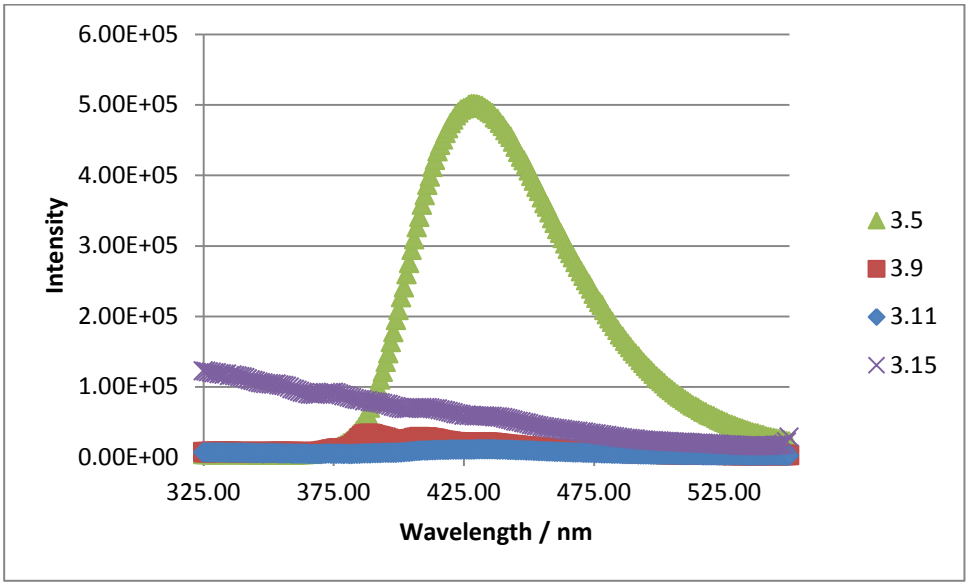

Figure 3.12 Emission profile of ligand **3.5** and corresponding complexes **3.9**, **3.11** and **3.15**. Recorded in DMSO at room temperature, with an excitation wavelength of 280 nm.

Figure 3.12 shows platinum(II) complex **3.9** and palladium(II) complex **3.11** appears to have negligible emission when excited at 280 nm, with gold complex, **3.15**, showing minimal fluorescence and no emission maxima in the range the emission maxima is observed for ligand **3.5**. Ligand **3.5** strongly fluoresces, with an emission maxima recorded at 429 nm giving a Stokes shift of 149 nm. Since fluorescence is observed for the ligand but quenched on coordination to the metals utilised here this may indicate the potential for ligand **3.5** to be used as a "turn-off" fluorescence sensor for the detection of metals such as Pt(II), Pd(II) and Au(I), though as shown here the "turn-off" sensing would not be specific to a metal. Future work could explore if there is also a reduction in fluorescence when **3.5** is coordinated to other metals.

Table 3.1 Summary of UV absorbance and fluorescence data for **3.5** and respective complexes.

Compound	Conc at 0.1 abs. ($x10^{-6}$) (mol dm^{-3})	Absorption Max (λ_{ex}) (nm)	Emission Max (λ_{em}) (nm)	Stokes shift ($\Delta\nu_{st}$) (nm)	Coeffiecent (ε) (cm^{-1} M^{-1})
3.5	8.44	280	429	149	9350
3.9	4.83	277	-	-	18900
3.11	2.60	279	-	-	21700
3.15	9.49	278	-	-	7900

To investigate the absorbance at 340 nm in the UV spectra for palladium(II) compound, **3.11**, related compounds **3.5**, **3.9** and **3.15** were made up to an identical concentration at which **3.11** had 0.1 absorbance at 340 nm. These solutions were measured on the Fluoromax spectrophotometer to identify their emission spectra. The UV excitation maxima, λ_{ex}, at 340 nm is of interest as it could be used to identify Pd(II) containing species. The emission spectra, a result of excitation at 340 nm, in shown in Figure 3.13. Palladium(II) complex, **3.11**, does not peak but has a flat emission between 430 – 440 nm, with ligand **3.5** and complexes **3.9** and **3.15** having irregular emission profiles when excited at 340 nm. Future work will be conducted to further explore fluorescence when excited at 340 nm.

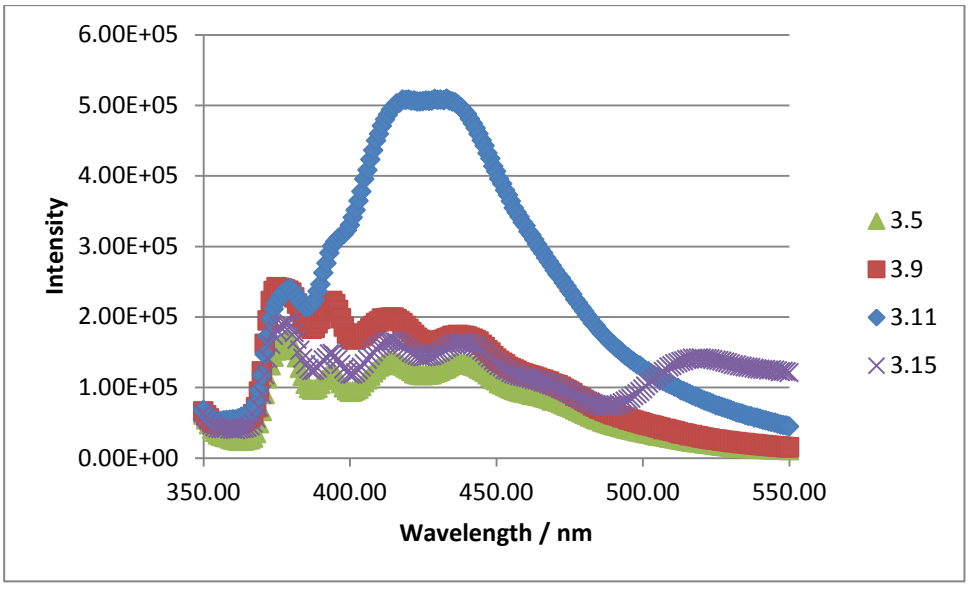

Figure 3.13 Emission profile of ligand **3.5** and corresponding complexes **3.9**, **3.11** and **3.15**. Recorded in DMSO at room temperature, with an excitation wavelength of 340 nm.

Ligand **3.6** and complexes **3.10**, **3.12** and **3.16** all showed an absorbance maxima at *ca.* 316 nm. However palladium(II) and platinum(II) complexes, **3.10** and **3.12** respectively, had an addition absorbance peak at 566 nm which was not observed in related compounds **3.6** and **3.16**. Spirocyclic rhodamine derivatives are non-fluorescent and colourless. It is possible that in Pt(II) and Pd(II) complexes **3.10** and **3.12**, the spirocyclic ring has ring-opened to produce an absorption band in the region expected for ring-open rhodamine derivatives (566 nm).[155] Complexes **3.10** and **3.12** are also pink in colour, which would support the theory of spirocyclic ring-opening since ring-closed derivative are colourless. The reason for the presence of an addition absorption band will be investigated in the future by further fluorescence studies and alternative techniques such as X-ray crystallography.

Using the 0.1 absorbance concentrations, fluorescence measurements were performed to find the emission maxima, λ_{em}, when exciting at 316 nm. The DMSO solutions of all compounds were purged with nitrogen before measurements in order to prevent the formation of phosphine oxide and to limit quenching by photobleaching (excited oxygen). The emission spectra for **3.6**, **3.10**, **3.12** and **3.16** when excited at 316 nm are shown in Figure 3.14.

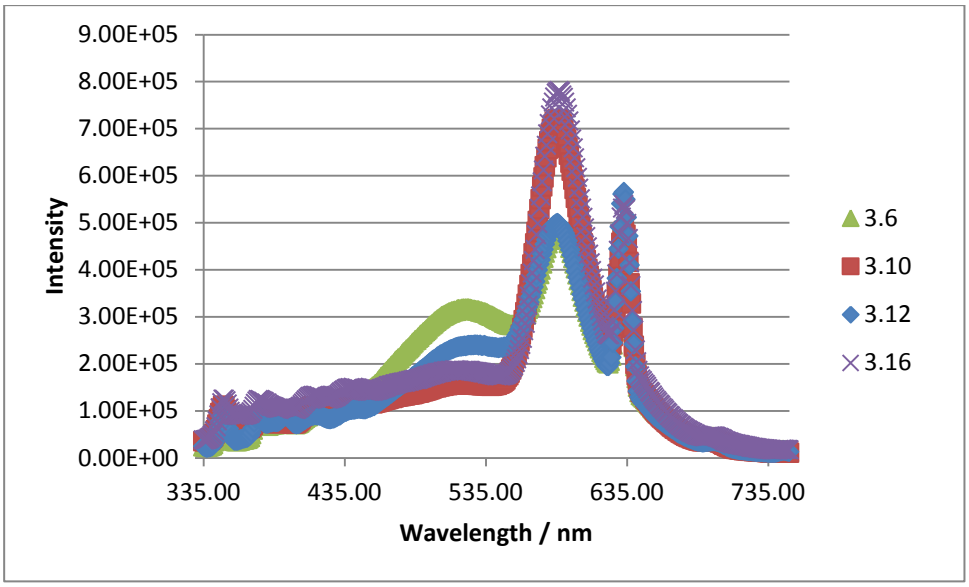

Figure 3.14 Emission profile of ligand **3.6** and corresponding complexes **3.10**, **3.12** and **3.16**. Recorded in DMSO at room temperature, with an excitation wavelength of 316 nm.

All compounds show an emission maximum at *ca.* 586 nm. Gold(I) complex, **3.16**, and platinum(II) complex, **3.10**, are the most fluorescent of the four compounds, with palladium complex, **3.12**, and ligand **3.6** showing similar lesser fluorescence

intensities. Since all of the compounds fluoresce at similar intensities and have similar Stokes shift, it is unlikely excitation at 316 nm could be used for sensing purposes. The graph also shows an additional peak at *ca.* 633 nm however this is twice the excitation wavelength and can be disregarded.

Table 3.2 Summary of UV absorbance and fluorescence data for **3.6** and respective complexes **3.10**, **3.12** and **3.16**.

Compound	Conc at 0.1 abs. ($x10^{-6}$) (mol dm^{-3})	Absorption Max (λ_{ex}) (nm)	Emission Max (λ_{em}) (nm)	Stokes shift ($\Delta\nu_{st}$) (nm)	Coeffiecent (ε)(cm^{-1} M^{-1})
3.6	8.44	316	587	271	11400
3.10	4.10	317	586	269	25500
3.12	3.18	316	586	270	24700
3.16	8.00	317	587	270	12850

To investigate the absorbance at 566 nm in the UV spectra for platinum(II) and palladium(II) compounds, **3.10** and **3.12**, a series of concentrations were made up in order to find 0.1 absorbance at 566 nm for the most absorbing compound **3.10**. Related compounds **3.6**, **3.12** and **3.16** were made up to an identical concentration at which **3.10** had 0.1 absorbance at 566 nm. These solutions were measured on the Fluoromax spectrophotometer to identify their emission spectra; the emission spectra is displayed in Figure 3.15.

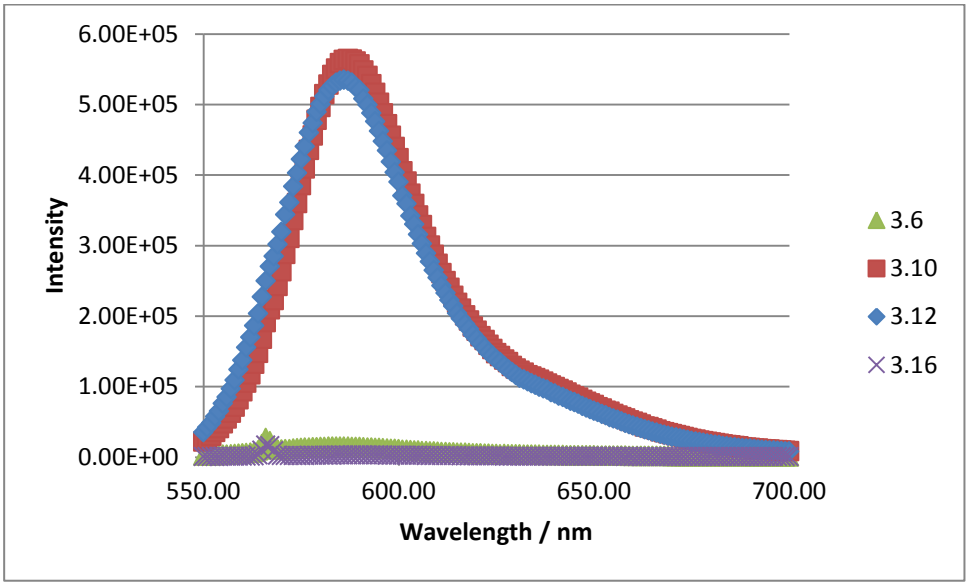

Figure 3.15 Emission profile of ligand **3.6** and corresponding complexes **3.10**, **3.12** and **3.16**. Recorded in DMSO at room temperature, with an excitation wavelength of 566 nm.

As shown in Figure 3.15, platinum and palladium compounds **3.10** and **3.12** strongly fluoresce, while ligand **3.6** and gold(I) complex **3.16** both show no fluorescence. This may suggest ligand **3.6** could be used as a "turn-on sensor" for the detection of Pt(II) and Pd(II) metals. Li *et al.* designed probe **1.71**, as shown in Figure 3.16.[108] Probe **1.71** is a colourless non-fluorescent compound, and much like ligand **3.6**, on addition of palladium(II) ions forms a pink, fluorescent solid; with palladium(II) coordinated **1.71** and **3.12** displaying similar absorption and emission bands (**1.71**: λ_{ex} 526 nm, λ_{em} 552 nm).[108] Probe **1.71** is ring opened on addition of Pd(II) ions, which leads to the change in fluorescence. It is likely that this is also the reason for the change in fluorescence of our rhodamine derivative (**1.71**) when coordinated to Pd(II) ions; though this needs to be investigated further.

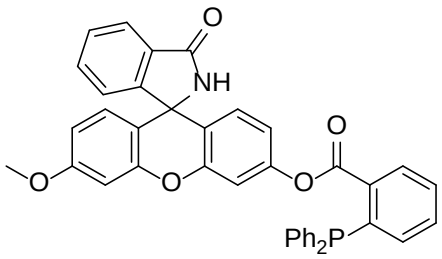

(1.71)

Figure 3.16 Chemical structure of palladium sensor, **1.71**, designed by Li *et al.*[108]

Since complexes **3.10** and **3.12** show an additional absorbance peak at 566 nm (unlike ligand **3.6** and gold complex **3.16**) and it is likely that spirocyclic ring-opening occurs on the complexation of ligand **3.6** to palladium(II) and platinum(II) metal centres, like that reported for **1.71**. Future work will further explore the photophysical properties of these compounds and investigate the photophysical properties of ligand **3.6** when coordinated to other metals to determine if spirocyclic ring-opening is limited to platinum(II) and palladium(II) complexes **3.10** and **3.12**.

3.4 The effect of pH on 3.5 and related coordination compounds

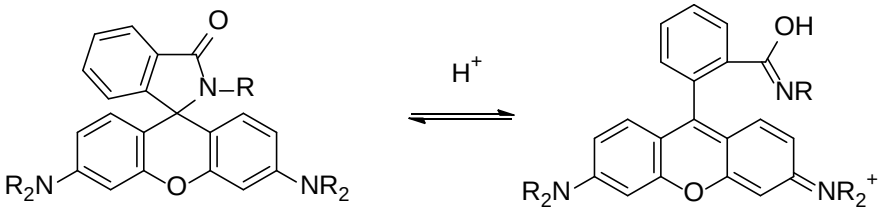

Figure 3.17 H^+ promoted ring opening of rhodamine amides.[103]

Some papers in the literature study utilise the ring opening of the spirolactam form of fluorescein and its derivatives for use in fluorescent sensors. The spirocyclic form of these fluorophores are often colourless and non-fluorescent, with the ring-open form coloured and highly fluorescent. Many researchers using fluorescein and rhodamine derivatives aim to synthesise a sensor which ring opens/closes allowing for the detection of the analyte of interest. In the presence of acid, the spirolactam ring will open, since the equilibrium is highly sensitive to pH of the solution. Many researchers try to exploit this for the synthesis of fluorescent sensors; Kang and colleagues are an example of this work. Kang and coworkers investigated rhodamine amides for the detection of volatile acids; the solid rhodamine amide changed from colourless to pink in the presence of H^+.

The writer of this thesis undertook an initial study on the effect acid had on the fluorescein derivative compounds synthesised as part of this thesis. Since a change in colour, observed by the naked eye, is known to be associated with the ring opened form of fluorescein derivatives, acid was added to solutions of ligand **3.5** and its associated coordination complexes and the colour of the solution was monitored by eye. Figure 3.18 shows the initial colour of a 0.01M DMSO (99+%) solutions of starting material fluorescein, **3.1**, fluorescein hydrazide, **3.3**, novel ligand **3.5** and subsequent coordination complexes **3.9**, **3.11** and **3.15**. Hydrochloric acid (100µL; 32%) was added to each 1 mL sample and the samples were monitored for a colour change to the naked eye over several hours.

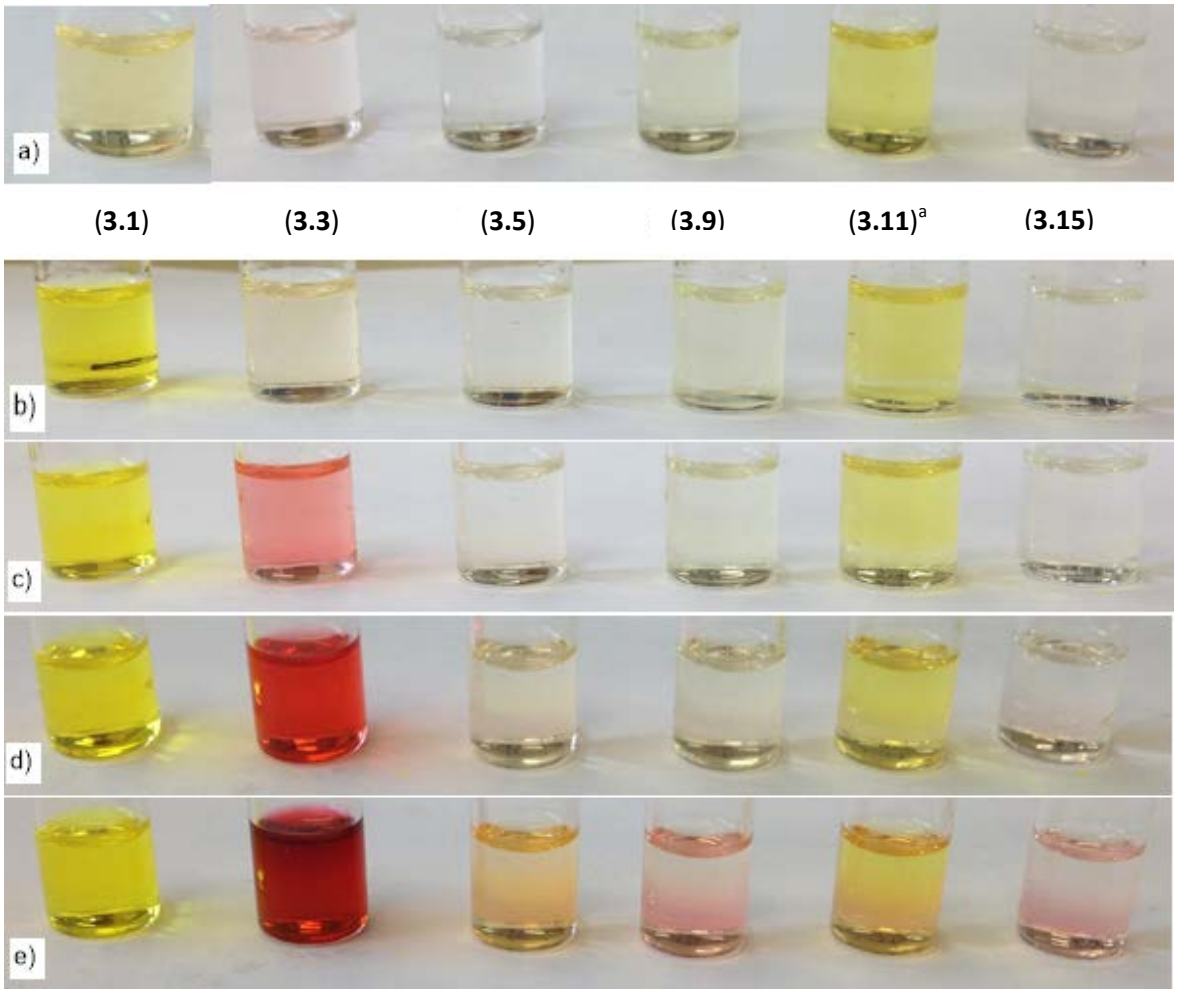

Figure 3.18 Colour change after addition of 100 microlitres 32% hydrochloric acids to 0.1M 1mL solutions of **3.1**, **3.3**, **3.5**, **3.9**, **3.11** and **3.15**. a) Solutions before addition of acid. b) Initial colour change of solutions on addition of acid. c) 30 mins after addition. d) 2h after addition. e) 5h after addition of acid. [a]Fine precipitate observed after the addition of acid.

On addition of hydrochloric acid (100µL; 32%), fluorescein, **3.1**, changes from pale yellow to dark yellow. All other solutions show minimal initial changes in colour. All metal complex solutions formed a precipitate on addition of the acid. Complexes **3.9** and **3.15** redissolved after a few seconds, but the fine precipitate formed for complex **3.11** took longer to redissolve and was not observed after 30 minutes. After 30 minutes the most notable change was the colour change for **3.3** which had become a bright pink solution. A pink solution indicates the ring-opening to the spirocyclic ring, as recorded in the literature.[108,103,161]

After two hours, **3.3** had further darkened in colour, but all other solutions appeared to remain the same. After five hours a light pink colour was observed in complexes **3.9**, **3.11** and **3.15** and a light orange colour formed in ligand **3.5**. This would indicate that

the fluorescein retains its spirolactam form in compounds **3.5**, **3.9**, **3.11** and **3.15** for up to five hours, unlike compounds **3.1** and **3.3**. While this rules out fluorescence sensing through activation on addition of acid, this was not an aim when synthesising the compounds described in this thesis, however it may indicate that compounds **3.5**, **3.9**, **3.11** and **3.15** have some stability in an acidic environment. Further studies need to be conducted to confirm the solution behaviour of these compounds before, during and after the addition of acid.

3.5 Synthesis of PCN containing fluoresceinamine isomer I derivatives

In order to investigate the influence the position the PCN moiety has, with respect to the fluorophore, on the photophysical properties of compounds synthesised as part of this thesis, a third compound, **3.18**, was synthesised for comparison purposes. Fluoresceinamine isomer I, **3.17**, is commercially available, low cost and has a primary amine located in the 5 position on the aromatic ring available for reaction with Ph_2PCH_2OH. A methanolic solution of 1 equiv. fluoresceinamine isomer I, **3.17**, and two equiv. Ph_2PCH_2OH was refluxed for 3h, followed by a 72h stir at r.t. The dark brown solution was reduced in volume by 50% to give a light brown precipitate, which was filtered to provide compound **3.18** with a yield of 63%. An increase in reflux and stirring time appeared to have little effect on yield. Reduction of the solution to 1-2mL followed by filtration of the resulting precipitate also gave no improvement in yield and was coupled with a less pure product, as determined by $^{31}P\{^1H\}$ NMR.

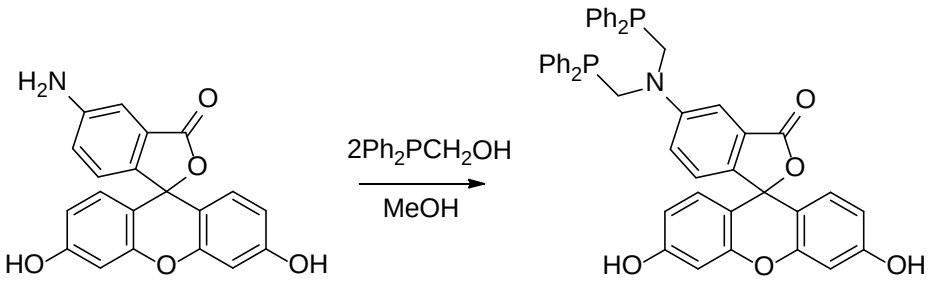

(**3.17**) (**3.18**)

Scheme 3.10 Synthesis of *bis*phosphine ligand **3.18**.

The $^{31}P\{^1H\}$ NMR spectrum of compound **3.18** recorded in d_6-DMSO gave a single resonance at -28.4 ppm, in the region typical for *bis*phosphine PCNCP ligands as discussed in Chapter 4 of this thesis and in the literature; *bis*(methylphosphino)aniline displays a $^{31}P\{^1H\}$ NMR resonance at -27.2 ppm.[140,139] A singlet resonance at 4.13 ppm

indicative of PCH_2 was observed in the ^1H NMR spectrum with an integration of four and there was no appearance of an NH peak, supporting the formation of *bis*-phosphine **3.18**. IR analysis displayed no NH stretches, with only one broad peak observed between 3000-4000 cm^{-1} corresponding to the OH vibration. ESI-MS also supported the formation of compound **3.18** exhibiting a $[M-H]^+$ fragment at *m/z* 744.2049. Despite numerous attempts, X-ray quality crystals of compound **3.18** were not obtained.

3.5.1 Coordination studies with platinum(II)

In a similar fashion to the synthesis of **3.9** and **3.10**, ligand **3.18** was reacted with equimolar amounts of $PtCl_2$(cod) to yield a chocolate brown solid **3.19** in a yield of 97%. A singlet resonance at -12.0 ppm with associated satellites ($^1J_{PtP}$ = 3440Hz) was observed in the $^{31}P\{^1H\}$ NMR spectra of *cis*-configured complex **3.19**. *Bis*phosphine compounds **2.16 – 2.19**, as described in Chapter 2, display similar $^1J_{PtP}$ coupling constants ($^1J_{PtP}$ = 3450 Hz) to ligand **3.19**; this would support the conclusion that platinum and the respective phosphine moieties in compounds **2.16 – 2.19** and ligand **3.19** are in similar chemical environments.

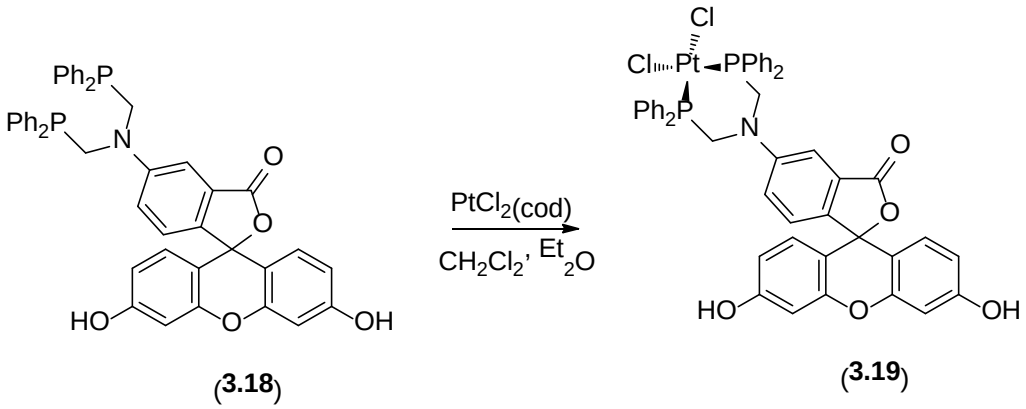

(**3.18**) (**3.19**)

Scheme 3.11 Synthesis of platinum(II) complex **3.19**.

FT-IR analysis of **3.19** also confirmed coordination to the dichloroplatinum fragment in a *cis*-configuration through the presence of two vPt-Cl stretches at 317 and 289 cm^{-1}.[146] In the ^1H NMR spectrum, the PCH_2 singlet peak for **3.19** shifted downfield in comparison to ligand **3.18** by 0.85 ppm. Formation of product **3.19** is supported by elemental analysis and also by ESI-MS which displayed fragmentation at *m/z* 973.1312 which is attributed to $[M-Cl]^+$. Unfortunately, crystals of **3.19** suitable for X-ray crystallography were not obtained.

3.5.2 Coordination studies with palladium(II)

Complex **3.20**, a brown solid, was synthesised from the reaction of equimolar amounts of ligand **3.18** and $PdCl_2$(cod) in a yield of 81%. Analysis by $^{31}P\{^1H\}$ NMR showed a single resonance at 2.6 ppm.

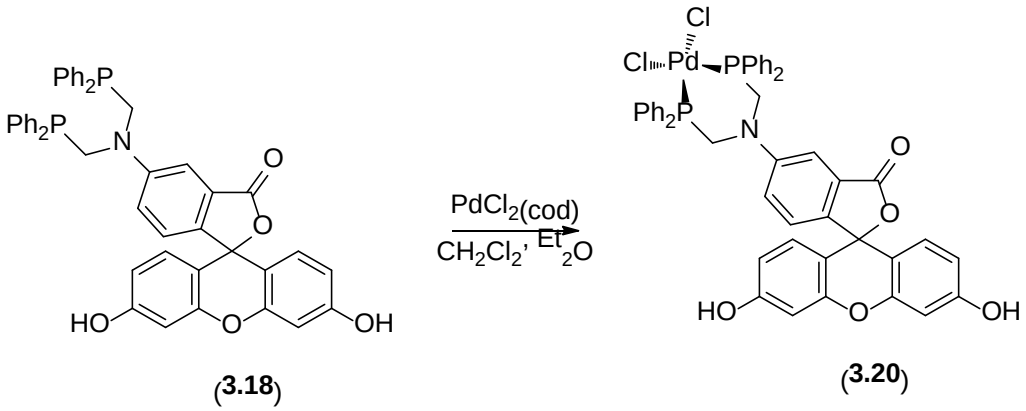

(**3.18**) (**3.20**)

Scheme 3.12 Synthesis of palladium(II) complex **3.20**.

Similarly to analogous platinum(II) compound **3.19**, the ^1H NMR showed a downfield shift of 0.85 ppm for the PCH_2 singlet resonance in **3.20** from parent **3.18**. ESI-MS displayed fragments representative of $[M+H]^+$ and $[M-Cl]^+$ at *m/z* 920.0461 and 884.0698, respectively. Elemental analyses confirmed the empirical formulae for **3.20**, though **3.20** had some CH_2Cl_2 present, as also seen in the ^1H NMR, which were taken into account. Despite numerous attempts, crystals of compound **3.20** suitable for X-ray crystallography were not obtained.

3.5.3 Coordination studies with gold(I)

Lastly, ligand **3.18** was reacted with Au(tht)Cl in a 1:2 ratio generating the binuclear compound **3.21**, a reddish-orange precipitate, in a yield of 74%. The $^{31}P\{^1H\}$ NMR spectrum of compound **3.21** in d_6-DMSO displayed a single resonance at 19.3 ppm, some 48 ppm downfield from the parent ligand **3.18**, a typical shift for linear P-Au-Cl coordination complexes, as observed in Chapter 2 and Chapter 4 of this thesis, as well as in literature.[145]

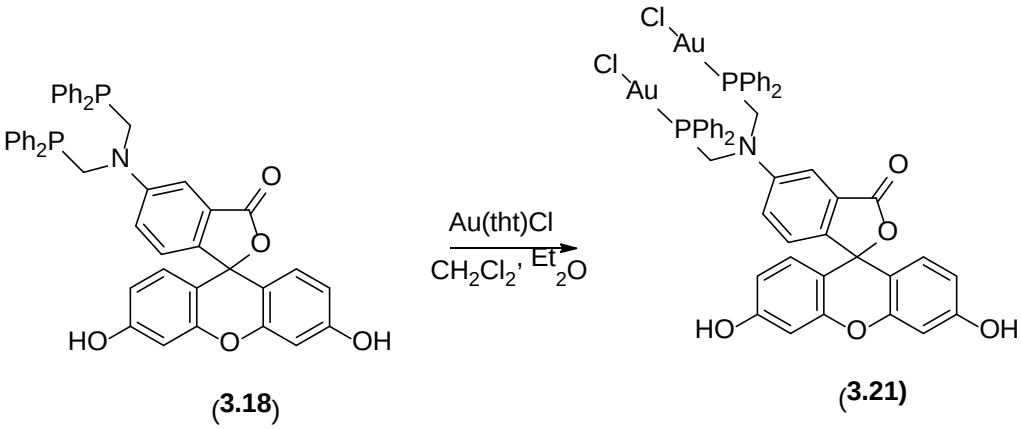

Scheme 3.13 Synthesis of gold(I) complex **3.21**.

ESI-MS analysis exhibits a $[M+H]^+$ fragment at *m/z* 1208.0760 and elemental analysis was in agreement with the empirical formula for **3.21** with some CH_2Cl_2 impurity present, also observed in the ^1H NMR. Lastly, examination of the IR spectrum of the complex showed an Au-Cl IR stretch at v326 cm^{-1}, a wavelength typical for complexes of this type.[145] Despite numerous attempts, crystals of compound **3.21** suitable for X-ray crystallography were not obtained.

3.6 Preliminary photophysical studies

An initial check for luminescence using a black light was performed on ligand **3.18** and respective complexes **3.19** – **3.21**; the results of which are shown in Figure 3.19. Ligand **3.18** appears to luminesce brightly, with no observed luminescence observed for corresponding complexes **3.19** – **3.21**.

Figure 3.19 Image in daylight, on left, and image of compounds under a black light, on the right. Compounds ordered **3.18** – **3.21**, from left to right, in both images.

Ligand **3.18** and its respective complexes **3.19** – **3.21** were dissolved in DMSO (99%+) and investigated by UV absorbance for their excitation maxima, λ_{ex}, and concentration at which the sample has 0.1 absorbance at said maxima. Fluoresceinamine isomer I, **3.17**, has limited fluorescence due to intramolecular quenching, as a result of the donation of the amine lone pair into the fluorophore's pi system.[162] Excitation and emission maxima are observed at λ_{ex}= 488 nm and λ_{em}= 530 nm for fluoresceinamine **3.17**, however for ligand **3.18** and related complexes **3.19** - **3.21** no UV absorbance in this region. This suggests that intramolecular quenching is also present here. Despite this ligand **3.18** and complexes **3.19** – **3.21** all showed a single absorbance maxima at 277 nm.

Using the 0.1 absorbance concentrations, fluorescence measurements were performed to find the emission maxima, λ_{em}, when exciting at 277 nm. The DMSO solutions of all compounds were purged with nitrogen before measurements in order to prevent the formation of phosphine oxide and to limit quenching by photobleaching (excited oxygen). The emission spectra for **3.18** – **3.21** when excited at 277 nm are shown in Figure 3.20.

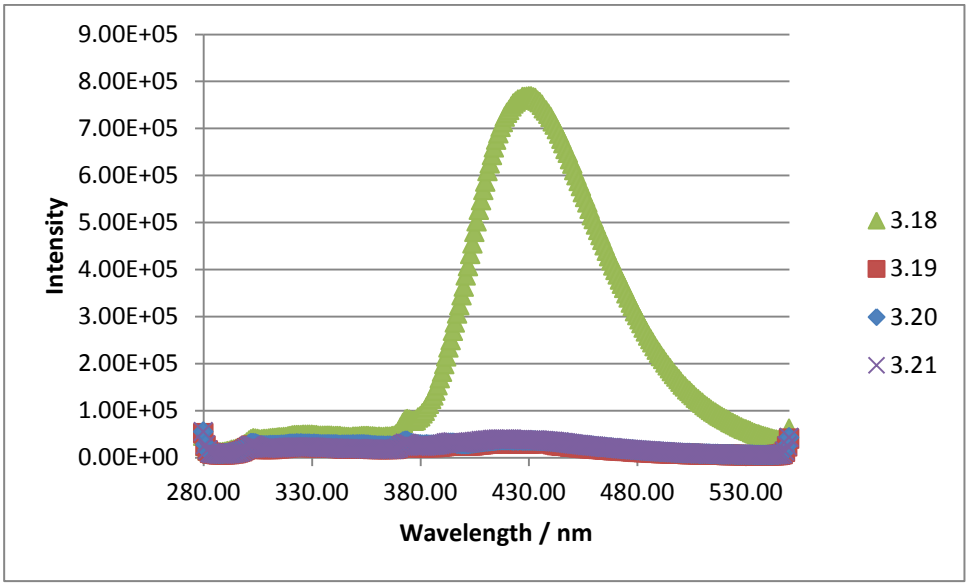

Figure 3.20 Emission profile of ligand **3.18** and corresponding complexes **3.19**, **3.20** and **3.21**. Recorded in DMSO at room temperature, with an excitation wavelength of 277 nm.

The UV spectra of ligand **3.18** and complexes **3.19** – **3.21** at a concentration of $1x10^{-4}$ $moldm^{-3}$ show ligand **3.18** and platinum(II) complex **3.19** have the greatest and similar

absorbance intensities at 277 nm. However the emission spectra does not reflect the emission spectra, with only the phosphine **3.18** showing any emission in the region 280 – 530 nm. This is also seen in Figure 3.19, where only ligand **3.18** appears to luminescence under black light. No emission for complexes **3.19** – **3.21** may be due to MLCT. The emission maxima, λ_{em}, for ligand **3.18** was observed at 430 nm giving a Stokes shift of 155 nm.

Table 3.3 Summary of UV and fluorescence data for **3.18** and respective complexes.

Compound	Conc at 0.1 abs. (x 10^{-6}) (mol dm^{-3})	Absorption Max (λ_{ex}) (nm)	Emission Max (λ_{em}) (nm)	Stokes shift ($\Delta\nu_{st}$) (nm)	Coeffiecent (ε)(cm^{-1} M^{-1})
3.18	3.54	275	430	155	39100
3.19	3.30	277	-	-	32450
3.20	1.09	274	-	-	30200
3.21	6.74	277	-	-	20750

Further work investigating the photophysical properties of ligand **3.18** and its corresponding complexes will be continued by the Smith group, with exploration of the potential of compound **3.18** to act as "turn-off" fluorescence sensor for the determination of metals, such as Pd(II), Pt(II) and Au(I), though future studies may investigate differences in fluorescence emission with a number of other metals.

3.7 Summary

Fluorescein and rhodamine spirolactams have undergone amidation, followed by the phosphorus analogous Mannich condensation using Ph_2PCH_2OH to successfully synthesize monofunctionalised PCN fluorescent probes **3.5** and **3.6**, the first of their kind. The coordination chemistries of these ligands have been investigated with a variety of metals and all metals used are known to possess medicinal properties, such as antitumour properties - as discussed in Section 1.4 of this thesis. Furthermore, ligand **3.5** underwent complexation with cyclopalladated species, which are of interest medicinally for the stabilisation of Pd(II) *in vivo*. Attempts to synthesise a *bis*(phosphine) ligand were not successful under the conditions trialled. The UV absorption and fluorescence of these ligands and their subsequent complexes have been briefly studied and require further work to determine their potential use as fluorescent sensors.

Fluoresceinamine isomer I was also investigated to explore the impact the position of the phosphine donors had on photophysical properties, as well as provide a *bis*-substituted PCN fluorescein derivative. Novel ligand **3.18** was successfully synthesised and fully characterised, as were related coordination compounds **3.19** - **3.21**. A preliminary study of the photophysical properties of **3.18** - **3.21** may suggest the potential for ligand **3.18** to be used as a "turn-off" fluorescence sensor.

Fluorescein derivatives have been explored in the literature for medicinal applications such as sensors in cellular imaging.[107] Therefore novel ligands **3.5**, **3.6** and **3.18** have potential for medicinal applications and will be explored further by the Smith group in the future.

Chapter 4 - Synthesis and characterisation of aminomethylphosphine functionalised amino acids and their subsequent coordination chemistries

4.1 Phosphine functionalised amino acids

Research into the synthesis of compounds with potential as radiopharmaceuticals has grown hugely in recent years.[3,163–165] Within this, a wide variety of chelating moieties have been studied; one area of interest is the use of phosphine donors to coordinate to radioactive metal centres. Phosphine donors are attractive since the chemical and physical properties of the phosphine, itself and subsequent coordinated metal-phosphine complexes can be manipulated through the modification of substituent groups on the phosphine. Blower and Katti were among the first to investigate phosphine containing chelators for radiopharmaceutical purposes.[41,54] Since then, a range of different variations have been investigated, including aminomethylphosphine coordination complexes with rhenium, as studied by Zhang *et al*.[3] Zhang and coworkers utilised the phosphorus analogous Mannich condensation reaction to synthesise aminomethylphosphines, ligands **4.1 – 4.3**, as an example, from amino acids and related derivatives. Once the phosphine moieties were added, ligands **4.1 – 4.3** underwent coordination, with the view that after coordination the amino acid could be extended through the carboxylic acid moiety to a peptide-based targeting vector in a "preformed chelate" fashion.[3]

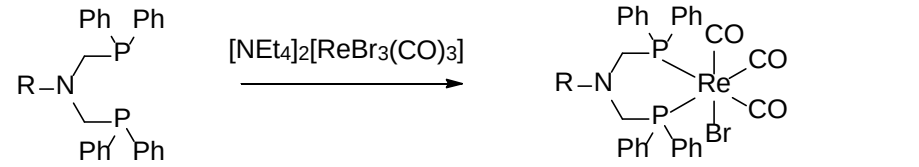

R = **(4.1)** $CH_2CH_2CO_2H$
(4.2) CH_2CO_2H
(4.3) $CH_2CONHCH_2CO_2H$

R = **(4.4)** $CH_2CH_2CO_2H$
(4.5) CH_2CO_2H
(4.6) $CH_2CONHCH_2CO_2H$

Scheme 4.1 Coordination reaction between ligands **4.1 – 4.3**, synthesised by the phosphorus analogous Mannich condensation, with a rhenium tricarbonyl precursor.[3]

Aminomethylphosphine compounds **4.1 – 4.3** are attractive as the phosphine moiety can coordinate to a broad range of metals; the Smith group previously investigated the synthesis of ligands **4.1**, **4.2**, **4.7** and their subsequent coordination with platinum(II), gold(I) and ruthenium(II) metal centres.[145] These compounds are attractive since a

range of different substituents can be attached to the amino acid group, including substituents for conjugation to a targeting vector or substituents for increased water solubility. Additionally, as observed by Zhang *et al.* through conjugation of the targeting vector through the central atom in the diphosphine backbone, steric hindrance is minimised between the targeting vector and the coordination sphere.[3]

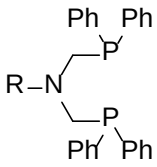

R = (**4.7**) $CH_2CONHCH_2CONHCH_2CO_2H$

Figure 4.1 Aminomethylphosphine ligand, **4.7**, synthesised by the Smith group.[145]

In the following sections, the syntheses of a number of aminomethylphosphines from a range of amino acids will be discussed, expanding the number of compounds of this type known in the literature. The coordination chemistries of known and unknown ligands of this type will also be investigated utilising, in the first instance, gold(I), platinum(II) and ruthenium(II) metals - this is a continuation of the work previously initated within the Smith group.[145] While medicinal applications are of interest here, it should also be noted that aminomethylphosphines of this type (**4.1** – **4.3**) also have applications elsewhere.[8,9,145]

4.2 Synthesis of Aminomethylphosphine containing Amino Acids

Utilising the phosphorus analogous Mannich based condensation reaction, a series of symmetric PCNCP ligands, **4.2**, **4.3**, **4.7**, **4.12** – **4.15** and **4.19** – **4.21**, were prepared by reacting two equivs. of PPh_2CH_2OH with one equiv. of the appropriate primary amine (Schemes 4.2 and 4.3). Conditions varied from ligand to ligand synthons, with the progress of all reactions monitored by $^{31}P\{^1H\}$ NMR.

Initially primary amines glycine, glycylglycine and triglycine were used; for the synthesis of **4.2**, a procedure described by Kellner *et al*. was followed, and for the synthesis of **4.3** and **4.7** a procedure described by the Smith group was replicated.[145,14] These procedures involved stirring the starting materials at rt. under N_2 for 18h in methanol. While this worked well for the synthesis of **4.2** and **4.3**, the triglycine counterpart **4.7** was improved through refluxing over 18h in methanol to give a purer

product than when using the original procedure.[145] Data collected for **4.2**, **4.3** and **4.7** agreed with analysis described in the literature.[14,145]

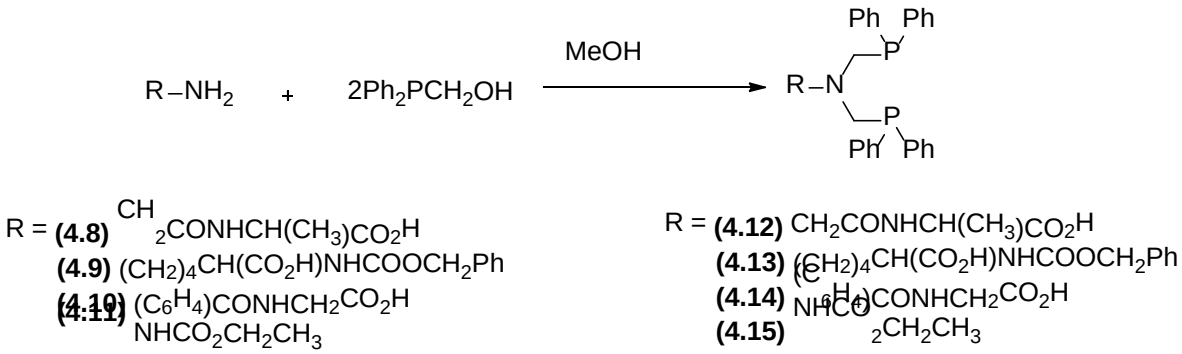

Scheme 4.2 Synthesis of ligands **4.12 – 4.15**.

Similarly novel *bis*phosphines **4.12 – 4.14** were synthesised using the same conditions as **4.2** and **4.3**. Glycyl-L-alanine was investigated for comparison against dipeptide glycylglycine, while *p*-aminohippuric acid was studied due to its known use as a diagnostic agent.[166] N-alpha-Cbz-L-lysine was explored as the second amine protected by the carboxybenzyl moiety provides an additional functional group suitable, once deprotected, for conjugation to a peptide or conjugation to alternative moieties for the purposes of modifying chemical properties or providing an additional donor site for coordination to another metal.

To synthesise **4.15** identical conditions to those utilised in the synthesis of **4.2** and **4.3** were investigated, however the reaction did not proceed fully under these conditions. Refluxing over 18h in methanol was also trialled, in a similar fashion to **4.7**, but again the reaction did not reach completion. Finally, a 24h reflux in toluene and methanol (3:1) was found to generate **4.15** in quantitative yields.

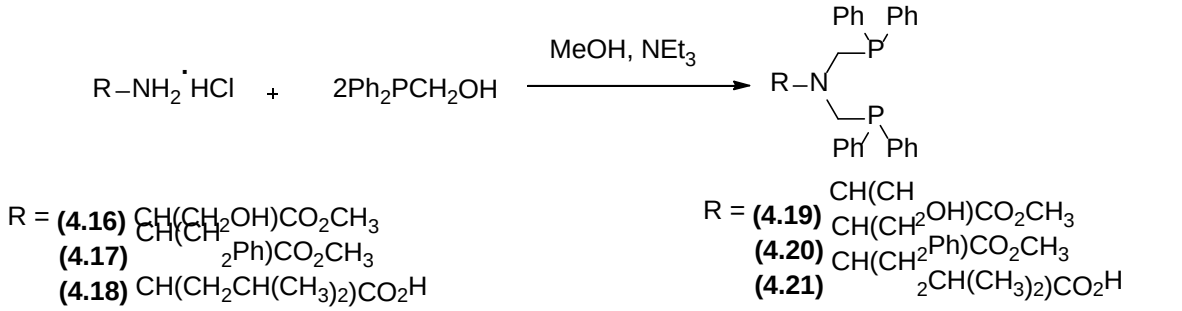

Scheme 4.3 Synthesis of ligands **4.19 – 4.21**.

Next, L-serine and L-phenylalanine underwent esterification with methanol in the presence of thionyl chloride (0.1 mL) using a known literature procedure, generating methyl esters **4.16** and **4.17**.[167] Data collected for **4.16** and **4.17** were in agreement with that recorded in the literature.[167] Amines **4.16**, **4.17** and commercially purchased L-leucine methyl ester, **4.18**, were then refluxed with PPh_2CH_2OH in methanol over 48h. Triethylamine was also added to each of the reaction mixtures since starting materials **4.16** - **4.18** are all hydrochloride salts, and in the presence of acid the phosphorus analogous Mannich condensation reaction is hindered.

Unlike similar compounds discussed here **4.19 – 4.21** were not white solids, but were colourless oils. This may be due to residual triethylamine hydrochloride, as supported by NMR analysis, which could not be removed under vacuum or through recrystallisation. As a result **4.19 – 4.21** oxidised much quicker than other aminomethylphosphines discussed here, and were difficult to handle. Compounds **4.19 – 4.21** have been synthesised previously and the data recorded matches that described in literature.[9]

The yields achieved for compounds, **4.2**, **4.3**, **4.7**, **4.12 – 4.15** and **4.19 – 4.21**, were in the region of 44 to 98%. All *bis*phosphines synthesised here exhibited a singlet resonance in their respective $^{31}P\{^1H\}$ NMR spectra in the range of δ(P) -25.7 and -27.4 ppm. This is fairly typical of *bis*(phosphino)amines incorporating the $–PPh_2CH_2$ group, and is approximately 16 ppm upfield from the PPh_2CH_2OH starting material [δ(P) -10.0 ppm].[139,168] It is worth noting that altering the R substituent on $(PPh_2CH_2)_2NCH(R)CO_2H$ has very little influence on the $^{31}P\{^1H\}$ signals of these compounds. Analyses of all previously recorded compounds match that recorded in the literature.[9,145] Formation of novel compounds is supported by ESI-MS, IR and CHN analysis.

4.2.1 Synthesis of monophosphine 4.24

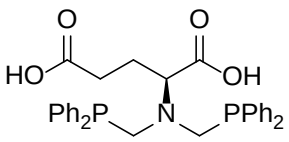

(4.22)

Figure 4.2 Desired product **4.22**.

L-glutamic acid was reacted with two equivs. of PPh_2CH_2OH in order to synthesise the intended product **4.22**, as shown in Figure 4.2. Despite varying the reaction conditions,

the $^{31}P\{^{1}H\}$ NMR spectra of resulting solutions, disregarding starting material phosphine peaks, showed a single resonance at δ -22.5 ppm with a maximum integration of 45%. A peak in the region of δ -20 to -25 ppm in an $^{31}P\{^{1}H\}$ NMR spectrum is indicative of monofunctionalised aminomethylphosphine compounds.[156] Coupled with the maximum yield obtained, it was likely a monosubstituted phosphine product had formed. L-glutamic acid and PPh_2CH_2OH were refluxed over 4h in methanol, in a 1:1 stoichiometry; this successfully resulted in the formation of a white solid, **4.24**, in a yield of 92%.

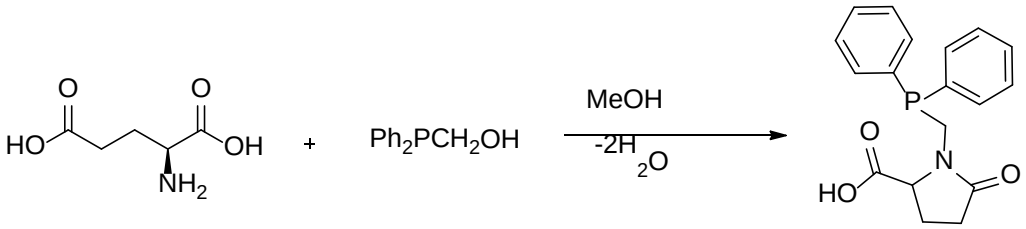

(4.23) **(4.24)**

Scheme 4.4 Synthesis of ligand **4.24**.

When refluxed, glutamic acid cyclises into pyroglutamic acid and can therefore undergo addition of only one phosphine moiety. The presence of the pyro form of glutamic acid is evident from the ^{1}H NMR spectrum; two CH_2 groups are indistinguishable from each other and are split into multiple peaks due to the fixed conformation of the 5-membered ring. The ^{1}H NMR spectrum shows no presence of uncyclised glutamic acid with only compound **4.24** present. This would indicate that in solution only one species is present - that being compound **4.24**. No vNH IR peaks are present, in agreement with the proposed compound; ESI-MS further confirmed the proposed structure as **4.24**. Compound **4.24** is air-stable as a solid, however if left in solution in the prescence of oxygen **4.24** will form the phosphine oxide.

4.2.2 Molecular structure of the oxide of phosphine 4.24

Crystals of the oxide of ligand **4.24** suitable for X-ray crystallography were grown by slow evaporation of a CH_2Cl_2/Et_2O filtrate of **4.24**. Selected bond lengths and angles for the oxide of **4.24** can be found in Table 4.1, with a molecular structure shown in Figure 4.3. According to the CSD database there are 100+ examples with a pyroglutamic acid moiety known, however no example contains a phosphine moiety directly attached to the pyroglutamic acid; therefore the oxide of **4.24**, shown in Figure 4.3, is the first of

its kind.[132] Bond lengths and angles of the pyroglutamic moiety of ligand **4.24** are in keeping with the literature.[169]

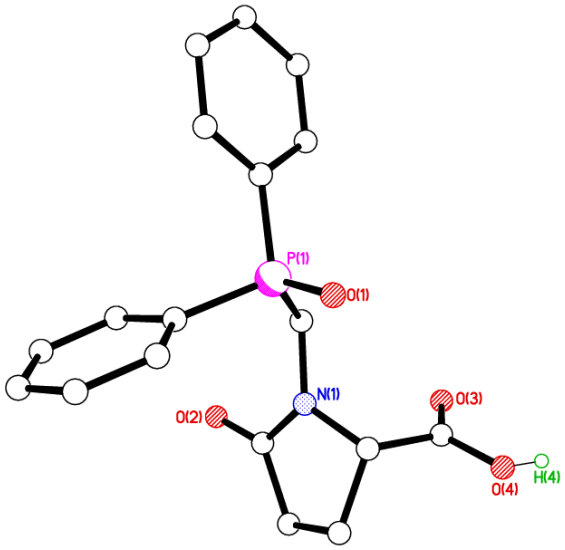

Figure 4.3 Molecular structure of **4.24** oxide. All hydrogen atoms, except H(4), and solvent molecules omitted for clarity.

There are six phosphine oxide ligands per unit cell, all of which are *R*-enantiomers at C(17) bearing the $-CO_2H$ group. The six molecules of **4.24** oxides in a unit cell are coupled in pairs with head-to-tail, but non-centrosymmetric, hydrogen bonding between the hydroxyl proton and the phosphine oxide [average bond length (O(4)—H4···O1X) is 2.557 Å] - this generates a 16-membered ring; an example is shown in Figure 4.4. One molecule of diethyl ether was also present per unit cell. This was modelled with all atoms two-fold disordered.

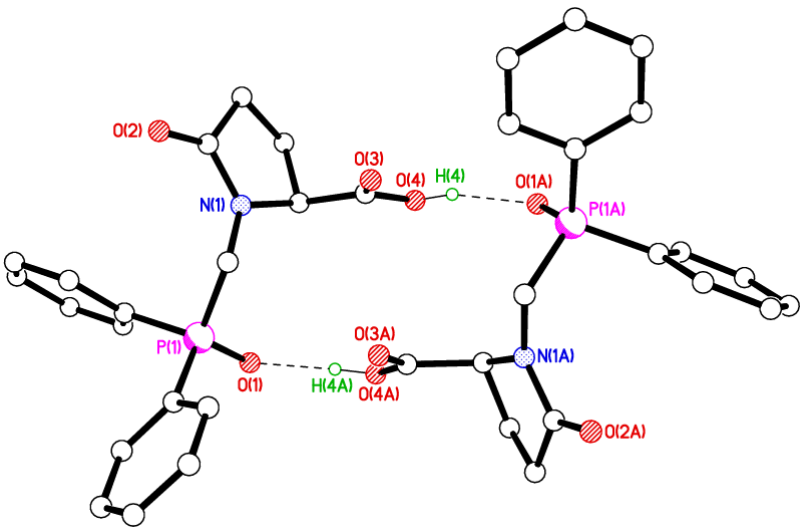

Figure 4.4 Packing structure of **4.24** oxides, showing the dimer pair. All hydrogen bonds, except H(4) and H(4A), and solvent molecules were removed for clarity.

Table 4.1 Selected bond lengths (Å) and angles (°) for the oxide of **4.24** (averaged from the six molecules in the unit cell)

O1—P1	1.5014 (17)	O1—P1—C8	111.50 (11)
P1—C2	1.797 (2)	C2—P1—C8	109.06 (11)
P1—C8	1.798 (2)	O1—P1—C1	112.95 (10)
P1—C1	1.820 (2)	C2—P1—C1	104.51 (10)
C1—N1	1.452 (3)	C8—P1—C1	106.00 (11)
O1—P1—C2	112.38 (10)	N1—C1—P1	112.70 (15)

4.2.3 Coordination studies with gold(I)

Ligands **4.12** – **4.15** and **4.19** – **4.21** were reacted with 2 equivs. of Au(tht)Cl (tht = tetrahydrothiophene) in CH_2Cl_2, resulting in air stable white powders of complexes **4.25** – **4.31** on addition of Et_2O to a reduced CH_2Cl_2 solution. Labile tht is replaced with one phosphine leading to the formation of neutral binuclear gold(I) complexes, as shown in Scheme 4.5. The yields achieved for complexes **4.25** – **4.31** ranged from 45 to 82%.

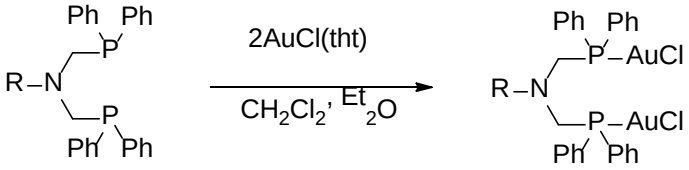

R = **(4.12)** $CH_2CONHCH(CH_3)CO_2H$
(4.13) $(CH_2)_4CH(CO_2H)NHCOOCH_2Ph$
(4.14) $(C_6H_4)CONHCH_2CO_2H$
(4.15) $CH(CH_2CH_2CH_3$
(4.19) $CH(CH_2OH)CO_2CH_3$
(4.20) $CH(CH_2Ph)CO_2CH_3$
(4.21) $_2CH(CH_3)_2)CO_2H$

R = **(4.25)** $CH_2CONHCH(CH_3)CO_2H$
(4.26) $(CH_2)_4CH(CO_2H)NHCOOCH_2Ph$
(4.27) $(C_6H_4)CONHCH_2CO_2H$
(4.28) $NHCO_2CH_2CH_3$
$CH(CH$
(4.29) $CH(CH_2OH)CO_2CH_3$
(4.30) $CH(CH_2Ph)CO_2CH_3$
(4.31) $_2CH(CH_3)_2)CO_2H$

Scheme 4.5 Synthesis of binuclear gold(I) complexes **4.25** – **4.31**.

A sharp single resonance was observed in the $^{31}P\{^1H\}$ NMR spectra for all complexes (**4.25** – **4.31**) at approximately δ 21 ppm (in $CDCl_3$) - a significant downfield shift from

free ligands **4.12** – **4.15** and **4.19** – **4.21**. This is in agreement with analogous complexes, **4.32** and **4.33**, also synthesised by the Smith group. Analysis of the data for complexes **4.32** and **4.33** (shown in Figure 4.5) are summarised alongside complexes **4.25** – **4.31** in Table 4.2.[145]

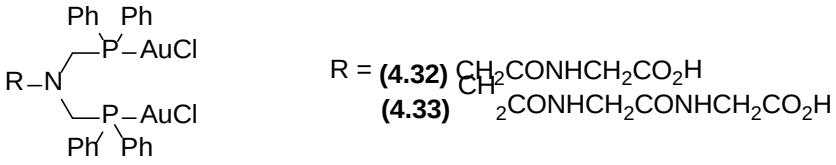

Figure 4.5 Binuclear gold(I) complexes previously synthesised by the Smith group.[145]

Additional analyses supported the formation of complexes **4.25** – **4.31**; ESI-MS data displayed $[M\text{-}Cl]^+$ fragments for all seven gold(I) coordination complexes and IR analyses featured vAuCl stretches in the range of 315 – 330 cm^{-1}, typical of gold chloride stretches.[170,171] Elemental analyses were also in agreement with the expected formulae for complexes **4.25** – **4.28**. Despite numerous attempts to crystallise complexes **4.25** – **4.31**, X-ray quality crystals could not be obtained.

Table 4.2 Selected $^{31}P\ \{^1H\}$ NMR, MS and IR data for complexes **4.25** to **4.33**[a]

Compound	δ(P)	ν_{AuCl}	*m/z* $[M\text{-}Cl]^+$ found (ppm difference)
4.25	19.4	327	971.0888 (1.5 ppm)
4.26	18.3	318	1105.1662 (2.0 ppm)
4.27	17.6	328	1019.0903 (0.1 ppm)
4.28	22.6	328	944.0778 (2.0 ppm)
4.29	21.2	319	944.0776 (1.9 ppm)
4.30	21.8	325	990.1001 (0.0 ppm)
4.31	21.9	327	970.1297 (1.7 ppm)
4.32[b,c]	23.1	-	957
4.33[b,c]	23.4	-	1014

[a] NMR data for complexes **4.25** – **4.31** were recorded in $CDCl_3$ (in ppm). All IRs were recorded as KBr discs (in cm^{-1}), [b] NMR was recorded in d-DMSO, [c] Data were taken from reference 145.

4.2.4 Coordination studies with gold(I) and ligand 4.24

Mono-phosphine ligand **4.24** also underwent coordination to Au(tht)Cl, following identical conditions to that of **4.25** – **4.31**, with alteration of only the stoichiometry of

starting materials. The reaction of 4.24 and Au(tht)Cl in a 1:1 ratio generated a white solid **4.34** in a yield of 53%.

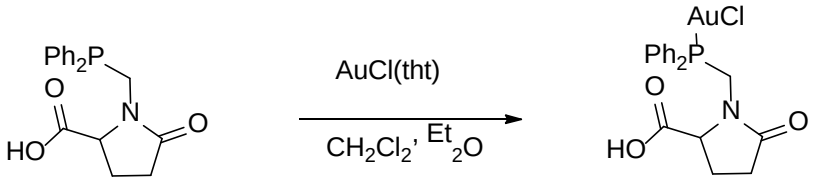

(4.24) **(4.34)**

Scheme 4.6 Synthesis of mononuclear gold(I) complex **4.34**.

The $^{31}P\{^{1}H\}$ NMR spectrum for complex **4.34** displayed a singlet peak at 22.4 ppm (in $CDCl_3$), at a similar resonance to complexes **4.25** – **4.31**. The ^{1}H NMR spectrum for complex **4.34** showed a downfield shift for the NCH and PCH_2 hydrogens from 4.8 and 3.6 ppm to 5.3 and 4.8 ppm respectively. Support for the preparation of **4.34** was also obtained from ESI-MS results which revealed a $[M\text{-}Cl]^+$ fragment for **4.34** at *m/z* 524.0667. Despite numerous attempts to obtain crystals of gold(I) complex, **4.34**, only powdered material was obtained. No additional analysis was performed on the powdered material yielded.

4.2.5 Coordination studies with platinum(II)

Ditertiary aminophosphine ligands **4.12** – **4.15** and **4.19** – **4.21** were reacted with a platinum(II) precursor, $PtCl_2$(cod) (cod = cycloocta-1,5-diene), in equimolar proportions to prepare mononuclear complexes **4.35** – **4.41** in yields of 52 - 94%. Similarly to the formation of gold(I) complexes **4.25** – **4.31**, the mechanism of reaction is ligand substitution, however in this case labile cod is removed. The $^{31}P\{^{1}H\}$ NMR spectra for these complexes featured a single resonance with a large downfield shift in comparison to the free ligand, and also featured associated ^{195}Pt satellites with $^{1}J_{PtP}$ coupling constants in the region expected for *cis* platinum-phosphine coupling (3400 to 3700 Hz).[158]

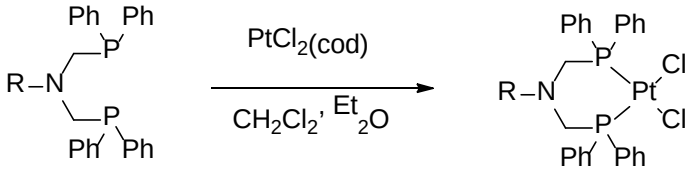

R = **(4.12)** $CH_2CONHCH(CH_3)CO_2H$
(4.13) $(CH_2)_4CH(CO_2H)NHCOOCH_2Ph$
(4.14) $(C_6H_4)CONHCH_2CO_2H$
(4.15) $CH(CH_2CH_2CH_3$
(4.19) $CH(CH_2OH)CO_2CH_3$
(4.20) $CH(CH_2Ph)CO_2CH_3$
(4.21) $_2CH(CH_3)_2)CO_2H$

R = **(4.35)** $CH_2CONHCH(CH_3)CO_2H$
(4.36) $(CH_2)_4CH(CO_2H)NHCOOCH_2Ph$
(4.37) $(C_6H_4)CONHCH_2CO_2H$
(4.38) $NHCO_2CH_2CH_3$
$CH(CH$
(4.39) $CH(CH_2OH)CO_2CH_3$
(4.40) $CH(CH_2Ph)CO_2CH_3$
(4.41) $_2CH(CH_3)_2)CO_2H$

Scheme 4.7 Synthesis of platinum(II) complexes **4.35** – **4.41**.

Cis conformation was further confirmed by the presence of two νPtCl stretches present in the FT-IR spectra of complexes **4.35** – **4.41**. $^{31}P\{^1H\}$ NMR and IR data is summarised in Table 4.3 along with data collected from analogous compounds, **4.42** and **4.43**, previously synthesised by the Smith group.[145] ESI-MS was collected for each of the synthesised complexes with $[M\text{-}Cl]^+$ fragments found in all cases. Elemental analyses were performed on all samples and were in agreement with the proposed empirical formulae for complexes **4.35**, **4.36** and **4.38**.

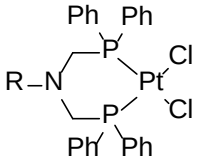

R = **(4.42)** $CH_2CONHCH_2CO_2H$
(4.43) $CH_2CONHCH_2CONHCH_2CO_2H$

Figure 4.6 Chemical structure of compounds **4.42** and **4.43** synthesised previously by the Smith group.[145]

Table 4.3 Summary of NMR and IR data for complexes **4.35** to **4.43**.[c]

Complex	δ(P)	^1J(PtP)	ν_{PtCl}
4.35[b]	-10.0	3392	294, 308
4.36[a]	-7.8	3407	294, 312
4.37[b]	-10.7	3487	292, 308
4.38[b]	-4.5	3404	-
4.39[a]	-8.1	3420	288, 299
4.40[a]	-8.0	3425	318
4.41[a]	-7.9	3437	282, 315
4.42 [b/d]	-10.6	3393	-
4.43[b/d]	-10.4	3474	-

[a]NMRs were recorded in $CDCl_3$ (in ppm). [b]NMRs were recorded in d_6-DMSO. [c]All IR spectra recorded as KBr discs (in cm^{-1}). [d]Data was taken from reference 145.

4.2.6 Molecular structure of 4.41

Crystals of **4.41** suitable for X-ray crystallography were grown by slow evaporation of a CH_2Cl_2 solution of **4.41**. The Smith group has previously studied related compounds **4.42** and **4.43** by X-ray crystallography. Selected bond lengths and angles for platinum(II) complexes **4.42**, **4.43** and **4.41** can be found in Table 4.4 and a molecular structure of **4.41** is shown in Figure 4.7.

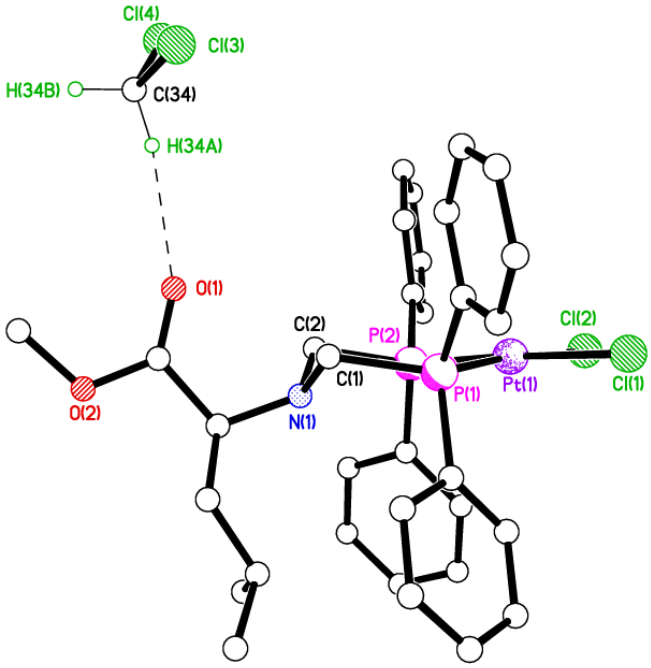

Figure 4.7 Molecular structure of **4.41** and solvent of crystallisation, CH_2Cl_2. All hydrogen atoms, excluding H(34A) and H(34B), were omitted for clarity.

The overall geometry of complex **4.41** is square planar with respect to the Pt(II) centre with the phosphorus atoms adopting a *cis* configuration forming a six membered chelate ring in a chair-like conformation. Analogous complexes **4.42** and **4.43** show similar bond lengths and angles to compound **4.41** and are all consistent with values reported in the literature.[145,170]

Table 4.4 Selected bond lengths (Å) and angles (°) for **4.41 - 4.43**.

	4.41	**4.42**	**4.43**
Pt(1)–Cl(1)	2.348(0)	2.3618(9)	2.3689(8)
Pt(1)–Cl(2)	2.357(2)	2.3593(7)	2.3520(9)
Pt(1)–P(1)	2.225(2)	2.2248(7)	2.2293(9)
Pt(1)–P(2)	2.226(2)	2.2283(8)	2.2210(8)
P(1)–Pt(1)–P(2)	95.99(6)	92.76(3)	92.89(3)
P(1)–Pt(1)–Cl(1)	86.56(7)	89.82(3)	89.97(3)
P(2)–Pt(1)–Cl(2)	86.63(8)	88.51(3)	88.93(3)
Cl(1)–Pt(1)–Cl(2)	90.65(6)	88.65(3)	88.93

Compounds **4.42** and **4.43** were observed to pack differently. Compound **4.42** formed a two dimensional structure with strong hydrogen bonding through the hydroxyl group on the carboxylic acid. In contrast compound **4.43** formed a one dimensional structure with hydrogen bonding through the (amide)C-O···H-N(amide) groups. Complex **4.41** packs differently to both compounds **4.42** and **4.43**, with no hydrogen bonding through the hydroxyl group of the carboxylic acid observed nor is there an amide bond present for intermolecular bonding. Hydrogen bonding *via* Pt-Cl···H-C(CH_2Cl_2) [3.556(9) – 3.604(9) Å] and (carboxylic acid)C-O···H-C(CH_2Cl_2) [3.372(9) Å] forms a one dimensional chain between molecules of **4.41** and solvent CH_2Cl_2, as shown in Figure 4.8.

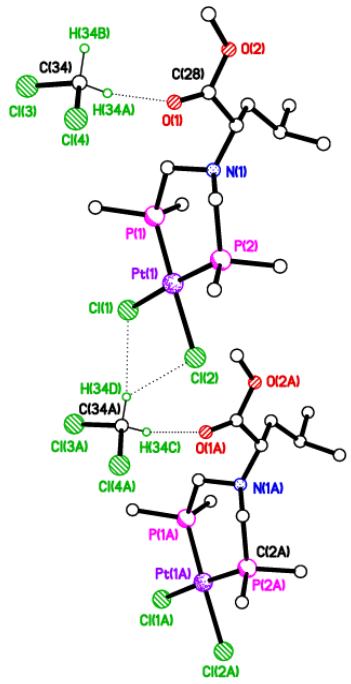

Figure 4.8 Packing plot of **4.41**. All hydrogen atoms, except H(34A), H(34B), H(34C) and H(34D), and phenyl rings omitted for clarity. Symmetry operator for equivalent molecule A: - x+1, y, z.

4.2.7 Coordination studies with platinum(II) and ligand 4.24

Mono-phosphine ligand **4.24** also underwent coordination to $PtCl_2$(cod), reacting starting materials **4.24** and $PtCl_2$(cod) in a two-to-one ratio respectively. After stirring the CH_2Cl_2 solution for 1h, the volume was reduced five-fold and Et_2O was added in order to precipitate a white solid, **4.44**, in a yield of 53%.

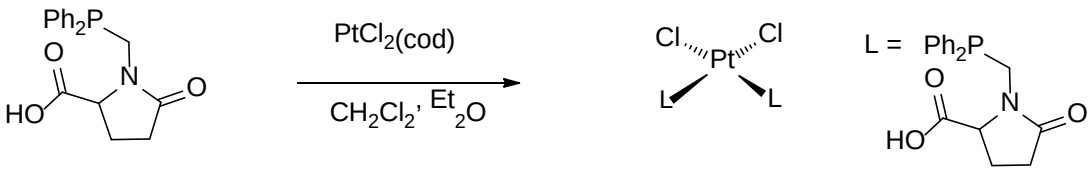

(4.24) **(4.44)**

Scheme 4.8 Synthesis of platinum(II) complex **4.44**.

The $^{31}P\{^{1}H\}$ NMR spectrum displayed a resonance at 3.0 ppm with associated satellites observed at $^{1}J_{PtP}$ 3625 Hz; these satellites are again within the region expected for *cis*

conformed Pt(II) complexes. ESI-MS data displayed fragments representative of $[M-Cl]^+$ for complex **4.44** (at *m/z* 884.1370). Elemental analysis results matched the expected empirical formula for compound **4.44**, though water was present and was also taken into account. Despite repeated attempts, crystals suitable for X-ray crystallography were not grown.

4.2.8 Coordination studies with ruthenium(II)

The coordination chemistry of ligands **4.12** – **4.15** and **4.19** – **4.21** were further explored through the formation of ruthenium(II) complexes **4.45** – **4.51**. Bimetallic ruthenium(II) complexes **4.45** – **4.51** were formed through the reaction of ligands **4.12** – **4.15** and **4.19** – **4.21** with a stirred CH_2Cl_2 solution of dichloro(*p*-cymene)ruthenium(II) dimer. After reduction in volume, the addition of Et_2O resulted in the precipitation of orange products **4.45** – **4.51**, affording a yield of 45-81%.

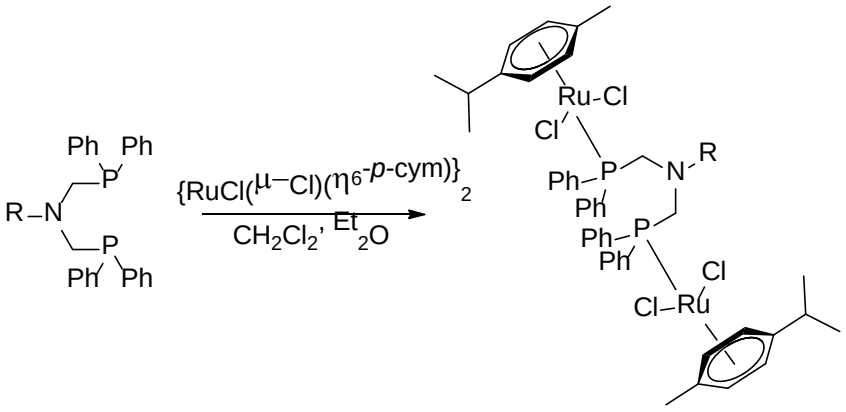

R = **(4.12)** $CH_2CONHCH(CH_3)CO_2H$
(4.13) $(CH_2)_4CH(CO_2H)NHCOOCH_2Ph$
(4.14) $(C_6H_4)CONHCH_2CO_2H$
(4.15) $CH(CH_2CH_2CH_3$
(4.19) $CH(CH_2OH)CO_2CH_3$
(4.20) $CH(CH_2Ph)CO_2CH_3$
(4.21) $CH_2CH(CH_3)_2)CO_2H$

R = **(4.45)** $CH_2CONHCH(CH_3)CO_2H$
(4.46) $(CH_2)_4CH(CO_2H)NHCOOCH_2Ph$
(4.47) $(C_6H_4)CONHCH_2CO_2H$
(4.48) $NHCO_2CH_2CH_3$
$CH(CH$
(4.49) $CH(CH_2OH)CO_2CH_3$
(4.50) $CH(CH_2Ph)CO_2CH_3$
(4.51) $CH_2CH(CH_3)_2)CO_2H$

Scheme 4.9 Synthesis of ruthenium(I) complexes **4.45** – **4.51**.

$^{31}P\{^1H\}$ NMR studies depicted a single major resonance for complexes **4.45** – **4.51**, with a *ca.* 45 ppm downfield shift from ligands **4.12** – **4.15** and **4.19** – **4.21**. The singlet resonances were observed between 16.8 – 21.0 ppm, with specific values for each complex shown in Table 4.5; the Smith group previously synthesized glycylglycine and triglycine analogues of complexes **4.45** – **4.51**, named **4.52** and **4.53** respectively,

which also feature in Table 4.5.[145] The ^{1}H NMR spectra of **4.45 – 4.51** show well resolved, distinct resonances for the η^{6}-*p*-cymene ancillary ligand – in the case of **4.45 – 4.51** the aromatic hydrgogens are observed between 5.42 – 4.93 ppm, the CH_3 groups are observed at 1.44 – 1.14 and 0.93 – 0.73 ppm. ESI-MS data displayed fragments representative of $[M\text{-}Cl]^{+}$ for complexes **4.45 – 4.51** (at *m/z* 1119.1218, 1253.1963, 1167.1244, 1079.1088, 1092.1138, 1166.1519 and 1132.1683).

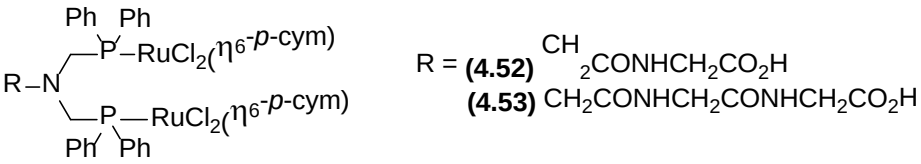

Figure 4.9 Chemical structure of compounds **4.52** and **4.53** synthesised by the Smith group.[145]

Table 4.5 - Summary of NMR and IR data for complexes **4.35** to **4.43**.[a]

Complex	δ(P)	*m/z* $[M\text{-}Cl]^{+}$ found (ppm difference)
4.45	16.8	1119.1218 (0.8 ppm)
4.46	19.5	1253.1963 (0.4 ppm)
4.47	20.7	1167.1244 (1.6 ppm)
4.48	20.0	1079.1088 (4.1 ppm)
4.49	18.8	1092.1138 (1.5 ppm)
4.50	18.6	1166.1519 (0.1 ppm)
4.51	21.0	1132.1683 (0.9 ppm)
4.52[b]	15.7	1104
4.53[b]	18.2	1162

[a]All NMRs were recorded in $CDCl_3$ (in ppm).[b] Data was taken from reference 145.

In addition to ESI-MS and NMR data, the formation of **4.45 – 4.51** was supported by IR analyses for complexes **4.45 – 4.51** and elemental analyses of **4.45**, **4.48** and **4.50**. Crystals suitable for X-ray crystallography were grown *via* slow evapration for complex **4.50**. Crystals also formed in the filtrate of **4.51**, however on analysis by single crystal X-ray diffraction, **4.54** had formed. A brown powder had precipitated before brown crystals of compound **4.54** were formed. It is likely that some of the unreacted starting material (dichloro(*p*-cymene)ruthenium(II) dimer) precipitated out leaving starting materials dichloro(*p*-cymene)ruthenium(II) dimer and **4.21** in stoichiometric ratios of 1:2 in the filtrate solution, resulting in the formation of compound **4.54**.

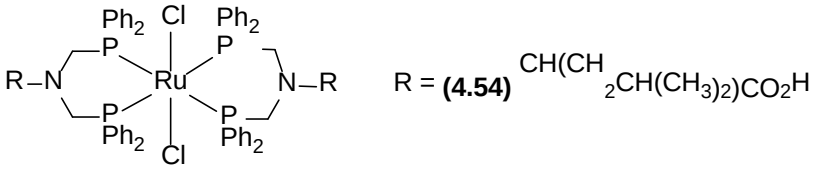

Figure 4.10 Chemical structure of **4.54** (crystals grown from filtrate of **4.51)**.

4.2.9 Molecular structures of ruthenium(II) complexes 4.50 and 4.54

Crystals of ruthenium(II) complex **4.54** suitable for X-ray crystallography were grown by slow evaporation of a CH_2Cl_2/Et_2O filtrate of **4.51**. The coordinated ligands around the metal centre are in an octahedral arrangement. Selected bond lengths and angles for compound **4.54** can be found in Table 4.6, with a molecular structure shown in Figure 4.11.

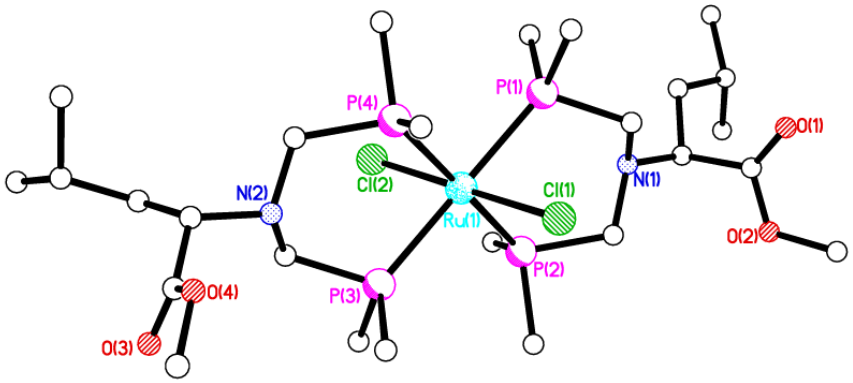

Figure 4.11 Molecular structure of **4.54**. All hydrogen atoms, phenyl rings, except the ipso carbons and solvent molecules have been omitted for clarity.

Six coordinate ruthenium(II) complexes with two chloride donors and four phosphine donors are known in the literature.[172] The chloride ligands in complex **4.54** arrange in a *trans* position to each other, with the phosphine donors taking the four equatorial positions. There is no significant distortion from 90° angles between each of the donors giving rise to an octahedral arrangement. The Ru-P distances are longer than those reported in literature for $[RuCl_2L_4]$ complexes (L = $PPhH_2$ 2.318(3)/2.319(3)Å, PTA 2.316-2.353Å); the longer Ru-P bonds in compound **4.54** may be due to steric hindrance from the bulky PPh_2 moieties.[173,174] A search of the CSD database found a number of ruthenium(II) complexes with four phosphine donor atoms, however there were no examples found with two PCNCP moieties; therefore complex **4.54** is the first of its type.[132]

Table 4.6 Selected bond lengths (Å) and angles (°) for **4.54**.

Ru1—P1	2.4347 (19)	P4—Ru1—P1	92.71 (6)
Ru1—P2	2.3680 (16)	P2—Ru1—P3	92.28 (6)
Ru1—P3	2.4213 (19)	P2—Ru1—P1	88.01 (6)
Ru1—P4	2.3718 (17)	P4—Ru1—P3	87.02 (6)
Ru1—Cl2	2.4379 (18)	P2—Ru1—Cl2	92.15 (6)
Ru1—Cl1	2.4415 (18)	P2—Ru1—Cl1	87.31 (6)

One molecule of **4.54** is observed per asymmetric unit with two half molecules of Et_2O also present. Molecules stack in columns along the *b* axis, with molecules of diethyl ether filling the voids between columns in a regular pattern. A number of intramolecular interactions are present however no intermolecular hydrogen bonding was observed. A list of intramolecular interactions is displayed in Table 4.7.

Table 4.7 Specified intermolecular interactions for **4.54**.

D—H···*A*	*D*—H	H···*A*	*D*···*A*	*D*—H···*A*
C1—H1*B*···Cl1	0.99	2.80	3.361 (7)	117
C4—H4···Cl2	0.95	2.45	3.338 (8)	155
C14—H14···Cl1	0.95	2.76	3.343 (7)	121
C16—H16···Cl1	0.95	2.58	3.413 (8)	147
C26—H26···N1	0.95	2.36	3.098 (10)	134
C34—H34*A*···Cl2	0.99	2.72	3.321 (7)	120
C37—H37···Cl1	0.95	2.43	3.330 (7)	158
C47—H47···Cl2	0.95	2.68	3.349 (7)	128
C49—H49···Cl2	0.95	2.58	3.424 (9)	148
C59—H59···N2	0.95	2.40	3.162 (11)	138

Crystals of **4.50** suitable for X-ray crystallography were grown by slow evaporation of a CH_2Cl_2 mother liquor of complex **4.50**. Selected bond lengths and angles for compound **4.50** can be found in Table 4.8, with a molecular structure shown in Figure 4.12. The Smith group has previously explored the molecular structure of ruthenium(II) complex **4.53**, in addition to other related structures by X-ray crystallography; the bond lengths and angles of **4.50** are in agreement with analogous structures previously synthesised.[145]

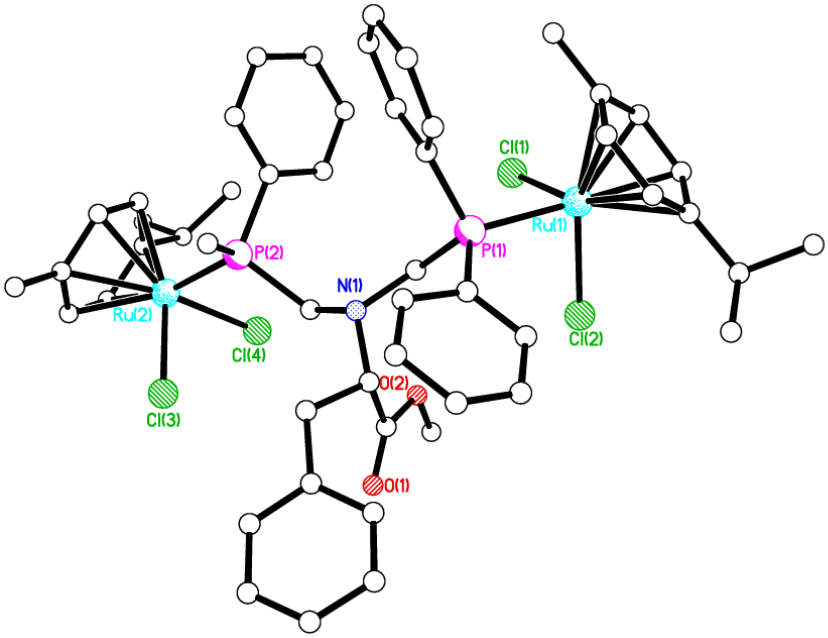

Figure 4.12 Molecular structure of **4.50**. All hydrogen atoms, one phenyl ring except the ipso carbon atom and the solvent molecule CH_2Cl_2 are omitted for clarity.

Compound **4.50** displays the classic "piano-stool" geometry formed by the η^6-*p*-cymene ancillary ligand, and the three "legs" being the two chlorides and the phosphorus donor atom of the P–C–N–C–P ligand. This is also observed in related ruthenium(II) complexes, such as **4.53**.[145] Compound **4.53** features intermolecular carboxylic acid-carboxylic acid head-to-tail hydrogen bonding, arranging molecules into dimers. In contrast, compound **4.50** possesses no hydroxyl groups for dimerisation and features no strong intermolecular or intramolecular bonding.

Table 4.8 Selected bond lengths (Å) and angles (°) for **4.50** and **4.53**.[145]

	4.50	**4.53**
Ru1—P1	2.3659 (14)	2.342(2)
Ru1—Cl2	2.4103 (14)	2.423(2)
Ru1—Cl1	2.4241 (14)	2.396(2)
Ru1 – cym centroid	1.703[b]	n.r[a]
P1—C1	1.867 (6)	1.881(7)
P2—Ru2	2.3574 (15)	2.341(2)
Ru2—Cl4	2.4251 (15)	2.401(2)
Ru2—Cl3	2.4304 (15)	2.408(2)
Ru1 - cym centroid	1.708 [b]	n.r[a]
C2—P2	1.861 (6)	1.875(8)
P1—Ru1—Cl2	86.12 (5)	86.35(8)
P1—Ru1—Cl1	84.53 (5)	83.03(8)
Cl2—Ru1—Cl1	89.66 (5)	88.01(8)
P2—Ru2—Cl4	85.97 (5)	83.17(8)
P2—Ru2—Cl3	85.44 (5)	90.15(8)
Cl4—Ru2—Cl3	88.37 (5)	87.26(8)

[a]n.r = not resolved, [b]no esd recorded

4.2.10 Coordination studies with ruthenium(II) and ligand 4.24

Mono-phosphine ligand **4.24** also underwent coordination with dichloro(*p*-cymene)ruthenium(II) dimer in a two-to-one reaction respectively. This generated an orange solid **4.55** in a modest yield of 44%.

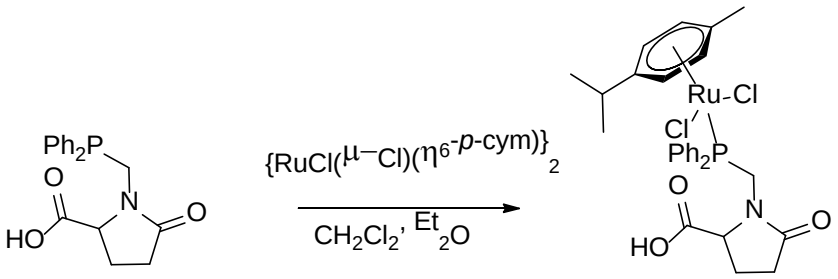

(4.24) **(4.55)**

Scheme 4.10 Synthesis of ruthenium complex **4.55**.

The $^{31}P\{^{1}H\}$ NMR spectrum showed a singlet resonance at 22.1 ppm - this is a similar downfield shift as complexes **4.45** – **4.51**. The predicted $[M–Cl]^+$ fragment for compound **4.55** was found in the respective spectrum with less than 1.5 ppm mass difference to the recorded fragment observed. Despite repeated attempts, crystals suitable for X-ray crystallography were not grown.

4.3 Coordination with group 11 metals

Metal-phosphine complexes, where the metal is from group 11, have been shown to have great promise in a number of areas of medicine, with metal complexes displaying antimicrobial, antibacterial, antiviral, cytotoxicity and antitumour activity - this is described in further detail in Section 1.4 of this thesis.[2,40,46,51] Inspiration for the following section of this thesis has been taken from the work described in literature involving diphosphine dppe and derivatives of dppe.

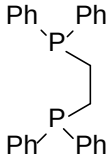

(4.56)

Figure 4.13 Chemical structure of dppe.

Metal centres coordinated to two dppe derivatives benefit from quick and easy synthesis, *in vivo* stability and the ability to control biodistribution through modification of the substituents on the phosphines.[44] This has resulted in many examples of these compounds being explored for antitumour drugs, as well as potential metallodrugs for PET imaging.[1,44,52–54] In the following section group 11 metals, copper(I), gold(I) and silver(I) are complexed with aminomethylphosphine ligands with amino acid backbones, as described in the first half of this chapter, in a ratio of 1:2 respectively.

4.3.1 Coordination studies with copper(I)

A CH_2Cl_2 solution of tetrakis(acetonitrile)copper(I) tetrafluoroborate was treated with two equivalents of ligand, **4.2**, **4.3**, **4.7** and **4.12** – **4.15** respectively, under an inert atmosphere. After 1h stirring the solution was reduced and Et_2O was used to precipitate white complexes **4.57** – **4.63**. It was observed that on leaving the

complexes in air during filtration for *ca.* 10 mins the white precipitate changes to a green oil, this would indicate hydration by water in the atmosphere as well as oxidation of copper(I) to copper(II). Therefore collection of material from the filter was performed quickly with yields for complexes **4.57 – 4.63** in the region of 39 - 96% were obtained.

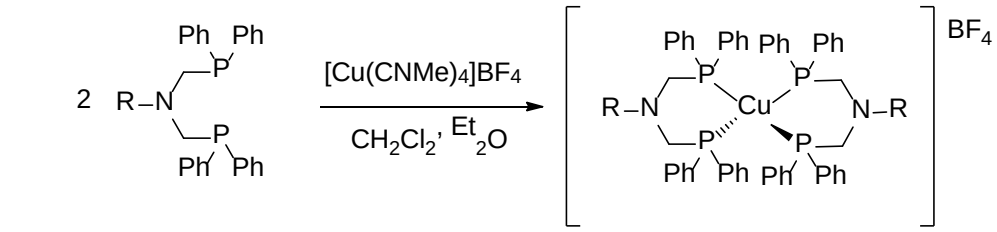

R = **(4.2)** CH_2CO_2H
(4.3) $CH_2CONHCH_2CO_2H$
(4.7) $CH_2CONHCH_2CONHCH_2CO_2H$
(4.12) $CH_2CONHCH(CH_3)CO_2H$
(4.13) $(CH_2)_4CH(CO_2H)NHCOOCH_2Ph$
(4.14) $(C_6H_4)CONHCH_2CO_2H$
(4.15) $NHCOOCH_2CH_3$

R = **(4.57)** CH_2CO_2H
(4.58) $CH_2CONHCH_2CO_2H$
(4.59) $CH_2CONHCH_2CONHCH_2CO_2H$
(4.60) $CH_2CONHCH(CH_3)CO_2H$
(4.61) $(CH_2)_4CH(CO_2H)NHCOOCH_2Ph$
(4.62) $(C_6H_4)CONHCH_2CO_2H$
(4.63) $NHCOOCH_2CH_3$

Scheme 4.11 Synthesis of copper(I) complexes **4.57 – 4.63**.

The $^{31}P\{^1H\}$ NMR spectra shows a broadening and downfield phosphorus chemical shift for complexes **4.57 – 4.63** from parent ligands **4.2**, **4.3**, **4.7** and **4.12** – **4.15**, with broad signals displayed in the region of -12.2 to -21.1 ppm. Broad signals in the same region have been observed for similar complexes in literature.[42, 175] Similarly the ^1H NMR spectra were also broad. Broadening may suggest dynamic behaviour or may be a result of the quadrupolar effect (^{63}Cu and ^{65}Cu I = 3/2), or both.

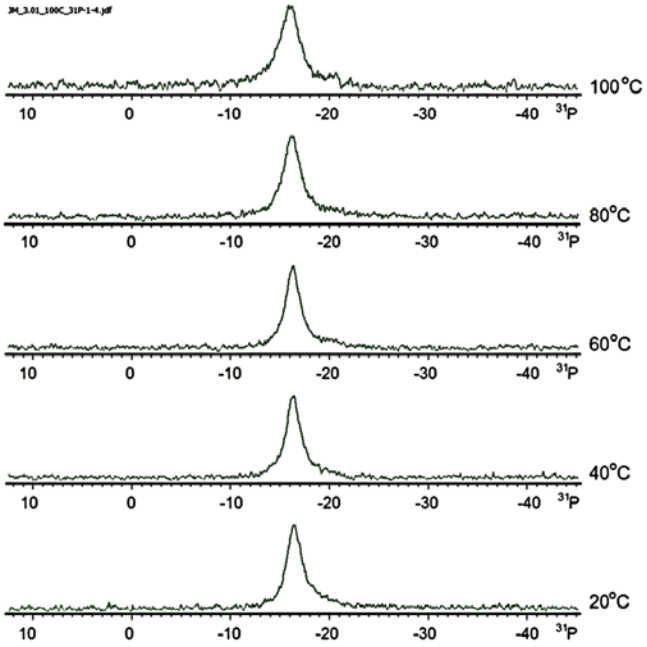

Figure 4.14 $^{31}P\{^{1}H\}$ NMR spectra of complex **4.58** at varying temperatures (in d^{6}-DMSO).

Temperature variant NMR studies on **4.58** showed an increase in temperature resulted in some broadening though not extensive; the $^{31}P\{^{1}H\}$ NMR spectra for **4.58** from 20°C to 100°C in 20°C intervals can be found in Figure 4.14; peak width at half height for each of the temperatures measured can be found in Table 4.9. This may suggest broadening is a result of the quadrupolar effect, since increased temperature and broadening are not strongly positively correlated.

Table 4.9 Width at half-height for $^{31}P\{^{1}H\}$ NMR peaks at varying temperatures for compound **4.58** (in d^{6}-DMSO).

Temperature (°C)	Width at half-height (Hz)
20	323
40	304
60	297
80	323
100	407

The ESI-MS confirmed the existence of complexes **4.57 – 4.63**, giving $[M]^{+}$ at *m/z* 1005.2302 (2.2 ppm), 1119.2739 (1.3 ppm), 1233.3178 (0.4 ppm), 1147.3050 (1.5 ppm), 1415.4491 (2.8 ppm), 1243.3058 (0.7 ppm) and 1063.2843 (1.2 ppm) respectively. Elemental analyses were in agreement with calculated values for desired

products **4.57 – 4.59** and **4.61 – 4.62**. The $^{31}P\{^{1}H\}$ NMR data are displayed in Table 4.10.

Table 4.10 Summary of $^{31}P\{^{1}H\}$ NMR data for compounds **4.57 – 4.63**.[a]

Complex	δ(P)	$^{31}P\{^{1}H\}$ peak width at half-height (Hz)
4.57[b]	-15.8	627
4.58	-16.4	277
4.59	-15.9	312
4.60	-12.2	332
4.61	-15.8	355
4.62	-16.3	280
4.63	-21.1	71

[a]NMRs recorded in $CDCl_3$ unless otherwise stated(in ppm). [b]NMR recorded in d_6-DMSO.

4.3.2 Molecular structures of 4.58 and 4.63

Colourless blocks of **4.58** were grown by slow diffusion of Et_2O into a DMF/CH_2Cl_2 solution of **4.58** and its molecular structure was determined, as shown in Figure 4.15. There is one molecule of DMF in the asymmetric unit and a partial water molecule. BF_4^-, the counterion for the copper-phosphine complex is also present in the asymmetric unit, but displayed some disorder. This was resolved by splitting the molecule into parts.

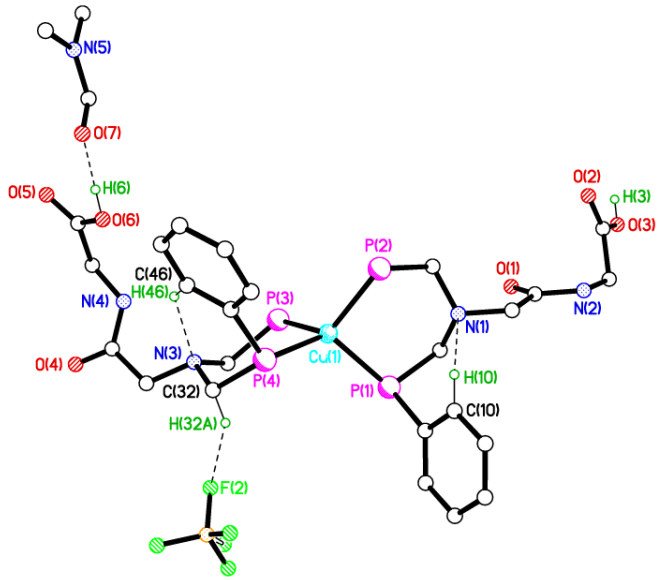

Figure 4.15 Molecular structure of **4.58**. All hydrogen atoms except those on O(3), O(6), C(10), C(32) and C(46) a partial water molecule of crystallisation and most of the phenyl rings have been omitted for clarity.

Molecules stack in columns along the *b* axis, with one neighbouring column interacting through hydrogen bonds between O(3)-H(3)···O(5) [contact length of 2.625(3)Å]. Phenyl rings from the phosphine moieties, as well as DMF and partial water molecules occupy the space between columns.

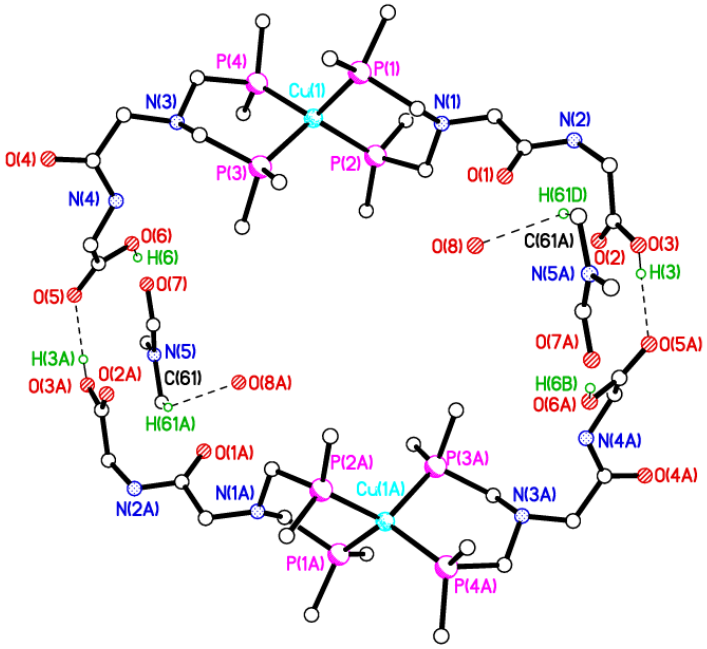

Figure 4.16 Packing structure of **4.58** highlighting the intermolecular interactions present. All hydrogen atoms except those on O(3A), O(6), C(61), O(3), O(6A) and C(61A) have been omitted for clarity. Symmetry operator for equivalent molecule A: -x+1, -y+1, -z+1.

Other neighbouring columns are hydrogen bonded through the amide C=O of one molecule and an Ar-H and CH_2 of the PCN moiety of another molecule. With intermolecular interaction also observed between amide N-H and the fluorine atoms of the BF_4^- counterion. This is shown in Figure 4.17.

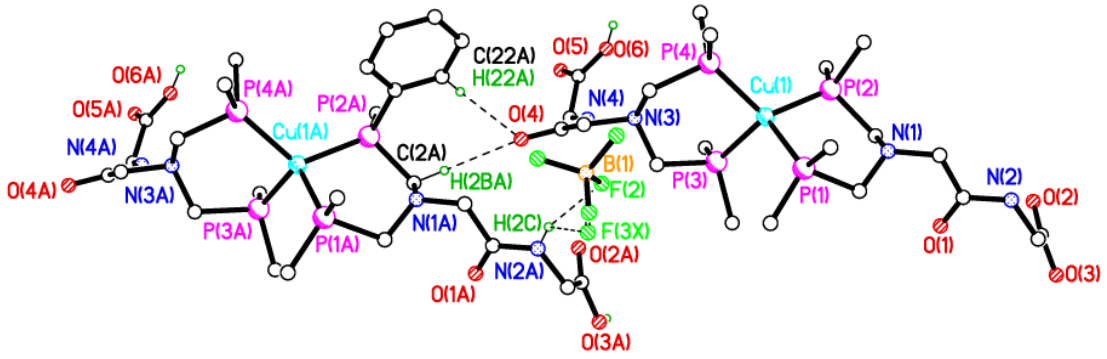

Figure 4.17 Packing structure of **4.58** highlighting the intermolecular interactions present. All hydrogen atoms except those on C(2A), C(22A), N(2A), O(3A), O(6) and O(6A) have been omitted for clarity. Symmetry operator for equivalent molecule A: x-1, y, z.

Crystals of related ligand **4.63** suitable for X-ray crystallography were grown by slow evaporation of a CH_2Cl_2/Et_2O filtrate of **4.63** and its molecular structure determined, as shown in Figure 4.18. One disordered molecule of Et_2O per asymmetric unit was resolved using Platon squeeze. The bond lengths and angles of complex **4.63** and **4.58** were comparable and furthermore, agreed with related structures in the literature.[176]

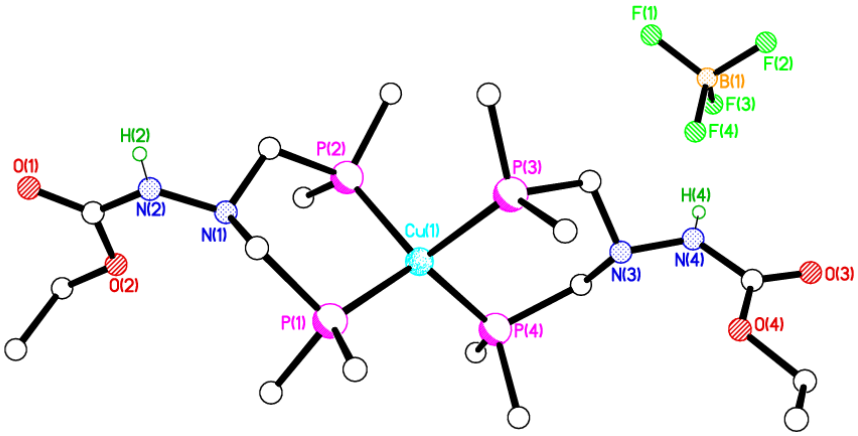

Figure 4.18 Molecular structures of **4.63** and the counterion BF_4^-. All hydrogen atoms except those on N(2) and N(4) and the phenyl rings, except the ipso carbons, have been omitted for clarity.

Complexes **4.63** and **4.58** both adopt a distorted tetrahedral geometry provided by four P atoms from two phosphine ligands. The Cu—P bond distances are in the range 2.2940 (5)– 2.3286 (5) Å. Relevant bond lengths and angles are displayed in Table 4.11; these values are in agreement with literature values.[176]

Table 4.11 Selected bond lengths (Å) and angles (°) for **4.58** and **4.63**.

	4.58	**4.63**
Cu1—P4	2.2890 (5)	2.2695 (4)
Cu1—P1	2.3286 (5)	2.2858 (5)
Cu1—P2	2.2812 (5)	2.2940 (5)
Cu1—P3	2.2951 (5)	2.3044 (5)
P4—Cu1—P1	121.93 (2)	119.084 (17)
P1—Cu1—P2	97.611 (19)	98.913 (17)
P4—Cu1—P3	96.518 (19)	96.954 (17)
P2—Cu1—P3	116.81 (2)	105.958 (16)

Unlike **4.58**, **4.63** has no hydroxyl groups to form a 20-membered hydrogen bonded ring, as shown in Figure 4.16, however there is an interaction observed between the carbonyl group of one molecule, and the CH_2 and aromatic CH groups on the neighbouring molecule [C(51)—H(51)···O(3A) 3.356(2) Å, C(31)—H(31A)···O(3A) 3.1950(19) Å] - this generates a 12-membered ring, as shown in Figure 4.19.

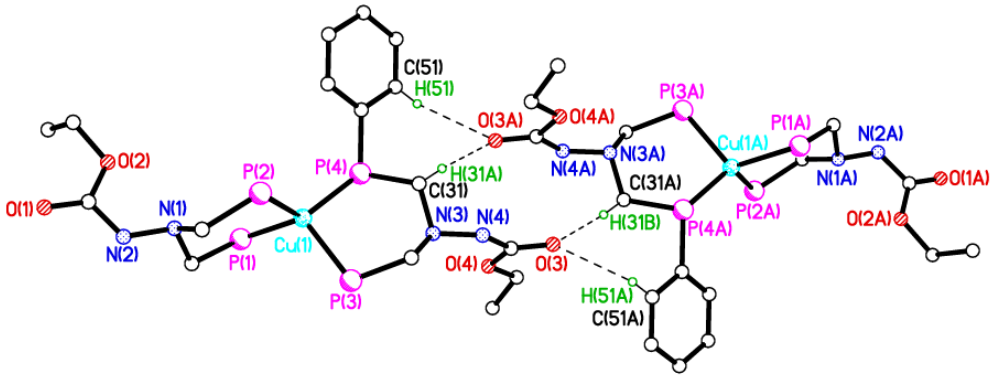

Figure 4.19 Packing structure of **4.63** highlighting the intermolecular interactions present. All hydrogen atoms except those on C(31), C(31A), C(51) and C(51A) have been omitted for clarity. Symmetry operator for equivalent molecule A: -*x*+2, -*y*+1, -*z*+1.

4.3.3 Coordination studies with gold(I)

Reaction between ligands **4.3**, **4.7** and **4.12** – **4.15** and Au(tht)Cl was again employed (previously described in Section 4.2.4) however on this occasion the reaction was performed on a 2:1 ratio, leading to substitution of both chloride and tht ligands

generating *bis*(diphosphine) complexes **4.64** – **4.69**, with a chloride ion as the counterion. Gold(I) complexes **4.64** – **4.69** were afforded in yield of 45 – 97%.

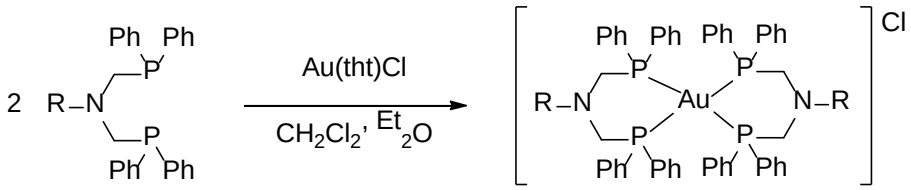

R = **(4.3)** $CH_2CONHCH_2CO_2H$
(4.7)
(4.12) $CH_2CONHCH_2CONHCH_2CO_2H$
$CH_2CONHCH(CH_3)CO_2H$
(4.13) $(CH_2)_4CH(CO_2H)NHCOOCH_2Ph$
(4.14) $C_6H_4CONHCH_2CO_2H$
(4.15) $NHCOOCH_2CH_3$

R = **(4.64)** $CH_2CONHCH_2CO_2H$
(4.65)
(4.66) $CH_2CONHCH_2CONHCH_2CO_2H$
$CH_2CONHCH(CH_3)CO_2H$
(4.67) $(CH_2)_4CH(CO_2H)NHCOOCH_2Ph$
(4.68) $C_6H_4CONHCH_2CO_2H$
(4.69) $NHCOOCH_2CH_3$

Scheme 4.12 Synthesis of gold(I) complexes **4.64** – **4.69**.

Coordination of ligands **4.3**, **4.7** and **4.12** – **4.15** to gold(I) resulted in a downfield shift of the singlet resonance in the $^{31}P\{^1H\}$ NMR signal by approximately δ 18 ppm (in d_6-DMSO). This is in contrast to the shift observed for linear gold(I) complexes **4.25** – **4.31** which exhibited a downfield shift of *ca.* δ 48 ppm (in $CDCl_3$). The differences in shift are too great to be a result of a change of NMR solvent, and support the removal of chloride ions. ESI-MS data displayed signals, as expected, for the positive molecular ion $[M]^+$ fragments. The expected empirical formulae for compounds **4.66** – **4.68** matched that recorded for the elemental analyses. IR spectra did not exhibit νAuCl stretches in the range of 315 – 330 cm^{-1}, confirming the loss of bound chloride ligands and the formation of cationic species.

4.3.4 Coordination studies with silver(I)

Similarly to the reactions generating copper(I) complexes **4.57** – **4.63**, reactions using ligands **4.2**, **4.3**, **4.7** and **4.12** – **4.15** with silver(I) salt, $AgBF_4$, were carried out using Schlenk line techniques due to the hydroscopic behaviour of the silver salt used. Additionally, aluminium foil was used to cover the glassware due to the light sensitivity of silver salts. Ligands **4.2**, **4.3**, **4.7** and **4.12** – **4.15** (two equivalents) and $AgBF_4$ (one equivalent) were dissolved in CH_2Cl_2 and stirred for 1h, before the solution was reduced in volume and Et_2O was added to precipitate solids **4.71** – **4.76**. In addition,

ligand **4.70**, the synthesis of which was repeated from literature, was also used in the reaction with $AgBF_4$ under identical conditions to that used for the formation of complexes **4.71 – 4.76**.[177,178] The reactions, as shown in Scheme 4.13, gave yields of between 44 - 96% for complexes **4.71 – 4.77**.

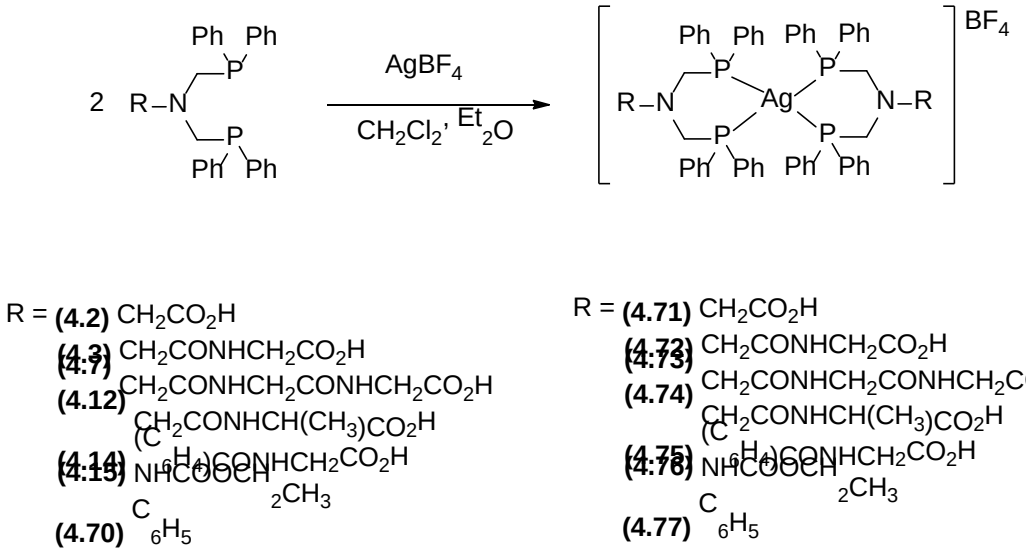

Scheme 4.13 Synthesis of silver complexes **4.71 – 4.77**.

The $^{31}P\{^1H\}$ NMR spectra of complexes **4.71 – 4.77** clearly display two doublets in the region of -9.3 - -12.6 ppm; an example is shown in Figure 4.20. Silver has two NMR-active isotopes, ^{107}Ag (I = 0.5, 52% natural abundance) and ^{109}Ag (I = 0.5, 48% natural abundance) which result in the appearance of two doublets arising from the ^{107}Ag-P and ^{109}Ag-P spin-spin coupling. Since the spin-spin coupling is observed at room temperature it reveals the complexes are stable in solution and there is no or minimal intermolecular ligand exchange. All complexes featured almost identical coupling constants(*ca.* $^1J_{^{107}AgP}$ = 257Hz; $^1J_{^{109}AgP}$ = 224Hz); the recorded coupling constants are typical for silver(I) complexes with two phosphines bound.[33,179]

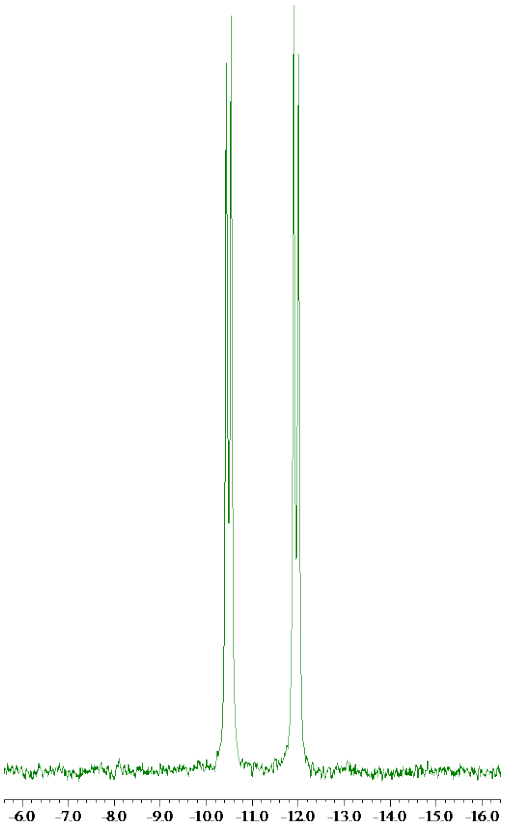

Figure 4.20 $^{31}P\{^{1}H\}$ NMR spectrum (in d_6-DMSO) of complex **4.72**. Chemical scale in δP/ppm.

ESI-MS further confirmed the formation of complexes **4.71** – **4.77** through the presence of $[M]^+$ fragments displayed in the respective spectra. Elemental analyses were also in agreement with the expected formulae for complexes **4.72**, **4.75** and **4.76**.

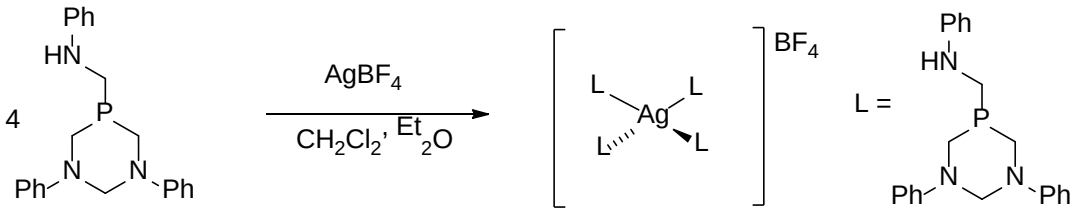

(4.78) **(4.79)**

Scheme 4.14 Formation of silver(I) complex **4.79**.

Ligand **4.78**, also synthesised by the Smith group, was reacted with $AgBF_4$ under the same conditions used for the formation of complexes **4.71** – **4.77**, generating complex **4.79** in a yield of 60%. The $^{31}P\{^{1}H\}$ NMR spectrum of complex **4.79** showed two

doublets ($^{1}J_{107AgP}$ = 424Hz; $^{1}J_{109AgP}$ = 218Hz). Elemental analysis agreed with the predicted formula for complex **4.79**, though half a molecule of CH_2Cl_2 was also present. ESI-MS data displayed a signal for the $[M\text{-}L]^+$ at *m/z* 1190.4149 (1.6ppm). Attempts to form crystals of X-ray crystallographic quality were unsuccessful.

4.3.5 Preliminary investigation of $[M(N\text{^}N)(P\text{^}P)]^+$ synthesis

1,10-Phenanthroline (phen) is planar, hydrophobic and has a rigid structure; these structural features allow phen to intercalate and groove bind to DNA and RNA.[67] $[Cu(phen)_2]^{2+}$ is one example of a commonly used DNA cleaving agent.[68] Phen derivatives also have applications in molecular recognition, molecular self-assembly and photoswitchable molecular devices, amongst others.[69–72]

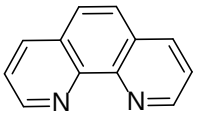

(4.80)

Figure 4.21 Chemical structure of 1,10-phenanthroline.

Copper(I)-phen complexes with the formula, $[Cu(N\text{^}N)(P\text{^}P)]^+$, where N^N is a diimine and P^P is a *bis*phosphine ligand are of interest since these complexes exhibit enhanced MLCT fluorescence in comparison to copper(I) complexes with the formula $[Cu(N\text{^}N)_2]^+$.[73] $[Cu(N\text{^}N)(P\text{^}P)]^+$ complexes where N^N is a fluorophore, in this case phen, and P^P is a bidentate aminomethylphosphine with an amino acid backbone have potential as mixed ligand bimodal radiopharmaceuticals. The amino acid backbone of the phosphine moiety can be extended to form a peptide based targeting vector.

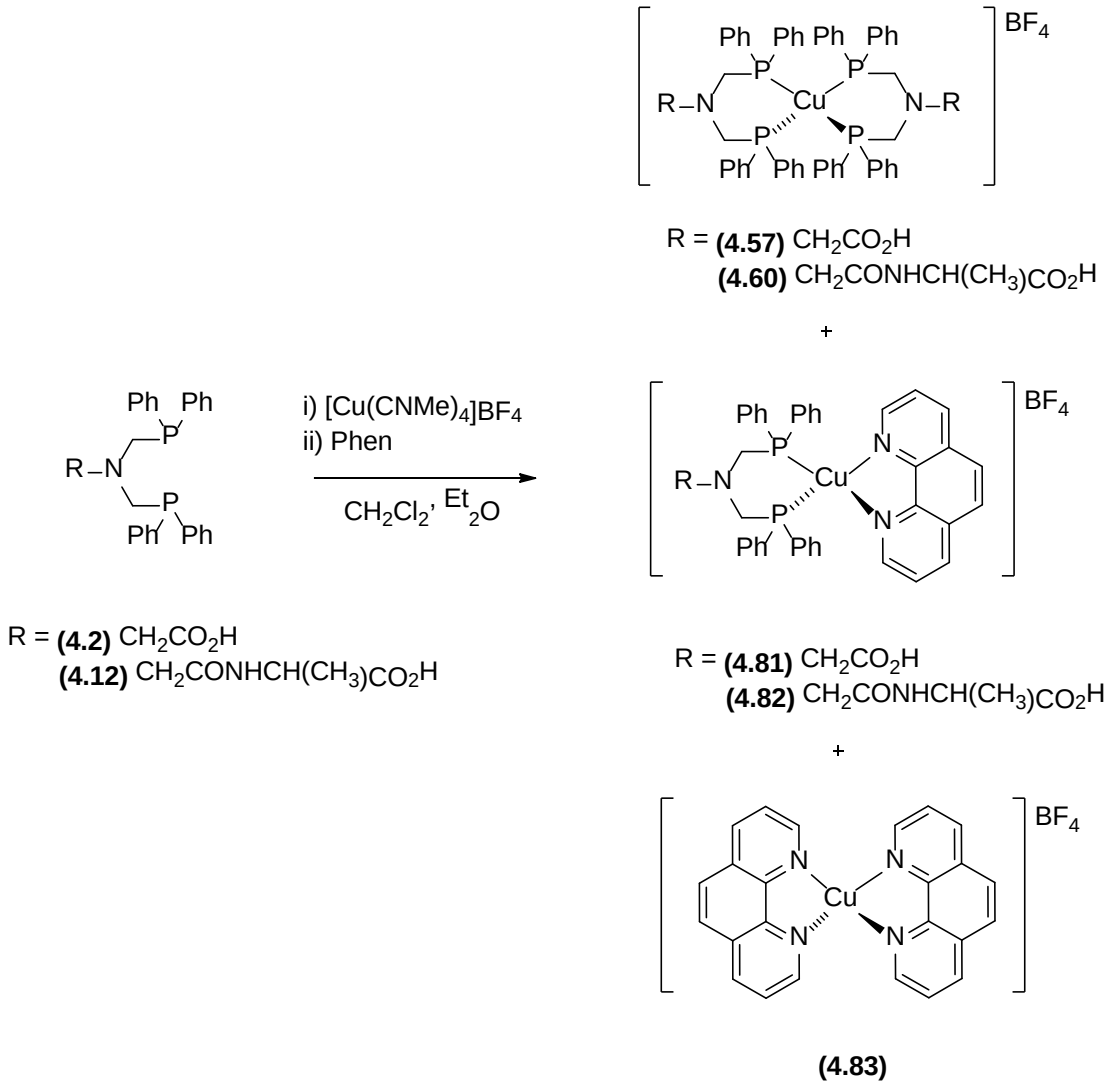

Scheme 4.15 Synthesis of $[Cu(N\text{^}N)(P\text{^}P)]^+$ complexes **4.81** and **4.82**.

Initially a reaction utilising ligand **4.2**, phen and tetrakis(acetonitrile)copper(I) tetrafluoroborate was performed. Metal precursor $[Cu(CNMe)_4]BF_4$ and ligand **4.2** were stirred in CH_2Cl_2/MeCN for 30 min, under inert conditions. Phen was added to the colourless solution and the resulting green solution was stirred a further 1h. The solution was reduced in volume and Et_2O was added, generating a green precipitate in a yield of 48%, assuming formation of desired product **4.81**.

$^{31}P\{^1H\}$ NMR analysis showed a broad peak at -15.3 ppm; this is a similar δ(P) value to $[Cu(P\text{^}P)_2]^+$ compound **4.57**. CHN analysis and ESI-MS results for the solid yielded illustrated that a mixture of products were formed and **4.81** was not the sole product present. ESI-MS analysis of the solid showed $[M]^+$ fragments for products **4.81**, **4.57** and **4.83**. Elemental analysis did not agree with the predicted formula for **4.81**, due to the impurities (**4.57** and **4.83**) present.

Kaesar *et al.* synthesised similar compounds (depicted and discussed in Section 1.5.4) which formed a mixture of products on reaction, but were isolated through recrystallisation in CH_2Cl_2/Et_2O.[77,76] Crystals suitable for X-ray diffraction were grown from a CH_2Cl_2/Et_2O solution of the yielded green precipitate and were analysed. Desired product **4.81** was observed and the description of the molecular structure of **4.81** can be found in Section 4.3.6. Elemental analysis of the crystals of **4.81** was in agreement with the expected formula for desired complex **4.81**. NMR analysis could not be performed on the crystals due to the small quantity formed.

To investigate the reactions with alternative ligands, the reaction was performed with related ligand **4.12** under the same conditions as **4.2**. This resulted in a similar outcome of mixed complexes ($[Cu(P\hat{}P)_2]^+$, $[Cu(N\hat{}N)(P\hat{}P)]^+$ and $[Cu(N\hat{}N)_2]^+$), but the desired component could not be isolated by crystallisation under the condition trialled. Since the ratio of the mixture of products formed was hard to determine due to the broad single $^{31}P\{^1H\}$ resonance, it was decided to investigate the reaction of *bis*phosphines **4.2** and **4.12** with a silver(I) precursor and phen.

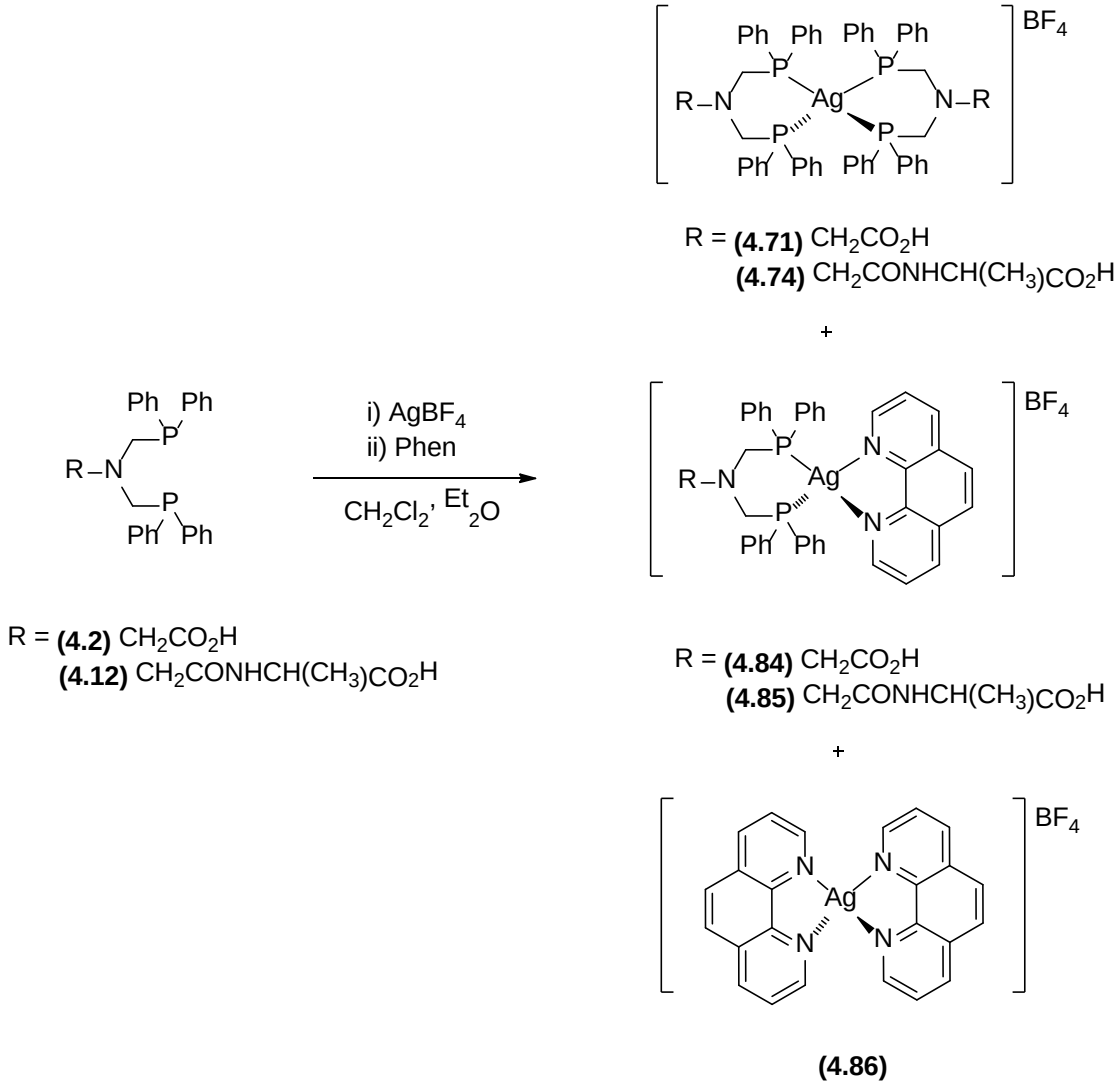

Scheme 4.16 Attempted synthesis of $[Ag(N\text{^}N)(P\text{^}P)]^+$ complexes **4.84** and **4.85**.

Respectively *bis*phosphines **4.2** and **4.12** were stirred under inert conditions for 30 mins with $AgBF_4$. Phen was added to the solution and the solution was stirred for a further 1h, before reduction in volume and addition of Et_2O gave solids for the attempted synthesis of **4.84** and **4.85** in a yield of 41 and 46% respectively, assuming **4.84** and **4.85** have formed. On analysis by $^{31}P\{^1H\}$ NMR, there was clearly two phosphorus containing compounds present in each product yielded. Two doublets, arising from ^{107}Ag-P and ^{109}Ag-P spin-spin coupling were clearly observed (at -10.50ppm for **4.84**; -10.2 ppm for **4.85**). These are attributed the $[Ag(P\text{^}P)_2]BF_4$ products **4.71** and **4.74**, due to the silver spin-coupling ($^1J_{107AgP}$ = 225Hz; $^1J_{109AgP}$ = 221Hz). Two additional peaks are observed (at -5.3 ppm for **4.84**; at -6.5 ppm for **4.85**). These were broad peaks and did not clearly show Ag-P coupling indicating cleavage of

the Ag-P bond in intermolecular phosphorus exchange and are likely attributed to the heteroleptic species **4.84** and **4.85**. Attempts were made to crystallise the two solids collected in order to isolate **4.84** and **4.85**, but were unsuccessful under the conditions trialled. The ratio of homoleptic to heteroleptic species formed, as determined by $^{31}P\{^{1}H\}$ NMR, were *ca.* 1.7:2.0 for **4.84** and *ca* 2.0:1.7 for **4.85**, as determined by $^{31}P\{^{1}H\}$ NMR.

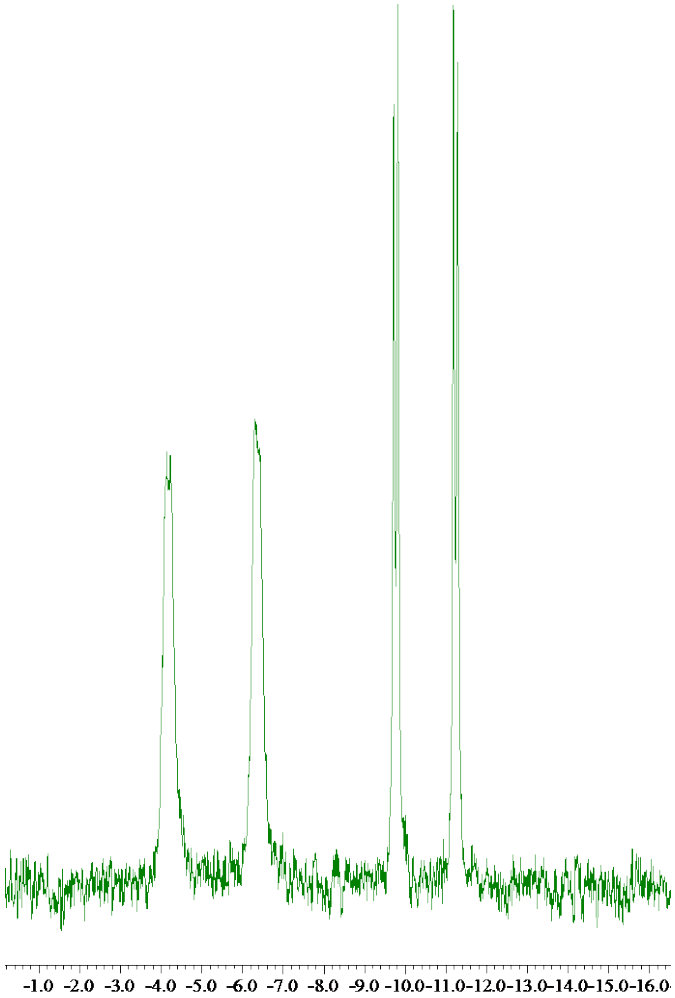

Figure 4.22 $^{31}P\{^{1}H\}$ NMR (in d_6-DMSO) for the attempted synthesis of complex **4.84**. δP/ppm scale

The attempted synthesis of **4.85** was repeated, however on addition of phen to the stirring solution of $AgBF_4$ and **4.12**, the time allowed for stirring before reduction in volume was increased from 1h to 18h. On analysis of the resulting precipitate after addition of Et_2O, the $^{31}P\{^{1}H\}$ NMR spectrum showed both the heteroleptic and

homoleptic species were present, however the ratio of heteroleptic to homoleptic had changed from *ca* 1.7:2.0 with 1h stirring to *ca* 1.4:1.9 with 18h stirring; therefore increased stirring time reduced the yield of the desired homoleptic species **4.85** slightly. Refluxing after addition of phen to a stirring solution of $AgBF_4$ and **4.12** was also trialled to investigate the effect this had on the ratio of homoleptic to heteroleptic species, however silver deposited on the flask when refluxed.

Section 4.3.5 has described a preliminary investigation into the synthesis of $[M(N\hat{}N)(P\hat{}P)]^+$, where M is silver(I) or copper(I) metal centre, N^N is a fluorescent diimine in this case phen and P^P is a *bis*phosphine ligand. Utilising a *bis*phosphine with an amino acid backbone can provide functional groups for coordination to a peptide based targeting vector providing a pathway to bimodal radiopharmaceuticals. Heteroleptic $[M(N\hat{}N)(P\hat{}P)]^+$ species were only isolated in the case of **4.81** through crystallisation under the condition trialled here. Alternative conditions may provide a pathway to a single heteroleptic species; such as the reaction of $[Ag(P\hat{}P)_2]BF_4$ and $[Ag(Phen)_2]BF_4$ to synthesis the desired compound, as shown in Scheme 4.17 or through utilising derivatives of phen with substitutents in the 2 - 9 positions which may result in the favourability of heteroleptic complexes, as shown in literature.[76,77]

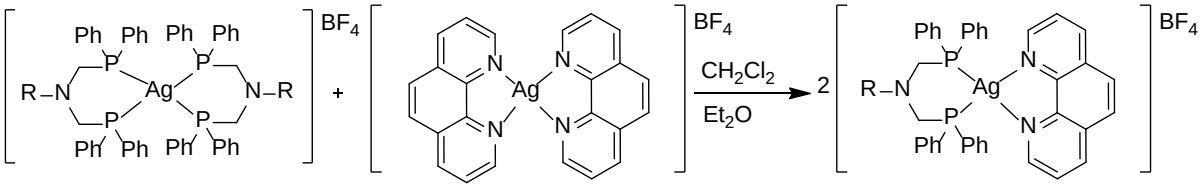

Scheme 4.17 Potential pathway to heteroleptic silver complexes.

4.3.6 Molecular structure of copper(I) complex 4.81

Crystals of the ligand **4.81** suitable for X-ray crystallography were isolated and grown by slow evaporation of a CH_2Cl_2/Et_2O filtrate of a mixture of compounds **4.81**, **4.83** and **4.57**. Selected bond lengths and angles for complex **4.81** can be found in Table 4.12, with a molecular structure shown in Figure 4.23. X-ray crystallograph analysis of compound **4.81** showed one molecule of **4.81** per asymmetric unit, with one Et_2O solvent molecule of crystallisation present. The BF_4 counterion was also present but was 2-fold disordered. Platon squeeze modelled one additional Et_2O molecule per asymmetric unit. The six memebered PCNCPCu ring adopted a chair conformation.

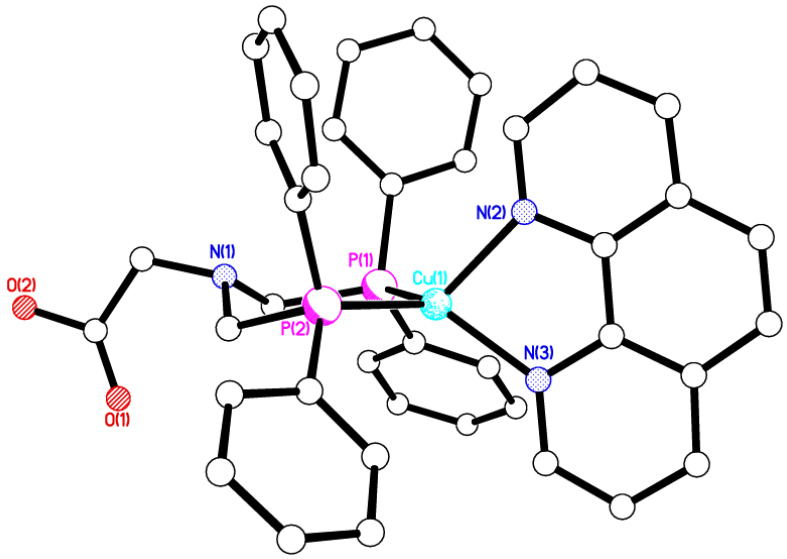

Figure 4.23 Molecular structure of **4.81**. All hydrogen atoms, BF_4^- counterion and solvent molecules omitted for clarity.

The copper ion in complex **4.81** shows a distorted tetrahedral geometry coordinated to bidentate phosphine ligand **4.2** and bidentate phenanthroline; this is in keeping with related $[Cu(N^N)(P^P)]^+$ complexes described in literature.[180,181] An example of a known $[Cu(N^N)(P^P)]^+$ complex described in the literature is copper(I) complex **4.87**; Table 4.12 lists selected bond lengths and angles for complex **4.87** and **4.81**.

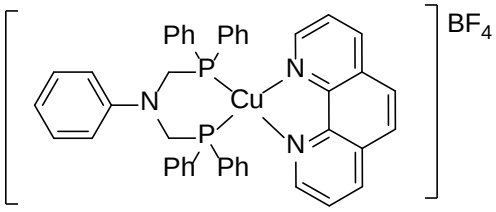

(4.87)

Figure 4.24 Chemical structure of copper(I) complex **4.87** synthesised by Hou *et al.*[180]

Molecules packed with the phen groups laying parallel to the *c* axis, with phosphine moieties perpendicular to the phen groups. Intermolecular bonding was observed between a disordered BF_4^- counterion and hydrogens on the phen moiety, linking neighboroughing phen moieties *via* the BF_4. The hydroxyl moiety on the bidentate ligand hydrogen bonded to the oxygen in the neighbouring Et_2O [O(2)—H(2)···O(3) 2.676(5) Å], as shown in Figure 4.25, along with intramolecular interactions observed.

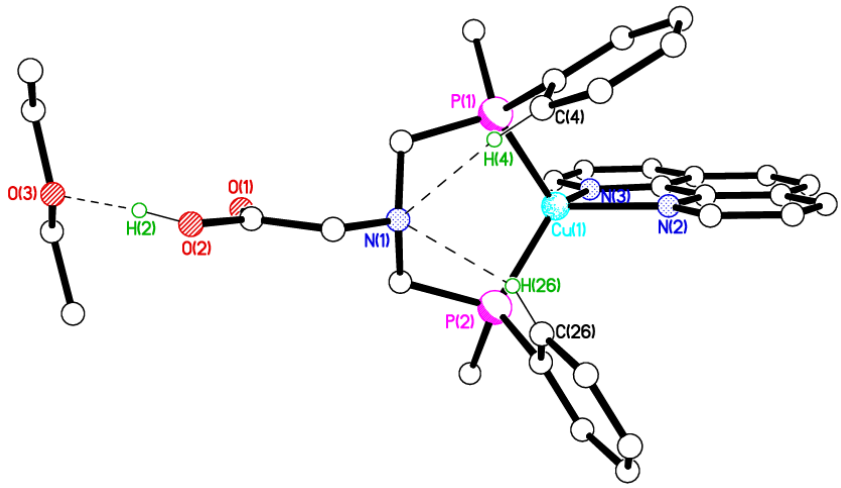

Figure 4.25 Molecular structure of **4.81** and Et_2O, solvent of crystallisation, highlighting the intramolecular interactions present. Counterion, BF_4^-, and all hydrogen atoms except those on C(26), C(4) and O(2) have been omitted for clarity.

Table 4.12 Selected bond lengths (Å) and angles (°) for **4.81** and **4.87**.[180]

	4.81	**4.87**
Cu1—N3	2.031 (4)	2.077 (3)
Cu1—N2	2.062 (4)	2.060 (3)
Cu1—P2	2.2133 (16)	2.2404 (11)
Cu1—P1	2.2213 (15)	2.2474 (10)
N3—Cu1—N2	81.87 (15)	80.95 (11)
N3—Cu1—P2	125.19 (13)	114.03 (8)
N2—Cu1—P2	115.10 (13)	125.85 (8)
N3—Cu1—P1	119.65 (14)	109.91 (8)
N2—Cu1—P1	111.99 (13)	118.03 (8)
P2—Cu1—P1	102.14 (6)	105.36 (3)

4.4 Preliminary antibacterial studies of silver(I) complexes 4.72 – 4.77 and 4.79

The growth inhibitory effects of the novel silver(I) complexes, **4.72** – **4.77** and **4.79**, $AgBF_4$ and ligands **4.2**, **4.3**, **4.12** **4.70** were investigated against Gram-negative *Escherichia Coli* and Gram-positive *Staphylococcus Aureus* bacteria using the agar disk

diffusion method. *E. Coli.* and *S. Aureus* are usually associated with medical-associated infections, which is why they were chosen for this study.[182]

Initially, *ca.* 5 mg of each complex (**4.72** - **4.77** and **4.79**) was dissolved in 20 mL DMSO (99+%) and the solution (20 μL) transferred to aseptic disks. Mueller-Hinton sterile agar plates were seeded with the respective bacteria and the sample disks were impregnated on Mueller-Hinton plates. Only a select sample of complexes could be studied due to solubility or availability issues. Most complexes displayed some growth inhibitory effects on both bacteria, with **4.74** and **4.76** showing negligible antibacterial activity against *S. Aureus,* as shown in Figure 4.27. The diameters of the area around the disks where bacteria could not grow were measured after 12 hours (zone of inhibition); this information is displayed in Table 4.13. The bigger the zone of inhibition, the higher the antibacterial activity of the complex.

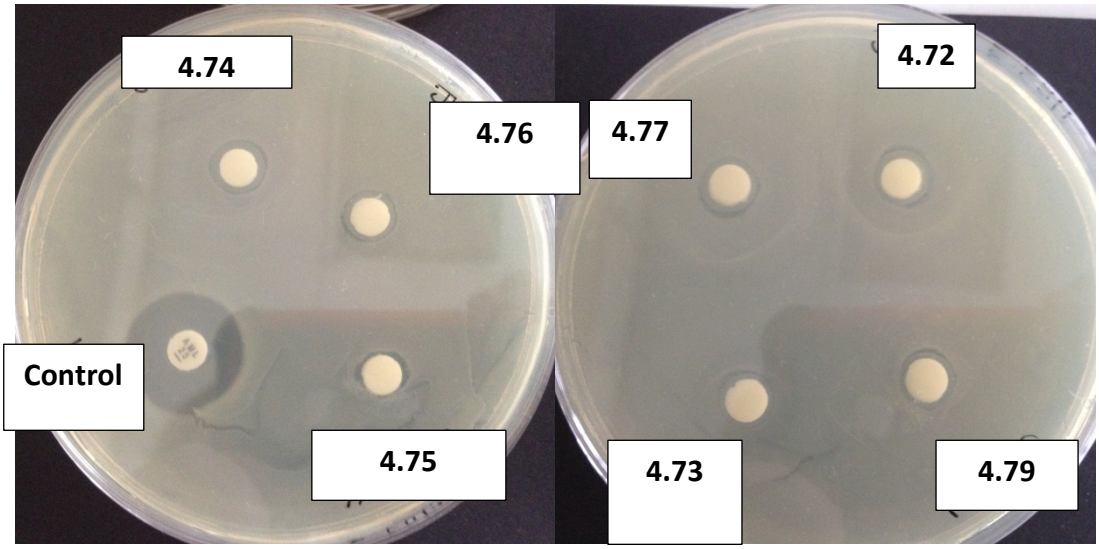

Figure 4.26 Photographs of the Mueller-Hinton plates containing *E.Coli.* bacteria and silver complexes **4.72** - **4.77** and **4.79** impregnated on aseptic disks (concentration 5 mg in 20 mL DMSO (99+%)).

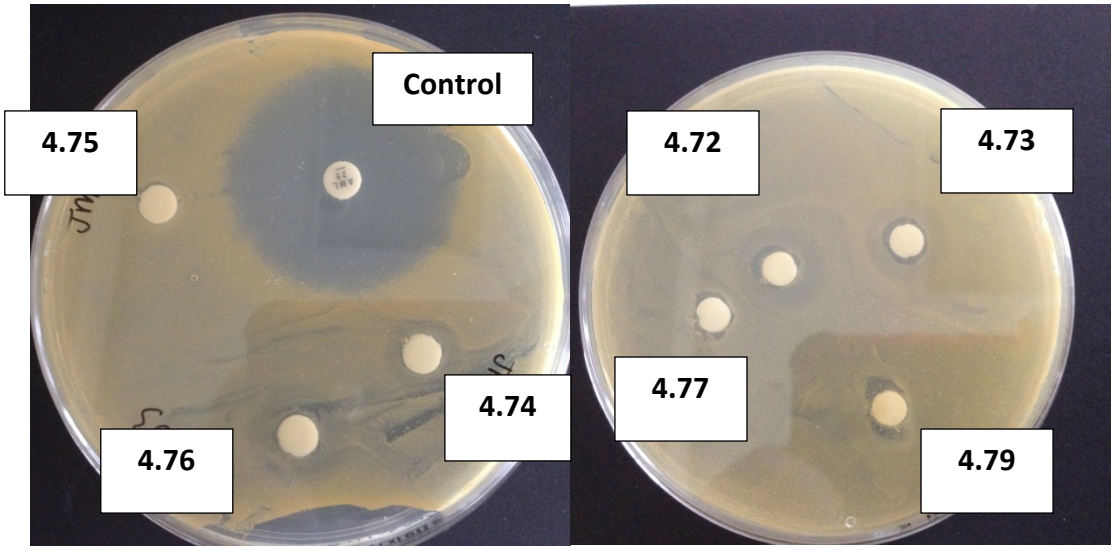

Figure 4.27 Photographs of the Mueller-Hinton plates containing *S. Aureus* bacteria and silver complexes **4.72** - **4.77** and **4.79** impregnated on aseptic disks (concentration 5 mg in 20 mL DMSO (99+%)).

All of the silver complexes (**4.72** - **4.77** and **4.79**) tested displayed antibacterial activity against *E.Coli.* Figures 4.26 and 4.27 displayed images of the resulting Mueller-Hinton plates. Between the two tested bacteria, *E. Coli* has a larger zone of inhibition for the majority of silver complexes tested than *S. Aureus.* In contrast, complex **4.79** is more antibacterial against *S. Aureus.* The differences observed in the diameter of the zone of inhibition may be due to the difference in the susceptibility of different bacteria to the prepared complexes having differing chemical structures.

Table 4.13 Zone of inhibition (diameter) measured for complexes **4.72** - **4.77** and **4.79** (concentration 5 mg in 20 mL DMSO (99+%)) against two types of bacteria.

Compound	*E. Coli* (in mm)	*S. Aureus* (in mm)
4.72	5.6	5.1
4.73	4.8	4.9
4.74	4.9	3.5
4.75	4.1	4.0
4.76	4.7	3.6
4.77	5.9	4.5
4.79	4.1	6.2
control	8.7	17.5

Increased concentrations of complexes **4.72** - **4.74**, **4.77** and **4.79** were then explored, again, using Gram-negative *E. Coli.* and Gram-positive *S. Aureus* bacteria. Related

ligands, **4.2**, **4.3**, **4.12**, **4.70**, and starting material $AgBF_4$ were also investigated in order to draw a comparison between starting material antibacterial activity and after complexation with Ag(I). The zone of inhibition results are tabulated in Table 4.14.

Table 4.14 Zone of inhibition (diameter) measured for complexes **4.72** - **4.75** and **4.77**, $AgBF_4$ and ligands **4.2**, **4.3**, **4.12 4.70**, at differing concentration (in DMSO (99+%)) against two types of bacteria.

Compound	***E. Coli* (in mm)**			***S. Aureus* (in mm)**		
	10mg in 20 mL	20mg in 20 mL	50mg in 20 mL	10mg in 20 mL	20mg in 20 mL	50mg in 20 mL
4.72	3.3	4.7	4.9	4.0	3.0	
4.73	5.1	6.2	7.1		3.0	3.0
4.74	3.2	4.7	4.9	4.2	4.2	
4.75	4.4	5.3	7.5	3.0	3.4	3.9
4.77	5.2	5.6	5.7	3.0	3.0	4.0
4.2			5.2		3.0	
4.3			3.5		3.0	
4.12			4.6		3.0	
4.70			3.9		3.0	
$AgBF_4$			3.2			5.0
control			9.5		17.1	

On increasing the concentration of the silver complexes on the impregnated disks, as expected, the zone of inhibition is increased for *E. Coli*. The highest antibacterial activity for silver complexes tested against *E. Coli*. are compounds **4.73** and **4.75**. Against *S. Aureus* silver complexes studied show limited or no improvement in antibacterial activity on increase of concentration.

Investigating the antibacterial activity of related ligands **4.2**, **4.3**, **4.12** and **4.70** showed the ligands themselves possessed antibacterial properties, especially against *E. Coli*. Ligand **4.2** showed the highest zone of inhibition against *E. Coli*., larger than the zones of inhibition recorded for some of the silver complexes tested against *E. Coli*. However, overall antibacterial activity against *E. Coli* was increased through coordination of PCN ligands to Ag(I).

Antibacterial activity against *E. Coli*. was improved from starting material $AgBF_4$ to final products, silver complexes **4.72** - **4.75** and **4.77**. The opposite was true against *S. Aureus*; $AgBF_4$ showed higher antibacterial activity than the silver complexes and

ligands trialled. Ligands **4.2**, **4.3**, **4.12** and **4.70** all showed a zone of inhibition of 3.0 mm, which would indicate that variation of the substituent on the chiral carbon does not influence antibacterial activity against *S. Aureus*. The silver complexes explored showed little improvement in antibacterial activity in comparison to the constituent ligands, with complex **4.74** showing the most improvement.

Further studies may be conducted to explore in more detail the antibacterial activity of the silver complexes synthesised as part of this thesis. This is likely to focus on *E. Coli.* since the preliminary studies discussed here show the presence of some antibacterial activity, though additional studies would determine on what scale the compounds are antibacterial through comparison studies. Future studies may also investigate the antibacterial activity of these complexes against additional strains of bacteria.

4.5 Summary

PCN ligands with amino acid moieties have previously been studied in literature, as discussed in Chapter 1 of this thesis.[3,9,14,145] Some of these ligands have been resynthesised, and the library of known PCN ligands with amino acid moieties has been broadened with dipeptides and unnatural amino acid substituents. L-glutamic acid was also investigated and found to cyclise to pyroglutamic acid under reflux undergoing addition of only one PCN moiety.

These ligands have undergone coordination with Pt(II), Ru(II) and Au(I), in an extension of the work previously conducted by the Smith group.[145] Coordination studies have been conducted with Cu(I), Au(I) and Ag(I) metal centres; inspired by the work by Katti and Blower, among others.[41,4,53,2,1] The silver(I) complexes formed were studied preliminarily for their antibacterial activity; the silver complexes **4.72** - **4.77** and **4.79** appeared to have activity against *E. Coli*., as did related ligands which were not explored to the same extent. Further studies on the antibacterial activity of complexes **4.72** - **4.77** and **4.79** would be of interest in future.

Several preliminary experiments were carried out to investigate mixed ligand complexes with the formula $[MPhen(P\hat{}P)]^{+}$. A mixture of heteroleptic and homoleptic complexes were yielded, as determined by $^{31}P\{^{1}H\}$ NMR. The heteroleptic complex **4.81** was isolated by slow evaporation of diethyl ether into a CH_2Cl_2 solution forming crystals suitable for X-ray crystallography. Further experimentation is required to resolve if heteroleptic and homoleptic species can be separated or if the heteroleptic species can be preferentially formed.

Chapter 5 – Conclusions and Future Work

5.1 Overview

This thesis has explored the synthesis of a number of PCN ligands, with the phosphine moieties (PPh_2CH_2-) introduced *via* the phosphorus analogous Mannich based condensation reaction. This included the formation of PCN ligands with fluorescent groups such as naphthlimides (Chapter 2), fluorescein and rhodamine derivatives (Chapter 3), and with non-fluorescent amino acids, both natural and unnatural (Chapter 4). All compounds synthesised as part of this thesis were analysed through standard spectroscopic techniques, with some compounds also studied by X-ray crystallography.

5.1.1 Chapter 2

Fluorescent sensors for medicinal applications, such as monitoring the biodistribution of metallodrugs or investigating the mode of action of metallodrugs, are an area of interest for researchers.[81,107,112] This chapter describes the synthesis of naphthalimide-based phosphine ligands, their corresponding metal complexes and a preliminary study of their photophysical properties.

Naphthalimides have been shown to possess antitumour, antiviral and medicinal imaging properties, as they can localise in cells, have DNA binding capabilities and strong fluorescent properties.[86–88] For this reason naphthalimdie fluorophores were chosen for the phosphine based probes. Phosphine moieties were chosen as donor atoms since phosphine chemistries are generally well established, as well as the benefits phosphine ligands bestow. These include the ability to manipulate physical properties, such as the electronic, steric and solubility capabilities of the metal complex they coordinate to, through the addition of different substituents on the phosphine moiety and the ability to stabilise low oxidation state metals.[6,7]

Four alkylamines were added to 4-bromo-1,8-naphthalic anhydride following a known literature procedure forming naphthalimides **2.5** – **2.8**.[129] Hydrazine hydrate was added to compounds **2.5** – **2.8** to synthesise hydrazides **2.12** – **2.15**; all hydrazides excluding **2.14** were known in the literature.[129] Analyses of novel hydrazide **2.14** were in agreement with the predicted chemical structure and correlated with analogous compounds **2.12**, **2.13** and **2.15**. Addition of the hydrazide substituent provided the free NH_2 group required for the addition of two PPh_2CH_2 moieties *via* the phosphorus analogous Mannich based condensation reaction and gave rise to novel PCN ligands **2.16** – **2.19**. While, during synthesis, ligands **2.16** – **2.18** precipitated out of solution allowing filtration, the reaction mixture for ligand **2.19** required evaporation to dryness in order to yield solid **2.19**; this is likely attributed to the hydroxyl group on

compound **2.19** enhancing solubility. The coordination capabilities of PCN ligands **2.16** – **2.19** were explored with platinum(II), palladium(II), gold(I) and silver(I) precursors. Silver(I) complexes **2.36** – **2.39** showed limited solubility and therefore analysis techniques which could be performed on these complexes were restricted and a study of their photophysical properties was not performed.

A preliminary study of the photophysical properties of two of the naphthalimide ligands (**2.16** – **2.19**) was conducted, with compounds **2.18** and **2.19** being chosen. Ligand **2.19** was especially of interest since the hydroxyl moiety of the alkyl chain aids solubility, as displayed during the synthesis of compound **2.19**. The respective coordination complexes of ligands **2.18** and **2.19** were also studied. Each compound was dissolved in DMSO (99+%) in varying concentrations (within the range: $2x10^{-6}$ to $1x10^{-5}$) and analysed by UV spectrophotometry to find the concentration at which the solution has 0.1 absorbance at the excitation maxima, λ_{ex}. Interestingly all compounds had a similar concentration at λ_{ex}. While ligand **2.19** had a similar absorbance maxima, λ_{ex}, as its related coordination complexes, ligand **2.18** differed from its related complexes by *ca.* 13 nm. This would suggest the alkyl chain influences the absorbance maxima. Future work could expand the study of photophysical properties to naphthalimides with different alkyl groups, like compounds **2.16** and **2.17**, but could also investigate the influence different moieties, not only alkyl chains, have on the photophysical properties. Due to the limited number of ligands studied here, future studies would limit uncertainity in the results presented in this thesis and confirm the difference in absorbance maxima is due to the influence of the alkyl chain.

Fluorescence measurements were taken of the 0.1 absorbance solutions of all of the compounds studied by UV spectrophotometry. For both **2.18** and **2.19**, the fluorescence intensity is reduced by a magnitude of 2-3 when coordinated to Pt(II) or Pd(II) most likely due to MLCT. This may suggest ligands **2.18** and **2.19** could be used in the detection of Pt(II) or Pd(II) through a change in intensity, though further study of the photophysical properties of these compounds is needed. For the respective gold(I) compounds synthesised, there was minimal difference in fluorescence intensity from parent ligands **2.18** and **2.19**. Due to the difference in the λ_{ex} for **2.18** and **2.19**, this results in a difference observed in the Stokes shift. Preliminary fluorescence lifetime measurements were conducted showing all compounds studied (**2.18**, **2.19**, **2.26**, **2.27**, **2.30**, **2.31**, **2.34** and **2.35**) had biexpontial decay and have similar lifetimes, though on coordination these lifetimes are reduced slightly; this would indicate static quenching is the cause of the reduction in intensity on coordination to Pt(II) and Pd(II).

Naphthalimides are versatile compounds which can undergo addition of a number of substituents in the imido position as well as in the 3-, 4-, 5- and 6- positions of the resulting naphthalimide. This was briefly explored and continues to be explored by the

Smith group; Section 2.4 discusses the attempt to add a diamine to 4-bromo-1,8-naphthalic anhydride, followed by the addition of PPh_2CH_2 groups to the free amine. Section 2.4 also describes how the addition of a substituent which can bond to targeting vectors, for example peptides, could aid the desired biodistribution of the naphthalimide if required.

5.1.2 Chapter 3

Similarly to Chapter 2, Chapter 3 aimed to synthesise fluorescent phosphine ligands with the potential to act as a fluorescent sensor for metals with medicinal properties, such as Pt(II), Pd(II) and Au(I). For example, these compounds may be useful in monitoring the biodistribution of a metallodrug or understanding the mechanism of action within a patient's body. Similarly to Chapter 2, Chapter 3 explores the addition of phosphine moieties to a fluorophore using the phosphorus analogous Mannich based condensation reaction, but the fluorophores of interest are fluorescein and rhodamine derivatives.

Hydrazine hydrate was added to the fluorescein/rhodamine fluorophores forming hydrazides **3.3** and **3.4**, following a procedure described by Shen *et al.*[154] Compounds **3.3** and **3.4** then underwent addition of PPh_2CH_2 *via* the phosphorus analogous Mannich based condensation to form ligands **3.5** and **3.6**. Attempts were made to add two PPh_2CH_2 moieties to **3.3** and **3.4**, however under the conditions trialled attempts were unsuccessful; this may be due to steric effects or from a change in basicity at the NH group. The coordination capabilities of monosubstituted phosphine ligands **3.5** and **3.6** were then explored using platinum(II), palladium(II) and gold(I). For platinum(II) coordination complexes, ligands arranged in a *cis* conformation, however in analogous palladium(II) complexes a mixture of both *cis* and *trans* arrangements were evident. This is likely due to the smaller atomic radius of palladium therefore making it more energetically favourable to arrange in a *trans* conformation. Ligand **3.5** was also investigated with cyclopalladated precursors forming complexes **3.13** and **3.14**. Cyclopalladated compounds are of interest as anticancer agents, in order to improve stability of metallodrugs and ensure they reach their biological target.[57,59]

UV spectrophotometry on ligands **3.5** and the respective complexes **3.9**, **3.11** and **3.15** all showed an excitation maxima, λ_{ex}, at 280 nm [in DMSO (99+%)]. Palladium(II) complex **3.11** showed an additional peak at 340 nm. Fluorescein derivatives often have an excitation maximum at *ca.* 516 nm, however this is not the case for compounds **3.5**, **3.9**, **3.11** and **3.15**, which potentially may be a result of an adopted spirolactam conformation.[154,160] Fluorescence measurements were taken of solutions **3.5**, **3.9**, **3.11**

and **3.15** at the concentration which they display 0.1 absorbance at excitation wavelength, 280 nm. Fluorescence spectrophotometry showed only ligand **3.5** fluoresced; this may suggest ligand **3.5** could be used as a "turn-off" fluorescence sensor in the detection of metals, however further work will need to be conducted. Research into the influence a broader range of metals has on the photophysical properties of **3.5** will determine if there is selective quenching, which is likely to give greater insight.

The UV absorbance peak at 340 nm for palladium complex **3.11** was also investigated. All compounds (**3.5**, **3.9** and **3.15**) were made up to the concentration at which **3.11** had 0.1 absorbance at 340 nm, and their photophyscial properties were explored using a fluorophotometer. All compounds displayed some fluorescence, though complex **3.11** displayed a 3-fold greater intensity than all other compounds trialled. However, fluorescence spectra collected were complex and there were no emission maximums for any of the compounds. Further work must be conducted to understand the photophysical properties of these compounds.

Rhodamine derivatives **3.6**, **3.10**, **3.12** and **3.16** were investigated using UV spectrophotometry. Ligand **3.6** and complexes **3.10**, **3.12** and **3.16** all showed an absorbance maxima at *ca.* 316 nm. The palladium(II) and platinum(II) complexes, **3.16** and **3.12** respectively, also had a peak at 566 nm which was not observed in the related compounds **3.6** and **3.16**. Spirocyclic rhodamine derivatives are non-fluorescent and colourless. It is possible that on complexation with Pt(II) and Pd(II) the spirocyclic ring has ring-opened to produce the pink products observed and an absorption band in the region expected for ring-open rhodamine derivatives.[155]

Investigating the fluorescence of compounds **3.6**, **3.10**, **3.12** and **3.16** at a fixed excitation wavelength of 316 nm, all compounds exhibited fluorescence and had a similar Stokes shift making it unlikely that excitation at 316 nm could be used for sensing purposes. On excitation at 516 nm however, both the platinum(II) and palladium(II) complex fluoresced (**3.10** and **3.12**) but the uncoordinated ligand **3.6** and its gold(I) complex **3.16** did not. This may suggest ligand **3.6** could be used as a "turn-on sensor" for the detection of Pt(II) and Pd(II) metals. Future work will further explore the photophysical properties of these compounds and investigate the photophysical properties of ligand **3.6** coordinated to other metals and to other platinum and palladium starting materials.

Fluoresceinamine isomer I was also investigated for several reasons, including the presence of a primary amine group which eliminates the need for the hydrazine hydrate step. Moving the position of the amine provides insight into the influence the position of the PPh_2CH_2- moieties has on the photophysical properties and it also

allows for the addition of two PPh_2CH_2- moieties to the fluorescein derivative. Two PPh_2CH_2 moieties were added to fluoresceinamine isomer I to form ligand **3.18**, followed by the coordination chemistries of ligand **3.18** being explored using platinum(II), palladium(II) and gold(I) precursors.

Fluoresceinamine isomer I, **3.17**, has limited fluorescence due to intramolecular quenching, as a result of the donation of the amine lone pair into the fluorophore's π system.[162] Excitation and emission maxima are observed at λ_{ex} = 488 nm and λ_{em} = 530 nm for fluoresceinamine isomer 1, **3.17**, however for the functionalised derivatives **3.18** - **3.21** no UV absorbance was recorded in this region. This suggests that intramolecular quenching is also present here. Despite this ligand **3.18** and complexes **3.19** – **3.21** all showed a single absorbance maxima at 277 nm. Fluorescence measurements of compounds **3.18** - **3.21** when excited at 277 nm showed complexes **3.19** – **3.21** displayed no fluorescence. Ligand **3.18**, however displayed fluorescence, with an emission maxima at 430 nm. No emission for complexes **3.19** – **3.21** may be due to MLCT.

Further work investigating the photophysical properties of ligand **3.18** and corresponding complexes will be researched in more detail with exploration of the potential of compound **3.18** to act as a "turn-off" fluorescence sensor for the determination of metals, such as Pd(II), Pt(II) and Au(I), though future studies may investigate any differences in fluorescence emission with a number of other metals.

Fluorescein derivatives have been explored in the literature for medicinal applications such as sensors in cellular imaging.[107] Therefore novel ligands **3.5**, **3.6**, **3.18** and derivatives of these compounds may have potential for medicinal applications and will be explored further by the Smith group in future.

5.1.3 Chapter 4

Aminomethylphosphine ligands with amino acid backbones have been explored in the literature for their potential towards a number of applications.[3,9,145,183] Zhang *et al.* utilised the phosphorus analogous Mannich based condensation reaction to synthesise aminomethylphosphines, ligands **4.1** – **4.3**, which were coordinated to rhenium, for the purposes of forming new radiopharmaceuticals for PET imaging.[3] The amino acid backbone could be extended through the carboxylic acid moiety to a peptide based targeting vector in a "preformed chelate" fashion.[3]

In continuation of the work our research group has already conducted, the number of amino acid backbones, both natural and unnatural, with PCNCP moieties was

expanded. This included using precusors such as aminohippuric acid, which is known for its use as a diagnostic agent and N-alpha-Cbz-L-lysine, which possesses a second amine protected by a carboxybenzyl moiety, therefore providing an additional functional group suitable, once deprotected, for conjugation to a peptide or conjugation to alternative moieties for the purposes of modifying chemical properties or providing an additional donor site for coordination to another metal.[166]

The coordination capabilities of the ligands synthesised were then explored with platinum(II), ruthenium(II) and gold(I) precursors. This was further expanded to group 11 metals: copper(I), silver(I) and gold(I). The silver(I) complexes formed were studied primarily for their antibacterial activity. Silver complexes **4.72** – **4.77** and **4.79** appeared to have activity against *E. Coli*. and therefore further studies on the antibacterial activity of complexes **4.72** – **4.77** and **4.79** would be of interest in the future.

L-glutamic acid was also explored. However under reaction conditions, L-glutamic acid cyclised to form pyroglutamic acid and only monoaddition of PPh_2CH_2 occurred. Monofunctionalised phosphine, **4.24**, underwent coordination with gold(I), platinum(II) and ruthenium(II) metal precursors.

Chapter 6 - Experimental

6.1 General Procedure

Unless otherwise stated, all reactions were carried out in air. All air- and/or water-sensitive reactions were carried out in the presence of an inert atmosphere using standard Schenk procedures, involving degassed solvents and, where required, freeze thaw cycles. Reagents and solvents were purchased from Aldrich or Alfa Aesar and were used as received. Metal precursors $PtCl_2(cod)$, $PdCl_2(cod)$,[184] AuCl(tht),[185] $\{RuCl(\mu\text{–}Cl)(\eta^6\text{–}p\text{–}cym)\}_2$,[186] $[Pd(\mu\text{-}Cl)(C_9H_{12}N)]_2$ and $[Pd(\mu\text{-}Cl)(C_{12}H_{12}N)]_2$ were prepared according to published procedures. The preparation of the tertiary phosphine, Ph_2PCH_2OH, was carried out utilising equimolar amounts of Ph_2PH and $(CH_2O)_n$ according to the literature.[187]

6.2 Instrumentation

NMR data was recorded in $CDCl_3$ or $(CD_3)_2SO$, and collected (*ca.* 298K) on a Bruker DPX–400 instrument or JEOL ECS spectrometer. Chemical shifts were recorded relative to $Si(CH_3)_4$ for ^1H and 85% H_3PO_4 for $^{31}P\{^1H\}$ NMR. The instrument operated at 400 MHz for ^1H and 161.98 MHz for $^{31}P\{^1H\}$ NMR when collecting spectra. The following abbreviations are used b, broad; s, singlet; d, doublet; t, triplet; q, quartet; p, pentet (quintet); sept, septuplet; m, multiplet. Infra–red spectra were recorded as KBr discs using a Perkin–Elmer Spectrum 100 FT–IR spectrometer (4000–250 cm^{-1}). All compounds were analysed (Thermo Scientific™ Exactive™ instrument) by high resolution (HRMS) electrospray in positive ionisation mode (ESI^+) using CH_2Cl_2 or CH_3OH as the solvent within the Chemistry Department, or using the EPSRC UK National Mass Spectrometry Service at Swansea University. ESI-MS was recorded when there was >5 ppm difference between the recorded and calculated mass for the ion. Elemental analyses (Exeter Analytical, Inc. CE-440 Elemental Analyzer) were performed by the Loughborough University Analytical Service within the Department of Chemistry. The errors limits were ± 0.5% for elemental analyses. Molar magnetic susceptibility was measured on a Sherwood Scientific Magnetic Susceptibility Balance within the Department of Chemistry.

6.3 Chapter 2 Experimental

Compounds **2.5** and **2.8** were prepared following a known procedure which is explained for **2.5** as an example and extended to **2.6**, **2.7** and **2.8**.[129]

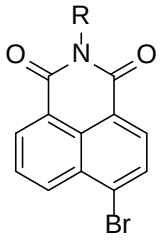

R = **(2.5)** $(CH_2)_3CH_3$
(2.6) $(CH_2)_7CH_3$
(2.7) $(CH_2)_2OCH_3$
(2.8) $(CH_2)_2O(CH_2)_2OH$

$C_{16}H_{14}BrNO_2$ (2.5)

4-Bromo-1,8-naphthalic anhydride (2.501g, 9.027 mmol) and butylamine (1.321g, 18.061 mmol) were suspended together in glacial acetic acid (20 mL) and refluxed, under a nitrogen atmosphere, for *ca*. 72h. The dark brown solution was allowed to cool to ambient temperature before slow addition to fast stirring ice/DH_2O (200mL). After stirring for *ca*. 60 min the light brown suspension was filtered, washed with a large volume of distilled H_2O and dried *in vacuo*. The light brown solid was recrystallized from a minimum volume of EtOH, filtered under suction and dried *in vacuo* to yield light brown/grey solid (2.40g, 80%). Crystals suitable for X-ray crystallographic analysis were obtained from slow evaporation of the mother liquor (EtOH). **^{1}H NMR** (400 MHz, $CDCl_3$) δ 8.64 (1H, dd, J = 7.3, 0.9Hz, Ar-H), 8.55 (1H, dd, J = 8.7, 0.9Hz, Ar-H), 8.40 (1H, d, J = 8.2Hz, Ar-H), 8.02 (1H, d, J = 8.2Hz, Ar-H), 7.83 (1H, dd, J = 7.6Hz, Ar-H), 4.16 (2H, t, J = 7.6Hz, N-CH_2), 1.75-1.65 (2H, m, CH_2), 1.49-1.37 (2H, m, CH_2), 0.96 (3H, t, J = 7.3Hz, CH_3) ppm; **FT-IR** (KBr): *v* = 3025(Ar-H), 1650(C=O), 1575(C=C), 1429(CH_2), 1359(CH_3) cm^{-1}; **CHN:** $C_{16}H_{14}BrNO_2$ requires C (57.85%), H (4.25%), N (4.22%), found: C (57.43%), H (4.19%), N (4.18%); **ESI-MS**: calcd for $C_{16}H_{15}BrNO_2$ $[M + H]^+$ requires m/z 332.0281, found *m/z* 332.0276 (1.3 ppm).

$C_{20}H_{22}BrNO_2$ (2.6)

From 4-bromo-1,8-naphthalic anhydride (2.505g, 9.041 mmol) and octylamine (2.332g, 18.044 mmol). **Yield:** 2.916g, 83%; **Appearance:** cream/light brown solid; **^{1}H NMR** (400

MHz, $CDCl_3$) δ 8.64 (1H, dd, J = 7.4, 0.8Hz, Ar-H), 8.54 (1H, dd, J = 8.7, 0.8Hz, Ar-H), 8.39 (1H, d, J = 8.2Hz, Ar-H), 8.02 (1H, d, J = 7.8Hz, Ar-H), 7.83 (1H, dd, J = 8.4, 7.2Hz, Ar-H), 4.14 (2H, t, J = 7.6Hz, N-CH_2), 1.75-1.65 (2H, m, CH_2), 1.44-1.19 (10H, m, CH_2), 0.85 (3H, t, J = 6.8Hz, CH_3) ppm; **FT-IR** (KBr): *v* = 1641(C=O), 1457(CH_2), 1570(C=C), 1365(CH_3), 1052(CN), 857(Ar-H), 784(Ar-H) cm^{-1}; **CHN:** Despite repeated attempts, a satisfactory elemental analysis was not obtained; **ESI-MS:** calcd for $C_{20}H_{23}BrNO_2$ $[M + H]^+$ requires m/z 388.0907, found *m/z* 388.0903 (0.3 ppm).

$C_{15}H_{12}BrNO_3$ (2.7)

From 4-bromo-1,8-naphthalic anhydride (2.495g, 9.005 mmol) and 2-methoxyethylamine (1.365g, 18.173 mmol). **Yield:** 2.617g, 87%; **Appearance:** light brown/grey solid; **^{1}H NMR** (500 MHz, $CDCl_3$) δ 8.69 (1H, d, J = 6.5Hz, Ar-H), 8.59 (1H, d, J = 9.0Hz, Ar-H), 8.44 (1H, d, J = 8.0Hz, Ar-H), 8.06 (1H, d, J = 8.0Hz, Ar-H), 7.87 (1H, dd, J = 7.5Hz, Ar-H), 4.46 (2H, t, J = 5.5Hz, N-CH_2-C<u>H</u>$_2$-O), 3.76 (2H, t, J = 5.5Hz, N-C<u>H</u>$_2$-CH_2-O), 3.40 (3H, s, CH_3) ppm; **FT-IR** (KBr): *v* = 3090(Ar-H), 1659(C=O), 1571(C=C), 1371(CH_3), 1232(C-O), 1113(CN), 780(Ar-H), cm^{-1}; **CHN:** $C_{15}H_{12}BrNO_3$ requires C (53.91%), H (3.62%), N (4.19%), found: C (53.95%), H (3.75%), N (3.83%); **ESI-MS:** calcd for $C_{15}H_{13}BrNO_3$ $[M + H]^+$ requires m/z 334.0073, found *m/z* 334.0068 (1.6 ppm).

$C_{16}H_{14}BrNO_4$ (2.8)

From 4-bromo-1,8-naphthalic anhydride (2.480g, 8.951 mmol) and 2-(2-aminoethoxy)ethanol (1.900g, 18.072 mmol). **Yield:** 2.945g, 90%; **Appearance:** light brown/grey solid; **^{1}H NMR** (500 MHz, $CDCl_3$) δ 8.68 (1H, d, J = 7.1Hz, Ar-H), 8.60 (1H, d, J = 8.5Hz, Ar-H), 8.44 (1H, d, J = 7.5Hz, Ar-H), 8.07 (1H, d, J = 8.0Hz, Ar-H), 7.88 (1H, t, J = 8.5Hz, Ar-H), 4.46 (2H, t, J = 6.0Hz, CH_2), 4.20 (2H, t, J = 5.0Hz, CH_2), 3.86 (2H, t, J = 6.0Hz, CH_2), 3.76 (2H, t, J = 5.0Hz, CH_2), 1.62 (1H, s, OH) ppm; **FT-IR** (KBr): *v* = 3470(OH), 1670(C=O), 1570(C=C), 1459(CH_2), 1231(C-O), 1055(CN), 863(Ar-H), cm^{-1}; **CHN:** $C_{16}H_{14}BrNO_4$ requires C (52.77%), H (3.87%), N (3.85%), found: C (52.36%), H (3.09%), N (3.74%); **ESI-MS:** calcd for $C_{16}H_{15}BrNO_4$ $[M + H]^+$ requires m/z 364.0179, found *m/z* 364.0172 (0.7 ppm).

Compounds **2.12** and **2.15** were prepared following a known procedure which is explained for **2.12** as an example and also extended to **2.14**.[129] Compound **2.13** required longer reflux times as specified below.

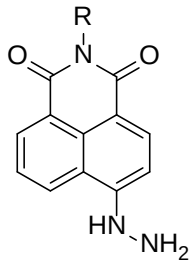

R = **(2.12)** $(CH_2)_3CH_3$
(2.13) $(CH_2)_7CH_3$
(2.14) $(CH_2)_2OCH_3$
(2.15) $(CH_2)_2O(CH_2)_2OH$

$C_{16}H_{17}N_3O_2$ (2.12)

Hydrazine monohydrate (0.9mL, 98%) and **2.5** (1.005g, 3.036 mmol) were added together to 2-methoxyethanol (30mL) and refluxed, under a nitrogen atmosphere, for 2h. The dark brown/orange solution was allowed to cool to ambient temperature and left to stand for *ca.* 12h. After this time an orange solid had formed. The suspension was filtered under suction, washed with a small volume of 2-methoxyethanol and dried *in vacuo* to yield an orange solid (0.665g, 76%). **^{1}H NMR** (400 MHz, d_6-DMSO) δ 9.07 (1H, s, NH), 8.55 (1H, d, J = 8.6Hz, Ar-H), 8.36 (1H, d, J = 6.4Hz, Ar-H), 8.23 (1H, d, J = 8.6Hz, Ar-H), 7.58 (1H, dd, J = 7.7 Hz, Ar-H), 7.19 (1H, d, J = 8.6Hz, Ar-H), 4.63 (2H, s, NH_2), 3.96 (2H, t, J = 7.5Hz, N-CH_2), 1.58-1.47 (2H, m, CH_2), 1.34-1.22 (2H, m, CH_2), 0.87 (3H, t, J = 7.3Hz, CH_3) ppm; **FT-IR** (KBr): *v* = 3379(NH), 3319(NH), 1638(C=O), 1356(CH_3), 777(Ar-H) cm^{-1}; **CHN:** Despite repeated attempts, a satisfactory elemental analysis was not obtained; **ESI-MS**: calcd for $C_{16}H_{18}N_3O_2$ $[M + H]^+$ requires m/z 284.1394, found *m/z* 284.1389 (1.6 ppm).

$C_{20}H_{25}N_3O_2$ (2.13)

Hydrazine monohydrate (2.2ml, 98%) and **2.6** (2.849g, 7.360 mmol) were added together to 2-methoxyethanol (50mL) and refluxed, under a nitrogen atmosphere, for *ca.* 24h. The dark brown/orange solution was allowed to cool to ambient temperature

and left to stand for *ca.* 12h. After this time, no solid had formed. To induce precipitation, distilled H_2O (50mL) was added to the brown/orange solution, forming an orange suspension. The suspension was filtered under suction, washed with a small volume of distilled H_2O and dried *in vacuo* to yield an orange solid (1.435g, 58%). **^{1}H NMR** (400 MHz, d_6-DMSO) δ 9.08 (1H, s, NH), 8.55 (1H, d, J = 7.8Hz, Ar-H), 8.36 (1H, d, J = 6.9Hz, Ar-H), 8.23 (1H, d, J = 8.7Hz, Ar-H), 7.58 (1H, dd, J = 7.8Hz, Ar-H), 7.19 (1H, d, J = 8.7Hz, Ar-H), 4.63 (2H, s, NH_2), 3.94 (2H, t, J = 7.6Hz, N-CH_2), 1.62-1.46 (2H, m, CH_2), 1.33-1.11 (10H, m, CH_2), 0.79 (3H, t, J = 6.6Hz, CH_3) ppm; **FT-IR** (KBr): *v* = 3469(NH), 3417(NH), 3298(NH), 1695(C=O), 1580(C=C), 1467(CH), 777(Ar-H) cm^{-1}; **CHN:** Despite repeated attempts, a satisfactory elemental analysis was not obtained; **ESI-MS**: calcd for $C_{20}H_{26}N_3O_2$ $[M + H]^+$ requires m/z 340.2020, found *m/z* 340.2020 (0.1 ppm).

$C_{15}H_{15}N_3O_3$ (2.14)

From hydrazine monohydrate (0.9mL, 98%) and **2.7** (1.006g, 3.021 mmol). **Yield:** 0.559g, 66%; **Appearance:** orange solid; **^{1}H NMR** (400 MHz, d_6-DMSO) δ 9.10 (1H, s, NH), 8.56 (1H, d, J = 8.2Hz, Ar-H), 8.36 (1H, d, J = 7.0Hz, Ar-H), 8.23 (1H, d, J = 8.2Hz, Ar-H), 7.58 (1H, dd, J = 7.8Hz, Ar-H), 7.19 (1H, d, J = 8.7Hz, Ar-H), 4.64 (2H, s, NH_2), 4.17 (2H, t, J = 6.4Hz, N-CH_2-C$\underline{H}_2$-O), 3.51 (2H, t, J = 6.4Hz, N-C$\underline{H}_2$-CH_2-O), 3.21 (3H, s, CH_3) ppm; **FT-IR** (KBr): *v* = 3372(NH), 3319(NH), 3269(NH), 1677(C=O), 1582(C=C), 1367(CH_3), 1249(C-O), 1084(CN), 775(Ar-H), 687(Ar-H) cm^{-1}; **CHN:** Despite repeated attempts, a satisfactory elemental analysis was not obtained; **ESI-MS**: calcd for $C_{15}H_{16}N_3O_3$ $[M + H]^+$ requires m/z 286.1186, found *m/z* 286.1180 (0.7 ppm).

$C_{16}H_{17}N_3O_4$ (2.15)

From hydrazine monohydrate (0.8mL, 98%) and **2.8** (1.011g, 2.785 mmol). **Yield:** 0.443g, 51%; **Appearance:** orange solid; **^{1}H NMR** (400 MHz, d_6-DMSO) δ 9.11 (1H, s, NH), 8.57 (1H, d, J = 8.2Hz, Ar-H), 8.37 (1H, d, J = 7.0Hz, Ar-H), 8.24 (1H, d, J = 8.7Hz, Ar-H), 7.59 (1H, dd, J = 7.8Hz, Ar-H), 7.20 (1H, d, J = 8.7Hz, Ar-H), 4.64 (2H, s, NH_2), 4.59-4.51 (1H, m, OH), 4.16 (2H, t, J = 6.6Hz, N-CH_2-C$\underline{H}_2$-O), 3.57 (2H, t, J = 6.6Hz, N-C$\underline{H}_2$-CH_2-O), 3.42 (4H, d, J = 2.5Hz, C$\underline{H}_2$-C$\underline{H}_2$-OH) ppm; **FT-IR** (KBr): *v* = 3412(OH), 3315(NH), 1675(C=O), 1574(C=C), 1541(NH), 1450(CH2), 1246(C-O), 1055(CN), cm^{-1}; **CHN:** $C_{16}H_{17}N_3O_4$ requires C (60.94%), H (5.43%), N (13.33%), found: C (60.55%), H (5.08%), N (13.17%); **ESI-MS**: calcd for $C_{16}H_{18}N_3O_4$ $[M + H]^+$ requires m/z 316.1292, found *m/z* 316.1287 (1.7 ppm).

Compounds **2.17** – **2.18** were prepared in an identical manner to that described for **2.16**. Compound **2.19** was isolated in an alternative manner, as described below.

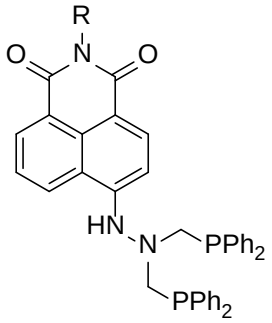

R = **(2.16)** $(CH_2)_3CH_3$
(2.17) $(CH_2)_7CH_3$
(2.18) $(CH_2)_2OCH_3$
(2.19) $(CH_2)_2O(CH_2)_2OH_3$

$C_{42}H_{39}N_3O_2P_2$ (2.16)

Ph_2PCH_2OH (80% purity, 0.741g, 2.744 mmol) and **2.12** (0.306g, 1.1081 mmol) in degassed MeOH (10mL) were refluxed, under a nitrogen atmosphere, for 90 min. The orange suspension was allowed to cool to ambient temperature and continued to stir for *ca.* 72h. The yellow suspension was filtered under suction, washed with a small volume of MeOH and dried *in vacuo* to yield a bright yellow solid (0.559g, 76%). **^{1}H NMR** (400 MHz, $CDCl_3$) δ 8.51 (1H, d, J = 6.8Hz, Ar-H), 8.19 (1H, d, J = 8.1Hz, Ar-H), 7.50 (1H, d, J = 8.1Hz, Ar-H), 7.43 (1H, dd, J = 7.7 Hz, Ar-H), 7.40-7.26 (20H, m, Ar-H), 6.76 (1H, d, J = 8.6Hz, Ar-H), 6.32 (1H, s, NH), 4.14 (2H, t, J = 7.5Hz, N-CH_2), 4.00 (4H, s, CH_2), 1.73-1.63 (2H, m, CH_2), 1.48-1.37 (2H, m, CH_2), 0.95 (3H, t, J = 7.3 Hz, CH_3) ppm; **^{31}P{^{1}H} NMR** (162 MHz, $CDCl_3$) δ -28.36 ppm; **FT-IR** (KBr): *v* = 3440(NH), 1681(C=O), 1584(C=C), 1360(CH_3), 1095(CN), 777(NH), 737(Ar-H), 695(Ar-H) cm^{-1}; **CHN:** $C_{42}H_{39}N_3O_2P_2$ requires C (74.21%), H (5.78%), N (6.18%), found: C (74.07%), H (5.74%), N (6.20%); **ESI-MS**: calcd for $C_{42}H_{40}N_3O_2P_2$ $[M + H]^+$ requires m/z 680.2590, found *m/z* 680.2579 (1.6 ppm).

$C_{46}H_{47}N_3O_2P_2$ (2.17)

From Ph_2PCH_2OH (90%, 0.423g, 1.763 mmol) and **2.13** (0.283g, 0.834 mmol). **Yield:** 0.529g, 86%; **Appearance:** bright yellow solid**; ^{1}H NMR** (400 MHz, $CDCl_3$) δ 8.51 (1H, d, J = 6.9Hz, Ar-H), 8.19 (1H, d, J = 8.2Hz, Ar-H), 7.50 (1H, d, J = 8.2Hz, Ar-H), 7.43 (1H, dd, J = 7.8Hz, Ar-H), 7.40-7.23 (20H, m, Ar-H), 6.76 (1H, d, J = 8.7Hz, Ar-H), 6.33 (1H, s, NH),

4.12 (2H, t, J = 7.6 Hz, N-CH_2), 4.00 (4H, s, CH_2), 1.74-1.64 (2H, m, CH_2), 1.44-1.19 (10H, m, CH_2), 0.85 (3H, t, J = 6.9 Hz, CH_3) ppm; **$^{31}P\{^1H\}$ NMR** (162 MHz, $CDCl_3$) δ -28.32 ppm; **FT-IR** (KBr): *v* = 3469(NH), 1687(C=O), 1573(C=C), 1464(CH), 777(Ar-H), 696(Ar-H) cm^{-1}; **CHN:** $C_{46}H_{47}N_3O_2P_2$·MeOH requires C (73.52%), H (6.69%), N (5.47%), found: C (73.18%), H (6.24%), N (6.08%); **ESI-MS**: calcd for $C_{46}H_{48}N_3O_2P_2$ $[M + H]^+$ requires m/z 736.3216, found *m/z* 736.3226 (0.9 ppm).

$C_{41}H_{37}N_3O_3P_2$ (2.18)

From Ph_2PCH_2OH (90%, 0.503g, 2.096 mmol) and **2.14** (0.300g, 1.052 mmol). **Yield:** 0.576g, 80%; **Appearance:** bright yellow solid; **^1H NMR** (400 MHz, $CDCl_3$) δ 8.52 (1H, d, J = 7.3Hz, Ar-H), 8.20 (1H, d, J = 8.6Hz, Ar-H), 7.50 (1H, d, J = 8.1Hz, Ar-H), 7.43 (1H, dd, J = 7.7Hz, Ar-H), 7.40-7.23 (20H, m, Ar-H), 6.76 (1H, d, J = 8.6Hz, Ar-H), 6.34 (1H, s, NH), 4.40 (2H, t, J = 6.0Hz, N-CH_2-C<u>H</u>$_2$-O), 4.00 (4H, s, CH_2), 3.70 (2H, t, J = 6.0 Hz, N-C<u>H</u>$_2$-CH_2-O), 3.37 (3H, s, CH_3) ppm; **$^{31}P\{^1H\}$ NMR** (162 MHz, $CDCl_3$) δ -28.33 ppm; **FT-IR** (KBr): *v* = 3434(NH), 1679(C=O), 1583(C=C), 1480(CH_2), 1381(CH_3), 1242(C-O), 1059(CN), 739(Ar-H), 695(Ar-H) cm^{-1}; **CHN:** $C_{41}H_{37}N_3O_3P_2$ requires C (72.24%), H (5.47%), N (6.16%), found: C (71.84%), H (5.20%), N (6.21%); **ESI-MS**: calcd for $C_{41}H_{38}N_3O_3P_2$ $[M + H]^+$ requires m/z 682.2383, found *m/z* 682.2383 (0.1 ppm).

$C_{42}H_{39}N_3O_4P_2$ (2.19)

Ph_2PCH_2OH (90% purity, 0.480g, 1.998 mmol) and **2.15** (0.300g, 0.952 mmol) in degassed MeOH (15mL) were refluxed, under a nitrogen atmosphere, for 3h. The orange/yellow solution was allowed to cool to ambient temperature and continued to stir for *ca.* 72h. The solution was reduced to dryness *in vacuo* to yield an orange/yellow solid (0.752g, 79%). **^1H NMR** (400 MHz, $CDCl_3$) δ 8.50 (1H, d, J = 7.3Hz, Ar-H), 8.19 (1H, d, J = 8.1 Hz, Ar-H), 7.53-7.23 (22H, m, Ar-H), 6.76 (1H, d, J = 8.6Hz, Ar-H), 6.38 (1H, s, NH), 4.40 (2H, t, J = 5.6Hz, CH_2), 4.00 (4H, s, CH_2), 3.83 (2H, t, J = 5.6Hz, CH_2), 3.71-3.64 (4H, m, CH_2), 2.67 (1H, *br.* s, OH) ppm; **$^{31}P\{^1H\}$ NMR** (162 MHz, $CDCl_3$) δ -28.32 ppm; **FT-IR** (KBr): *v* =3468(OH), 3419(NH), 1638(C=O), 1579(C=C), 1433(CH2), 1244(C-O), 1048(CN), 861(Ar-H), cm^{-1}; **CHN:** $C_{42}H_{39}N_3O_4P_2$ requires C (70.88%), H (5.52%), N (5.90%), found: C (70.70%), H (5.34%), N (6.00%); **ESI-MS**: calcd for $C_{42}H_{40}N_3O_4P_2$ $[M + H]^+$ requires m/z 712.2489, found *m/z* 712.2484 (0.6 ppm).

Coordination Compounds (2.24 – 2.35)

Unless otherwise stated, the following Pt(II), Pd(II) and Au(I) complexes were synthesised through the reaction of appropriate metal precursors, $PtCl_2$(cod), $PdCl_2$(cod) and AuCl(tht), with ligands **2.16 – 2.19**. Following 1h stirring in CH_2Cl_2, the solvent volume was reduced to 1-2mL and Et_2O was added resulting in the precipitation of complexes **2.24 – 2.35**.

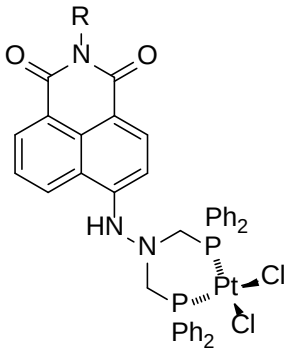

R = **(2.24)** (CH
(2.25) $(CH_2)_3CH_3$
$(CH_2)_7CH_3$
(2.26) $(CH_2)_2OCH_3$
(2.27) $_2)_2O(CH_2)_2OH$

$C_{42}H_{39}N_3O_2P_2PtCl_2$ (2.24)

From **2.16** (0.100g, 0.147 mmol) and $PtCl_2$(cod) (0.056g, 0.150 mmol). **Yield:** 0.130g, 92%; **Appearance:** yellow solid;**^{1}H NMR** (400 MHz, d_6-DMSO) δ 9.63 (1H, s, NH), 8.40-8.32 (2H, m, Ar-H), 8.13-7.94 (3H, m, Ar-H), 7.77-7.35 (19H, m, Ar-H), 5.52 (1H, d, J = 8.2Hz, Ar-H), 4.47-4.28 (2H, m, CH_a), 4.11-3.96 (2H, m, CH_b), 3.92 (2H, t, J = 7.3Hz, N-CH_2), 1.56-1.45 (2H, m, CH_2), 1.32-1.23 (2H, m, CH_2), 0.86 (3H, t, J = 7.3Hz, CH_3) ppm; **^{31}P{^{1}H} NMR** (162 MHz, d_6-DMSO) δ 0.13 ($^1J_{PtP}$ = 3449Hz) ppm; **FT-IR** (KBr): *v* = 3420(NH), 1688(C=O), 1582(C=C), 1359(CH_3), 777(Ar-H), 692(Ar-H), 318(PtCl), 296(PtCl) cm^{-1}; **CHN:** $C_{42}H_{39}N_3O_2P_2PtCl_2$ requires C (53.34%), H (4.16%), N (4.44%), found: C (53.19%), H (4.14%), N (4.27%); **ESI-MS**: calcd for $C_{42}H_{39}N_3O_2P_2PtCl$ $[M - Cl]^+$ requires m/z 909.1848, found *m/z* 909.1836 (1.2 ppm).

$C_{46}H_{47}N_3O_2P_2PtCl_2$ (2.25)

From **2.17** (0.100g, 0.136 mmol) and $PtCl_2$(cod) (0.048g, 0.128 mmol). **Yield:** 0.113g, 87%; **Appearance:** orange solid; **^{1}H NMR** (400 MHz, d_6-DMSO) δ 9.62 (1H, s, NH), 8.40-

8.31 (2H, m, Ar-H), 8.11-7.97 (3H, m, Ar-H), 7.75-7.35 (19H, m, Ar-H), 5.52 (1H, d, J = 8.6Hz, Ar-H), 4.44-4.27 (2H, m, CH_a), 4.09-3.96 (2H, m, CH_b), 3.91 (2H, t, J = 7.3Hz, N-CH_2), 1.56-1.45 (2H, m, CH_2), 1.28-1.14 (10H, m, CH_2), 0.81 (3H, t, J = 6.6Hz, CH_3) ppm; **$^{31}P\{^1H\}$ NMR** (162 MHz, d_6-DMSO) δ 0.13 ($^1J_{PtP}$ = 3456Hz) ppm; **FT-IR** (KBr): *v* = 3469(NH), 1688(C=O), 1582(C=C), 1385(CH), 1358(CH), 776(Ar-H), 739(Ar-H), 690(Ar-H), 312(PtCl) cm^{-1}; **CHN:** $C_{46}H_{47}N_3O_2P_2PtCl_2$ requires C (55.15%), H (4.73%), N (4.19%), found: C (55.35%), H (4.77%), N (4.14%); **ESI-MS**: calcd for $C_{46}H_{47}N_3O_2P_2PtCl$ $[M-Cl]^+$ requires m/z 965.2474, found *m/z* 965.2469 (0.6 ppm).

$C_{41}H_{37}N_3O_3P_2PtCl_2$ (2.26)

From **2.18** (0.100g, 0.147 mmol) and $PtCl_2$(cod) (0.055g, 0.147 mmol). **Yield:** 0.116g, 83%; **Appearance:** orange solid; **^{1}H NMR** (400 MHz, d_6-DMSO) δ 9.63 (1H, s, NH), 8.35 (2H, dd, J = 12.6, 7.9Hz, Ar-H), 8.13-7.94 (3H, m, Ar-H), 7.75-7.37 (19H, m, Ar-H), 5.54 (1H, d, J = 8.1Hz, Ar-H), 4.48-4.23 (2H, m, CH_a), 4.13 (2H, t, J = 6.2Hz, N-CH_2-C$\underline{H}_2$-O), 4.08-3.91 (2H, m, CH_b), 3.49 (2H, t, J = 6.4Hz, N-C$\underline{H}_2$-CH_2-O), 3.20 (3H, s, CH_3) ppm; **$^{31}P\{^1H\}$ NMR** (162 MHz, d_6-DMSO) δ 0.05 ($^1J_{PtP}$ = 3460Hz) ppm; **FT-IR** (KBr): *v* = 3468(NH), 1691(C=O), 1585(C=C), 1376(CH_3), 1241(C-O), 778(Ar-H), 741(Ar-H), 692(Ar-H), 311(PtCl) cm^{-1}; **CHN:** $C_{41}H_{37}N_3O_3P_2PtCl_2$ requires C (51.96%), H (3.94%), N (4.43%), found: C (51.44%), H (3.83%), N (4.40%); **ESI-MS**: calcd for $C_{41}H_{37}N_3O_3P_2PtCl$ $[M-Cl]^+$ requires m/z 911.1641, found *m/z* 911.1629 (1.2 ppm).

$C_{42}H_{39}N_3O_4P_2PtCl_2$ (2.27)

From **2.19** (0.100g, 0.141 mmol) and $PtCl_2$(cod) (0.050g, 0.134 mmol). **Yield:** 0.103g, 80%; **Appearance:** orange solid; **^{1}H NMR** (400 MHz, d_6-DMSO) δ 9.67 (1H, s, NH), 8.43-8.33 (2H m, Ar-H), 8.14-7.95 (3H, m, Ar-H), 7.75-7.35 (19H, m, Ar-H), 5.52 (1H, d, J = 8.6Hz, Ar-H), 4.54 (1H, s, OH), 4.46-4.27 (2H, m, CH_a), 4.19-3.96 (4H, m, CH_b, N-CH_2-C$\underline{H}_2$-O), 3.54 (2H, t, J = 6.6Hz, N-C$\underline{H}_2$-CH_2-O), 3.41 (4H, s, C$\underline{H}_2$-C$\underline{H}_2$-OH) ppm; **$^{31}P\{^1H\}$ NMR** (162 MHz, d_6-DMSO) δ 0.14 ($^1J_{PtP}$ = 3455Hz) ppm; **FT-IR** (KBr): *v* = 3468(OH), 1682(C=O), 1583(C=C), 1244(C-O), 1060(CN), 856(Ar-H), 311(PtCl) cm^{-1}; **CHN:** $C_{42}H_{39}N_3O_4P_2PtCl_2$requires C (51.59%), H (4.02%), N (4.30%), found: C (51.39%), H (3.91%), N (4.03%); **ESI-MS**: calcd for $C_{42}H_{39}N_3O_4P_2PtCl$ $[M-Cl]^+$ requires m/z 941.1747, found *m/z* 941.1732 (1.5 ppm).

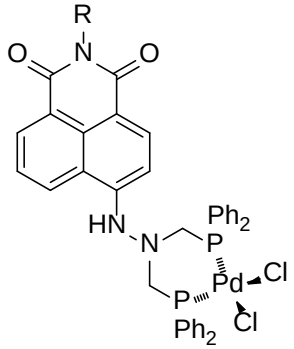

R = **(2.28)** $(CH_2)_3CH_3$
(2.29) $(CH_2)_7CH_3$
(2.30) $(CH_2)_2OCH_3$
(2.31) $(CH_2)_2O(CH_2)_2OH$

$C_{42}H_{39}N_3O_2P_2PdCl_2$ (2.28)

From **2.16** (0.103g, 0.152 mmol) and $PdCl_2$(cod) (0.043g, 0.151 mmol). **Yield:** 0.107g, 84%; **Appearance:** yellow solid;**^{1}H NMR** (400 MHz, d_6-DMSO) δ 9.66 (s, 1H, NH), 8.43-8.30 (m, 2H, Ar-H), 8.13-7.97 (m, 3H, Ar-H), 7.74-7.22 (m, 19H, Ar-H), 5.44 (d, J = 8.2 Hz, 1H, Ar-H), 4.38-4.17 (m, 2H, CH_a), 4.11-3.88 (m, 4H, CH_b, N-CH_2), 1.56-1.46 (m, 2H, CH_2), 1.32-1.23 (m, 2H, CH_2), 0.86 (t, J = 7.3 Hz, 3H, CH_3) ppm; **^{31}P{^{1}H} NMR** (162 MHz, d_6-DMSO) δ 17.67 ppm; **FT-IR** (KBr): *v* = 3423(NH), 1686(C=O), 1582(C=C), 1357(CH_3), 777(Ar-H), 694(Ar-H), 343(PdCl), 315(PdCl) cm^{-1}; **CHN:** $C_{42}H_{39}N_3O_2P_2PdCl_2 \cdot 0.5H_2O$ requires C (58.25%), H (4.65%), N (4.85%), found: C (58.21%), H (4.70%), N (4.72%); **ESI-MS**: calcd for $C_{42}H_{39}N_3O_2P_2PdCl$ $[M - Cl]^+$ requires m/z 820.1235, found *m/z* 820.1217 (2.2 ppm).

$C_{46}H_{47}N_3O_2P_2PdCl_2$ (2.29)

From **2.17** (0.100g, 0.136 mmol) and $PdCl_2$(cod) (0.037g, 0.130 mmol). **Yield:** 0.070g, 59%; **Appearance:** yellow solid; **^{1}H NMR** (400 MHz, d_6-DMSO) δ 9.66 (1H, s, NH), 8.41-8.31 (2H, m, Ar-H), 8.14-7.96 (3H, m, Ar-H), 7.78-7.35 (19H, m, Ar-H), 5.45 (1H, d, J = 8.6Hz, Ar-H), 4.39-4.19 (2H, m, CH_a), 4.13-3.97 (2H, m, CH_b), 3.91 (2H, t, J = 7.1Hz, N-CH_2), 1.57-1.44 (2H, m, CH_2), 1.31-1.10 (10H, m, CH_2), 0.80 (3H, t, J = 6.4Hz, CH_3) ppm; **^{31}P{^{1}H} NMR** (162 MHz, d_6-DMSO) δ 17.68 ppm; **FT-IR** (KBr): *v* = 3469(NH), 1683(C=O), 1582(C=C), 1359(CH), 775(Ar-H), 746(Ar-H), 691(Ar-H) cm^{-1}; **CHN:** Despite repeated attempts, a satisfactory elemental analysis was not obtained; **ESI-MS:** calcd for $C_{46}H_{47}N_3O_2P_2PdCl$ $[M - Cl]^+$ requires m/z 876.1861, found *m/z* 876.1860 (0.2 ppm).

$C_{41}H_{37}N_3O_3P_2PdCl_2$ (2.30)

From **2.18** (0.099g, 0.145 mmol) and $PdCl_2$(cod) (0.042g, 0.148mmol). **Yield:** 0.112g, 90%; **Appearance:** yellow solid; **^{1}H NMR** (400 MHz, d_6-DMSO) δ 9.68 (1H, s, NH), 8.39 (1H, d, J = 8.1Hz, Ar-H), 8.34 (1H, d, J = 7.3Hz, Ar-H), 8.15-7.97 (3H, m, Ar-H), 7.80-7.36 (19H, m, Ar-H), 5.45 (1H, d, J = 8.6Hz, Ar-H), 4.42-4.21 (2H, m, CH_a), 4.13 (2H, t, J = 6.2Hz, 2H, N-CH_2-C<u>H</u>$_2$-O), 4.09-3.96 (2H, m, CH_b), 3.48 (2H, t, J = 6.2Hz, N-C<u>H</u>$_2$-CH_2-O), 3.19 (3H, s, CH_3) ppm; **^{31}P{^{1}H} NMR** (162 MHz, d_6-DMSO) δ 17.66 ppm; **FT-IR** (KBr): *v* = 3434(NH), 1691(C=O), 1584(C=C), 1483(CH_2), 1376(CH_3), 1241(C-O), 741(Ar-H), 691(Ar-H) cm^{-1}; **CHN:** $C_{41}H_{37}N_3O_3P_2PdCl_2 \cdot H_2O$ requires C (56.15%), H (4.48%), N (4.79%), found: C (56.41%), H (4.22%), N (4.71%); **ESI-MS:** calcd for $C_{41}H_{37}N_3O_3P_2PdCl$ $[M-Cl]^+$ requires m/z 822.1028, found *m/z* 822.1013 (1.5 ppm).

$C_{42}H_{39}N_3O_4P_2PdCl_2$ (2.31)

From **2.19** (0.101g, 0.142 mmol) and $PdCl_2$(cod) (0.032g, 0.113 mmol). **Yield:** 0.085g, 86%; **Appearance:** yellow solid; **^{1}H NMR** (400 MHz, d_6-DMSO) δ 9.72 (1H, s, NH), 8.41 (1H, d, J = 8.7Hz, Ar-H), 8.35 (2H, d, J = 7.3Hz, Ar-H), 8.13-8.00 (3H, m, Ar-H), 7.79-7.26 (19H, m, Ar-H), 5.44 (1H, d, J = 8.7Hz, Ar-H), 4.55 (1H, s, OH), 4.40-4.22 (2H, m, CH_a), 4.19-3.98 (4H, m, CH_b, N-CH_2-C<u>H</u>$_2$-O), 3.54 (2H, t, J = 6.6Hz, N-C<u>H</u>$_2$-CH_2-O), 3.40 (4H, *br.* s, C<u>H</u>$_2$-C<u>H</u>$_2$-OH) ppm; **^{31}P{^{1}H} NMR** (162 MHz, d_6-DMSO) δ 17.65 ppm; **FT-IR** (KBr): *v* = 3469(OH), 3416(NH), 1681(C=O), 1582(C=C), 1243(C-O), 1060(CN), 854(CH), 334 (PdCl) cm^{-1}; **CHN:** $C_{42}H_{39}N_3O_4P_2PdCl_2$ requires C (56.74%), H (4.42%), N (4.73%), found: C (56.29%), H (4.38%), N (4.44%); **ESI-MS:** calcd for $C_{42}H_{39}N_3O_4P_2PdCl$ $[M-Cl]^+$ requires m/z 852.1134, found *m/z* 852.1115 (2.2 ppm).

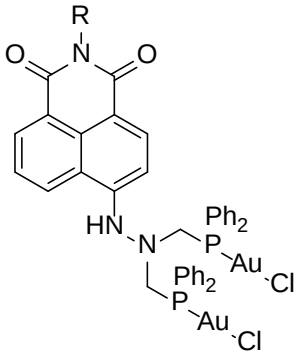

R = **(2.32)** $(CH_2)_3CH_3$
(2.33) $(CH_2)_7CH_3$
(2.34) $(CH_2)_2OCH_3$
(2.35) $(CH_2)_2O(CH_2)_2OH$

$C_{42}H_{39}N_3O_2P_2Au_2Cl_2$ (2.32)

From **2.16** (0.100g, 0.147 mmol) and AuCl(tht) (0.094g, 0.293 mmol). **Yield:** 0.139g, 83%; **Appearance:** yellow solid; **^{1}H NMR** (400 MHz, d_6-DMSO) δ 9.15 (1H, s, NH), 8.28 (1H, d, J = 7.3Hz, Ar-H), 7.96 (1H, d, J = 8.6Hz, Ar-H), 7.78-7.65 (8H, m, Ar-H), 7.58-7.41 (8H, m, Ar-H), 7.33-7.23 (6H, m, Ar-H), 6.16 (1H, d, J = 8.6Hz, Ar-H), 4.97 (2H, dd, J = 14.1, 5.1Hz, CH_a), 4.59 (2H, d, J = 15.8 Hz, CH_b), 3.94 (2H, t, J = 7.3Hz, N-CH_2), 1.58-1.48 (2H, m, CH_2), 1.34-1.23 (2H, m, CH_2), 0.88 (3H, t, J = 7.5Hz, CH_3) ppm; **^{31}P{^{1}H} NMR** (162 MHz, d_6-DMSO) δ 23.62 ppm; **FT-IR** (KBr): *v* = 3426(NH), 1688(C=O), 1582(C=C), 1358(CH_3), 775(Ar-H), 691(Ar-H), 330(AuCl), 319(AuCl) cm^{-1}; **CHN:** $C_{42}H_{39}N_3O_2P_2Au_2Cl_2$ requires C (44.07%), H (3.43%), N (3.67%), found: C (43.78%), H (3.35%), N (3.85%); **ESI-MS:** calcd for $C_{42}H_{39}N_3O_4P_2Au_2Cl$ $[M - Cl]^+$ requires m/z 941.1747, found *m/z* 941.1732 (1.5 ppm).

$C_{46}H_{47}N_3O_2P_2Au_2Cl_2$ (2.33)

From **2.17** (0.099g, 0.135 mmol) and AuCl(tht) (0.083g, 0.259 mmol). **Yield:** 0.119g, 78%; **Appearance:** yellow solid; **^{1}H NMR** (400 MHz, d_6-DMSO) δ 9.14 (1H, s, NH), 8.28 (1H, d, J = 6.8Hz, Ar-H), 7.96 (1H, d, J = 8.6Hz, Ar-H), 7.78-7.64 (8H, m, Ar-H), 7.59-7.40 (8H, m, Ar-H), 7.32-7.22 (6H, m, Ar-H), 6.16 (1H, d, J = 8.6Hz, Ar-H), 4.97 (2H, dd, J = 14.5, 4.7Hz, CH_a), 4.59 (2H, d, J = 15.0Hz, CH_b), 3.92 (2H, t, J = 7.3Hz, N-CH_2), 1.59-1.48 (2H, m, CH_2), 1.31-1.14 (10H, m, CH_2), 0.81 (3H t, J = 6.6Hz, , CH_3) ppm; **^{31}P{^{1}H} NMR** (162 MHz, d_6-DMSO) δ 23.63 ppm; **FT-IR** (KBr): *v* = 3469(NH), 1686(C=O), 1583(C=C), 1384(CH), 777(Ar-H), 693(Ar-H), 318(AuCl) cm^{-1}; **CHN:** $C_{46}H_{47}N_3O_2P_2Au_2Cl_2$ requires C (46.02%), H (3.95%), N (3.50%), found: C (45.93%), H (3.95%), N (3.57%); **ESI-MS:** calcd for $C_{46}H_{47}N_3O_2P_2Au_2Cl$ $[M - Cl]^+$ requires m/z 1164.2158, found *m/z* 1164.2141 (1.4 ppm).

$C_{41}H_{37}N_3O_3P_2Au_2Cl_2$ (2.34)

From **2.18** (0.099g, 0.145 mmol) and AuCl(tht) (0.094g, 0.29 3mmol). **Yield:** 0.140g, 84%; **Appearance:** yellow solid; **^{1}H NMR** (400 MHz, d_6-DMSO) δ 9.17 (1H, s, NH), 8.29 (1H, d, J = 7.3Hz, Ar-H), 7.97 (1H, d, J = 8.6Hz, Ar-H), 7.78-7.65 (8H, m, Ar-H), 7.59-7.40 (8H, m, Ar-H), 7.33-7.22 (6H, m, Ar-H), 6.16 (1H, d, J = 8.6Hz, Ar-H), 4.97 (2H, dd, J = 14.3, 4.9Hz, CH_a), 4.60 (2H, d, J = 15.8Hz, CH_b), 4.14 (2H, t, J = 6.2Hz, N-CH_2-$\underline{CH_2}$-O), 3.51 (2H, t, J = 6.2Hz, N-$C\underline{H_2}$-CH_2-O), 3.22 (3H, s, CH_3) ppm; **^{31}P{^{1}H} NMR** (162 MHz, d_6-DMSO) δ 23.68 ppm; **FT-IR** (KBr): *v* = 3290(NH), 1681(C=O), 1586(C=C), 1483(CH_2), 1384(CH_3), 1243(C-O), 745(Ar-H), 695(Ar-H), 331(Au-Cl) cm^{-1}; **CHN:** $C_{41}H_{37}N_3O_3P_2Au_2Cl_2$

requires C (42.95%), H (3.25%), N (3.66%), found: C (42.76%), H (2.98%), N (3.69%); **ESI-MS:** calcd for $C_{41}H_{37}N_3O_3P_2Au_2Cl$ $[M - Cl]^+$ requires m/z 1110.1324, found *m/z* 1110.1327 (0.2 ppm).

$C_{42}H_{39}N_3O_4P_2Au_2Cl_2$ (2.35)

From **2.19** (0.100g, 0.141 mmol) and AuCl(tht) (0.072g, 0.225 mmol). **Yield:** 0.085g, 66%; **Appearance:** yellow solid; **^{1}H NMR** (400 MHz, d_6-DMSO) δ 9.18 (1H, s, NH), 8.29 (1H, d, J = 6.8Hz, Ar-H), 7.97 (1H, d, J = 8.1Hz, Ar-H), 7.80-7.62 (8H, m, Ar-H), 7.59-7.38 (8H, m, Ar-H), 7.33-7.21 (6H, m, Ar-H), 6.15 (1H, d, J = 8.6Hz, Ar-H), 4.97 (2H, d, J = 14.1Hz, CH_a), 4.59 (2H, m, CH_b), 4.13 (2H, t, J = 6.4Hz, N-CH_2-$C\underline{H}_2$-O), 3.56 (2H, t, J = 6.6Hz, N-$C\underline{H}_2$-CH_2-O), 3.43 (4H, s, $C\underline{H}_2$-$C\underline{H}_2$-OH) ppm; **^{31}P{^{1}H} NMR** (162 MHz, d_6-DMSO) δ 23.71 ppm; **FT-IR** (KBr): *v* = 3435(OH), 3286(NH), 1667(C=O), 1582(C=C), 1243(C-O), 1059(CN), 861(Ar-H), 324(AuCl) cm^{-1}; **CHN** $C_{42}H_{39}N_3O_4P_2Au_2Cl_2$ requires C (42.87%), H (3.34%), N (3.57%), found: C (43.05%), H (3.25%), N (3.57%); **ESI-MS:** calcd for $C_{42}H_{39}N_3O_4P_2Au_2Cl$ $[M - Cl]^+$ requires m/z 1140.1430, found *m/z* 1140.1416 (1.2 ppm).

Compounds **2.36** – **2.39** were prepared in an identical manner to that described for **2.36**.

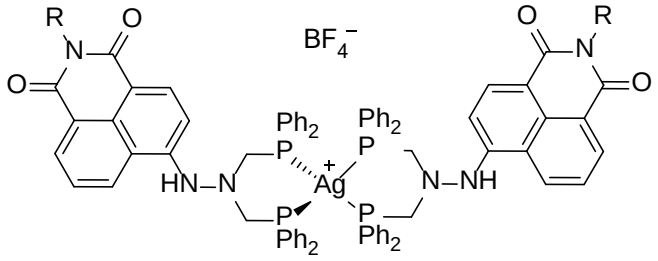

R = **(2.36)** $(CH_2)_3CH_3$
(2.37) $(CH_2)_7CH_3$
(2.38) $(CH_2)_2OCH_3$
(2.39) $(CH_2)_2O(CH_2)_2OH$

$C_{84}H_{78}N_6O_4P_4AgBF_4$ (2.36)

Using a Schlenk procedure, ligand **2.16** (0.200g, 0.293 mmol) and $AgBF_4$ (0.028g, 0.144 mmol) were dissolved in CH_2Cl_2 and stirred for 1h, the solvent volume was reduced to 1-2mL and Et_2O was added to ensure the product had precipitated fully. This yielded a

yellow solid (0.116g, 52%). **FTIR** (KBr): *v* = 3468(N-H), 2959(C-H), 1681(C=O) cm^{-1}; **CHN**: $C_{84}H_{78}N_6O_4P_4AgBF_4$ requires C (64.92), H (5.06), N (5.41), found: C (64.47), H (4.82), N (5.41); **ESI-MS:** calcd for $C_{84}H_{78}N_6O_4P_4Ag$ $[M]^+$ requires m/z 1465.4080, found *m/z* 1465.4133 (3.6 ppm).

$C_{92}H_{94}N_6O_4P_4AgBF_4$ (2.37)

From **2.17** (0.103g, 0.140 mmol) and $AgBF_4$ (0.017g, 0.088 mmol). **Yield:** 0.066g, 56%; **Appearance:** yellow solid; **FTIR** (KBr): *v* = 2924(C-H), 1686(C=O), 1643 and 1584(C=C) cm^{-1}; **CHN**: $C_{92}H_{94}N_6O_4P_4AgBF_4 \cdot H_2O$ requires C (65.60), H (5.74), N (5.04), found: C (65.52), H (5.56), N (5.08); **ESI-MS:** calcd for $C_{92}H_{94}N_6O_4P_4Ag$ $[M]^+$ requires m/z 1577.5332, found *m/z* 1577.5390 (3.6 ppm).

$C_{82}H_{74}N_6O_6P_4AgBF_4$ (2.38)

From **2.18** (0.098g, 0.143 mmol) and $AgBF_4$ (0.014g, 0.073 mmol). **Yield:** 0.070g, 63%; **Appearance:** yellow solid; **FTIR** (KBr): *v* = 3327(N-H), 3053(Ar-H), 2972 and 2870(C-H), 1686(C=O), 1644 and 1583(C=C) cm^{-1}; **CHN**: $C_{82}H_{74}N_6O_6P_4AgBF_4$ requires C (63.21), H (4.79), N (5.39), found: C (62.83), H (4.72), N (5.43); **ESI-MS:** calcd for $C_{82}H_{75}N_6O_6P_4Ag$ $[M+H]^{+2}$ requires m/z 1470.3744, found *m/z* 1470.3744 (0.0 ppm).

$C_{84}H_{78}N_6P_4AgBF_4$ (2.39)

From **2.19** (0.199g, 0.285 mmol) and $AgBF_4$ (0.026g, 0.134 mmol). **Yield:** 0.128g, 60%; **Appearance:** yellow solid; **FTIR** (KBr): *v* = 3467(N-H), 1682(C=O), 1641 and 1581(C=C), 1616(N-H) cm^{-1}; **CHN**: $C_{84}H_{78}N_6P_4AgBF_4 \cdot 3H_2O$ requires C (60.34), H (5.06), N (5.03), found: C (59.99), H (4.64), N (4.94); **ESI-MS:** calcd for $C_{84}H_{78}N_6P_4Ag$ $[M]^+$ requires m/z 1529.3877, found *m/z* 1529.3929 (3.4 ppm).

Compounds described in Further Work:

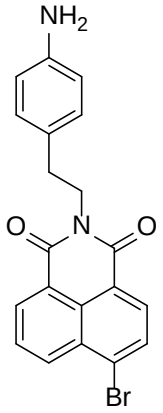

(2.41)

$C_{20}H_{16}N_2O_2Br$ (2.41)

2-(4-aminophenyl)-ethylamine (0.983g; 7.210mmol). 4-bromo naphthalic anhydride (1.003g; 3.621mmol) and glacial acetic acid (10 mL) were transferred into a round-bottomed flask and refluxed over 72h. The mixture was stirred over 20h, before being poured into an ice-water mixture (100 mL). The light brown precipitate was collected by filtration and dried *in vacuo.* The light brown solid was recrystallized from a minimum volume of EtOH, filtered under suction and dried *in vacuo* to yield light brown/grey solid. **Yield:** 1.013g, 71%; **Appearance:** light brown powder; **^{1}H NMR** (400 MHz, CDCl3) δ 8.66 (2H, dd, J = 6.8, 13.2Hz, Ar-H), 8.43 (1H, d, J = 7.6Hz, Ar-H), 8.07 (1H, d, J = 7.6Hz, Ar-H), 7.88 (1H, dd, J = 7.2Hz, Ar-H), 7.34 (2H, m, Ar-H), 7.25 (2H, m, Ar-H), 5.74 (1H, *br.* s, NH), 3.57 (2H, m, CH_2), 2.90 (2H, m, CH_2) ppm; **FTIR** (KBr): *v* = 3415(NH), 3275(NH), 1710(C=O) cm^{-1}; **CHN:** Despite repeated attempts, a satisfactory elemental analysis was not obtained; **ESI-MS:** calcd for $C_{20}H_{16}N_2O_2Br$ $[M+H]^+$ requires m/z 395.0390, found *m/z* 395.0398 (2.2 ppm).

Photophysical Measurements

Absorption spectra were recorded with a Shimadzu UV-1650PC spectrophotometer while fluorescence studies were performed on a Spex model Fluoromax fluorescence spectrophotometer. Absorption and emission spectra were recorded in dimethylsulfoxide (DMSO) at room temperature (*ca.* 298K) using a standard quartz cell. Samples were purged with nitrogen before measurement to reduce photobleaching and oxidation of the phosphine moiety. Dyes were excited at 440 nm

and excitation and emission slits were both set to 0.6 mm. Lifetime measurements were recorded with a FLS920 Fluorescence Spectrometer equipped with a TMS300 monochromator, a S900 single photon photomultiplier detection system and an EPL-375 ps pulsed diode laser (Edinburgh Instruments).

6.4 Chapter 3 Experimental

Compounds **3.3** and **3.4** were prepared following a known procedure which is explained for **3.3**.[154]

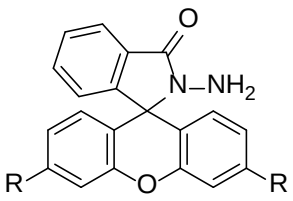

R = (**3.3**) OH
(**3.4**) $N(CH_2CH_3)_2$

$C_{20}H_{14}O_4N_2$ (3.3)

Hydrazine monohydrate (20mL, 98%) was added to a suspension of fluorescein (6.001g, 18.058 mmol) in ethanol (50mL). The reaction mixture was refluxed for 7h, after which the solution was poured into ice-water (400mL) and left to settle overnight. The resulting yellow precipitate was filtered under suction and washed with water and ethanol, before drying *in vacuo.* **Yield:** 5.077g; 81%; **^{1}H NMR** (400MHz, d_6-DMSO) δ 9.66 (2H, s, 2OH), 7.72 (1H, m, Ar-H), 7.45 (2H, m, Ar-H), 6.95 (1H, m, Ar-H), 6.55 (2H, d, J = 2Hz, Ar-H), 6.41 (2H, dd, J = 2, 6,4Hz, Ar-H), 6.36 (2H, d, J = 8.4Hz, Ar-H), 4.35 (2H, br. s, NH_2) ppm; **ESI-MS:** calcd for $C_{20}H_{15}O_4N_2$ $[M+H]^+$ requires m/z 347.1026, found *m/z* 347.1024 (0.7 ppm). Data was comparable to the previously published procedure.[154]

$C_{28}H_{32}O_2N_4$ (3.4)

From hydrazine monohydrate (5mL, 98%) and Rhodamine B base (2.007g, 4.508 mmol). **Yield:** 2.267g, quantitative; **Appearance:** orange solid; **^{1}H NMR** (400 MHz, $CDCl_3$) δ 7.96 (1H, m , Ar-H), 7.47 (2H, m, Ar-H), 7.13 (1H, m, Ar-H), 6.48 (2H, d, J = 9.2Hz, Ar-H), 6.42 (2H, d, J = 2Hz, Ar-H), 6.31 (2H, dd, J = 2.4, 6.4Hz, Ar-H), 3.64 (2H, *br*. s, NH_2), 3.36 (8H, q, J = 6.8Hz, $4CH_2$), 1.19 (12H, t, J = 6.8Hz, $4CH_3$) ppm; **ESI-MS:** calcd for $C_{28}H_{33}O_2N_4$ $[M+H]^+$ requires m/z 457.2598, found *m/z* 457.2597 (0.1 ppm). Compound known in literature; data comparable to that recorded in literature.[101]

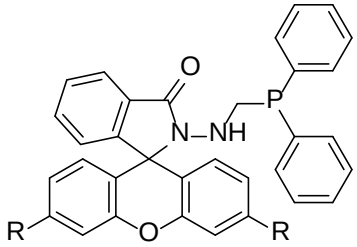

R = (**3.5**) OH
(**3.6**) $N(CH_2CH_3)_2$

$C_{33}H_{25}O_4N_2P$ (3.5)

A suspension of fluorescein hydrazide (0.585g, 1.691 mmol) and hydroxymethyldiphenylphosphine (0.406g, 1.880 mmol) in methanol (10mL) was refluxed for 4h. On cooling of the colourless solution a white precipitate is observed. The mixture is left to stir for 72hrs at r.t. The white powder was filtered under suction. **Yield:** 0.830g, 90%; **^{1}H NMR** (400MHz, d_6-DMSO) δ 9.83 (2H, s, 2OH), 7.75 (1H, d, J = 6.8, Ar-H), 7.50 (2H, p, J = 6Hz, Ar-H), 7.25 (6H, m, Ar-H), 7.02 (5H, m, Ar-H), 6.57 (2H, s, Ar-H), 6.40 (4H, s, Ar-H), 5.29 (1H, t, J = 6.8Hz, NH), 3.13 (2H, d, J = 4.4, CH_2); **^{31}P{^{1}H} NMR** (162 MHz, d_6-DMSO) δ -22.82 ppm;); **FT-IR** (KBr): *v* = 3412(NH), 3242(OH), 1665(C=O), 1504(C=C), 1468(CH_2), 846 and 820(Ar-H) cm^{-1}; **CHN:** $C_{33}H_{25}O_4N_2P{\cdot}H_2O$ requires C (70.51%), H (4.84%), N (4.98%), found: C (70.27%), H (4.68%), N (5.34%); **ESI-MS:** calcd for $C_{33}H_{26}O_4N_2P$ $[M+H]^+$ requires m/z 545.1625, found *m/z* 545.1619 (1.1 ppm).

$C_{41}H_{43}O_2N_4P$ (3.6)

A suspension of rhodamine hydrazide (0.299g, 0.658 mmol) and hydroxymethyldiphenylphosphine (0.120g, 0.548 mmol) in methanol (10mL) was refluxed for 24h. The pink suspension is left to stir for 72hrs at r.t. The white powder is filtered under suction and washed with methanol (3-5mL). **Yield:** 0.236g, 72%; **Appearance:** white with a slight pink tinge; **^{1}H NMR** (400 MHz, d_6-DMSO) δ 7.74 (1H, d, J = 6.8Hz, Ar-H), 7.48 (2H, p, J = 7.2Hz, Ar-H), 7.22 (6H, m, Ar-H), 7.07 (4H, t, J = 6.8Hz, Ar-H), 7.00 (1H, d, J = 6.8Hz, Ar-H), 6.35-6.28 (6H, m, Ar-H), 5.16 (1H, t, J = 6.8Hz, NH), 3.27 (10H, m, $5CH_2$), 1.01 (12H, t, J = 6.8Hz, $4CH_3$) ppm; **^{31}P{^{1}H} NMR** (162 MHz, d_6-DMSO) δ -23.38ppm; **FT-IR** (KBr): *ν* = 3465(NH), 1703(C=O), 782(Ar-H), 747(Ar-H), 697(Ar-H) cm^{-1}; **CHN** $C_{41}H_{43}PN_4O_2$ requires C (75.20%), H (6.62%), N (8.56%), found: C (74.78%), H (6.47%), N (8.47%); **ESI-MS:** calcd for $C_{41}H_{44}O_2N_4P$ $[M+H]^+$ requires m/z 655.3196, found *m/z* 655.3206 (1.5 ppm).

Coordination Compounds (3.9 – 3.14)

Unless otherwise stated, the following Pt(II), Pd(II) and Au(I) complexes were synthesised through the reaction of appropriate metal precursors, $PtCl_2$(cod), $PdCl_2$(cod), $[Pd(\mu\text{-}Cl)(C_{12}H_{12}N)]_2$, $Pd_2C_{18}H_{24}N_2Cl_2$ and AuCl(tht), with ligands **3.5** and **3.6**. Following 1h stirring in CH_2Cl_2, the solvent volume was reduced to 1-2mL and Et_2O/C_6H_{14} was added resulting in the precipitation of complexes **3.9 – 3.14**.

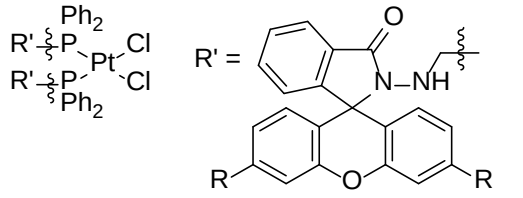

R = (**3.9**) OH
(**3.10**) $N(CH_2CH_3)_2$

$C_{66}H_{50}O_8N_4P_2PtCl_2$ (3.9)

From **3.5** (0.100g, 0.184 mmol) and $PtCl_2$(cod) (0.032g, 0.086 mmol). **Yield:** 0.099g, 85%; **Appearance:** white solid; **^{1}H NMR** (400 MHz, d_6-DMSO) δ 9.78 (2H, s, 2OH), 7.72 (1H, m, Ar-H), 7.45 (2H, m, Ar-H), 7.28 (2H, dd, J = 7.2Hz, Ar-H), 7.00-6.86 (9H, m, Ar-H), 6.41 (2H, s, Ar-H), 6.33 (4H, s, Ar-H), 4.88 (1H, t, J = 8Hz, NH), 3.60 (2H, s, CH_2) ppm;

$^{31}P\{^{1}H\}$ NMR (162 MHz, d_6-DMSO) δ 1.77 ppm ($^{1}J_{PtP}$ 3644 Hz); **FT-IR** (KBr): *v* = 3418(OH), 1667(C=O), 1504(C=C), 849(Ar-H), 317 and 293(PtCl) cm^{-1}; **CHN:** $C_{66}H_{50}O_8N_4P_2PtCl_2$ requires C (58.50%), H (3.72%), N (4.13%), found: C (58.20%), H (3.82%), N (3.85%); **ESI-MS:** calcd for $C_{66}H_{50}O_8N_4P_2PtCl$ $[M\text{-}Cl]^+$ requires m/z 1318.2435, found *m/z* 1318.2416 (1.4 ppm).

$C_{82}H_{86}P_2N_8O_4PtCl_2$ (3.10)

From **3.6** (0.151g, 0.231 mmol) and $PtCl_2$(cod) (0.043g, 0.115 mmol). **Yield:** 0.113g; 62%; **Appearance:** bright pink/purple powder; **^{1}H NMR** (400 MHz, d_6-DMSO) δ 7.76 (1H, m, Ar-H), 7.47 (3H, m, Ar-H), 7.29 (2H, dd, J = 6.4Hz, Ar-H), 6.94 (8H, m, Ar-H), 6.29 (4H, m, Ar-H), 6.17 (2H, s, Ar-H), 5.07 (1H, t, J = 7.6Hz, NH), 3.58 (2H, *br.* s, CH_2), 3.28 (8H, m, $4CH_2$), 1.05 (12H, t, J = 7.2Hz, $4CH_3$) ppm; **$^{31}P\{^{1}H\}$ NMR** (162 MHz, d_6-DMSO) δ 1.19 ppm ($^{1}J_{PtP}$ = 3646 Hz); **FT-IR** (KBr): *v* = 3468(NH), 1701(C=O), 786(Ar-H), 744(Ar-H), 698(Ar-H), 317(PtCl), 294(PtCl) cm^{-1}; **CHN:** $C_{82}H_{86}P_2N_8O_4PtCl_2{\cdot}CH_2Cl_2$ requires C (60.04%), H (5.34%), N (6.75%), found: C (60.16%), H (5.16%), N (6.69%); **ESI-MS:** calcd for $C_{82}H_{86}O_4N_8P_2PtCl$ $[M\text{-}Cl]^+$ requires m/z 1538.5578, found *m/z* 1538.5566 (0.8 ppm).

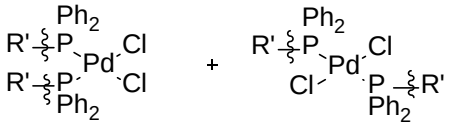

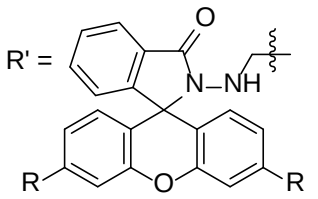

R = (**3.11**) OH
(**3.12**) $N(CH_2CH_3)_2$

$C_{66}H_{50}P_2N_4O_8PdCl_2$ (3.11)

From **3.5** (0.098g, 0.180 mmol) and $PdCl_2$(cod) (0.025g, 0.089 mmol). **Yield:** 0.096g, 86%; **Appearance:** off-white solid; **^{1}H NMR** (400 MHz, d_6-DMSO) δ 9.81 (2H, s, *trans*-2OH), 9.78 (2H, s, *cis*-2OH), 7.74 (2H, m, *cis* + *trans* Ar-H), 7.46 (4H, m, *cis* + *trans* Ar-H), 7.33 (4H, m, *cis* + *trans* Ar-H), 6.93 (18H, m, *cis* + *trans* Ar-H), 6.56 (2H, s, *trans*-Ar-H),

6.51 (2H, s, *cis*-Ar-H), 6.33 (4H, m, *cis* + *trans* Ar-H), 5.07 (1H, m, *cis*-NH), 4.90 4.88 (1H, t, J = 7.6Hz, *trans*-NH), 3.75 (2H, m, *trans*-CH_2), 3.67 (2H, *br.* s, *cis*-CH_2) ppm; **$^{31}P\{^1H\}$ NMR** (162 MHz, d_6-DMSO) δ 10.91, 21.47 ppm; **FT-IR** (KBr): *v* = 3467(OH), 1670(C=O), 1504(C=C), 1466(CH_2), 853(Ar-H), 353(*trans*-PdCl), 326(*cis*-PdCl) cm^{-1}; **CHN** $C_{66}H_{50}P_2N_4O_8PdCl_2 \cdot 2H_2O$ requires C (60.94%), H (4.18%), N (4.31%), found: C (60.66%), H (4.42%), N (4.01%); **ESI-MS:** calcd for $C_{66}H_{50}O_8N_4P_2PdCl$ $[M\text{-}Cl]^+$ requires m/z 1229.1822, found *m/z* 1229.1835 (1.1 ppm).

$C_{82}H_{86}P_2N_8O_4PdCl_2$ (3.12)

From **3.6** (0.148g, 0.226 mmol) and $PdCl_2$(cod) (0.033g, 0.115 mmol). **Yield:** 0.104g, 62%; **Appearance:** purple powder; **^{1}H NMR** (500 MHz, d_6-DMSO) δ 7.75 (2H, m, *cis* + *trans* Ar-H), 7.45-7.26 (16H, m, *cis* + *trans* Ar-H), 6.96-6.88 (10H, m, *cis* + *trans* Ar-H), 6.29-6.19 (12H, m, *cis* + *trans* Ar-H), 5.19 (1H, t, J = 9Hz, cis-NH), 5.04 (1H, t, J = 7Hz, trans-NH), 3.69 (2H, m, *trans*-CH_2), 3.61 (2H, m, *cis*-CH_2), 3.41-3.25 (16H, m, *cis* + *trans* 4CH_2), 1.07-0.10 (24H, m, *cis* + *trans* 4CH_3) ppm; **$^{31}P\{^1H\}$ NMR** (162 MHz, d_6-DMSO) δ 10.08, 20.93 ppm; **FT-IR** (KBr): *v* = 3468(NH), 1700(C=O), 786(Ar-H), 743(Ar-H), 692(Ar-H), 358(*trans*-PdCl), 336(*cis*-PdCl), 314(*cis*-PdCl) cm^{-1}; **CHN** $C_{82}H_{86}P_2N_8O_4PdCl_2 \cdot 0.5CH_2Cl_2$ requires C (64.83%), H (5.73%), N (7.33%), found: C (64.32%), H (5.48%), N (7.22%); **ESI-MS:** calcd for $C_{82}H_{86}O_4N_8P_2PdCl$ $[M\text{-}Cl]^+$ requires m/z 1449.4965, found *m/z* 1449.4982 (1.2 ppm).

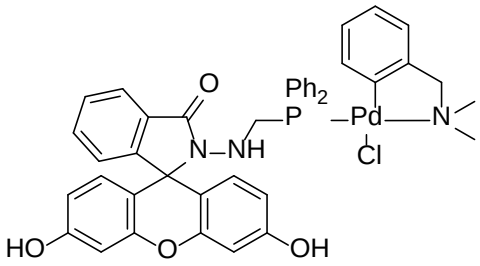

(**3.13**)

$C_{42}H_{37}PN_3O_4PdCl$ (3.13)

From **3.5** (0.102g, 0.186 mmol) and $Pd_2C_{18}H_{24}N_2Cl_2$ (0.047g, 0.085 mmol). **Yield:** 0.095g, 65%; **Appearance:** white powder; **^{1}H NMR** (400 MHz, d_6-DMSO) δ 9.81 (2H, s, 2OH), 7.71 (1H, m, Ar-H), 7.49-7.42 (8H, m, Ar-H), 7.33 (4H, m, Ar-H), 6.90 (2H, m, Ar-H), 6.69 (1H, dd, J = 7.6Hz, Ar-H), 6.47 (2H, d, J = 2Hz, Ar-H), 6.34 (2H, m, Ar-H), 6.29-

6.23 (3H, m, Ar-H), 6.00 (1H, dd, J = 6.8Hz, Ar-H), 5.01 (1H, t, J = 7.6Hz, NH), 3.92 (2H, s, NCH_2), 3.74 (2H, t, J = 5.6Hz, PCH_2), 2.47 (6H, s, $2CH_3$) ppm; **$^{31}P\{^1H\}$ NMR** (162 MHz, d_6-DMSO) δ 29.40 ppm; **FT-IR** (KBr): *v* = 3467(OH), 1631(C=O), 1503(C=C), 1463(CH_2), 1384(CH_3), 850(Ar-H) cm^{-1}; **CHN** $C_{42}H_{37}PN_3O_4PdCl{\cdot}H_2O$ requires C (60.18%), H (4.57%), N (5.01%), found: C (60.16%), H (4.31%), N (5.01%); **ESI-MS:** calcd for $C_{42}H_{37}O_4N_3PPd$ $[M\text{-}Cl]^+$ requires m/z 784.1551, found *m/z* 784.1560 (1.2 ppm).

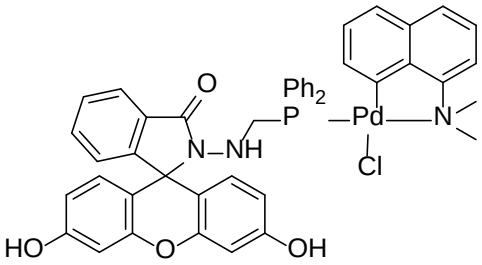

(**3.14**)

$C_{45}H_{37}PN_3O_4PdCl$ (3.14)

From **3.5** (0.101g, 0.186 mmol) and $Pd_2C_{24}H_{24}N_2Cl_2$ (0.054g, 0.087 mmol). **Yield:** 0.074g, 47%; **Appearance:** white solid; **^1H NMR** (400 MHz, d_6-DMSO) δ 9.80 (2H, s, 2OH), 7.71 (2H, m, Ar-H), 7.60-7.54 (5H, m, Ar-H), 7.50-7.40 (5H, m, Ar-H), 7.36-7.30 (5H, m, Ar-H), 6.90 (1H, m, Ar-H), 6.53 (1H, dd, J = 7.6Hz, Ar-H), 6.46 (2H, d, J = 2.4Hz, Ar-H), 6.42-6.29 (4H, m, Ar-H), 6.09 (1H, dd, J = 7.6Hz, Ar-H) , 5.24 (1H, t, J = 7.6Hz, NH), 3.85 (2H, t, J = 6Hz, PCH_2), 3.24 (6H, s, $2CH_3$) ppm; **$^{31}P\{^1H\}$ NMR** (162 MHz, d_6-DMSO) δ 31.35 ppm; **FT-IR** (KBr): *v* = 3467(OH), 1631(C=O), 1504(C=C), 1464(CH_2), 1384(CH_3), 852(Ar-H), 331(PdCl), 316 (PdCl) cm^{-1}; **CHN** $C_{45}H_{37}PN_3O_4PdCl{\cdot}H_2O$ requires C (61.87%), H (4.38%), N (4.81%), found: C (61.89%), H (4.09%), N (4.76%); **ESI-MS:** calcd for $C_{45}H_{37}O_4N_3Pd$ $[M\text{-}Cl]^+$ requires m/z 820.1551, found *m/z* 820.1548 (0.4 ppm).

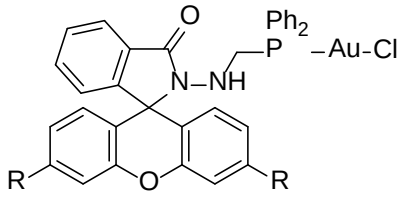

R = (**3.15**) OH
(**3.16**) $N(CH_2CH_3)_2$

$C_{33}H_{26}O_4N_2PAuCl$ (3.15)

From **3.5** (0.100g, 0.184 mmol) and AuCl(tht) (0.055g, 0.172 mmol). **Yield:** 0.100g, 70%; **Appearance:** white solid; **^{1}H NMR** (400 MHz, d_6-DMSO) δ 9.86 (2H, s, 2OH), 7.76 (1H, d, J = 7.2Hz, Ar-H), 7.54-7.41 (8H, m, Ar-H), 7.31 (4H, q, J = 8, 4.8Hz, Ar-H), 6.98 (1H, d, J = 7.2Hz, Ar-H), 6.52 (4H, m, Ar-H), 6.41 (2H, dd, J = 2.4, 6.4Hz, Ar-H), 5.99 (1H, t, J = 6.8Hz, NH), 3.81 (2H, t, J = 5.6Hz, CH_2) ppm; **^{31}P{^{1}H} NMR** (162 MHz, d_6-DMSO) δ 20.16 ppm; **FT-IR** (KBr): *v* = 3434(OH), 1665(C=O), 1502(C=C), 1464(CH_2), 856(Ar-H), 327(AuCl) cm^{-1}; **CHN** $C_{33}H_{25}PN_2O_4AuCl$ requires C (49.06%), H (3.12%), N (3.47%), found: C (49.43%), H (2.81%), N (3.49%); **ESI-MS:** calcd for $C_{33}H_{26}O_4N_2PAuCl$ $[M+H]^+$ requires m/z 777.0979, found *m/z* 777.0979 (0.4 ppm).

$C_{41}H_{43}PN_4O_2AuCl$ (3.16)

From **3.6** (0.101g, 0.153 mmol) and AuCl(tht) (0.048g, 0.153 mmol). **Yield:** 0.096g, 72%; **Appearance:** lilac powder; **^{1}H NMR** (400 MHz, d_6-DMSO) δ 7.80 (1H, d, J = 7.6Hz, Ar-H), 7.59-7.37 (12H, m, Ar-H), 7.07 (1H, d, J = 6Hz, Ar-H), 6.48 (2H, d, J = 8.8Hz, Ar-H), 6.38-6.33 (4H, m, Ar-H), 5.87 (1H, m, NH), 3.75 (2H, t, J = 5.2Hz, CH_2), 3.34 (8H, m, $4CH_2$), 1.07 (12H, t, J = 7.2, $4CH_3$) ppm; **^{31}P{^{1}H} NMR** (162 MHz, d_6-DMSO) δ 24.14 ppm; **FT-IR** (KBr): *v* = 3467(NH), 1697(C=O), 785(Ar-H), 751(Ar-H), 695(Ar-H), 319(AuCl) cm^{-1}; **CHN** $C_{41}H_{43}PN_4O_2AuCl$ requires C (55.51%), H (4.88%), N (6.32%), found: C (55.18%), H (4.77%), N (6.06%); **ESI-MS:** calcd for $C_{41}H_{43}O_2N_4PAu$ $[M-Cl]^+$ requires m/z 851.2784, found *m/z* 851.2784 (0.1 ppm).

Photophysical Measurements

Absorption spectra were recorded with a Shimadzu UV-1650PC spectrophotometer while fluorescence studies were performed on a Spex model Fluoromax fluorescence spectrophotometer. Absorption and emission spectra were recorded in

dimethylsulfoxide (DMSO 99+%) at room temperature (*ca.* 298K) using a standard quartz cell. Samples were purged with nitrogen before measurement to reduce photobleaching and oxidation of the phosphine moiety. Fluorescein derivative dyes were excited at 280 and 340 nm and excitation and emission slits were both set to 0.5 nm. Rhodamine derivative dyes were excited at 316 and 566 nm and excitation and emission slits were both set to 0.5 and 0.4 nm respectively.

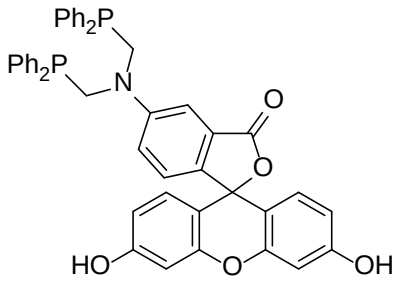

(**3.18**)

$C_{46}H_{35}O_5NP_2$ (3.18)

A suspension of fluoresceinamine isomer 1 (0.182g, 0.524 mmol) and hydroxymethyldiphenylphosphine (0.250g, 1.157 mmol) in methanol (10mL) was refluxed for 3h to yield a dark brown solution. The solution was stirred for 44h at r.t., before the volume was reduced by 50% generating a light brown suspension. The light brown solid collected by filtration under vaccum. **Yield:** 0.245g, 63%; **^{1}H NMR** (400 MHz, d_6-DMSO) δ 10.13 (2H, s, 2OH), 7.39 (20H, br. s, Ar-H), 7.20 (2H, m, Ar-H), 6.87 (1H, d, J = 8.4Hz, Ar-H), 6.67 (2H, d, J = 2Hz, Ar-H), 6.61 (2H, dd, J = 2, 6.4Hz, Ar-H), 6.51 (2H, d, J = 8.4Hz, Ar-H), 4.13 (4H, s, $2CH_2$) ppm; **^{31}P{^{1}H} NMR** (162 MHz, d_6-DMSO) δ -28.38 ppm; **FT-IR** (KBr): *v* = 3468(OH), 1727(C=O), 1507(C=C), 1384(CO), 851(Ar-H) cm^{-1}; **CHN** Despite repeated attempts, a satisfactory elemental analysis was not obtained; **ESI-MS:** calcd for $C_{46}H_{36}O_5NP_2$ $[M-H]^+$ requires m/z 744.2063, found *m/z* 744.2049 (2.0 ppm).

Coordination Compounds (3.19 – 3.21)

Unless otherwise stated, the following Pt(II), Pd(II) and Au(I) complexes were synthesised through the reaction of appropriate metal precursors, $PtCl_2$(cod), $PdCl_2$(cod) and AuCl(tht), with ligand **3.18**. Following 1h stirring in CH_2Cl_2, the solvent

volume was reduced to 1-2mL and Et_2O was added resulting in the precipitation of complexes **3.19 – 3.21**.

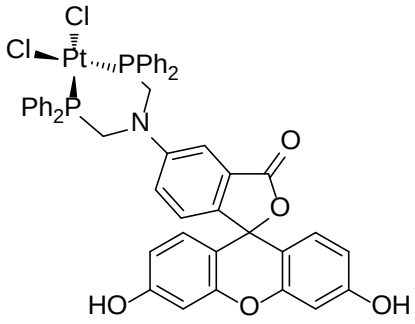

(**3.19**)

$C_{46}H_{35}P_2NO_5PtCl_2$ (3.19)

From **3.18** (0.099g, 0.133 mmol) and $PtCl_2$(cod) (0.050g, 0.134 mmol). **Yield:** 0.130g, 97%; **Appearance:** chocolate brown solid; **^{1}H NMR** (400 MHz, d_6-DMSO) δ 10.01 (2H, s, 2OH), 7.99 (8H, m, Ar-H), 7.50 (12H, m, Ar-H), 6.77 (1H, s, Ar-H), 6.58 (2H, d, J = 2.8Hz, Ar-H), 6.51 (3H, m, Ar-H), 6.40 (1H, d, J = 9.2Hz, Ar-H), 6.21 (2H, d, J = 8.4Hz, Ar-H), 4.98 (4H, s, $2CH_2$) ppm; **^{31}P{^{1}H} NMR** (162 MHz, d_6-DMSO) δ -12.00 ppm ($^1J_{PtP}$ = 3440Hz); **FT-IR** (KBr): *v* = 3466(OH), 1745(C=O), 1503(C=C), 1384(CO), 852(Ar-H), 781(Ar-H), 317(PtCl), 289(PtCl) cm^{-1}; **CHN** $C_{46}H_{35}P_2NO_5PtCl_2 \cdot H_2O$ requires C (53.82%), H (3.44%), N (1.36%), found: C (53.86%), H (3.53%), N (1.59%); **ESI-MS:** calcd for $C_{46}H_{35}O_5NP_2PtCl$ $[M\text{-}Cl]^+$ requires m/z 973.1321, found *m/z* 973.1312 (0.9 ppm).

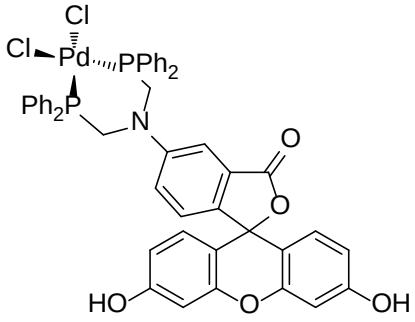

(**3.20**)

$C_{46}H_{35}O_5NP_2PdCl_2$ (3.20)

From **3.18** (0.082g, 0.110 mmol) and $PdCl_2$(cod) (0.031g, 0.109 mmol). **Yield:** 0.082g; 81%; **Appearance:** chocolate brown solid; **^{1}H NMR** (400 MHz, d_6-DMSO) δ 10.14 (2H, br. s, 2OH), 8.06 (8H, m, Ar-H), 7.57 (12H, m, Ar-H), 6.80 (1H, s, Ar-H), 6.64 (2H, d, J = 2Hz, Ar-H), 6.56 (3H, m, Ar-H), 6.47 (1H, d, J = 8.4Hz, Ar-H), 6.26 (2H, d, J = 8.4Hz, Ar-H), 4.98 (4H, s, $2CH_2$) ppm; **^{31}P{^{1}H} NMR** (162 MHz, d_6-DMSO) δ 2.57 ppm; **FT-IR** (KBr): *v* = 3468(OH), 1748(C=O), 1503(C=C), 1384(CO), 851(Ar-H), 780(Ar-H), cm^{-1}; **CHN** $C_{46}H_{35}P_2NO_5PdCl_2{\cdot}CH_2Cl_2$ requires C (56.12%), H (3.71%), N (1.40%), found: C (56.60%), H (3.74%), N (1.55%); **ESI-MS:** calcd for $C_{46}H_{35}O_5NP_2PdCl$ $[M\text{-}Cl]^+$ requires m/z 884.0719, found *m/z* 884.0698 (2.4 ppm); calcd for $C_{46}H_{36}O_5NP_2PdCl_2$ $[M+H]^+$ requires m/z 920.0486, found *m/z* 920.0461 (2.7 ppm).

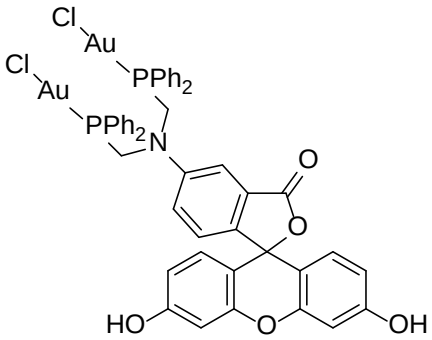

(**3.21**)

$C_{46}H_{35}O_5NP_2Au_2Cl_2$ (3.21)

From **3.18** (0.099g, 0.133 mmol) and AuCl(tht) (0.086g, 0.268 mmol). **Yield:** 0.120g, 74%; **Appearance:** red/orange solid; **^{1}H NMR** (400 MHz, d_6-DMSO) δ 10.08 (2H, s,

2OH), 7.80-7.75 (8H, m, Ar-H), 7.74 (1H, s, Ar-H), 7.59-7.55 (12H, m, Ar-H), 7.48 (1H, d, J = 6Hz, Ar-H), 6.77 (1H, d, J = 8Hz, Ar-H), 6.65 (2H, s, Ar-H), 6.60 (4H, s, Ar-H), 5.08 (4H, s, $2CH_2$) ppm; **$^{31}P\{^1H\}$ NMR** (162 MHz, d_6-DMSO) δ 19.34 ppm; **FT-IR** (KBr): *v* = 3467(OH), 1745(C=O), 1503(C=C), 1384(CO), 850(Ar-H), 326(AuCl) cm^{-1}; **CHN** $C_{46}H_{35}P_2NO_5Au_2Cl_2 \cdot CH_2Cl_2$ requires C (43.69%), H (2.89%), N (1.08%), found: C (43.69%), H (2.75), N (1.29%); **ESI-MS:** calcd for $C_{46}H_{36}O_5NP_2Au_2Cl_2$ $[M+H]^+$ requires m/z 1208.0771, found *m/z* 1208.0760 (0.9 ppm).

Photophysical Measurements

Absorption spectra were recorded with a Shimadzu UV-1650PC spectrophotometer while fluorescence studies were performed on a Spex model Fluoromax fluorescence spectrophotometer. Absorption and emission spectra were recorded in dimethylsulfoxide (DMSO 99+%) at room temperature (*ca.* 298K) using a standard quartz cell. Samples were purged with nitrogen before measurement to reduce photobleaching and oxidation of the phosphine moiety. Compounds were excited at 277 nm and excitation and emission slits were both set to 0.7 nm.

6.5 Chapter 4 Experimental

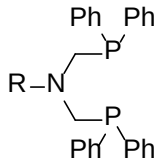

R = **(4.2)** CH_2CO_2H
(4.3) $CH_2CONHCH_2CO_2H$
(4.7) $CH_2CONHCH_2CONHCH_2CO_2H$
(4.12) $(CH_2)_4CH(CO_2H)NHCOOCH_2Ph$
(4.13) $(C_6H_4)CONHCH_2CO_2H$
(4.14) $NHCO_2CH_2CH_3$
(4.15)

$C_{28}H_{27}NO_2P_2$ (4.2)

Compound **4.2** was synthesised according to literature procedures with only slight modifications. Gathered data matched that recorded in the literature.[3,14] From glycine

(0.088g; 1.172mmol) and hydroxymethyldiphenylphosphine (0.503g; 2.329mmol). **Yield:** 0.397g, 81%; **Appearance:** white solid; **^{1}H NMR** (400 MHz, $CDCl_3$) δ 7.50-7.10 (20H, m, Ar-H), 3.95 (2H, d, J = 13.6Hz, PCH_2), 3.56 (2H, s, PCH_2), 3.48 (2H, dd, J = 5.6Hz, 7.6Hz, NCH_2) ppm; **^{31}P{^{1}H} NMR** (162 MHz, $CDCl_3$) δ -26.74 ppm.

$C_{30}H_{30}N_2O_3P_2$ (4.3)

Prepared in accordance with the procedure described in literature.[145] From glycylglycine (0.024g; 0.183mmol) and hydroxymethyldiphenylphosphine (0.080g; 0.370mmol). **Yield:** 0.080g, 82%; **Appearance:** white solid;**^{1}H NMR** (400 MHz, $CDCl_3$) δ 10.76 (1H, s, OH), 8.07 (1H, s, NH), 7.39-7.34 (20H, m, Ar-H), 4.16 (2H, s, CH_2), 3.29 (2H, s, CH_2), 2.17 (4H, s, CH_2) ppm; **^{31}P{^{1}H} NMR** (162 MHz, $CDCl_3$) δ -27.44 ppm.

$C_{32}H_{33}N_3O_4P_2$ (4.7)

Compound **4.7** has been previously synthesised in literature, however the method has been modified. Analysis of **4.7** matches that in the literature.[145] A methanolic solution (20mL) of hydroxymethyldiphenylphosphine (0.413g; 1.912mmol) and triglycine (0.177g; 0.936mmol) was refluxed over 20hr. under N_2. The clear solution was evaporated to dryness to give white solid **4.7**. **Yield:** 0.314g, 57%; **Appearance:** white solid; **^{1}H NMR** (400 MHz, $CDCl_3$) δ 10.64 (1H, s, OH), 8.12 (1H, s, NH), 8.23 (1H, s, NH), 7.42-7.31 (20H, m, Ar-H), 4.19 (2H, s, CH_2), 3.98 (2H, s, CH_2), 3.27 (2H, s, CH_2), 2.38 (4H, s, CH_2) ppm; **^{31}P{^{1}H} NMR** (162 MHz, $CDCl_3$) δ -26.36 ppm.

$C_{31}H_{32}N_2O_3P_2$ (4.12)

Prepared in the same manner as **4.2**; from glycyl-L-alanine (0.097g; 0.665mmol) and hydroxymethyldiphenylphosphine (0.287g; 1.330mmol). **Yield:** 0.191g, 53%; **Appearance:** white solid; **^{1}H NMR** (400 MHz, $CDCl_3$) δ 7.50-7.10 (20H, m, Ar-H), 6.88 (1H, d, J = 7.2Hz, NH), 4.29 (1H, quintet, J = 7.2Hz, CH), 3.75 (2H, d, J = 12.8Hz, PCH_2), 3.65 (2H, s, PCH_2), 3.56 (2H, dd, J = 4.8Hz, 8Hz, NCH_2), 0.93 (3H, d, J = 7.2Hz, CH_3) ppm; **^{31}P{^{1}H} NMR** (162 MHz, $CDCl_3$) δ -27.17 ppm; **FTIR** (KBr): *v* = 3468(NH), 1640(C=O), 695(Ar-H) cm^{-1}; **CHN:** Despite repeated attempts, a satisfactory elemental analysis was not obtained; **ESI-MS:** calcd for $C_{19}H_{22}O_4N_2P$ $[M\text{-}PPh_2]^+$ requires m/z 357.1355, found *m/z* 357.1367 (3.6 ppm).

$C_{40}H_{42}O_4N_2P_2$ (4.13)

Prepared in the same manner as **4.2**; from N-alpha-Cbz-L-Lysine (0.292g; 1.042mmol) and hydroxymethyldiphenylphosphine (0.498g; 2.305mmol).**Yield:** 0.310g, 44%; **Appearance:** white solid; **^{1}H NMR** (400 MHz, $CDCl_3$) δ 7.74 (1H, m, NH), 7.49-7.28 (25H, m, Ar-H), 5.02 (4H, s, CH_2), 3.78 (1H, m, CH), 3.50 (4H, s, CH_2), 1.50 (2H, m, CH_2), 1.39 (2H, m, CH_2), 1.24 (2H, m, CH_2), 1.07 (2H, m, CH_2) ppm; **^{31}P{^{1}H} NMR** (162 MHz, $CDCl_3$) δ -28.89 ppm; **FTIR** (KBr): *v* = 3441(NH), 2934(OH), 1714(C=O), 694(ArH) cm^{-1}; **CHN:** Despite repeated attempts, a satisfactory elemental analysis was not obtained; **ESI-MS:** calcd for $C_{40}H_{43}O_4N_2P_2$ $[M+H]^+$ requires m/z 677.2693, found *m/z* 677.2686 (1.0 ppm).

$C_{35}H_{32}P_2N_2O_3$ (4.14)

Prepared in the same manner as **4.2**; from *p*-aminohippuric acid (0.119g; 0.613mmol) and hydroxymethyldiphenylphosphine (0.250g; 1.157mmol). **Yield:** 0.355g, 98%; **Appearance:** white solid; **^{1}H NMR** (400 MHz, $CDCl_3$) δ 8.42 (1H, t, J = 6Hz, CH_2NH), 8.34 (isomeric eq. to 8.42), 7.60 (2H, d, J = 10Hz, 2Ar H), 7.35-7.3 (20H, m, Ar H), 6.76 (2H, d, J = 8Hz, 2Ar H), 6.68 (6.76 isomeric eq.), 3.96 (4H, s, $2PCH_2$), 3.80 (2H, s, CH_2CO_2H) ppm; **^{31}P{^{1}H} NMR** (162 MHz, $CDCl_3$) δ -26.17 ppm; **FTIR** (KBr): *v* = 3418(NH), 1734(C=O), 1604(C=O), 695(Ar-H) cm^{-1}; **CHN** $C_{35}H_{32}P_2N_2O_3{\cdot}H_2O$ requires C (69.06%), H (5.64%), N (4.60%), found C (69.13%), H (5.47%), N (4.83%); **ESI-MS:** calcd for $C_{35}H_{33}O_5N_2P_2$ $[(M+O_2)+H]^+$ requires m/z 623.1859, found *m/z* 623.1854 (1.0 ppm).

$C_{29}H_{30}P_2N_2O_2$ (4.15)

A mixture of hydroxymethyldiphenylphosphine (0.251g; 1.162mmol) and ethyl carbazate (0.070g; 0.673mmol) in methanol:toulene (1:3; 20 ml) was refluxed under N_2 for 24hs. The clear solution was then evaporated to dryness under vacuum. **Yield:** 0.33g, 115%; **Appearance:** white solid; **^{1}H NMR** (400 MHz, $CDCl_3$) δ 7.11-7.34 (20H, m, Ar-H), 3.97 (4H, m, PCH_2), 3.87 (2H, s, CH_2), 1.12 (3H, m, CH_3) ppm; **^{31}P{^{1}H} NMR** (162 MHz, $CDCl_3$) δ -25.71 ppm; **FTIR** (KBr): *v* = 3428(NH), 1702(C=O), 1480(C=C), 1383(CH_3), 1261(C-O), 739(Ar-H), 694(Ar-H) cm^{-1}; **CHN** $C_{29}H_{30}P_2N_2O_2{\cdot}2CH_3OH$ requires C (65.94%), H (6.80%), N (4.96%), found C (66.08%), H (6.35%), N (5.41%); **ESI-MS:** calcd for $C_{29}H_{31}O_2N_2P_2$ $[M+H]^+$ requires m/z 501.1855, found *m/z* 501.1844 (2.2 ppm).

Compounds **4.16** and **4.17** were synthesised according to a literature procedure.[187] ^{1}H NMR analysis was comparable to that in the literature.[167]

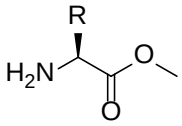

R = **(4.16)** CH_2OH
(4.17) CH_2Ph

$C_4H_9NO_3$ (4.16)

Methanol (25mL) was added to thionyl chloride (3.45mL; 47.578mmol) at 0°C. L-serine (1.000g; 9.516mmol) was added to the mixture and the solution was stirred over 24h. The solution was evaporated to dryness to yield white solid **4.16**.[167] **Yield:** 1.451g, 98%; **Appearance:** white solid; **^{1}H NMR** (400 MHz, CD_3OD) δ 4.07 (1H, t, J = 4.0Hz, CH), 3.98 (2H, d, J = 4.0Hz, CH_2), 3.83 (3H, s, CH_3) ppm.[188]

$C_{10}H_{13}NO_2$ (4.17)

From thionyl chloride (2.202mL; 30.270mmol), methanol (25mL) and L-phenylalanine (1.000g; 6.055mmol). **Yield:** 1.266g, 97%; **Appearance:** white solid; **^{1}H NMR** (400 MHz, CD_3OD) δ 7.37 (2H, t, J = 7.1Hz, Ar-H), 7.31 (1H, dd, J = 4.9, 9.6Hz, Ar-H), 7.27 (2H, d, J = 7.1Hz, Ar-H), 4.32 (1H, t, J = 6.8Hz, CH), 3.80 (3H, s, CH_3), 3.26 (1H, dd, J = 6.2, 14.3Hz, CH_2), 3.19 (1H, dd, J = 6.2, 14.3Hz, CH_2), 2.03 (2H, s, NH_2) ppm.[167]

The following general method was used for the synthesis of ligand **4.19** – **4.21**. A mixture of hydroxymethyldiphenylphosphine (2 eq), triethylamine (0.1mL) and primary amine phenylalanine methyl ester hydrochloride, serine methyl ester hydrochloride and leucine methyl ester hydrochloride (1 eq) in methanol (20 ml) was refluxed under N_2 for 48 hs. The solutions were evaporated to dryness under vaccum to give colourless oils. Data for all three compound match that recorded in the literature.[9]

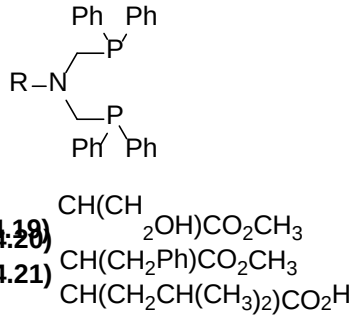

$C_{30}H_{31}O_3NP_2$ (4.19)

From L-serine methyl ester hydrochloride, **4.16**, (0.093g; 0.600mmol) and hydroxymethyldiphenylphosphine (0.243g; 1.125mmol). **Yield:** 0.385g, 79%; **Appearance:** colourless oil; **^{1}H NMR** (400 MHz, $CDCl_3$) δ 7.81-7.31 (20H, m, Ar H), 4.38 (1H, m, CH), 3.97 (2H, d, J = 9.2Hz, PCH_2), 3.71 (3H, s, CH_3), 3.58-3.49 (4H, m, CH_2P, CH_2) ppm; **^{31}P{^{1}H} NMR** (162 MHz, $CDCl_3$) δ -27.23 ppm.

$C_{356}H_{35}O_2NP_2$ (4.20)

From L-phenylalanine methyl ester hydrochloride, **4.17**, (0.132g; 0.612mmol) and hydroxymethyldiphenylphosphine (0.265g; 1.227mmol). **Yield:** 0.322g, 94%; **Appearance:** colourless oil; **^{1}H NMR** (400 MHz, $CDCl_3$) δ 7.33-7.25 (20H, m, Ar H), 7.15 (3H, m, H^d), 6.96 (2H, d, J = 1.6Hz, H^c), 4.45 (1H, m, CH (H^e)), 3.94 (2H, d, J = 13.2Hz, PCH_2 (H^f)), 3.56 (3H, s, CH_3), 3.47 (2H, name, J = 4.8Hz, 8Hz, PCH_2 (H^f)), 2.97 (1H, name, J =8.8Hz, 4.4Hz, H^a/H^b), 2.56 (1H, dd, J = 5.6Hz, 8Hz, H^a/H^b) ppm; **^{31}P{^{1}H} NMR** (162 MHz, $CDCl_3$) δ -26.78 ppm.

$C_{33}H_{37}O_2NP_2$ (4.21)

From L-leucine methyl ester hydrochloride (0.108g; 0.593mmol) and hydroxymethyldiphenylphosphine (0.258g; 1.19mmol). **Yield:** 0.238g, 74%; **Appearance:** colourless oil; **^{1}H NMR** (400 MHz, $CDCl_3$) δ 7.8-7.4 (20H, m, Ar H), 4.22 (1H, m, CH), 4.00 (2H, d, J = 13.2Hz, CH_2P), 3.66 (3H, s, CH_3), 3.41 (2H, m, CH_2P), 1.22 (1H, m, $CH(CH_3)_2$), 0.72 (3H, d, J = 6.4Hz, CH_3), 0.61 (3H, d, J = 6.4Hz, CH_3) ppm; **^{31}P{^{1}H} NMR** (162 MHz, $CDCl_3$) δ -26.56 ppm.

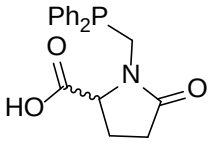

(4.24)

$C_{18}H_{18}O_3NP$ (4.24)

Hydroxymethyldiphenylphosphine (1 eq), and glutamic acid (1 eq) in methanol (20 ml) was refluxed under nitrogen for 4 hours. The solution was then evaporated to dryness under vaccum to give a white solid. **Yield:** 0.919g, 92%; **Appearance:** white solid; **^{1}H NMR** (400MHz, $CDCl_3$) δ 7.90 – 7.40 (10H, m, PPh_2), 4.82 (1H, d, J = 14.4Hz, NCH), 3.61 (2H, dd, J = 8.4Hz, 6Hz, PCH_2) 2.48 – 2.04 (4H, m, $2CH_2$); **^{31}P{^{1}H} NMR** (400MHz, $CDCl_3$) δ -22.47 ppm; **FTIR** (KBr): *v* = 3400-2400(OH), 1723(C=O), 1629(C=O), 1280(C-O) cm^{-1}; **CHN** $C_{18}H_{18}PNO_3$ requires C (66.05%), H (5.54%), N (4.28%), found: C (65.66%), H (5.32%), N (4.09%); **ESI-MS:** calcd for $C_{18}H_{19}O_3NP$ $[M+H]^+$ requires m/z 328.1103, found *m/z* 328.1112 (2.7 ppm).

Coordination Compounds

Unless otherwise stated, the following Au(I), Ru(II) and Pt(II) complexes were synthesised through the reaction of appropriate metal precursors, Au(tht)Cl, Pt(cod)Cl and $\{RuCl(\mu\text{-}Cl)(\eta^6\text{-}p\text{-cym})\}_2$, with ligands **4.12** – **4.15**, **4.19** – **4.21** and **4.24**. Following 1h stirring in CH_2Cl_2, the solvent volume was reduced to 1-2mL and Et_2O was added resulting in the precipitation of respective coordination complexes.

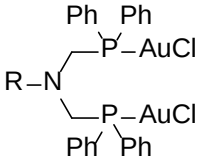

R = **(4.25)** $CH_2CONHCH(CH_3)CO_2H$
(4.26) $(CH_2)_4CH(CO_2H)NHCOOCH_2Ph$
(4.27) $(C_6H_4)CONHCH_2CO_2H$
(4.28) $CH(CH_2NHCO_2CH_2CH_3)CO_2CH_3$
(4.29) $CH(CH_2OH)CO_2CH_3$
(4.30) $CH(CH_2Ph)CO_2CH_3$
(4.31) $CH_2CH(CH_3)_2)CO_2H$

$C_{31}H_{32}N_2O_3P_2Au_2Cl_2$ (4.25)

From **4.12** (0.055; 0.101mmol) and AuCl(tht) (0.065g; 0.203mmol). **Yield:** 0.048g, 47%; **Appearance:** white solid; **^{1}H NMR** (400 MHz, $CDCl_3$) δ 7.76-7.42 (20H, m, Ar H $2PPh_2$), 6.61 (1H, s, NH), 4.35 (6H, m, CH_2, $2CH_2$), 3.45 (1H, m, CH), 1.42 (3H, d, J = 5.2Hz, CH_3) ppm; **^{31}P{^{1}H} NMR** (162 MHz, $CDCl_3$) δ 19.40 ppm; **FTIR** (KBr): *v* = 3401(NH), 2963(OH), 1735 and 1667(C=O), 692(Ar-H), 327(AuCl) cm^{-1}; **CHN** $C_{31}H_{32}P_2N_2O_3Au_2Cl_2$ requires C (36.96%), H (3.20%), N (2.78%), found: C (37.23%), H (2.91%), N (2.67%); **ESI-MS:** calcd for $C_{31}H_{32}O_3N_2P_2Au_2Cl$ $[M\text{-}Cl]^+$ requires m/z 971.0902, found *m/z* 971.0888 (1.5 ppm).

$C_{40}H_{42}P_2N_2O_4Au_2Cl_2$ (4.26)

From **4.13** (0.067g; 0.099mmol) and AuCl(tht) (0.064g; 0.200mmol). **Yield:** 0.059g, 52%; **Appearance:** white solid; **^{1}H NMR** (400 MHz, $CDCl_3$) δ 7.67-7.44 (20H, m, Ar-H), 7.35-7.23 (5H, m, Ar-H), 5.39 (1H, d, J = 7.6Hz, NH), 5.09 (2H, s, CH_2), 4.23 (1H, m, CH), 4.14 (4H, s, CH_2), 2.76 (2H, br. s , CH_2), 1.56-1.41 (2H, m, CH_2), 1.07-0.96 (4H, m, CH_2) ppm; **^{31}P{^{1}H} NMR** (162 MHz, $CDCl_3$) δ 18.26 ppm; **FTIR** (KBr): *v* = 3443(NH), 2932(OH), 1717(C=O), 693(ArH), 319(AuCl) cm^{-1}; **CHN** $C_{40}H_{42}P_2N_2O_4Au_2Cl_2{\cdot}H_2O$ requires C (41.43%), H (3.65%), N (2.42%), found: C (41.12%), H (3.05%), N (2.25%); **ESI-MS:** calcd for $C_{40}H_{42}P_2N_2O_4Au_2Cl$ $[M\text{-}Cl]^+$ requires m/z 1105.1640, found *m/z* 1105.1662 (2.0 ppm).

$C_{35}H_{32}P_2N_2O_3Au_2Cl_2$ (4.27)

From **4.14** (0.055g; 0.093mmol) and AuCl(tht) (0.064g; 0.200mmol). **Yield:** 0.044g, 45%; **Appearance:** white solid; **^{1}H NMR** (400 MHz, $CDCl_3$) δ 8.11 (1H, s, NH), 8.10-7.45 (20H, m, Ar-H), 6.91 (2H, t, J = 4.8Hz, Ar-H), 6.66 (2H, d, J = 8.8Hz, Ar-H), 4.80 (4H, s, CH_2), 4.22 (2H, d, J = 5.2Hz, CH_2) ppm; **^{31}P{^{1}H} NMR** (162 MHz, $CDCl_3$) δ 17.58 ppm; **FTIR** (KBr): *v* = 3401(NH), 1642(C=O), 1605(C=O), 1505(NH), 328(AuCl) cm^{-1}; **CHN** $C_{35}H_{32}P_2N_2O_3Au_2Cl_2$ requires C (39.83%), H (3.06%), N (2.65%), found C (39.47%), H (3.05%), N (2.99%); **ESI-MS:** calcd for $C_{35}H_{32}O_3N_2P_2Au_2Cl$ $[M\text{-}Cl]^+$ requires m/z 1019.0902, found *m/z* 1019.0903 (0.1 ppm).

$C_{29}H_{30}P_2N_2O_2Au_2Cl_2$ (4.28)

From **4.15** (0.118g; 0.236mmol) and AuCl(tht) (0.122g; 0.381mmol). **Yield:** 0.125g, 69%; **Appearance:** white solid; **^{1}H NMR** (400 MHz, $CDCl_3$) δ 7.72-7.67 (8H, m, Ar-H), 7.53-7.44 (12H, m, Ar-H), 6.42 (1H, br s, NH), 4.46 (4H, s, $2CH_2$), 3.93 (2H, q, J = 6Hz, CH_2), 1.12 (3H, t, J = 7.2Hz, CH_3) ppm; **^{31}P{^{1}H} NMR** (162 MHz, $CDCl_3$) δ 22.57 ppm;

FTIR (KBr): *v* = 3821(NH), 1718(C=O), 328(AuCl) cm^{-1}; **CHN** $C_{29}H_{30}P_2N_2O_2Au_2Cl_2$ requires C (36.08%), H (3.13%), N (2.90%), found C (36.32%), H (3.04%), N (2.98%); **ESI-MS:** calcd for $C_{29}H_{31}O_2N_2P_2Au_2Cl$ $[M\text{-}Cl]^+$ requires m/z 929.0797, found *m/z* 944.0778 (2.0 ppm)

$C_{30}H_{31}O_3NP_2Au_2Cl_2$ (4.29)

From **4.19** (0.051g; 0.099mmol) and AuCl(tht) (0.063g; 0.197mmol). **Yield:** 0.049g, 51%; **Appearance:** white solid; **^{1}H NMR** (400 MHz, $CDCl_3$) δ 11.17 (1H, br s, OH), 7.84-7.48 (20H, m, Ar-H), 4.56 (2H, dd, J = 4.8, 8.8Hz, CH_2P), 4.33 (2H, dd, J = 4.4, 10.4Hz, CH_2P), 3.76 (1H, m, CH), 3.67 (3H, s, CH_3), 3.54-3.41(2H, m, CH_2) ppm; **^{31}P{^{1}H} NMR** (162 MHz, $CDCl_3$) δ 21.18 ppm; **FTIR** (KBr): *v* = 3436(NH), 691(Ar-H), 319(AuCl) cm^{-1}; **CHN:** Despite repeated attempts, a satisfactory elemental analysis was not obtained; **ESI-MS:** calcd for $C_{30}H_{31}O_3NP_2Au_2Cl$ $[M\text{-}Cl]^+$ requires m/z 944.0793, found *m/z* 944.0776 (1.9 ppm).

$C_{36}H_{35}O_2NP_2Au_2Cl_2$ (4.30)

From **4.20** (0.072; 0.125mmol) and AuCl(tht) (0.061g; 0.191mmol). **Yield:** 0.052g, 53%; **Appearance:** white solid; **^{1}H NMR** (400 MHz, $CDCl_3$) δ 7.77-7.73 (8H, m, Ar-H), 7.56-7.48 (12H, m, Ar-H), 7.15 (3H, m, Ar-H), 6.64 (2H, m, Ar-H), 4.41 (2H, dd, J = 5.2Hz, 9.2Hz, CH_2P), 4.26 (2H, d, J = 14.8Hz, CH_2P), 3.79 (1H, dd, J = 3.6, 5.6Hz, CH), 3.53 (3H, s, CH_3), 2.69 (1H, dd, J = 9.6Hz, 4Hz, CH_2), 2.35 (1H, dd, J = 5.2, 8Hz, CH_2) ppm; **^{31}P{^{1}H} NMR** (162 MHz, $CDCl_3$) δ 21.81 ppm; **FTIR** (KBr): *v* = 1731(C=O), 325(AuCl) cm^{-1}; **CHN:** Despite repeated attempts, a satisfactory elemental analysis was not obtained; **ESI-MS:** calcd for $C_{36}H_{35}O_2NP_2Au_2Cl$ $[M\text{-}Cl]^+$ requires m/z 990.1001, found *m/z* 990.1001 (0.0 ppm).

$C_{33}H_{37}O_2NP_2Au_2Cl_2$ (4.31)

From **4.21** (0.054; 0.100mmol) and AuCl(tht) (0.064g; 0.200mmol). **Yield:** 0.050g, 50%; **Appearance:** white solid; **^{1}H NMR** (400 MHz, $CDCl_3$) δ 7.84-7.75 (8H, m, Ar-H), 7.55-7.49 (12H, m, Ar-H), 4.39 (2H, m, CH_2), 4.20 (2H, d, J = 13.2Hz, CH_2P), 3.63 (3H, s, CH_3), 3.49 (1H, m, CH), 1.22 (1H, m, CH), 0.52 (3H, d, J = 6.4Hz, CH_3), 0.41 (3H, d, J = 6.4Hz, CH_3) ppm; **^{31}P{^{1}H} NMR** (162 MHz, $CDCl_3$) δ 21.86 ppm; **FTIR** (KBr): *v* = 3444(NH), 695(Ar-H), 327(AuCl) cm^{-1}; **CHN:** Despite repeated attempts, a satisfactory elemental analysis was not obtained; **ESI-MS:** calcd for $C_{33}H_{37}O_2NP_2Au_2Cl$ $[M\text{-}Cl]^+$ requires m/z 970.1314, found *m/z* 970.1297 (1.7 ppm).

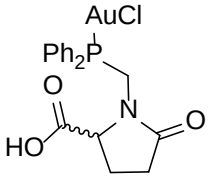

(4.34)

$C_{18}H_{18}O_3NPAu$ (4.34)

From **4.24** (0.256g; 0.379mmol) and $PtCl_2$(cod) (0.144g; 0.385mmol). Yield: 0.068g, 53%; **Appearance:** white solid; **^{1}H NMR** (400 MHz, $CDCl_3$) δ 7.88 – 7.48 (10H, m, PPh_2), 5.26 (1H, dd, J = 5.2, 10Hz, NCH), 4.82 (2H, m, J = 8.4Hz, 6Hz, PCH_2) 2.41 – 2.08 (4H, m, $2CH_2$) ppm; **^{31}P{^{1}H} NMR** (162 MHz, $CDCl_3$) δ 22.43 ppm; **FTIR** (KBr): *v* = 3330(OH), 1732(C=O) cm^{-1}; **CHN:** Despite repeated attempts, a satisfactory elemental analysis was not obtained; **ESI-MS:** calcd for $C_{18}H_{18}O_3NPAu$ $[M\text{-}Cl]^+$ requires m/z 524.0684, found *m/z* 524.0667 (3.3 ppm).

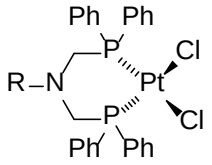

R = **(4.35)** $CH_2CONHCH(CH_3)CO_2H$
(4.36) $(CH_2)_4CH(CO_2H)NHCOOCH_2Ph$
(4.37) $(C_6H_4)CONHCH_2CO_2H$
(4.38) $CH(CH_2NHCO_2CH_2CH_3$
(4.39) $CH(CH_2OH)CO_2CH_3$
(4.40) $CH(CH_2Ph)CO_2CH_3$
(4.41) $CH_2CH(CH_3)_2)CO_2H$

$C_{31}H_{32}P_2N_2O_3PtCl_2$ (4.35)

From **4.12** (0.050g; 0.092mmol) and $PtCl_2$(cod) (0.034g; 0.091mmol). **Yield:** 0.620g, 94%; **Appearance:** white solid; **^{1}H NMR** (400 MHz, d_6-DMSO) δ 8.08 (1H, d, J = 7.2Hz, OH)7.46-7.55 (20H, m, Ar H $2PPh_2$), 5.77 (1H, s, NH), 4.13 (2H, q, J = 7.2Hz, CH_2), 3.93 (4H, d, J, 7.6Hz, J_{sat} = 14.8Hz, $2CH_2$), 2.31 (1H, s, CH), 1.15 (3H, d, J = 7.2Hz, CH_3) ppm; **^{31}P{^{1}H} NMR** (162 MHz, d_6-DMSO) δ -10.06 ($^1J_{PtP}$ 3392 Hz) ppm; **FTIR** (KBr): *v* =

3467(NH), 1737(C=O), 695(Ar-H), 308(PtCl), 294(PtCl) cm^{-1}; **CHN** $C_{31}H_{32}P_2N_2O_3PtCl_2 \cdot H_2O$ requires C (45.04%), H (4.15%), N (3.39%), found: C (45.27%), H (4.08%), N (3.72%); **ESI-MS:** calcd for $C_{31}H_{32}O_3N_2P_2PtCl$ $[M\text{-}Cl]^+$ requires m/z 772.1219, found *m/z* 772.1201 (0.4 ppm).

$C_{40}H_{42}P_2N_2O_4PtCl_2$ (4.36)

From **4.13** (0.256g; 0.379mmol) and $PtCl_2$(cod) (0.144g; 0.385mmol). **Yield:** 0.219g, 61%; **Appearance:** white solid; **^{1}H NMR** (400 MHz, $CDCl_3$) δ 7.88-7.407 (25H, m, Ar-H), 5.36 (1H, s, NH), 5.05 (2H, s, CH_2), 4.20 (1H, s, CH), 3.33 (4H, s, CH_2), 2.47 (2H, br. s, CH_2), 1.64-1.50 (4H, m, CH_2), 1.04 (2H, m, CH_2) ppm; **^{31}P{^{1}H} NMR** (162 MHz, $CDCl_3$) δ -7.75 ($^1J_{PtP}$ 3407 Hz) ppm; **FTIR** (KBr): *v* = 3416(NH), 2930(OH), 1714(C=O), 693(Ar-H), 312(Pt-Cl), 294(PtCl) cm^{-1}; **CHN** $C_{40}H_{42}P_2N_2O_4PtCl_2$ requires C (50.97%), H (4.49%), N (2.97%), found C (50.65%), H (4.30%), N (2.97%); **ESI-MS:** calcd for $C_{40}H_{42}O_4N_2P_2PtCl$ $[M\text{-}Cl]^+$ requires m/z 906.1951, found *m/z* 906.1950 (0.0 ppm).

$C_{35}H_{32}O_3N_2P_2PtCl_2$ (4.37)

From **4.14** (0.118g; 0.200mmol) and $PtCl_2$(cod) (0.073g; 0.195mmol). **Yield:** 0.121g, 71%; **Appearance:** white solid; **^{1}H NMR** (400 MHz, d_6-DMSO) δ 8.38 (1H, t, J = 9.6Hz, CH_2NH), 8.01-7.45 (20H, m, Ar H 4Ph), 7.25 (2H, d, J = 7.6Hz, 2Ar-H), 6.36 (2H, d, J = 8Hz, 2Ar-H), 4.23 (4H, s, $2CH_2$), 3.74 (2H, s, CH_2) ppm; **^{31}P{^{1}H} NMR** (162 MHz, d_6-DMSO) δ 10.70 ppm ($^1J_{PtP}$ 3487 Hz); **FTIR** (KBr): *v* = 3420(NH), 1605(C=O), 1505(NH), 308(PtCl), 292(PtCl) cm^{-1}; **CHN:** Despite repeated attempts, a satisfactory elemental analysis was not obtained; **ESI-MS:** calcd for $C_{35}H_{32}O_3N_2P_2PtCl$ $[M\text{-}Cl]^+$ requires m/z 820.1219, found *m/z* 820.1218 (0.1 ppm);

$C_{29}H_{30}P_2N_2O_2PtCl_2$ (4.38)

From **4.15** (0.105g; 0.203mmol) and $PtCl_2$(cod) (0.070g; 0.187mmol). **Yield:** 0.097g, 68%; **Appearance:** white solid; **^{1}H NMR** (400MHz, d_6-DMSO) δ 7.51-7.61 (20H, m, Ar H $2PPh_2$), 5.58 (1H, s, NH), 4.03-4.10 (6H, m, $2PCH_2$ + CH_2), 1.19 (3H, t, J = 7.2Hz, CH_3); **^{31}P{^{1}H} NMR** (162 MHz, d_6-DMSO) δ -4.45 ($^1J_{PtP}$ 3404 Hz) ppm; **FTIR** (KBr): *v* = 3468(NH), 1706(C=O), 1638(C=O), 689(Ar-H) cm^{-1}; **CHN** $C_{29}H_{30}P_2N_2O_2PtCl_2 \cdot H_2O$ requires C (44.40%), H (4.12%), N (3.57%), found C (44.34%), H (3.91%), N (3.69%); **ESI-MS:**

calcd for $C_{29}H_{30}O_2N_2P_2PtCl$ [M-Cl]$^+$ requires m/z 730.1113, found *m/z* 730.1096 (2.3 ppm).

$C_{30}H_{31}O_3NP_2PtCl_2$ (4.39)

From **4.19** (0.071g; 0.138mmol) and $PtCl_2$(cod) (0.037g; 0.099mmol). **Yield:** 0.041g, 55%; **Appearance:** white solid; **^{1}H NMR** (400MHz, $CDCl_3$) δ 7.89-7.40 (20H, m, Ar H), 4.39 (1H, m, CH), 3.83 (2H, m, PCH_2), 3.71 (3H, s, CH_3), 3.50-3.10 (4H, m, CH_2P, CH_2); **^{31}P{^{1}H} NMR** (162 MHz, $CDCl_3$) δ -8.07 ($^1J_{PtP}$ 3420 Hz) ppm; **FTIR** (KBr): *v* = 3435(OH), 693(Ar-H), 299(PtCl) cm^{-1}; **CHN:** Despite repeated attempts, a satisfactory elemental analysis was not obtained; **ESI-MS:** calcd for $C_{30}H_{31}O_3NP_2PtCl$ [M-Cl]$^+$ requires m/z 745.1110, found *m/z* 745.1107 (0.4 ppm).

$C_{36}H_{35}O_2NP_2PtCl_2$ (4.40)

From **4.20** (0.081g; 0.141mmol) and $PtCl_2$(cod) (0.037g; 0.099mmol). **Yield:** 0.044g, 52%; **Appearance:** white solid; **^{1}H NMR** (400MHz, $CDCl_3$) δ 7.88-7.36 (20H, m, Ar H), 7.10 (3H, m, H^d), 6.65 (2H, d, J = 6.8Hz, H^c), 3.67 (4H, m, $2CH_2P$), 3.51 (3H, s, CH_3), 3.38 (1H, m, CH), 2.81 (1H, dd, J = 8Hz, 6Hz, H^a/H^b), 2.27 (1H, m, H^a/H^b) ppm; **^{31}P{^{1}H} NMR** (162 MHz, $CDCl_3$) δ -8.04 ($^1J_{PtP}$ 3427 Hz) ppm; **FTIR** (KBr): <u>v</u> = 693(ArH), 318(Pt-Cl) cm^{-1}; **CHN:** Despite repeated attempts, a satisfactory elemental analysis was not obtained; **ESI-MS:** calcd for $C_{36}H_{35}O_2NP_2PtCl$ [M-Cl]$^+$ requires m/z 805.1474, found *m/z* 805.1475 (0.1 ppm).

$C_{33}H_{37}O_2NP_2PtCl_2$ (4.41)

From **4.21** (0.054g; 0.100mmol) and $PtCl_2$(cod) (0.036g; 0.096mmol). **Yield:** 0.048g, 55%; **Appearance:** white solid; **^{1}H NMR** (400MHz, $CDCl_3$) δ 7.79-7.25 (20H, m, Ar H), 4.45 (1H, s, CH), 3.78-3.59 (7H, m, $2CH_2P$, CH_3), 1.22 (1H, m, $CH(CH_3)_2$), 0.90 (3H, m, CH_3), 0.48 (3H, m, CH_3) ppm; **^{31}P{^{1}H} NMR** (162 MHz, $CDCl_3$) δ -7.93 ($^1J_{PtP}$ 3437 Hz) ppm; **FTIR** (KBr): *v* = 3436(NH), 692(C-H), 315(PtCl), 282(PtCl) cm^{-1}; **CHN:** Despite repeated attempts, a satisfactory elemental analysis was not obtained; **ESI-MS:** calcd for $C_{33}H_{37}O_2NP_2PtCl$ [M-Cl]$^+$ requires m/z 771.1630, found *m/z* 771.1627 (0.1 ppm).

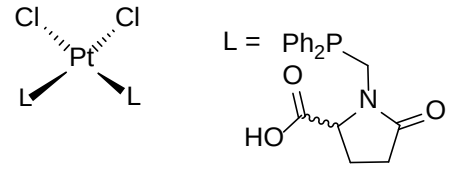

(4.44)

$C_{36}H_{36}O_6N_2P_2PtCl_2$ (4.44)

From **4.24** (0.101g; 0.306mmol) and $PtCl_2$(cod) (0.057g; 0.153mmol). Yield: 0.131g, 93%; **Appearance:** white solid; **^{1}H NMR** (400 MHz, d_6-DMSO) δ 8.02 – 6.87 (10H, m, PPh_2), 4.70 (1H, m, NCH), 4.36 (2H, m, PCH_2) 2.07 – 1.96 (4H, m, $2CH_2$) ppm; **^{31}P{^{1}H} NMR** (162 MHz, $CDCl_3$) δ 3.02 ($^1J_{PtP}$ 3625 Hz) ppm; **FTIR** (KBr): *v* = 3423(OH), 1736(C=O) cm^{-1}; **CHN** $C_{36}H_{36}P_2N_2O_6PtCl_2{\cdot}H_2O$ requires C (46.03%), H (4.08%), N (2.98%), found C (46.11%), H (3.77%), N (2.86%); **ESI-MS:** calcd for $C_{36}H_{36}O_6N_2P_2PtCl$ $[M\text{-}Cl]^+$ requires m/z 884.1379, found *m/z* 884.1370 (1.1 ppm).

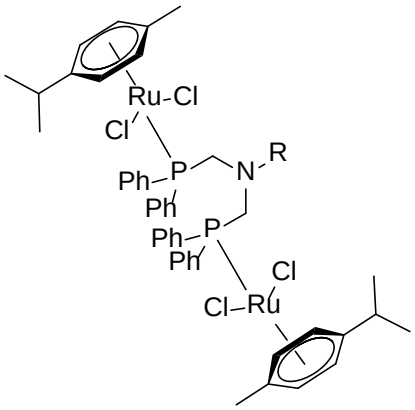

R = **(4.45)** $CH_2CONHCH(CH_3)CO_2H$
(4.46) $(CH_2)_4CH(CO_2H)NHCOOCH_2Ph$
(4.47) $(C_6H_4)CONHCH_2CO_2H$
(4.48) $CH(CH_2OH)CO_2CH_3$
(4.49) $CH(CH_2Ph)CO_2CH_3$
(4.50) $NHCO_2CH_2CH_3$
(4.51) $CH(CH_2CH(CH_3)_2)CO_2H$

$C_{51}H_{60}P_2N_2O_3Ru_2Cl_4$ (4.45)

From **4.12** (0.102g; 0.187mmol) and $[RuCl(\mu\text{-}Cl)(\eta^6\text{-}p\text{-cym})]_2$ (0.110g; 0.180mmol). **Yield:** 0.168g, 81%; **Appearance:** orange solid; **^{1}H NMR** (400MHz, $CDCl_3$) δ 7.36-7.76

(20H, m, Ar H on $2PPh_2$), 6.69 (1H, s, NH), 4.93-5.11 (8H, m, Ar H on 2(η^6-p-cymene)), 3.97 (1H, m, HNCH), 3.80 (4H, d, J = 10Hz, J_{sat} = 15.6Hz $2PCH_2$), 3.41 (2H, q, J = 6.8Hz, CH_2), 1.23 (3H, d, J = 4.4Hz, Ala CH_3), 1.14 (6H, t, J = 6.8Hz, CH_3, 2(η^6-p-cymene)), 0.79 (12H, m, $2CH_3$ on 2(η^6-p-cymene)); **^{31}P {^{1}H} NMR** (162 MHz, $CDCl_3$) δ 16.84 ppm; **FTIR** (KBr): *v* = 3413(NH), 2962(OH), 1734 (C=O), 1639 (C=O), 696 (Ar-H) cm^{-1}; **CHN** $C_{51}H_{60}P_2N_2O_3Ru_2Cl_4$ requires C (53.04%), H (5.24%), N (2.43%), found: C (52.82%), H (5.47%), N (2.39%); **ESI-MS:** calcd for $C_{51}H_{60}O_3N_2P_2Ru_2Cl_3$ $[M\text{-}Cl]^+$ requires m/z 1119.1226, found *m/z* 1119.1218 (0.8 ppm).

$C_{60}H_{70}O_4N_2P_2Ru_2Cl_4$ (4.46)

From **4.13** (0.067g; 0.099mmol) and $[RuCl(\mu\text{-}Cl)(\eta^6\text{-}p\text{-cym})]_2$ (0.061g; 0.100mmol). Yield: 0.068g, 53%; **Appearance:** orange solid; **^{1}H NMR** (400 MHz, $CDCl_3$) δ 7.84-6.94 (25H, m, Ar-H), 5.29 (1H, d, J = 6.8Hz, NH), 5.11 (2H, d, J =4.8Hz, CH_2), 5.03 (4H, d, J = 5.2Hz, (η^6-p-cymene)), 4.95 (4H, d, J = 6.4Hz, (η^6-p-cymene)), 4.06 (1H, m, CH), 4.14 (4H, s, CH_2), 2.76 (2H, br. s , CH_2), 1.56-1.41 (2H, m, CH_2), 1.07-0.96 (4H, m, CH_2) ppm; **^{31}P{^{1}H} NMR** (162 MHz, $CDCl_3$) δ 19.52 ppm; **FTIR** (KBr): *v* =3444(NH), 2960(OH), 1719(C=O), 697(ArH) cm^{-1}; **CHN:** Despite repeated attempts, a satisfactory elemental analysis was not obtained; **ESI-MS:** calcd for $C_{60}H_{70}O_4N_2P_2Ru_2Cl_3$ $[M\text{-}Cl]^+$ requires m/z 1253.1958, found *m/z* 1253.1963 (0.4 ppm)

$C_{55}H_{60}O_3N_2P_2Ru_2Cl_4$ (4.47)

From **4.14** (0.107g; 0.181mmol) and $[RuCl(\mu\text{-}Cl)(\eta^6\text{-}p\text{-cym})]_2$ (0.123g; 0.201mmol). **Yield:** 0.168g, 77%; **Appearance:** orange solid; **^{1}H NMR** (400MHz, $CDCl_3$) δ 8.88 (1H, m, CH_2NH), 7.47-7.37 (20H, m, Ar H on $2PPh_2$), 7.33 (2H, d, J = 8.8Hz, 2Ar H), 6.18 (isomeric eq. to 7.33), 5.65 (2H, d, J = 6Hz, Ar H $2PPh_2$), 5.57 (isomeric eq. to 5.65), 5.31 (2H, d, J = 5.6Hz, Ar H on 2(η^6-p-cymene)), 5.22 (2H, d, J = 6.4 Hz, Ar H on 2(η^6-p-cymene)), 4.51 (4H, s, $2PCH_2$), 4.10 (2H, s, CH_2CO_2H), 2.55 (3H, m, CH_3), 2.46 (1H, m, $CH(CH_3)_2$), 1.32 (6H, d, J = 6.8Hz, $2CH_3$) ppm; **^{31}P{^{1}H} NMR** (162MHz, $CDCl_3$) δ 20.72 ppm; **FTIR** (KBr): *v* = 3463(NH), 1639(C=O), 1509(NH) cm^{-1}; **CHN:** Despite repeated attempts, a satisfactory elemental analysis was not obtained; **ESI-MS:** calcd for $C_{55}H_{60}O_3N_2P_2Ru_2Cl_3$ $[M\text{-}Cl]^+$ requires m/z 1167.1226, found *m/z* 1167.1244 (1.6 ppm).

$C_{49}H_{58}P_2N_2O_2Ru_2Cl_4$ (4.48)

From **4.15** (0.099g; 0.198mmol) and $[RuCl(\mu\text{-}Cl)(\eta^6\text{-}p\text{-cym})]_2$ (0.120g; 0.196mmol). **Yield**: 0.139g, 62%; **Appearance:** orange solid; **^{1}H NMR** (400MHz, $CDCl_3$) δ 7.25-7.41 (20H, m, Ar H on $2PPh_2$), 5.39-5.42 (2H, m, Ar H on 2(η^6-p-cymene)), 5.24-5.28 (2H, m, Ar H on 2(η^6-p-cymene)), 5.05-4.96 (4H, m, $2PCH_2$), 3,46 (2H, m, CH_2), 2.85 (1H, m, $CH(CH_3)_2$), 2.35 (3H, m, CH_3), 1.21 (6H, d, J = 7.2Hz, $2CH_3$), 1.16 (3H, t, J = 6Hz, CH_3) ppm; **^{31}P {^{1}H} NMR** (400MHz, $CDCl_3$) δ 20.03 ppm; **FTIR** (KBr): *v* = 3468 (NH), 1727 (C=O), 1470 (C=C), 1384 (CH_3), 695 (Ar-H) cm^{-1}; **CHN** $C_{49}H_{58}P_2N_2O_2Ru_2Cl_4 \cdot 2H_2O$ requires C (51.22%), H (5.45%), N (2.49%), found C (50.76%), H (5.15%), N (2.48%); **ESI-MS:** calcd for $C_{49}H_{58}O_2N_2P_2Ru_2Cl_2{}^{37}Cl$ $[M\text{-}Cl]^+$ requires m/z 1079.1131, found *m/z* 1079.1088 (4.1 ppm).

$C_{50}H_{59}P_2NO_3Ru_2Cl_4$ (4.49)

From **4.19** (0.052g; 0.101mmol) and $[RuCl(\mu\text{-}Cl)(\eta^6\text{-}p\text{-cym})]_2$ (0.061g; 0.100mmol). **Yield:** 0.044g, 54%. **Appearance:** orange solid; **^{1}H NMR** (400MHz, $CDCl_3$) δ 7.80-7.34 (20H, m, Ar H), 5.01 (8H, m, Ar H), 4.22 (2H, d, J = 3.6Hz, CH_2P), 3.99 (2H, d, J = 14.8Hz, CH_2P), 3.35 (3H, s, CH_3), 3.02 (1H, m, CH), 2.37 (2H, m, CH_2), 1.23 (3H, t, J = 7.2Hz, CH_3), 0.91 (6H, m, $2CH_3$) ppm; **^{31}P{^{1}H} NMR** (162 MHz, $CDCl_3$) δ 18.80 ppm; **FTIR** (KBr): *v* = 3444(OH), 695(Ar-H) cm^{-1}; **CHN:** Despite repeated attempts, a satisfactory elemental analysis was not obtained; **ESI-MS:** calcd for $C_{50}H_{59}P_2NO_3Ru_2Cl_3$ $[M\text{-}Cl]^+$ requires m/ 1092.1122, found *m/z* 1 1092.1138 (1.5 ppm).

$C_{56}H_{63}P_2NO_2Ru_2Cl_4$ (4.50)

From **4.20** (0.068g; 0.118mmol) and $[[RuCl(\mu\text{-}Cl)(\eta^6\text{-}p\text{-cym})]_2$ $Ru(\eta^6\text{-p-cymene})Cl_2]_2$ (0.061g; 0.100mmol). **Yield:** 0.071g, 85%; **Appearance:** orange solid; **^{1}H NMR** (400MHz, $CDCl_3$) δ 7.89 – 7.37 (20H, m, Ar H), 7.03 (3H, m, H^d), 6.59 (2H, dd, J = 2Hz, 6Hz, H^c), 5.01 – 4.93 (8H, m, Ar H on 2p-cym), 4.02 (4H, s, $2CH_2P$), 3.25 (1H, m, CH), 3.06 (3H, s, CH_3), 2.40 (2H, m, H^a/H^b), 1.44 (6H, t, J = 6.8Hz, CH_3 on 2p-cym), 0.93 (12H, t, 5.6Hz, $2CH_3$ on 2p-cym) ppm; **^{31}P{^{1}H} NMR** (162 MHz, $CDCl_3$) δ 18.64 ppm; **FTIR** (KBr): *v* = 1735(C=O), 696(Ar-H) cm^{-1}; **CHN** $C_{56}H_{63}P_2NO_2Ru_2Cl_4 \cdot H_2O$ requires C (55.80%), H (5.28%), N (1.16%), found C (55.08%), H (5.69%), N (1.79%); **ESI-MS:** calcd for $C_{56}H_{63}O_2N_2P_2Ru_2Cl_3$ $[M\text{-}Cl]^+$ requires m/z 1152.1486, found *m/z* 1166.1519 (0.1 ppm).

$C_{66}H_{65}O_2N_2P_2Ru_2Cl_4$ (4.51)

From **4.21** (0.054g; 0.100mmol) and $[RuCl(\mu\text{-}Cl)(\eta^6\text{-}p\text{-cym})]_2$ (0.060g; 0.098mmol). **Yield**: 0.056g, 45%; **Appearance:** orange solid; **^{1}H NMR** (400MHz, $CDCl_3$) δ 7.89–7.25 (20H, m, Ar H), 5.37–5.26 (8H, m, Ar H on 2p-cym), 4.15 (1H, m, CH), 3.67 (4H, s, $2CH_2P$), 1.41 (6H, m, CH_3 on 2p-cym), 0.93 (12H, t, 5.6Hz, $2CH_3$ on 2p-cym) ppm; **^{31}P{^{1}H} NMR** (400MHz, $CDCl_3$) δ 21.02 ppm; **FTIR** (KBr): *v* = 2944(CH), 1732(C=O), 851(Ar-H), 697(Ar-H) cm^{-1}; **CHN:** Despite repeated attempts, a satisfactory elemental analysis was not obtained; **ESI-MS:** calcd for $C_{66}H_{65}O_2N_2P_2Ru_2Cl_3$ $[M\text{-}Cl]^+$ requires m/z 1288.1673, found *m/z* 1132.1683 (0.9 ppm).

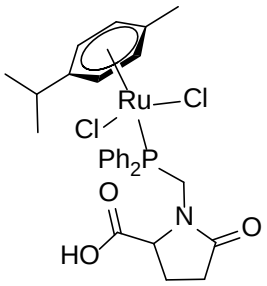

(4.53)

$C_{28}H_{32}O_3NPRuCl_2$ (4.53)

From **4.24** (0.096g; 0.298mmol) and $[RuCl(\mu\text{-}Cl)(\eta^6\text{-}p\text{-cym})]_2$ (0.092g; 0.150mmol). Yield: 0.081g, 44%; **Appearance:** orange solid; **^{1}H NMR** (400 MHz, $CDCl_3$) δ 8.0 – 7.48 (10H, m, ArH), 5.41 (2H, q, J = 6Hz, ArH), 5.18 (1H, d, J = 5.6Hz, ArH), 4.98 (2H, q, J = 7.2Hz, ArH), 4.28 (2H, dd, J = 2.4, 12.8Hz, PCH_2), 3.60(1H, d, J = 9.6Hz, CH), 2.46 (1H, p, J = 6.8, $CH(CH_3)_2$), 1.70 - 1.90 (4H, m, CH_2), 1.25 (3H, t, J = 6.8Hz, CH_3), 0.76 (6H, d, J = 6.8Hz, $2CH_3$) ppm; **^{31}P{^{1}H} NMR** (162 MHz, $CDCl_3$) δ 26.06 ppm; **FTIR** (KBr): *v* = 3330(OH), 1718(C=O) cm^{-1}; **CHN:** Despite repeated attempts, a satisfactory elemental analysis was not obtained; **ESI-MS:** calcd for $C_{28}H_{32}O_3NPRuCl$ $[M\text{-}Cl]^+$ requires m/z 598.0846, found *m/z* 598.0831 (2.5 ppm).

Coordination Compounds 4.57 – 4.77

Unless otherwise stated, the following Cu(I), Ag(I) and Au(I) complexes were synthesised through the reaction of appropriate metal precursors, $[Cu(CNMe)_4]BF_4$, $AgBF_4$ and AuCl(tht), with ligands **4.2**, **4.3**, **4.7** and **4.12 – 4.15**. Following 1h stirring in

CH_2Cl_2, the solvent volume was reduced to 1-2mL and Et_2O was added resulting in the precipitation of complexes **4.57** – **4.61** and **4.71** – **4.77**. Cu(I) and Ag(I) complexes were synthesised using Schlenk techniques.

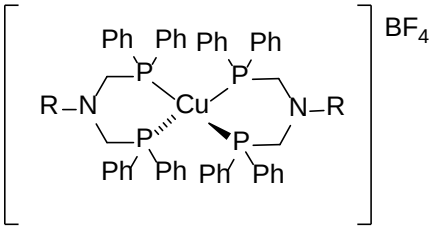

R = **(4.57)** CH_2CO_2H
(4.58) $CH_2CONHCH_2CO_2H$
(4.59)
(4.60) $CH_2CONHCH_2CONHCH_2CO_2H$
$CH_2CONHCH(CH_3)CO_2H$
(4.61) $(CH_2)_4CH(CO_2H)NHCOOCH_2Ph$
(4.62) $C_6H_4CONHCH_2CO_2H$
(4.63) $NHCOOCH_2CH_3$

$C_{56}H_{54}P_4N_2O_4CuBF_4$ (4.57)

From **4.2** (0.201g, 0.425mmol) and $[Cu(MeCN)_4]BF_4$ (0.069g, 0.196mmol). **Yield:** 0.151g, 64%; **Appearance:** white solid; **^{1}H NMR** (400 MHz, $CDCl_3$) δ 7.63-7.03 (40H, m, Ar-H), 4.00 (8H, s, CH_2P), 3.56 (4H, s, CH_2) ppm; **^{31}P{^{1}H} NMR** (162 MHz, $CDCl_3$) δ -15.81 ($W_{0.5}$ = 627Hz) ppm; **FTIR** (KBr): *v* = 3469(OH), 1719(C=O), 1384(CH_2) cm^{-1}; **CHN** $C_{56}H_{54}P_4N_2O_4CuBF_4 \cdot 2H_2O$ requires C (59.63%), H (5.18%), N (2.48%), found C (59.50%), H (4.82%), N (2.64%); **ESI-MS:** calcd for $C_{56}H_{54}O_4N_2P_4Cu$ $[M]^+$ requires m/z 1005.2325, found *m/z* 1005.2302 (2.2 ppm).

$C_{60}H_{60}P_4N_4O_6CuBF_4$ (4.56)

From **4.3** (0.137g, 0.259mmol) and $[Cu(MeCN)_4]BF_4$ (0.034g, 0.108mmol). **Yield:** 0.084g, 72%; **Appearance:** white solid; **^{1}H NMR** (400MHz, d_6-DMSO) δ 7.77 (2H, t, J = 6Hz, 2NH), 7.33-7.09 (40H, m, Ar-H), 3.93 (8H, s, $4CH_2$), 3.62 (4H, d, J =6Hz, $2CH_2$), 2.95 (4H, s, $2CH_2$) ppm; **^{31}P{^{1}H} NMR** (162 MHz, d_6-DMSO) δ -16.41 ppm ($W_{0.5}$ = 277Hz); **FTIR** (KBr): *v* = 3385(NH), 3055(OH), 1737(C=O), 1664(C=O), 695(Ar-H) cm^{-1}; **CHN** $C_{60}H_{60}P_4N_4O_6CuBF_4 \cdot 2H_2O$ requires C (57.96%), H (4.86%), N (4.51%), found C (57.63%), H (4.63%), N (5.04%); **ESI-MS:** calcd for $C_{60}H_{60}O_6N_4P_4Cu$ $[M]^+$ requires m/z 1119.2754, found *m/z* 1119.2739 (1.3 ppm).

$C_{64}H_{66}P_4N_6O_8CuBF_4$ (4.57)

From **4.7** (0.199g, 0.340mmol) and $[Cu(MeCN)_4]BF_4$ (0.041g 0.130mmol). **Yield:** 0.125g, 73%; **Appearance:** white solid; **^{1}H NMR** (400 MHz, d_6-DMSO) δ 7.51-6.84 (40H, m, Ar-H), 3.64 (12H, m, $4CH_2$), 2.76 (4H, s, $2CH_2$), 2.31 (4H, s, $2CH_2$) ppm; **^{31}P{^{1}H} NMR** (162 MHz, d_6-DMSO) δ -15.92 ppm ($W_{0.5}$ = 312Hz); **FTIR** (KBr): *v* = 3410(NH), 2964(OH), 1661(C=O), 695(Ar-H) cm^{-1}; **CHN** $C_{64}H_{66}P_4N_6O_8CuBF_4 \cdot 2H_2O$ requires C (56.68%), H (5.20%), N (6.20%), found C (56.12%), H (5.03%), N (6.13%); **ESI-MS:** calcd for $C_{64}H_{66}O_8N_6P_4Cu$ $[M]^+$ requires m/z 1233.3183, found *m/z* 1233.3178 (0.4 ppm).

$C_{62}H_{64}O_6N_4P_4CuBF_4$ (4.58)

From **4.12** (0.240g, 0.443mmol) and $[Cu(MeCN)_4]BF_4$ (0.069g, 0.220mmol). **Yield:** 0.104g, 39%**; Appearance:** white solid; **^{1}H NMR** (400 MHz, d_6-DMSO) δ 8.01 (2H, d, J = 7.2Hz, 2NH), 7.48-7.11 (40H, m, Ar-H), 4.18 (2H, p, J = 7.2Hz, 2CH), 3.97 (8H, q, J = 14.4, $4CH_2$), 2.87 (4H, d, J = 15.6, 9.6Hz, $2CH_2$), 1.21 (6H, d, J = 7.6, $2CH_2$) ppm; **^{31}P{^{1}H} NMR** (162 MHz, d_6-DMSO) δ -12.24 ppm ($W_{0.5}$ = 332Hz); **FTIR** (KBr): *v* = 3468(NH), 2963(OH), 1735(C=O), 1648(C=O), 693(Ar-H) cm^{-1}; **CHN:** Despite repeated attempts, a satisfactory elemental analysis was not obtained; **ESI-MS:** calcd for $C_{62}H_{64}O_6N_4P_4Cu$ $[M]^+$ requires m/z 1147.3067, found *m/z* 1147.3050 (1.5 ppm).

$C_{80}H_{84}P_4N_4O_8CuBF_4$ (4.59)

From **4.13** (0.199g, 0.294mmol) and $[Cu(MeCN)_4]BF_4$ (0.033g, 0.103mmol). **Yield:** 0.084g, 54%; **Appearance:** white solid; **^{1}H NMR** (400 MHz, d_6-DMSO) δ 7.51-7.12 (50H, m, Ar-H), 5.03 (4H, m, CH_2), 4.00 (8H, br. s, CH_2), 2.18 (4H, m, CH_2), 1.06 (4H, m, CH_2), 0.78 (4H, m, CH_2), 0.53 (4H, m, CH_2) ppm; **^{31}P{^{1}H} NMR** (162 MHz, d_6-DMSO) δ -15.76 ppm ($W_{0.5}$ = 355Hz); **FTIR** (KBr): *v* = 3442(NH), 2942(OH), 1718(C=O), 1630(C=O), 695(CH) cm^{-1}; **CHN** $C_{80}H_{84}P_4N_4O_8CuBF_4$ requires C (63.90%), H (5.63%), N (3.73%), found C (64.05%), H (5.55%), N (3.85%); **ESI-MS:** calcd for $C_{80}H_{84}O_8N_4P_4Cu$ $[M]^+$ requires m/z 1415.4530, found *m/z* 1415.4491 (2.8 ppm).

$C_{70}H_{64}P_4N_4O_6CuBF_4$ (4.60)

From **4.14** (0.166g, 0.298mmol) and $[Cu(MeCN)_4]BF_4$ (0.050g, 0.161mmol). **Yield:** 0.192g, 96%; **Appearance:** white solid; **^{1}H NMR** (400 MHz, d_6-DMSO) δ 8.28 (2H, s,

2NH), 7.84-7.25 (44H, m, Ar-H), 6.06 (4H, d, J = 8.0Hz, Ar-H), 4.80 (8H, s, $4CH_2$), 3.68 (4H, m, $2CH_2$) ppm; **$^{31}P\{^1H\}$ NMR** (162 MHz, d_6-DMSO) δ -16.29 ppm ($W_{0.5}$ = 280Hz); **FTIR** (KBr): *v* = 3400(NH), 3054(OH), 1734(C=O), 1637(C=O), 693(Ar-H) cm^{-1}; **CHN** $C_{70}H_{64}P_4N_4O_6CuBF_4 \cdot CH_2Cl_2$ requires C (60.27%), H (4.70%), N (3.95%), found C (60.12%), H (5.19%), N (3.83%); **ESI-MS:** calcd for $C_{70}H_{64}O_6N_4P_4Cu$ $[M]^+$ requires m/z 1243.3067, found *m/z* 1243.3058 (0.7 ppm).

$C_{58}H_{60}O_4N_4P_4CuBF_4$ (4.61)

From **4.15** (0.645g, 1.290mmol) and $[Cu(MeCN)_4]BF_4$ (0.203g, 0.645mmol). **Yield:** 0.053g, 71%; **Appearance:** white solid; **^{1}H NMR** (400 MHz, d_6-DMSO) δ 7.57-7.11 (40H, m, Ar-H), 4.07 (8H, s, $4CH_2$), 3.94 (4H, s, CH_2), 1.10 (6H, s, $2CH_3$) ppm; **$^{31}P\{^1H\}$ NMR** (162 MHz, d_6-DMSO) δ -21.12 ppm ($W_{0.5}$ = 71Hz); **FTIR** (KBr): *v* = 3416(NH), 1618 (C=O), 695(Ar-H) cm^{-1}; **CHN:** Despite repeated attempts, a satisfactory elemental analysis was not obtained; **ESI-MS:** calcd for $C_{58}H_{60}O_4N_4P_4Cu$ $[M]^+$ requires m/z 1063.2856, found *m/z* 1063.2843 (1.2 ppm).

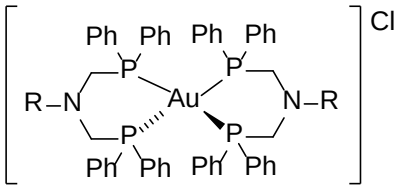

R = **(4.64)** $CH_2CONHCH_2CO_2H$
(4.65) $CH_2CONHCH_2CONHCH_2CO_2H$
(4.66) $CH_2CONHCH(CH_3)CO_2H$
(4.67) $(CH_2)_4CH(CO_2H)NHCOOCH_2Ph$
(4.68) $C_6H_4CONHCH_2CO_2H$
(4.69) $NHCOOCH_2CH_3$

$C_{60}H_{60}O_6N_4P_4AuCl$ (4.64)

From **4.3** (0.099g, 0.188 mmol) and AuCl(tht) (0.030g, 0.094 mmol). **Yield:** 0.069g, 57%; **Appearance:** white solid; **^{1}H NMR** (400 MHz, d_6-DMSO) δ 7.83 (2H, t, J = 5.2Hz, NH), 7.37-7.03 (40H, m, Ar-H), 5.71 (2H, s, OH), 4.12 (8H, s, $2CH_2$), 3.62 (4H, d, J = 6Hz, CH_2), 2.76 (2H, s, CH_2) ppm; **$^{31}P\{^1H\}$ NMR** (162 MHz, d_6-DMSO) δ -8.85 ppm; **FTIR** (KBr): *v* = 2928(OH), 1752(C=O), 1626(C=O), 693(Ar-H) cm^{-1}; **CHN:** Despite repeated

attempts, a satisfactory elemental analysis was not obtained; **ESI-MS:** calcd for $C_{60}H_{60}O_6N_4P_4Au$ $[M]^+$ requires m/z 1253.3123, found *m/z* 1253.3089 (2.7 ppm).

$C_{64}H_{66}O_8N_6P_4AuCl$ (4.65)

From **4.7** (0.120g; 0.203mmol) and AuCl(tht) (0.033g; 0.103mmol). **Yield:** 0.100g, 69%; **Appearance:** white solid; **^{1}H NMR** (400 MHz, d_6-DMSO) δ 7.53-7.09 (40H, m, Ar-H), 4.42 (4H, s, $2CH_2$), 3.70-3.69 (8H, m, $4CH_2$), 2.82 (8H, s, $4CH_2$) ppm; **^{31}P{^{1}H} NMR** (162 MHz, d_6-DMSO) δ -9.39 ppm; **FTIR** (KBr): *v* = 3278(NH), 2927(OH), 1662(C=O), 694(Ar-H) cm^{-1}; **CHN:** Despite repeated attempts, a satisfactory elemental analysis was not obtained; **ESI-MS:** calcd for $C_{64}H_{66}O_8N_6P_4Au$ $[M]^+$ requires m/z 1367.3553, found *m/z* 1367.3520 (2.4 ppm).

$C_{62}H_{64}O_6N_4P_4AuCl$ (4.66)

From **4.12** (0.100g, 0.185 mmol) and AuCl(tht) (0.030g, 0.094 mmol). **Yield:** 0.051g, 45%; **Appearance:** white solid; **^{1}H NMR** (400 MHz, d_6-DMSO) δ 7.25-6.90 (40H, m, Ar-H), 4.22 (2H, m, 2CH), 3.94 (8H, s, $4CH_2$), 2.68 (4H, m, $2CH_2$), 1.16 (6H, d, J = 7.2Hz, $2CH_3$) ppm; **^{31}P{^{1}H} NMR** (162 MHz, d_6-DMSO) δ -9.30 ppm; **FTIR** (KBr): *v* = 3444(NH), 2933(OH), 1733(C=O), 1664(C=O), 694(Ar-H) cm^{-1}; **CHN** $C_{62}H_{64}P_4N_4O_6AuCl{\cdot}CH_2Cl_2$ requires C (53.95%), H (4.74%), N (3.99%), found C (53.70%), H (4.38%), N (3.82%); **ESI-MS:** calcd for $C_{62}H_{64}O_6N_4P_4Au$ $[M]^+$ requires m/z 1281.3436, found *m/z* 1281.3405 (2.4 ppm).

$C_{80}H_{84}P_4N_4O_8AuCl$ (4.67)

From **4.13** (0.070g, 0.103mmol) and AuCl(tht) (0.017g, 0.053mmol). **Yield:** 0.069g, 87%; **Appearance:** white solid; **^{1}H NMR** (400 MHz, d_6-DMSO) δ 7.48-7.08 (50H, m, Ar-H), 4.96 (4H, m, CH_2), 4.00 (8H, br. s, CH_2), 2.15 (4H, m, CH_2), 1.06 (4H, m, CH_2), 0.74 (4H, m, CH_2), 0.54 (4H, m, CH_2) ppm; **^{31}P{^{1}H} NMR** (162 MHz, d_6-DMSO) δ -7.99 ppm; **FTIR** (KBr): *v* = 3441(NH), 2935(OH), 1710(C=O), 694(Ar-H) cm^{-1}; **CHN** $C_{80}H_{84}P_4N_4O_8AuCl$ requires C (60.59%), H (5.34%), N (3.53%), found C (60.73%), H (5.25%), N (3.69%); **ESI-MS:** calcd for $C_{80}H_{84}O_8N_4P_4Au$ $[M]^+$ requires m/z 1549.4900, found *m/z* 1549.4864 (2.3 ppm).

$C_{70}H_{64}O_6N_4P_4AuCl$ (4.68)

From **4.14** (0.151g; 0.255mmol) and AuCl(tht) (0.040g; 0.125mmol). **Yield:** 0.105g, 59%; **Appearance:** white solid; **^{1}H NMR** (400 MHz, d_6-DMSO) δ 7.41-6.95 (20H, m, Ar-H), 6.88 (2H, m, Ar-H), 5.65 (2H, d, J =8.8Hz, Ar-H), 4.40 (4H, s, PCH_2), 3.78 (2H, m, CH_2) ppm; **^{31}P{^{1}H} NMR** (162 MHz, d_6-DMSO) δ -8.24 ppm; **FTIR** (KBr): *v* = 3265(NH), 2924(OH), 1723(C=O), 1643(C=O), 692(Ar-H) cm^{-1}; **CHN:** Despite repeated attempts, a satisfactory elemental analysis was not obtained; **ESI-MS:** calcd for $C_{70}H_{64}O_6N_4P_4Au$ $[M]^+$ requires m/z 1377.3436, found *m/z* 1377.3407 (2.1 ppm);

$C_{58}H_{60}O_4N_4P_4AuCl$ (4.69)

From **4.15** (0.118g, 0.236mmol) and AuCl(tht) (0.122g, 0.381mmol). **Yield:** 0.125g, 69%; **Appearance:** white solid; **^{1}H NMR** (400 MHz, d_6-DMSO) δ 7.31-7.07 (40H, m, Ar-H), 4.26 (8H, s, $4CH_2$), 3.97 (4H, *br*. s, $2CH_2$), 1.12 (6H, *br.* s, $2CH_3$) ppm;**^{31}P{^{1}H} NMR** (162 MHz, d_6-DMSO) δ -5.40 ppm; **FTIR** (KBr): *v* = 3052(NH), 1703(C=O), 1631(C=O), 693(Ar-H) cm^{-1}; **CHN** $C_{58}H_{60}P_4N_4O_4AuCl{\cdot}2H_2O$ requires C (54.91%), H (5.08%), N (4.41%), found C (55.03%), H (4.92%), N (4.42%); **ESI-MS:** calcd for $C_{58}H_{60}O_4N_4P_4Au$ $[M]^+$ requires m/z 1197.3225, found *m/z* 1197.3194 (2.6 ppm).

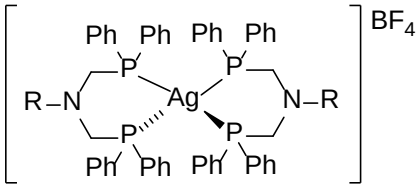

R = **(4.71)** CH_2CO_2H
(4.72) $CH_2CONHCH_2CO_2H$
(4.73) $CH_2CONHCH_2CONHCH_2CO_2H$
(4.74) $CH_2CONHCH(CH_3)CO_2H$
(4.75) $(C_6H_4)CONHCH_2CO_2H$
(4.76) $NHCOOCH_2CH_3$
(4.77) C_6H_5

$C_{56}H_{54}N_2O_4P_4AgBF_4$ (4.71)

From **4.2** (0.100g, 0.245 mmol) and $AgBF_4$ (0.023g, 0.118 mmol). **Yield:** 0.096g, 76%; **Appearance:** white solid; **^{1}H NMR** (400 MHz, $CDCl_3$) δ 7.13-7.54 (40H, m, Ar-H), 4.014

(8H, s, N-CH_2-P), 3.66 (4H, s, CH_2); **$^{31}P\{^1H\}$ NMR** (162 MHz, $CDCl_3$): δ -12.11 (d, $^1J_{107AgP}$ = 256Hz), -12.11 (d, $^1J_{109AgP}$ = 224Hz) ppm; **FTIR** (KBr): *v* = 2923(OH), 694(Ar-H) cm^{-1}; **CHN:** Despite repeated attempts, a satisfactory elemental analysis was not obtained; **ESI-MS**: calcd for $C_{56}H_{54}N_2O_4P_4Ag$ $[M]^+$ requires m/z 1049.2079, found *m/z* 1049.2066 (1.3 ppm).

$C_{60}H_{60}P_4N_4O_6AgBF_4$ (4.72)

From **4.3** (0.101g, 0.191 mmol) and $AgBF_4$ (0.018g, 0.092 mmol). **Yield:** 0.056g, 49%; **Appearance:** white solid; **^1H NMR** (400 MHz, d_6-DMSO) δ 7.86 (2H, t, J = 5.6Hz, 2NH), 7.33-7.11 (40H, m, Ar-H), 4.12 (8H, s, $4CH_2$), 3.64 (4H, d, J =5.6Hz, $2CH_2$), 2.86 (4H, s, $2CH_2$); **$^{31}P\{^1H\}$ NMR** (162 MHz, d_6-DMSO) δ -11.22 (d, $^1J_{107AgP}$ = 255Hz), -11.22 (d, $^1J_{109AgP}$ = 221Hz) ppm; **FTIR** (KBr): *v* = 3443(NH), 2926(OH), 1738(C=O), 1674(C=O), 693(Ar-H) cm^{-1}; **CHN** $C_{60}H_{60}P_4N_4O_6AgBF_4 \cdot H_2O$ requires C (56.76%), H (4.76%), N (4.41%), found C (56.54%), H (4.60%), N (4.62%); **ESI-MS:** calcd for $C_{60}H_{60}O_6N_4P_4Ag$ $[M]^+$ requires m/z 1163.2509, found *m/z* 1163.2497 (1.0 ppm).

$C_{64}H_{66}O_8N_6P_4AgBF_4$ (4.73)

From **4.7** (0.100g, 0.171 mmol) and $AgBF_4$ (0.013g 0.067 mmol). **Yield:** 0.079g, 83%; **Appearance:** white solid; **^1H NMR** (400 MHz, $CDCl_3$): δ 8.10 (2H, m, 2OH), 7.90 (2H, m, 2NH), 7.50-7.10 (40H, m, Ar-H), 3.98 (8H, s, N-CH_2-P), 3.70 (4H, s, CH_2), 2.80 (4H, s, CH_2), 2.49 (4H, s, CH_2) ppm; **$^{31}P\{^1H\}$ NMR** (162 MHz, $CDCl_3$): δ -12.62 (d, $^1J_{107AgP}$ = 256Hz), δ -12.62 (d, $^1J_{109AgP}$ = 222 Hz) ppm; **FTIR** (KBr): *v* = 2928(OH), 1629(C=O), 695(Ar-H) cm^{-1}; **CHN:** Despite repeated attempts, a satisfactory elemental analysis was not obtained; **ESI-MS:** calcd for $C_{64}H_{66}O_8N_6P_4Ag$ $[M]^+$ requires m/z 1277.2938, found *m/z* 1277.2926 (0.9 ppm);

$C_{62}H_{64}O_6N_4P_4AgBF_4$ (4.74)

From **4.12** (0.100g, 0.184 mmol) and $AgBF_4$ (0.020g, 0.103 mmol). **Yield:** 0.062g, 47%; **Appearance:** white/yellow solid; **^1H NMR** (400 MHz, d_6-DMSO) δ 7.93 (2H, d, J = 6.8Hz, 2NH), 7.39-7.11 (40H, m, Ar-H), 4.17 (10H, m, $4CH_2$, 2CH), 2.88 (4H, q, J = 4, 16.4Hz, $2CH_2$), 1.16 (6H, d, J = 7.2Hz, $2CH_2$); **$^{31}P\{^1H\}$ NMR** (162 MHz, d_6-DMSO) δ -11.19 (d, $^1J_{107AgP}$ = 255Hz), -11.19 (d, $^1J_{109AgP}$ = 221Hz) ppm; **FTIR** (KBr): *v* = 3345(NH), 2900(OH), 1731(C=O), 1629(C=O), 694(Ar-H) cm^{-1}; **CHN:** Despite repeated attempts, a satisfactory

elemental analysis was not obtained; **ESI-MS:** calcd for $C_{62}H_{64}O_6N_4P_4Ag$ $[M]^+$ requires m/z 1191.2822, found *m/z* 1191.2802 (1.7 ppm).

$C_{70}H_{64}P_4N_4O_6AgBF_4$ (4.75)

From **4.14** (0.150g, 0.342 mmol) and $AgBF_4$ (0.034g, 0.176 mmol). **Yield:** 0.066g, 44%; **Appearance:** white solid; **^{1}H NMR** (400 MHz, d_6-DMSO) δ 8.29 (2H, t, J = 5.6Hz, 2NH), 7.52-7.07 (44H, m, Ar-H), 6.13 (4H, d, J = 9.2Hz, Ar-H), 4.95 (8H, s, PCH_2), 3.70 (4H, d, J = 5.6Hz, $2CH_2$); **^{31}P{^{1}H} NMR** (162 MHz, d_6-DMSO) δ -9.34 (d, $^1J_{107AgP}$ = 255Hz), -9.34 (d, $^1J_{109AgP}$ = 221Hz) ppm; **FTIR** (KBr): *v* = 2925(OH), 1730(C=O), 1647(C=O), 693(Ar-H) cm^{-1}; **CHN** $C_{70}H_{64}P_4N_4O_6AgBF_4 \cdot CH_2Cl_2$ requires C (57.67%), H (4.50%), N (3.79%), found C (57.80%), H (4.37%), N (3.80%); **ESI-MS:** calcd for $C_{70}H_{56}O_6N_4P_4Ag$ $[M]^+$ requires m/z 1279.2196, found *m/z* 1279.2154 (4.2 ppm).

$C_{58}H_{60}O_4N_4P_4AgBF_4$ (4.76)

From **4.15** (0.255g, 0.510 mmol) and $AgBF_4$ (0.043g, 0.222 mmol). **Yield**: 0.255g, 96%; **Appearance:** white solid; **^{1}H NMR** (400 MHz, $CDCl_3$) δ 7.31-7.10 (40H, m, Ar-H), 6.95 (1H, s, NH), 4.29 (8H, s, $4CH_2$), 4.04 (4H, s, $2CH_2$), 1.17 (6H, m, $2CH_3$); **^{31}P{^{1}H} NMR** (162 MHz, $CDCl_3$) δ -10.17 (d, $^1J_{107AgP}$ = 257Hz), -10.17 (d, $^1J_{109AgP}$ = 224Hz) ppm; **FTIR** (KBr): *v* = 3302(NH), 1714(C=O), 692(Ar-H) cm^{-1}; **CHN** $C_{58}H_{60}O_4N_4P_4AgBF_4 \cdot H_2O$ requires C (57.40%), H (5.15%), N (4.62%), found C (57.25%), H (4.96%), N (4.71%); **ESI-MS:** calcd for $C_{58}H_{60}O_4N_4P_4Ag$ $[M]^+$ requires m/z 1107.2610, found *m/z* 1107.2588 (2.0 ppm).

$C_{64}H_{58}N_2P_4AgBF_4$ (4.77)

From **4.70** (0.097g, 0.198 mmol) and $AgBF_4$ (0.018g, 0.093 mmol). **Yield:** 0.055g, 51%; **Appearance:** white solid; **^{1}H NMR** (400 MHz, $CDCl_3$): δ 7.38-6.68 (25H, m, Ar-H), δ 4.47 (4H, s, N-CH_2-P) ppm; **^{31}P{^{1}H} NMR** (162 MHz, $CDCl_3$): δ -9.82 (d, $^1J_{107AgP}$ = 253Hz), -9.82 (d, $^1J_{109AgP}$ = 222Hz) ppm; **FTIR** (KBr): *v* = 3055(C-H), 1596(C=C), 1202(C-N) cm^{-1}; **CHN:** Despite repeated attempts, a satisfactory elemental analysis was not obtained; **ESI-MS**: calcd for $C_{64}H_{58}N_2P_4Ag$ $[M]^+$ requires m/z 1085.259, found *m/z* 1085.2611(1.4 ppm).

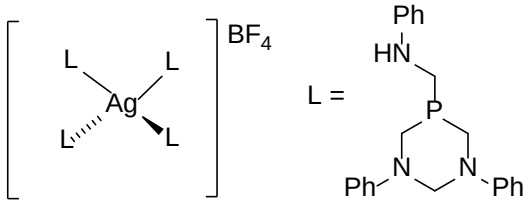

(4.79)

$C_{88}H_{96}N_{12}P_4AgBF_4$ (4.79)

$AgBF_4$ (0.028g, 0.114 mmol) and ligand **4.78** (0.201g, 0.553 mmol) were added to DCM (10 mL) and stirred, under a nitrogen atmosphere and in darkness for 1h. The solution was reduced to 1-2 mL by volume and diethyl ether (10 mL) and n-hexane (10 mL) were added. The resulting white suspension was filtered, washed with diethyl ether and dried in *vacuo* to yield white solid (0.137, 60%). The white solid was recrystallized from a minimum volume of DCM. **^{1}H NMR** (400 MHz, $CDCl_3$): δ 7.27 (24H, m, Ar-H), 7.09 (16H, m, Ar-H), 6.92 (12H, t, J = 7.6 Hz, Ar-H), 6.61 (8H, m, Ar-H), 4.96 (1H, d, J =12.8 Hz, N<u>H</u>-CH_2), 4.44 (2H, d, J =13.2 Hz, N-CH_2-N), 4.04 (12H, d, J = 12.8, N-CH_2-P), 3.74 (2H, d, J = 14 Hz, P- C<u>H</u>$_2$-NH); **^{31}P{^{1}H } NMR** (162 MHz, $CDCl_3$): δ -22.82 (d, $^1J_{107AgP}$ = 424 Hz), δ -23.03 (d, $^1J_{109AgP}$ = 218 Hz); **FTIR** (KBr): *v* = 3414(NH), 1598(NH), 1384(CH_2), cm^{-1}; **CHN** $C_{88}H_{96}N_{12}P_4AgBF_4 \cdot 0.5CH_2Cl_2$ requires C (63.16%), H (5.81%), N (9.99%), found C (63.41%), H (5.43%), N (9.64%); **HRMS** (ESI^+) calcd for $C_{66}H_{72}N_9P_3Ag$ $[M]^+$ requires m/z 1190.4169, found *m/z* 1190.4149 (1.6ppm).

Attempted synthesis of complexes 4.81, 4.82, 4.84 and 4.85

Ligand (1 eq) and metal precursor (1 eq), AgBF4 or $[Cu(CNMe)_4]BF_4$, were stirred under inert conditions for 30 mins in CH_2Cl_2. Phen (1 eq) was then added to the stirring solution and the resulting solution was stirred for 1h. The volume was reduced to 1-2mL and Et_2O was added, precipitating the resulting solids. The resulting solids were a mixture of heteroleptic and homoleptic complexes in all cases.

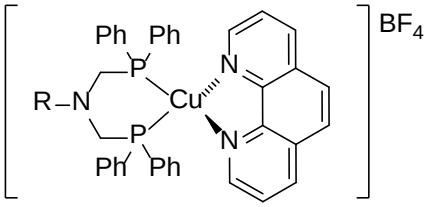

R = **(4.81)** CH_2CO_2H
(4.82) $CH_2CONHCH(CH_3)CO_2H$

$C_{40}H_{35}P_2N_3O_2CuBF_4$ (4.81)

From **4.2** (0.100g, 0.212mmol), phen (0.038g; 0.212mmol) and $[Cu(CNMe)_4]BF_4$ (0.067g, 0.212mmol). **Yield:** 0.081g, 48%; **Appearance:** green solid; **^{1}H NMR** (400 MHz, $CDCl_3$) δ 8.56 (2H, br. s, Phen Ar-H), 8.52 (2H, d, J = 6.4Hz, Phen Ar-H), 8.03 (2H, s, Phen Ar-H), 7.78 (2H, br. s, Phen Ar-H), 7.51-6.98 (20H, m, Ar-H), 4.20 (4H, br. s, PCH_2), 2.61 (2H, s, CH_2) ppm; **^{31}P{^{1}H} NMR** (162 MHz, $CDCl_3$) δ -15.27 ppm; **FTIR** (KBr): *v* = 3417(OH), 1717(C=O), 696(ArH) cm^{-1}; **CHN** $C_{40}H_{35}P_2N_3O_2CuBF_4$ (crystal) requires C (59.90%), H (4.40%), N (5.24%), found C (59.31%), H (4.08%), N (5.06%); **ESI-MS:** calcd for $C_{40}H_{35}P_2N_3O_2Cu$ $[M]^+$ requires m/z 715.2183, found *m/z* 715.2167 (2.2 ppm).

$C_{43}H_{40}P_2N_3O_3CuBF_4$ (4.82)

From **4.12** (0.101g, 0.189mmol), phen (0.034g; 0.189mmol) and $[Cu(CNMe)_4]BF_4$ (0.058g, 0.189mmol). **Yield:** 0.083g, 51%; **Appearance:** green solid; **^{1}H NMR** (400 MHz, $CDCl_3$) δ 8.70 (2H, br. s, Phen Ar-H), 8.50 (2H, d, J = 7.6Hz, Phen Ar-H), 8.02 (2H, s, Phen Ar-H), 7.80 (2H, br. s, Phen Ar-H), 7.62-6.98 (20H, m, Ar-H), 4.25 (4H, br. s, PCH_2), 3.67 (2H, br. s, CH_2), 2.16 (2H, s, CH_2) ppm;**^{31}P{^{1}H} NMR** (162 MHz, $CDCl_3$) δ -14.98 ppm.

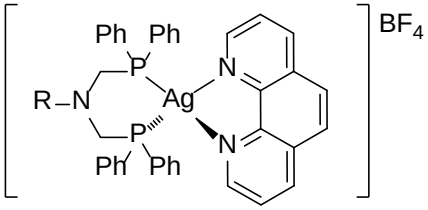

R = **(4.84)** CH_2CO_2H
(4.85) $CH_2CONHCH(CH_3)CO_2H$

$C_{40}H_{35}P_2N_3O_2AgBF_4$ (4.84)

From **4.2** (0.099g, 0.210mmol), phen (0.038g; 0.212mmol) and $AgBF_4$ (0.041g, 0.212mmol). **Yield:** 0.073g, 41%; **Appearance:** green solid; **^{1}H NMR** (400 MHz, d_6-DMSO) δ 9.14 (2H, d, J = 3.6Hz, Phen Ar-H), 8.72 (2H, d, J = 7.6Hz, Phen Ar-H), 8.15 (2H, s, Phen Ar-H), 7.98 (2H, m, Phen Ar-H), 7.50-7.01 (20H, m, Ar-H), 4.29 (4H, br. s, PCH_2), 2.81 (2H, s, CH_2) ppm; **^{31}P{^{1}H} NMR** (162 MHz, d_6-DMSO) δ -5.33 (d, J = 352Hz, $[M(N\text{^}N)(P\text{^}P)]BF_4$), -10.50 (d, $^1J_{107AgP}$ = 255Hz, $[M(P\text{^}P)_2]BF_4$), -10.50 (d, $^1J_{109AgP}$ = 221Hz, $[M(P\text{^}P)_2]BF_4$) ppm.

$C_{43}H_{40}P_2N_3O_3AgBF_4$ (4.85)

From **4.12** (0.100g, 0.185mmol), phen (0.033g; 0.185mmol) and $AgBF_4$ (0.030g, 0.155mmol). **Yield:** 0.185g, 46%; **Appearance:** green solid; **^{1}H NMR** (400 MHz, d_6-DMSO) δ 9.12 (2H, m, Phen Ar-H), 8.60 (2H, m, Phen Ar-H), 8.07 (2H, s, Phen Ar-H), 7.87 (2H, m, Phen Ar-H), 7.47-7.19 (20H, m, Ar-H), 4.13 (4H, m, PCH_2), 3.34 (2H, m, CH_2), 2.88 (2H, s, CH_2) ppm; **^{31}P{^{1}H} NMR** (162 MHz, d_6-DMSO) δ -6.54 (d, J = 355Hz, $[M(N\text{^}N)(P\text{^}P)]BF_4$), -10.20 (d, $^1J_{107AgP}$ = 255Hz, $[M(P\text{^}P)_2]BF_4$), -10.20 (d, $^1J_{109AgP}$ = 221Hz, $[M(P\text{^}P)_2]BF_4$) ppm.

Antibacterial Studies

The antibacterial studies were conducted under the guidance of Dr Sweta Ladwa. 0.1 mL of adjusted *E. Coli* (ATC25922) or *S.Aureus* (NCIMB 8625) culture was placed on the Mueller-Hinton plate using an aseptic technique and spread by using a sterile hockey stick around the plate. For the preparation of the antibiotic disks, 20 µL silver complex solution was absorbed per disk. The disks were placed onto the plates which had been divided into several sectors and labelled. These plates were inverted and incubated at RT. After 24h, the diameter of the zone of inhibition was determined and noted.

6.6 X-ray Crystallography

Measurements were made by utilising multiple diffractometers and radiation sources in the home laboratory and by the EPSRC National Crystallographic Service at Southampton University (see Appendix for compound specific details). All data collections were performed at low temperature (100–150K) using a single crystal mounted onto a glass fibre on the goniometer head using a drop of inert oil. Each data

collection took place in two stages; firstly the orientation matrix, unit cell and crystal system were determined, secondly a longer data collection was undertaken in order to measure a full sphere or hemisphere of the diffraction pattern. Programs used were APEX 2[285] or Rigaku CrystalClear[286] for diffractometer control and Bruker SAINT[287] or Rigaku CrystalClear[286] for frame integration. A semi–empirical absorption correction was applied using the SADABS[288-291] program based on equivalent and repeated reflections and subsequent data reduction carried out. The program XPREP within the SHELXTL[292] suite of programs was used to check for any higher or missed symmetry, and the space group was determined. The structure was solved using the program XS[293], using either direct methods or Patterson synthesis as appropriate. The structure was refined using the program SHELXL–97[293] or SHELX–2013/4[293] by full–matrix least squares methods on F^2. Non–hydrogen atoms were initially refined isotropically, then later anisotropically. Hydrogen atoms were placed in geometrically calculated positions. Platon[294] was used to model highly disordered molecules as diffuse regions of electron density (SQUEEZE), and also to generate estimated standard deviation values for molecular structures obtained from the CSD[199] for comparison purposes. See appendix for summary tables of data relating to each structure discussed, in addition to additional details of individual refinements. A CD is enclosed at the back of this document containing complete refinement data and tables for each molecular structure.

7 – References

1. S. J. Berners-Price, R. K. Johnson, C. K. Mirabelli, L. F. Faucette, F. L. McCabe, and P. J. Sadler, *Inorg. Chem.*, 1987, **26**, 3383.

2. S. J. Berners-Price, R. K. Johnson, A. J. Giovenella, L. F. Faucette, C. K. Mirabelli, and P. J. Sadler, *J. Inorg. Biochem.*, 1988, **33**, 285.

3. J. Zhang, J. J. Vittal, W. Henderson, J. R. Wheaton, I. H. Hall, T. S. A. Hor, and Y. Kai, *J. Organomet. Chem.*, 2002, **650**, 123.

4. D. E. Berning, K. V. Katti, C. L. Barnes, and W. a. Volkert, *J. Am. Chem. Soc.*, 1999, **121**, 1658.

5. J. H. Downing and M. B. Smith, in *'Comprehensive Coordination Chemistry II'*, 2004, p. 253.

6. P. C. J. Kramer and M. Van Leeuwen, P. W. N, Eds., *Phosphorus(III) ligands in homogenous catalysis: design and synthesis*, John Wiley and Sons Ltd, Chichester, UK, First Ed., 2012.

7. B. M. Sutton, *Gold Bull*, 1986, **19**, 15.

8. A. Agarkov, S. Greenfield, D. Xie, R. Pawlick, G. Starkey, and S. Gilbertson, *Biopolym. Pept. Sci.*, 2006, **84**, 48.

9. K. Kellner, W. Hanke, and A. Tzschach, *Zeitschrift fur Chemie*, 1984, **24**, 193.

10. A. M. LaPointe, *J. Comb. Chem.*, 1999, **1**, 101.

11. P. Servin, R. Laurent, A. Romerosa, M. Peruzzini, J.-P. Majoral, and A.-M. Caminade, *Organometallics*, 2008, **27**, 2066.

12. C. D. Swor, K. R. Hanson, L. N. Zakharov, and D. R. Tyler, *Dalt. Trans.*, 2011, **40**, 8604.

13. K. Kellner, *J. Organomet. Chem*, 1978, **149**, 167.

14. K. Kellner and A. Tzschach, *J. Organomet. Chem*, 1980, **193**, 307.

15. G. Markl and G. Yu Jin, *Tetrahedron Lett.*, 1981, **22**, 223.

16. J. Fawcett, P. A. T. Hoye, R. D. W. Kemmitt, D. J. Law, and D. R. Russell, *J. Chem. Soc. Dalt. Trans.*, 1993, **7**, 2563.

17. J. Lach, J. Heinicke, K. R. Basvani, N. Peulecke, P. G. Jones, and M. Kockerling, *Phosphorus, Sulfur, and Silicon*, 2011, **186**, 666.

18. D. Evans and T. C. Britton, *J. Am. Chem. Soc*, 1987, **109**, 6881.

19. D. A. Evans, T. C. Britton, J. A. Ellman, and R. L. Dorow, *J. Am. Chem. Soc.*, 1990, **112**, 4011.

20. D. A. Evans and J. A. Ellman, *J. Am. Chem. Soc*, 1989, **111**, 1063.

21. D. A. Blinn, R. S. Button, V. Farazi, M. K. Neeb, C. L. Tapley, T. E. Trehearne, S. D. West, T. L. Kruger, and B. N. Storhoff, *J. Organomet. Chem*, 1990, **393**, 143.

22. P. Bartlett and R. Davis, *J. Am. Chem. Soc*, 1958, **80**, 2513.

23. P. Knockel, M. C. P. Yeh, S. C. Berk, and J. Talbert, *J. Org. Chem.*, 1988, **53**, 2390.

24. D. J. Brauer, S. Schenk, S. Roßenbach, M. Tepper, O. Stelzer, T. Ha, and W. S. Sheldrick, *J. Organomet. Chem.*, 2000, **598**, 116.

25. B. M. Zeglis and J. S. Lewis, *Dalt. Trans.*, 2011, **40**, 6168.

26. M. Shokeen and C. J. Anderson, *Acc. Chem. Res.*, 2009, **42**, 832.

27. J. D. G. Correia, P. D. Raposinho, and I. Santos, *Dalt. Trans.*, 2011, **40**, 6144.

28. M. D. Bartholoma, A. S. Louie, J. F. Valliant, and J. Zubieta, *Chem. Rev.*, 2010, **110**, 2903.

29. J. D. Kelly, A. M. Forster, B. Higley, C. M. Archer, F. S. Booker, L. R. Canning, K. W. Chiu, B. Edwards, H. K. Gill, and M. McPartlin, *J. Nucl. Med.*, 1993, **34**, 222.

30. J. E. Cyr, D. A. Pearson, C. A. Nelson, B. A. Lyons, Y. Zheng, J. Bartis, J. He, M. V Cantorias, R. C. Howell, and L. C. Francesconi, *J. Med. Chem.*, 2007, **50**, 4295.

31. M. V Cantorias, R. C. Howell, L. Todaro, J. E. Cyr, D. Berndorff, R. D. Rogers, and L. C. Francesconi, *Inorg. Chem.*, 2007, **46**, 7326.

32. P. J. Blower, J. S. Lewis, and J. Zweit, *Nucl. Med. Biol.*, 1996, **23**, 957.

33. L. H. Davies, R. W. Harrington, W. Clegg, and L. J. Higham, *Dalt. Trans.*, 2014, **43**, 13485.

34. P. J. Blower, *Dalt. Trans.*, 2015, **44**, 4819.

35. D. Brasse and A. Nonat, *Dalt. Trans.*, 2015, **44**, 4845.

36. C. J. Anderson and M. J. Welch, *Chem. Rev.*, 1999, **99**, 2219.

37. W. Wadsak and M. Mitterhauser, *Eur. J. Radiol.*, 2010, **73**, 461.

38. P. S. Donnelly, *Dalt. Trans.*, 2011, **40**, 999.

39. D. J. Williamson, S. Ejaz, S. Sitnikov, T. D. Fryer, S. J. Sawiak, P. Burke, J.-C. Baron, and F. I. Aigbirhio, *Nucl. Med. Biol.*, 2013, **40**, 338.

40. S. Alidori, G. Gioia Lobbia, G. Papini, M. Pellei, M. Porchia, F. Refosco, F. Tisato, J. S. Lewis, and C. Santini, *J. Biol. Inorg. Chem.*, 2008, **13**, 307.

41. J. S. Lewis, J. Zweit, J. L. J. Dearling, B. C. Rooneya, and P. J. Blower, *Chem.*

Commun., 1996, 1093.

42. J. S. Lewis, S. L. Heath, A. K. Powell, and P. J. Blower, *Dalt. Trans.*, 1997, 855.

43. J. S. Lewis, P. J. BloweR, and J. Zweit, *Polyhedron*, 1998, **17**, 513.

44. J. S. Lewis, J. L. J. Dearling, J. K. Sosabowski, J. Zweit, P. Carnochan, L. R. Kelland, H. M. Coley, and P. J. Blower, *Eur. J. Nucl. Med.*, 2000, **27**, 638.

45. C. Marzano, V. Gandin, M. Pellei, D. Colavito, G. Papini, G. G. Lobbia, E. Del Giudice, M. Porchia, F. Tisato, and C. Santini, *J. Med. Chem.*, 2008, **51**, 798.

46. K. D. Mjos and C. Orvig, *Chem. Rev.*, 2014, **114**, 4540.

47. M. J. McKeage, S. J. Berners-Price, P. Galettis, R. J. Bowen, W. Brouwer, L. Ding, L. Zhuang, and B. C. Baguley, *Cancer Chemother. Pharmacol.*, 2000, **46**, 343.

48. Z. Human, A. Munyaneza, B. Omondi, N. M. Sanabria, R. Meijboom, and M. J. Cronjé, *BioMetals*, 2015, **28**, 219.

49. R. Meijboom, R. J. Bowen, and S. J. Berners-Price, *Coord. Chem. Rev.*, 2009, **253**, 325.

50. J. C. Dabrowiak, *Metals in Medicine*, 2009.

51. W. F. Kean, L. Hart, and W. W. Buchanan, *Br. J. Rheumatol.*, 1997, **36**, 560.

52. S. J. Berners-Price and P. J. Sadler, *Inorg. Chem.*, 1986, **25**, 3822.

53. S. J. Berners-Price, C. K. Mirabelli, R. K. Johnson, M. R. Mattern, F. L. . McCabe, L. F. Faucette, C.-M. Sung, S.-M. Mong, P. J. Sadler, and S. T. Crooke, *Cancer Res.*, 1986, **46**, 5486.

54. D. E. Berning, K. V. Katti, W. A. Volkert, C. J. Higginbotham, and A. R. Ketring, *Nucl. Med. Biol.*, 1998, **25**, 577.

55. B. Rosemberg, L. Van Camp, and T. Krigas, *Nature*, 1965, **205**, 698.

56. R. D. Graham and D. R. Williams, *J. Inorg. Nucl. Chem.*, 1979, **41**, 1245.

57. A. R. Kapdi and I. J. S. Fairlamb, *Chem. Soc. Rev.*, 2014, **43**, 4751.

58. L. Tusek-Bozic, I. Matijasic, G. Bocelli, G. Calestani, A. Furlani, V. Scarcia, and A. Papaioannou, *J. Chem. Soc. Dalt. Trans.*, 1991, 195.

59. E. G. Rodrigues, L. S. Silva, D. M. Fausto, M. S. Hayashi, S. Dreher, E. L. Santos, J. B. Pesquero, L. R. Travassos, and A. C. F. Caires, *Int. J. Cancer*, 2003, **107**, 498.

60. S. Page, *Educ. Chem.*, 2012, 26.

61. C. Scolaro, A. Bergamo, L. Brescacin, R. Delfino, M. Cocchietto, and P. J. Dyson, *J. Med. Chem.*, 2005, **48**, 4161.

62. A. D. Phillips, L. Gonsalvi, A. Romerosa, F. Vizza, and M. Peruzzini, *Coord. Chem. Rev.*, 2004, **248**, 955.

63. S. Chatterjee, S. Kundu, A. Bhattacharyya, C. G. Hartinger, and P. J. Dyson, *J. Biol. Inorg. Chem.*, 2008, **13**, 1149.

64. B. Valeur, *Molecular Fluorescence: Principles and Applications*, Wiley-VCH, Weinheim, 2002.

65. J. R. Lakowicz, *Principles of Fluorescence Spectroscopy*, Springer, New York, 3rd edn., 2006.

66. R. C. Evans, P. Douglas, and C. J. Winscom, *Coord. Chem. Rev.*, 2006, **250**, 2093.

67. A. Bencini and V. Lippolis, *Coord. Chem. Rev.*, 2010, **254**, 2096.

68. K. E. Erkkila, D. T. Odom, and J. K. Barton, *Chem. Rev.*, 1999, **99**, 2777.

69. G. Accorsi, A. Listorti, K. Yoosaf, and N. Armaroli, *Chem. Soc. Rev.*, 2009, **38**, 1690.

70. P. G. Sammes and G. Yahioglu, *Chem. Soc. Rev.*, 1994, **23**, 327.

71. J. M. Lehn, *Angew. Chem. Int. Ed. Engl.*, 1990, **29**, 1304.

72. J.-M. Lehn, *Angew. Chem. Int. Ed. Engl.*, 1988, **27**, 89.

73. A. Barbieri, G. Accorsi, and N. Armaroli, *Chem. Commun.*, 2008, 2185.

74. R. A. Rader, D. R. Mcmillin, M. T. Buckner, T. G. Matthews, D. J. Casadonte, R. K. Lengel, S. B. Whittaker, L. M. Darmon, and F. E. Lytle, *J. Am. Chem. Soc*, 1981, 5906.

75. M. T. Buckner and D. R. McMillin, *J. Chem. Soc. Chem. Commun.*, 1978, 759.

76. A. Kaeser, M. Mohankumar, J. Mohanraj, F. Monti, M. Holler, J.-J. Cid, O. Moudam, I. Nierengarten, L. Karmazin-Brelot, C. Duhayon, B. Delavaux-Nicot, N. Armaroli, and J.-F. Nierengarten, *Inorg. Chem.*, 2013, **52**, 12140.

77. A. Kaeser, B. Delavaux-Nicot, C. Duhayon, Y. Coppel, and J.-F. Nierengarten, *Inorg. Chem.*, 2013, **52**, 14343.

78. S. Banerjee, E. B. Veale, C. M. Phelan, S. a. Murphy, G. M. Tocci, L. J. Gillespie, D. O. Frimannsson, J. M. Kelly, and T. Gunnlaugsson, *Chem. Soc. Rev.*, 2013, **42**, 1601.

79. E. E. Langdon-Jones, N. O. Symonds, S. E. Yates, A. J. Hayes, D. Lloyd, R. Williams, S. J. Coles, P. N. Horton, and S. J. A. Pope, *Inorg. Chem.*, 2014, **53**, 3788.

80. S. Banerjee, J. A. Kitchen, T. Gunnlaugsson, and J. M. Kelly, *Org. Biomol. Chem.*,

2013, **11**, 5642.

81. T. Gunnlaugsson, M. Glynn, G. M. Tocci (née Hussey), P. E. Kruger, and F. M. Pfeffer, *Coord. Chem. Rev.*, 2006, **250**, 3094.

82. A. Pardo, J. M. L. Poyato, and E. Martin, *J. Photochem.*, 1987, **36**, 323.

83. A. Pardo, E. Martin, J. M. L. Poyato, J. J. Camacho, J. M. Castellano, and M. Braña, *J. Photochem. Photobiol.*, 1987, **41**, 69.

84. X. Qian, A. Zhu, K. Chen, Q. Yin, and G. Zhu, *Mater. Chem. Phys.*, 1989, **23**, 335.

85. X. Qian, Z. Zhu, K. Chen, and Q. Yin, *Dye. Pigment.*, 1989, **11**, 13.

86. C. Bailly, M. Braña, and M. J. Waring, *Eur. J. Biochem.*, 1996, **240**, 195.

87. D. Rideout, R. Schinazi, C. D. Pauza, K. Lovelace, L. C. Chiang, T. Calogeropoulou, M. McCarthy, and J. H. Elder, *J. Cell Biochem.*, 1993, **51**, 446.

88. M. F. Braña and A. Ramos, *Curr. Med. Chem. Anticancer agents*, 2001, **1**, 237.

89. E. B. Veale and T. Gunnlaugsson, *J. Org. Chem.*, 2010, **75**, 5513.

90. S. Banerjee, S. A. Bright, J. A. Smith, J. Burgeat, M. Martinez-calvo, D. C. Williams, J. M. Kelly, and T. Gunnlaugsson, *J. Org. Chem.*, 2014, **79**, 9272.

91. N. R. Deprez, K. A. McNitt, M. E. Petersen, R. G. Brown, and D. E. Lewis, *Tetrahedron Lett.*, 2005, **46**, 2149.

92. J. Tröger, *J. Prakt. Chem.*, 1887, **36**, 225.

93. M. A. Spielman, *J. Am. Chem. Soc*, 1935, **57**, 583.

94. Ö. V. Rúnarsson, J. Artacho, and K. Wärnmark, *European J. Org. Chem.*, 2012, **2012**, 7015.

95. J. L. A. Tatibouet, M. Demeunynck, C. Andraud, A. Collett, *J. Chem. Soc. Chem. Commun.*, 1991, 161.

96. I. Ott, X. Qian, Y. Xu, D. H. W. Vlecken, I. J. Marques, D. Kubutat, J. Will, W. S. Sheldrick, P. Jesse, A. Prokop, and C. P. Bagowski, *J. Med. Chem.*, 2009, **52**, 763.

97. H. Scheffler, Y. You, and I. Ott, *Polyhedron*, 2010, **29**, 66.

98. C. P. Bagowski, Y. You, H. Scheffler, D. H. Vlecken, D. J. Schmitz, and I. Ott, *Dalt. Trans.*, 2009, 10660.

99. K. J. Kilpin, C. M. Clavel, F. Edafe, and P. J. Dyson, *Organometallics*, 2012, **31**, 7031.

100. C. S. Allardyce, P. J. Dyson, D. J. Ellis, and S. L. Heath, *Chem. Commun.*, 2001, **2**, 1396.

101. J. Zhang, L. Zhang, Y. Zhou, T. Ma, and J. Niu, *Microchim Acta*, 2013, **180**, 211.

102. J. Panchompoo, L. Aldous, M. Baker, M. I. Wallace, and R. G. Compton, *Analyst*, 2012, **137**, 2054.

103. S. Kang, S. Kim, Y.-K. Yang, S. Bae, and J. Tae, *Tetrahedron Lett.*, 2009, **50**, 2010.

104. C. Castelló Beltrán, E. A. Palmer, B. R. Buckley, and F. Iza, *Chem. Commun.*, 2014, **51**, 1579.

105. L. Wei, Z. Zhu, Y. Li, L. Yi, and Z. Xi, *Chem. Commun.*, 2015, **51**, 10463.

106. W. R. Kitley, P. J. Santa Maria, R. a. Cloyd, and L. M. Wysocki, *Chem. Commun.*, 2015, **51**, 8520.

107. M. P. Tracey, D. Pham, and K. Koide, *Chem. Soc. Rev.*, 2015, **44**, 4769.

108. H. Li, J. Fan, M. Hu, G. Cheng, D. Zhou, T. Wu, F. Song, S. Sun, C. Duan, and X. Peng, *Chem. E*, 2012, **18**, 12242.

109. Z. Miao, J. A. Reisz, S. M. Mitroka, J. Pan, M. Xian, and S. B. King, *Bioorg. Med. Chem. Lett*, 2015, **25**, 16.

110. E. E. Langdon-Jones, D. Lloyd, A. J. Hayes, S. D. Wainwright, H. J. Mottram, S. J. Coles, P. N. Horton, and S. J. a. Pope, *Inorg. Chem.*, 2015, **54**, 6606.

111. V. Fernández-Moreira, F. L. Thorp-Greenwood, and M. P. Coogan, *Chem. Commun.*, 2010, **46**, 186.

112. H. Kobayashi, M. Ogawa, R. Alford, P. L. Choyke, and Y. Urano, *Chem. Rev.*, 2010, **110**, 2620.

113. F. L. Thorp-Greenwood, *Organometallics*, 2012, **43**, 5686.

114. L. K. Griffeth, *Proc. (Bayl. Univ. Med. Cent).*, 2005, **18**, 321.

115. M. Suchý, R. Bartha, and R. H. E. Hudson, *RSC Adv.*, 2013, **3**, 3249.

116. F. L. Thorp-Greenwood and M. P. Coogan, *Dalt. Trans.*, 2011, **40**, 6129.

117. T. Esteves, C. Xavier, S. Gama, F. Mendes, P. D. Raposinho, F. Marques, A. Paulo, J. C. Pessoa, J. Rino, G. Viola, and I. Santos, *Org. Biomol. Chem.*, 2010, **8**, 4104.

118. P. Häfliger, N. Agorastos, B. Spingler, O. Georgiev, G. Viola, and R. Alberto, *Chembiochem*, 2005, **6**, 414.

119. P. Haefliger, N. Agorastos, A. Renard, G. Giambonini-brugnoli, C. Marty, and R. Alberto, *Bioconjugate Chem.*, 2005, **15**, 582.

120. K. A. Stephenson, S. R. Banerjee, T. Besanger, O. O. Sogbein, M. K. Levadala, N. Mcfarlane, J. A. Lemon, D. R. Boreham, K. P. Maresca, J. D. Brennan, J. W.

Babich, J. Zubieta, and J. F. Valliant, *J. Am. Chem. Soc*, 2004, **126**, 8598.

121. M. L. Ortego, C. F. Williams, M. P. Coogan, M. D. Villacampa, and M. Concepcio, *Organometallics*, 2012, **31**, 5950.

122. C. Uptake, C. Mari, M. Panigati, L. D. Alfonso, I. Zanoni, D. Donghi, L. Sironi, M. Collini, S. Maiorana, C. Baldoli, G. D. Alfonso, E. Licandro, D. Chimica, and I.-Milano, *Organometallics*, 2012, **31**, 5918.

123. M.-W. Louie, A. W.-T. Choi, H.-W. Liu, B. T.-N. Chan, and K. K.-W. Lo, *Organometallics*, 2012, **31**, 5844.

124. J. D. Lee, *Concise Inorganic Chemistry*, Blackwell Science Ltd, London, 4th Ed., 1991.

125. K. K. Lo, W. Hui, D. C. Ng, K. Cheung, P. Road, and H. Kong, *Inorg. Chem.*, 2002, **41**, 40.

126. A. Leonidova, V. Pierroz, R. Rubbiani, J. Heier, S. Ferrari, and G. Gasser, *Dalt. Trans.*, 2014, **43**, 4287.

127. L. H. Davies, B. B. Kasten, P. D. Benny, R. L. Arrowsmith, H. Ge, S. I. Pascu, S. W. Botchway, W. Clegg, R. W. Harrington, and L. J. Higham, *Chem. Commun.*, 2014, **50**, 15503.

128. S. Mundwiler, M. Kündig, K. Ortner, and R. Alberto, *Dalt. Trans.*, 2004, 1320.

129. P. Jin, C. Jiao, Z. Guo, Y. He, S. Zhu, H. Tian, and W. Zhu, *Chem. Sci.*, 2014, **5**, 4012.

130. S. Tan, D. Sun, J. Lyu, X. Sun, F. Wu, Q. Li, Y. Yang, J. Lui, X. Wang, Z. Chen, H. Li, X. Qian, and Y. Xu, *Bioorg. Med. Chem.*, 2015, **23**, 5672.

131. L. A. Montoya and M. D. Pluth, *Chem. Commun.*, 2012, **48**, 4767.

132. F. H. Allen, *Acta Cryst.*, 2002, **B58**, 380.

133. L. N. Shok, G. A. Golder, L. A. Chetkina, and M. A. Davydova, *Krist.*, 1971, **16**, 923.

134. B. Chen and Y. Shi, *Acta. Crystallogr. Sect. E. Struct. Rep. Online.*, 2006, o3294.

135. J. Lv, X. Peng, B. Kishore, and C. Zhou, *Acta. Crystallogr. Sect. E. Struct. Rep. Online.*, 2012, **68**, o1852.

136. J. Lv, X. Peng, B. Kishore, and C. Zhou, *Biochem. Med. Chem. Lett.*, 2014, **24**, 308.

137. V. R. Pedireddi, D. Shekhar Reddy, B. Satish Goud, D. C. Craig, A. D. Rae, and G. R. Desiraju, *J. Chem. Soc., Perkin Trans*, 1994, **2**, 2353.

138. J. Cao and X. Wang, *Tetrahedron*, 2013, **69**, 10267.

139. S. E. Durran, M. R. J. Elsegood, N. Hawkins, M. B. Smith, and S. Talib, *Tetrahedron Lett.*, 2003, **44**, 5255.

140. M. R. J. Elsegood, A. J. Lake, C. L. Elliott, M. B. Smith, and G. W. Weaver, *Phosphorus. Sulfur. Silicon Relat. Elem.*, 2008, **183**, 435.

141. S. De Xu, C. H. Fang, G. X. Tian, Y. Chen, Y. H. Dou, and J. F. Kou, *J. Mol. Struct.*, 2015, **1102**, 197.

142. T. Dyad, R. Shritz, R. Shapira, E. Borzin, B. Tumanskii, W. Reichstein, C. Meichner, F. Schwaiger, P. M. Reichstein, J. Kreyenschmidt, D. Haarer, L. Kador, and Y. Eichen, *Chem. Eur. J.*, 2015, **21**, 11531.

143. I. I. Ponomarev, M. V. Zharinova, Z. S. Klemenkova, P. V. Petrovskii, and Z. A. Starikova, *Russ. Chem. Bull., Int. Ed.*, 2011, **60**, 512.

144. S. Hanessian, G. Charron, and J. Marin, *J. Org. Chem.*, 2006, **71**, 2760.

145. N. M. Sanchez-Ballester, Loughborough University, PhD thesis, 2009.

146. V. Gutmann, Ed., Academic Press Inc. Ltd., London, 1967, p. 111.

147. L. Rigamonti, A. Forni, M. Manassero, C. Manassero, and A. Pasini, *Inorg. Chem.*, 2010, **49**, 123.

148. L. Rigamonti, C. Manassero, M. Rusconi, M. Manassero, and A. Pasini, *Dalt. Trans.*, 2009, **2**, 1206.

149. C. M. Hartshorn and P. J. Steel, *Inorg. Chem.*, 1996, **35**, 6902.

150. M. Keles and M. K. Yilmaz, *Heteroat. Chem.*, 2012, **23**, 466.

151. M. C. Laudio, C. M. Fierro, A. Pintado-Alba, H. Riva, and S. Betanzos-Lara, *Gold Bull.*, 2007, **40**, 135.

152. A. Pintado-Alba, H. de la Riva, M. Nieuwhuyzen, D. Bautista, P. R. Raithby, H. A. Sparkes, S. J. Teat, J. M. López-de-Luzuriaga, and M. C. Lagunas, *Dalt. Trans.*, 2004, **2**, 3459.

153. M. Y. Berezin and S. Achilefu, *Chem. Rev.*, 2010, **110**, 2641.

154. C. Shen, B. D. W. Harris, L. J. Dawson, K. A. Charles, T. W. Hambley, and E. J. New, *Chem. Commun.*, 2015, **51**, 6312.

155. V. Dujols, F. Ford, and A. W. Czarnik, *J. Am. Chem. Soc*, 1997, **119**, 7386.

156. T. A. Noble, Loughborough University, PhD thesis, 2014.

157. D. X. Wanga and G.-H. Wub, *Acta. Crystallogr. Sect. E. Struct. Rep. Online.*, 2008, **64**, o397.

158. D. J. Law, University of Leicester, PhD thesis, 1990.

159. K. M. Anderson and A. G. Orpen, *Chem. Commun.*, 2001, 2682–2683.

160. A. M. Christianson and F. P. Gabbai, *Inorg. Chem.*, 2016, **55**, 5828.

161. J.-S. Wu, H. J. Kim, M. H. Lee, J. H. Yoon, J. H. Lee, and J. S. Kim, *Tetrahedron Lett.*, 2007, **48**, 3159.

162. C. Munkholm, D.-R. Parkinson, and D. R. Walt, *J. Am. Chem. Soc*, 1990, **112**, 2608.

163. S. L. Pimlott and A. Sutherland, *Chem. Soc. Rev.*, 2011, **40**, 149.

164. M. A. Deri, B. M. Zeglis, L. C. Francesconi, and J. S. Lewis, *Nucl. Med. Biol.*, 2013, **40**, 3.

165. N. Gillings, *MAGMA*, 2013, **26**, 149.

166. R. A. Phillips and P. B. Hamilton, *Am. J. Physiol*, 1948, **152**, 523.

167. C. F. Da Costa, A. C. Pinheiro, M. V De Almeida, M. C. S. Lourenço, and M. V. N. De Souza, *Chem. Biol. Drug Des.*, 2012, **79**, 216.

168. C. Klemps, E. Payet, L. Magna, L. Saussine, X. F. Le Goff, and P. Le Floch, *Chem. Eur. J.*, 2009, **15**, 8259.

169. E. Van Zoeren, H. A. J. Oonk, and J. Kroon, *Acta Cryst.*, 1978, **B34**, 1898.

170. M. B. Smith, S. H. Dale, S. J. Coles, T. Gelbrich, M. B. Hursthouse, and M. E. Light, *Cryst. Eng. Comm.*, 2007, **9**, 165.

171. V. Gee, A. G. Orpen, H. Phetmung, P. G. Pringle, and R. I. Pugh, *Chem. Commun.*, 1999, 901.

172. M. Bernechea, J. Fern, E. Lalinde, M. T. Moreno, S. Ruiz, and S. Sergio, *Organometallics*, 2011, **30**, 4665.

173. A. J. Blake, N. R. Champness, R. J. Forder, C. S. Frampton, C. A. Frost, G. Reid, and R. H. Simpson, *J. Chem. Soc. Dalt. Trans.*, 1994, 3377.

174. R. Girotti, A. Romerosa, S. Manas, M. Serrano-Ruiz, and R. N. Perutz, *Inorg. Chem.*, 2009, **48**, 3692.

175. J. R. Black, W. Levason, M. D. Spicer, and M. Webster, *J. Chem. Soc. Dalt. Trans.*, 1993, 3129.

176. J. Shang, L.-L. Huang, T.-H. Huang, K. Ma, and Q.-L. Ni, *Acta Cryst.*, 2011, **E67**, m96.

177. Z. Fei, R. Scopelliti, and P. J. Dyson, *Dalt. Trans.*, 2003, 2772.

178. M. T. Reetz, S. R. Waldvogel, and R. Goddard, *Tetrahedron Lett.*, 1997, **38**, 5967.

179. E. L. Muetterties and C. W. Alegranti, *J. Am. Chem. Soc.*, 1972, **94**, 6386.

180. R. Hou, T.-H. Huang, X.-J. Wang, X.-F. Jiang, Q.-L. Ni, L.-C. Gui, Y.-J. Fan, and Y.-L. Tan, *Dalt. Trans.*, 2011, **40**, 7551.

181. G.-Q. Yin, H.-C. Lian, Q.-L. Ni, L.-C. Gui, K.-G. Yang, and X.-J. Wang, *Inorg. Chem. Comm.*, 2012, **21**, 160.

182. A. F. De Faria, D. S. T. Martinez, S. M. M. Meira, A. C. M. de Moraes, A. Brandelli, A. G. S. Filho, and O. L. Alves, *Colloids Surfaces B Biointerfaces*, 2014, **113**, 115.

183. K. K. W. Hanke;, *J. Organomet. Chem*, 1987, **326**, C9.

184. D. Drew and R. Doyle, *Inorg. Synth.*, 1972, **13**, 47.

185. R. Uson and A. Laguna, *Inorg. Synth.*, 1989, **26**, 85.

186. M. A. Bennett and A. K. Smith, *J. Chem. Soc.*, 1974, 233.

187. H. Hellmann, J. Bader, H. Birkner, and O. Schumacher, *Ann. Der Chemie Justus Liebig*, 1962, **659**, 49.

188. F. W. Foss Jr., A. H. Snyder, M. D. Davies, M. Rouse, M. D. Okusa, K. R. Lynch, and T. L. Macdonald, *Bioorg. Med. Chem.*, 2007, **15**, 663.

189. Y. N. Kukushkin, *Platinum Metals Rev*., 1991, 35, 28.

8 – Appendix

2.5 A single molecule present in the asymmetric unit.

2.16 A single molecule present in the asymmetric unit.

2.18 A single molecule present in the asymmetric unit.

2.19 A single molecule present in the asymmetric unit, along with one molecule of Et_2O.

2.24 A single molecule present in the asymmetric unit, along with with one molecule of Et_2O and a disordered molecule of CH_2Cl_2.

2.27 A single molecule present in the asymmetric unit, along with with one molecule of DMSO and a disordered molecule of modelled as part DMSO, part CH_2Cl_2.

2.28 A single molecule present in the asymmetric unit, along with 1.5 molecules of Et_2O and 0.5 molecules of CH_2Cl_2.

3.5 A single molecule present in the asymmetric unit, along with three molecules of DMSO and one molecule of H_2O.

3.11 Half a molecule in the assymetric unit. Pd lies on a centre of symmetry. One molecule of Et_2O per asymmetric unit, with a further molecule of Et_2O per assymetric unit, modelled by Platon squeeze.

3.13 A single molecule present in the asymmetric unit, along with one molecule of Et_2O and a disordered molecule of $CHCl_3$.

4.24 Six molecules present in the asymmetric unit, along with one molecule of Et_2O.

4.41 A single molecule present in the asymmetric unit, along with one molecule of CH_2Cl_2.

4.50 1.5 molecules present in the asymmetric unit, along with one molecule of CH_2Cl_2.

4.54 A single molecule present in the asymmetric unit, along with two 0.5 molecules of Et_2O.

4.58 A single molecule present in the asymmetric unit, along with one molecule of DMF and a partial H_2O molecule.

4.63 A single molecule present in the asymmetric unit, along with one molecule of Et_2O modelled using Platon squeeze.

4.81 A single molecule present in the asymmetric unit, along with one molecule of Et_2O modelled using Platon squeeze and an additional molecule of Et_2O refined as point atoms.

2.5

Crystal data

$C_{16}H_{14}BrNO_2$	$F(000) = 672$
$M_r = 332.19$	$D_x = 1.607$ Mg m^{-3}
Monoclinic, $P2_1/n$	Mo $K\alpha$ radiation, $\lambda = 0.71073$ Å
$a = 12.6132$ (14) Å	Cell parameters from 3003 reflections
$b = 4.5217$ (5) Å	$\theta = 2.8–26.2°$
$c = 24.326$ (3) Å	$\mu = 2.99$ mm^{-1}
$\beta = 98.1336$ (14)°	$T = 150$ K
$V = 1373.4$ (3) Å^3	Rod, colourless
$Z = 4$	0.39 × 0.12 × 0.07 mm^3

Data collection

Bruker APEX 2 CCD area detector diffractometer	2827 independent reflections
Radiation source: fine-focus sealed tube	2144 reflections with $I > 2\sigma(I)$
Graphite monochromator	$R_{int} = 0.031$
ω rotation with narrow frames scans	$\theta_{max} = 26.4°$, $\theta_{min} = 1.7°$
Absorption correction: multi-scan *SADABS* v2012/1, Sheldrick, G.M., (2012)	$h = -15\rightarrow15$
$T_{min} = 0.388$, $T_{max} = 0.818$	$k = -5\rightarrow5$
10999 measured reflections	$l = -30\rightarrow30$

Refinement

Refinement on F^2	Primary atom site location: structure-invariant direct methods
Least-squares matrix: full	Secondary atom site location: difference Fourier map
$R[F^2 > 2\sigma(F^2)] = 0.036$	Hydrogen site location: inferred from neighbouring sites
$wR(F^2) = 0.096$	H-atom parameters constrained
$S = 1.03$	$w = 1/[\sigma^2(F_o^2) + (0.0469P)^2 + 0.9557P]$ where $P = (F_o^2 + 2F_c^2)/3$
2827 reflections	$(\Delta/\sigma)_{max} = 0.001$
187 parameters	$\Delta\rangle_{max} = 0.61$ e Å^{-3}
0 restraints	$\Delta\rangle_{min} = -0.48$ e Å^{-3}

2.16

Crystal data

$C_{42}H_{39}N_3O_2P_2$	D_x = 1.256 Mg m^{-3}
M_r = 679.70	Mo $K\alpha$ radiation, λ = 0.71073 Å
Orthorhombic, *Pbca*	Cell parameters from 4867 reflections
a = 11.9502 (10) Å	θ = 2.2–23.1°
b = 19.9252 (17) Å	μ = 0.16 mm^{-1}
c = 30.200 (3) Å	T = 150 K
V = 7190.9 (11) Å^3	Plate, green
Z = 8	0.66 × 0.10 × 0.05 mm^3
F(000) = 2864	

Data collection

Bruker APEX 2 CCD area detector diffractometer	7401 independent reflections
Radiation source: fine-focus sealed tube	4882 reflections with $I > 2\sigma(I)$
Graphite monochromator	R_{int} = 0.103
ω rotation with narrow frames scans	θ_{max} = 26.5°, θ_{min} = 2.0°
Absorption correction: multi-scan *SADABS* v2012/1, Sheldrick, G.M., (2012)	h = -14→14
T_{min} = 0.901, T_{max} = 0.992	k = -24→24
60503 measured reflections	l = -37→37

Refinement

Refinement on F^2	Secondary atom site location: dual
Least-squares matrix: full	Hydrogen site location: mixed
$R[F^2 > 2\sigma(F^2)]$ = 0.048	H atoms treated by a mixture of independent and constrained refinement
$wR(F^2)$ = 0.128	$w = 1/[\sigma^2(F_o^2) + (0.052P)^2 + 4.2567P]$ where $P = (F_o^2 + 2F_c^2)/3$
S = 1.02	$(\Delta/\sigma)_{max} < 0.001$
7401 reflections	$\Delta\rangle_{max}$ = 1.11 e Å^{-3}
448 parameters	$\Delta\rangle_{min}$ = -0.29 e Å^{-3}
0 restraints	Extinction correction: *SHELXL2014*/7 (Sheldrick 2014, $Fc^*=kFc[1+0.001xFc^2\lambda^3/\sin(2\theta)]^{-1/4}$
Primary atom site location: structure-invariant direct methods	Extinction coefficient: 0.00083 (17)

2.18

Crystal data

$C_{41}H_{37}N_3O_3P_2$	$F(000) = 1432$
$M_r = 681.67$	$D_x = 1.297$ Mg m^{-3}
Monoclinic, $P2_1/c$	Mo $K\alpha$ radiation, $\lambda = 0.71073$ Å
$a = 13.3702$ (10) Å	Cell parameters from 20314 reflections
$b = 25.391$ (2) Å	$\theta = 2.5–27.5°$
$c = 11.2527$ (9) Å	$\mu = 0.17$ mm^{-1}
$\beta = 113.951$ (2)°	$T = 100$ K
$V = 3491.1$ (5) Å^3	Needle, yellow
$Z = 4$	0.22 × 0.04 × 0.03 mm^3

Data collection

Rigaku Saturn724+ (2x2 bin mode) diffractometer	7900 independent reflections
Radiation source: Sealed Tube	5567 reflections with $I > 2\sigma(I)$
Mirrors monochromator	$R_{int} = 0.048$
Detector resolution: 28.5714 pixels mm^{-1}	$\theta_{max} = 27.5°$, $\theta_{min} = 2.6°$
profile data from ω–scans	$h = -17 \rightarrow 17$
Absorption correction: multi-scan *CrystalClear*-SM Expert 3.1 b27 (Rigaku, 20112)	$k = -32 \rightarrow 31$
$T_{min} = 0.664$, $T_{max} = 1.000$	$l = -14 \rightarrow 12$
23816 measured reflections	

Refinement

Refinement on F^2	Primary atom site location: iterative
Least-squares matrix: full	Hydrogen site location: mixed
$R[F^2 > 2\sigma(F^2)] = 0.047$	H atoms treated by a mixture of independent and constrained refinement
$wR(F^2) = 0.116$	$w = 1/[\sigma^2(F_o^2) + (0.0474P)^2 + 1.4013P]$ where $P = (F_o^2 + 2F_c^2)/3$
$S = 1.01$	$(\Delta/\sigma)_{max} < 0.001$
7900 reflections	$\Delta\rangle_{max} = 0.35$ e Å^{-3}
447 parameters	$\Delta\rangle_{min} = -0.38$ e Å^{-3}
0 restraints	

2.19

Crystal data

$C_{42}H_{39}N_3O_4P_2 \cdot CH_4O$	$Z = 2$
$M_r = 743.74$	$F(000) = 784$
Triclinic, $P\bar{1}$	$D_x = 1.296$ Mg m^{-3}
$a = 10.1966$ (7) Å	Mo $K\alpha$ radiation, $\lambda = 0.71073$ Å
$b = 10.6686$ (7) Å	Cell parameters from 29901 reflections
$c = 18.2356$ (15) Å	$\theta = 2.3$–$27.5°$
$\alpha = 94.674$ (5)°	$\mu = 0.16$ mm^{-1}
$\beta = 103.108$ (3)°	$T = 100$ K
$\gamma = 96.992$ (4)°	Block, yellow
$V = 1905.4$ (2) Å^3	0.07 × 0.05 × 0.05 mm^3

Data collection

Rigaku Saturn724+ (2x2 bin mode) diffractometer	8704 independent reflections
Radiation source: Sealed Tube	7066 reflections with $I > 2\sigma(I)$
Graphite Monochromator monochromator	$R_{int} = 0.052$
Detector resolution: 28.5714 pixels mm^{-1}	$\theta_{max} = 27.6°$, $\theta_{min} = 2.3°$
profile data from ω–scans	$h = -13 \rightarrow 10$
Absorption correction: multi-scan *CrystalClear*-SM Expert 3.1 b27 (Rigaku, 20112)	$k = -13 \rightarrow 13$
$T_{min} = 0.765$, $T_{max} = 1.000$	$l = -23 \rightarrow 23$
32949 measured reflections	

Refinement

Refinement on F^2	Primary atom site location: structure-invariant direct methods
Least-squares matrix: full	Secondary atom site location: dual
$R[F^2 > 2\sigma(F^2)] = 0.043$	Hydrogen site location: mixed
$wR(F^2) = 0.111$	H atoms treated by a mixture of independent and constrained refinement
$S = 1.03$	$w = 1/[\sigma^2(F_o^2) + (0.0484P)^2 + 0.9795P]$ where $P = (F_o^2 + 2F_c^2)/3$
8704 reflections	$(\Delta/\sigma)_{max} = 0.001$
491 parameters	$\Delta\rangle_{max} = 0.54$ e Å^{-3}
0 restraints	$\Delta\rangle_{min} = -0.30$ e Å^{-3}

2.24

Crystal data

$C_{42}H_{39}Cl_2N_3O_2P_2Pt\cdot CH_4O\cdot 0.5CHCl_3$	$F(000)$ = 2064
M_r = 1036.41	D_x = 1.629 Mg m^{-3}
Monoclinic, $P2_1/n$	Mo $K\alpha$ radiation, λ = 0.71073 Å
a = 10.0582 (7) Å	Cell parameters from 21052 reflections
b = 13.0873 (9) Å	θ = 2.1–27.5°
c = 32.102 (2) Å	μ = 3.66 mm^{-1}
β = 90.840 (3)°	T = 100 K
V = 4225.3 (5) Å^3	Block, yellow
Z = 4	0.07 × 0.05 × 0.02 mm^3

Data collection

Rigaku Saturn724+ (2x2 bin mode) diffractometer	9149 independent reflections
Radiation source: Sealed Tube	6277 reflections with $I > 2\sigma(I)$
Mirrors monochromator	R_{int} = 0.081
Detector resolution: 28.5714 pixels mm^{-1}	θ_{max} = 27.5°, θ_{min} = 2.5°
profile data from ω–scans	h = -13→13
Absorption correction: multi-scan *CrystalClear*-SM Expert 3.1 b27 (Rigaku, 20112)	k = -16→16
T_{min} = 0.563, T_{max} = 1.000	l = -38→41
25176 measured reflections	

Refinement

Refinement on F^2	Primary atom site location: structure-invariant direct methods
Least-squares matrix: full	Secondary atom site location: dual
$R[F^2 > 2\sigma(F^2)]$ = 0.095	Hydrogen site location: inferred from neighbouring sites
$wR(F^2)$ = 0.238	H-atom parameters constrained
S = 1.17	$w = 1/[\sigma^2(F_o^2) + (0.0692P)^2 + 113.4854P]$ where $P = (F_o^2 + 2F_c^2)/3$
9149 reflections	$(\Delta/\sigma)_{max}$ = 0.001
527 parameters	$\Delta\rangle_{max}$ = 5.00 e Å^{-3}
44 restraints	$\Delta\rangle_{min}$ = -2.36 e Å^{-3}

2.27

Crystal data

$C_{42}H_{39}Cl_2N_3O_4P_2Pt \cdot 1.43C_2H_6OS \cdot 0.57CH_2Cl_2$	$F(000) = 2280$
$M_r = 1137.72$	$D_x = 1.661$ Mg m^{-3}
Monoclinic, $P2_1/n$	Mo $K\alpha$ radiation, $\lambda = 0.71073$ Å
$a = 9.9379$ (7) Å	Cell parameters from 34419 reflections
$b = 17.7822$ (12) Å	$\theta = 2.4$–$27.5°$
$c = 25.7529$ (18) Å	$\mu = 3.46$ mm^{-1}
$\beta = 91.2848$ (15)°	$T = 100$ K
$V = 4549.9$ (5) Å^3	Plate, yellow
$Z = 4$	$0.05 \times 0.03 \times 0.01$ mm^3

Data collection

Rigaku Saturn724+ (2x2 bin mode) diffractometer	10390 independent reflections
Radiation source: Sealed Tube	7789 reflections with $I > 2\sigma(I)$
Mirrors monochromator	$R_{int} = 0.073$
Detector resolution: 28.5714 pixels mm^{-1}	$\theta_{max} = 27.5°$, $\theta_{min} = 2.4°$
profile data from ω–scans	$h = -12 \rightarrow 10$
Absorption correction: multi-scan *CrystalClear*-SM Expert 3.1 b27 (Rigaku, 20112)	$k = -22 \rightarrow 22$
$T_{min} = 0.645$, $T_{max} = 1.000$	$l = -33 \rightarrow 33$
39845 measured reflections	

Refinement

Refinement on F^2	Primary atom site location: structure-invariant direct methods
Least-squares matrix: full	Secondary atom site location: dual
$R[F^2 > 2\sigma(F^2)] = 0.041$	Hydrogen site location: mixed
$wR(F^2) = 0.089$	H atoms treated by a mixture of independent and constrained refinement
$S = 1.06$	$w = 1/[\sigma^2(F_o^2) + (0.0308P)^2 + 5.8921P]$ where $P = (F_o^2 + 2F_c^2)/3$
10390 reflections	$(\Delta/\sigma)_{max} = 0.002$
593 parameters	$\Delta\rangle_{max} = 1.58$ e Å^{-3}
35 restraints	$\Delta\rangle_{min} = -0.90$ e Å^{-3}

2.28

Crystal data

$C_{42}H_{39}Cl_2N_3O_2P_2Pd \cdot 1.5(CH_4O) \cdot 0.5(CH_2Cl_2)$	$F(000) = 3888$
$M_r = 947.53$	$D_x = 1.510$ Mg m^{-3}
Monoclinic, $P2_1/c$	Mo $K\alpha$ radiation, $\lambda = 0.71073$ Å
$a = 19.4930$ (14) Å	Cell parameters from 45182 reflections
$b = 15.6855$ (11) Å	$\theta = 2.1–27.5°$
$c = 27.901$ (2) Å	$\mu = 0.76$ mm^{-1}
$\beta = 102.188$ (2)°	$T = 100$ K
$V = 8338.7$ (10) Å^3	Plate, yellow
$Z = 8$	0.09 × 0.06 × 0.01 mm^3

Data collection

Rigaku CrystalClear-SM Expert 3.1 b27 diffractometer	19058 independent reflections
Radiation source: Sealed Tube	12108 reflections with $I > 2\sigma(I)$
Graphite Monochromator monochromator	$R_{int} = 0.072$
Detector resolution: 28.5714 pixels mm^{-1}	$\theta_{max} = 27.6°$, $\theta_{min} = 2.3°$
profile data from ω–scans	$h = -25 \rightarrow 17$
Absorption correction: multi-scan *CrystalClear*-SM Expert 3.1 b27 (Rigaku, 20112)	$k = -14 \rightarrow 20$
$T_{min} = 0.669$, $T_{max} = 1.000$	$l = -36 \rightarrow 36$
57122 measured reflections	

Refinement

Refinement on F^2	Primary atom site location: iterative
Least-squares matrix: full	Hydrogen site location: mixed
$R[F^2 > 2\sigma(F^2)] = 0.053$	H atoms treated by a mixture of independent and constrained refinement
$wR(F^2) = 0.126$	$w = 1/[\sigma^2(F_o^2) + (0.0407P)^2 + 17.0248P]$ where $P = (F_o^2 + 2F_c^2)/3$
$S = 1.01$	$(\Delta/\sigma)_{max} = 0.001$
19058 reflections	$\Delta\rangle_{max} = 0.98$ e Å^{-3}
1039 parameters	$\Delta\rangle_{min} = -1.09$ e Å^{-3}
0 restraints	

3.5

Crystal data

$C_{33}H_{25}N_2O_4P \cdot 3(C_2H_6OS) \cdot H_2O$	$Z = 2$
$M_r = 796.92$	$F(000) = 840$
Triclinic, $P\bar{1}$	$D_x = 1.368$ Mg m^{-3}
$a = 12.5904$ (3) Å	Mo $K\alpha$ radiation, $\lambda = 0.71073$ Å
$b = 13.5773$ (3) Å	Cell parameters from 32399 reflections
$c = 13.7755$ (4) Å	$\theta = 2.2–29.7°$
$\alpha = 113.061$ (3)°	$\mu = 0.29$ mm^{-1}
$\beta = 113.542$ (3)°	$T = 120$ K
$\gamma = 92.026$ (2)°	Prism, colourless
$V = 1934.28$ (10) Å^3	0.11 × 0.08 × 0.05 mm^3

Data collection

Rigaku AFC12 (Right) diffractometer	10135 independent reflections
Radiation source: Rotating Anode	8972 reflections with $I > 2\sigma(I)$
Confocal mirrors, HF Varimax monochromator	$R_{int} = 0.026$
Detector resolution: 28.5714 pixels mm^{-1}	$\theta_{max} = 29.8°$, $\theta_{min} = 2.3°$
profile data from ω–scans	$h = -17 \rightarrow 17$
Absorption correction: multi-scan *CrysAlis PRO* 1.171.38.41 (Rigaku Oxford Diffraction, 2015) Empirical absorption correction using spherical harmonics, implemented in SCALE3 ABSPACK scaling algorithm.	$k = -18 \rightarrow 18$
$T_{min} = 0.916$, $T_{max} = 1.000$	$l = -18 \rightarrow 18$
45470 measured reflections	

Refinement

Refinement on F^2	Primary atom site location: iterative
Least-squares matrix: full	Secondary atom site location: difference Fourier map
$R[F^2 > 2\sigma(F^2)] = 0.043$	Hydrogen site location: mixed
$wR(F^2) = 0.111$	H atoms treated by a mixture of independent and constrained refinement
$S = 1.03$	$w = 1/[\sigma^2(F_o^2) + (0.0528P)^2 + 1.4546P]$ where $P = (F_o^2 + 2F_c^2)/3$
10135 reflections	$(\Delta/\sigma)_{max} = 0.001$
508 parameters	$\Delta\rangle_{max} = 0.79$ e Å^{-3}
3 restraints	$\Delta\rangle_{min} = -0.78$ e Å^{-3}

3.11

Crystal data

$C_{66}H_{50}Cl_2N_4O_8P_2Pd \cdot 4(C_4H_{10}O)$	$F(000) = 3264$
$M_r = 1562.81$	$D_x = 1.403$ Mg m^{-3}
Monoclinic, $C2/c$	Mo $K\alpha$ radiation, $\lambda = 0.71073$ Å
$a = 29.617$ (2) Å	Cell parameters from 41546 reflections
$b = 15.0816$ (11) Å	$\theta = 2.4–27.5°$
$c = 18.7920$ (13) Å	$\mu = 0.43$ mm^{-1}
$\beta = 118.1580$ (14)°	$T = 100$ K
$V = 7400.5$ (9) Å^3	Blade, orange
$Z = 4$	0.28 × 0.09 × 0.06 mm^3

Data collection

Rigaku AFC12 (Right) diffractometer	8497 independent reflections
Radiation source: Rotating Anode	5879 reflections with $I > 2\sigma(I)$
Detector resolution: 28.5714 pixels mm^{-1}	$R_{int} = 0.075$
profile data from ω–scans	$\theta_{max} = 27.5°$, $\theta_{min} = 2.5°$
Absorption correction: multi-scan *CrystalClear*-SM Expert 3.1 b27 (Rigaku, 20112)	$h = -38 \rightarrow 38$
$T_{min} = 0.628$, $T_{max} = 1.000$	$k = -19 \rightarrow 19$
44806 measured reflections	$l = -24 \rightarrow 21$

Refinement

Refinement on F^2	Primary atom site location: iterative
Least-squares matrix: full	Secondary atom site location: difference Fourier map
$R[F^2 > 2\sigma(F^2)] = 0.072$	Hydrogen site location: mixed
$wR(F^2) = 0.222$	H atoms treated by a mixture of independent and constrained refinement
$S = 1.06$	$w = 1/[\sigma^2(F_o^2) + (0.118P)^2 + 12.1276P]$ where $P = (F_o^2 + 2F_c^2)/3$
8497 reflections	$(\Delta/\sigma)_{max} = 0.001$
436 parameters	$\Delta\rangle_{max} = 1.79$ e Å^{-3}
27 restraints	$\Delta\rangle_{min} = -0.73$ e Å^{-3}

3.13

Crystal data

$C_{42}H_{37}ClN_3O_4PPd \cdot C_4H_{10}O \cdot CHCl_3$	D_x = 1.484 Mg m^{-3}
M_r = 1014.05	Mo $K\alpha$ radiation, λ = 0.71073 Å
Orthorhombic, $P2_12_12_1$	Cell parameters from 15893 reflections
a = 9.9250 (3) Å	θ = 2.3–27.5°
b = 18.4117 (4) Å	μ = 0.73 mm^{-1}
c = 24.8404 (6) Å	T = 100 K
V = 4539.2 (2) Å^3	Plate, colourless
Z = 4	0.09 × 0.02 × 0.01 mm^3
F(000) = 2080	

Data collection

Rigaku AFC12 (Right) diffractometer	10337 independent reflections
Radiation source: Rotating Anode	8853 reflections with $I > 2\sigma(I)$
Detector resolution: 28.5714 pixels mm^{-1}	R_{int} = 0.053
profile data from ω–scans	θ_{max} = 27.5°, θ_{min} = 2.2°
Absorption correction: multi-scan *CrysAlis PRO*, Agilent Technologies, Version 1.171.37.35 (release 13-08-2014 CrysAlis171 .NET) (compiled Aug 13 2014,18:06:01) Empirical absorption correction using spherical harmonics, implemented in SCALE3 ABSPACK scaling algorithm. Empirical absorption correction using spherical harmonics, implemented in SCALE3 ABSPACK scaling algorithm.	h = -11→12
T_{min} = 0.900, T_{max} = 1.000	k = -23→23
31289 measured reflections	l = -19→32

Refinement

Refinement on F^2	Hydrogen site location: inferred from neighbouring sites
Least-squares matrix: full	H-atom parameters constrained
$R[F^2 > 2\sigma(F^2)]$ = 0.044	$w = 1/[\sigma^2(F_o^2) + (0.0423P)^2 + 2.4748P]$ where $P = (F_o^2 + 2F_c^2)/3$
$wR(F^2)$ = 0.094	$(\Delta/\sigma)_{max}$ = 0.001
S = 1.05	$\Delta\rangle_{max}$ = 0.86 e Å^{-3}
10337 reflections	$\Delta\rangle_{min}$ = -0.59 e Å^{-3}
520 parameters	Absolute structure: Flack x determined using 3287 quotients [(I+)-(I-)]/[(I+)+(I-)] (Parsons, Flack and Wagner, Acta Cryst. B69 (2013) 249-259).

0 restraints	Absolute structure parameter: 0.021 (12)
Primary atom site location: iterative	

4.24

Crystal data

$C_{18}H_{18}NO_4P \cdot 0.1667C_4H_{10}O$	$Z = 6$
$M_r = 355.66$	$F(000) = 1122$
Triclinic, $P1$	$D_x = 1.327$ Mg m^{-3}
$a = 12.2310$ (6) Å	Mo $K\alpha$ radiation, $\lambda = 0.71073$ Å
$b = 15.3876$ (7) Å	Cell parameters from 23513 reflections
$c = 15.6323$ (7) Å	$\theta = 2.2–30.6°$
$\alpha = 100.3631$ (6)°	$\mu = 0.18$ mm^{-1}
$\beta = 99.4849$ (7)°	$T = 150$ K
$\gamma = 108.2373$ (6)°	Block, colourless
$V = 2670.7$ (2) Å^3	0.51 × 0.10 × 0.02 mm^3

Data collection

Bruker APEX 2 CCD area detector diffractometer	31641 independent reflections
Radiation source: fine-focus sealed tube	29482 reflections with $I > 2\sigma(I)$
Graphite monochromator	$R_{int} = 0.013$
ω rotation with narrow frames scans	$\theta_{max} = 30.6°$, $\theta_{min} = 1.7°$
Absorption correction: multi-scan *SADABS* v2012/1, Sheldrick, G.M., (2012)	$h = -17 \rightarrow 17$
$T_{min} = 0.915$, $T_{max} = 0.996$	$k = -21 \rightarrow 22$
42985 measured reflections	$l = -22 \rightarrow 22$

Refinement

Refinement on F^2	Hydrogen site location: mixed
Least-squares matrix: full	H atoms treated by a mixture of independent and constrained refinement
$R[F^2 > 2\sigma(F^2)] = 0.037$	$w = 1/[\sigma^2(F_o^2) + (0.0588P)^2 + 0.2992P]$ where $P = (F_o^2 + 2F_c^2)/3$
$wR(F^2) = 0.099$	$(\Delta/\sigma)_{max} = 0.001$
$S = 1.02$	$\Delta\rangle_{max} = 0.80$ e Å^{-3}
31641 reflections	$\Delta\rangle_{min} = -0.43$ e Å^{-3}
1406 parameters	Absolute structure: Flack x determined using 13361 quotients [(I+)-(I-)]/[(I+)+(I-)] (Parsons, Flack and Wagner, Acta Cryst. B69 (2013) 249-259).
193 restraints	Absolute structure parameter: 0.023 (12)
Primary/secondary atom site location: iterative/difmap	

4.41

Crystal data

$C_{33}H_{37}Cl_2NO_2P_2Pt \cdot CH_2Cl_2$	D_x = 1.628 Mg m^{-3}
M_r = 892.49	Mo $K\alpha$ radiation, λ = 0.71075 Å
Orthorhombic, $P2_12_12_1$	Cell parameters from 25843 reflections
a = 11.6882 (8) Å	θ = 0.9–27.5°
b = 14.4263 (10) Å	μ = 4.27 mm^{-1}
c = 21.5957 (15) Å	T = 120 K
V = 3641.4 (4) Å^3	Block, light brown
Z = 4	0.66 × 0.21 × 0.18 mm^3
F(000) = 1768	

Data collection

Rigaku RAXIS conversion diffractometer	8308 independent reflections
Radiation source: Sealed Tube	7266 reflections with $I > 2\sigma(I)$
Graphite Monochromator monochromator	R_{int} = 0.059
Detector resolution: 10.0000 pixels mm^{-1}	θ_{max} = 27.5°, θ_{min} = 1.7°
profile data from ω–scans	h = -15→15
Absorption correction: multi-scan *CrystalClear*-SM Expert 3.1 b27 (Rigaku, 20112)	k = -16→18
T_{min} = 0.165, T_{max} = 0.514	l = -26→28
31742 measured reflections	

Refinement

Refinement on F^2	Hydrogen site location: inferred from neighbouring sites
Least-squares matrix: full	H-atom parameters constrained
$R[F^2 > 2\sigma(F^2)]$ = 0.035	$w = 1/[\sigma^2(F_o^2) + (0.0334P)^2]$ where $P = (F_o^2 + 2F_c^2)/3$
$wR(F^2)$ = 0.075	$(\Delta/\sigma)_{max}$ = 0.001
S = 0.96	$\Delta\rangle_{max}$ = 2.58 e Å^{-3}
8308 reflections	$\Delta\rangle_{min}$ = -2.72 e Å^{-3}
401 parameters	Extinction correction: *SHELXL*, $Fc^*=kFc[1+0.001xFc^2\lambda^3/\sin(2\theta)]^{-1/4}$
0 restraints	Extinction coefficient: 0.00155 (13)
Primary atom site location: structure-invariant direct methods	Absolute structure: Flack x determined using 2903 quotients [(I+)-(I-)]/[(I+)+(I-)] (Parsons, Flack and Wagner, Acta Cryst. B69 (2013) 249-259).
Secondary atom site location: difference Fourier map	Absolute structure parameter: 0.001 (5)

4.50

Crystal data

$C_{55.67}H_{62.33}Cl_{3.33}NO_2P_2Ru_2 \cdot CH_2Cl_2$	$F(000) = 3816$
$M_r = 1244.57$	$D_x = 1.502$ Mg m^{-3}
Monoclinic, $C2$	Mo $K\alpha$ radiation, $\lambda = 0.71073$ Å
$a = 57.695$ (4) Å	Cell parameters from 55538 reflections
$b = 13.0936$ (9) Å	$\theta = 2.3–27.5°$
$c = 10.9280$ (8) Å	$\mu = 0.91$ mm^{-1}
$\beta = 90.8561$ (9)°	$T = 100$ K
$V = 8254.5$ (10) Å^3	Plate, orange
$Z = 6$	0.16 × 0.08 × 0.02 mm^3

Data collection

Bruker APEX 2 CCD area detector diffractometer	18180 independent reflections
Radiation source: fine-focus sealed tube	16849 reflections with $I > 2\sigma(I)$
Graphite monochromator	$R_{int} = 0.068$
ω rotation with narrow frames scans	$\theta_{max} = 27.5°$, $\theta_{min} = 2.3°$
Absorption correction: multi-scan *SADABS* v2012/1, Sheldrick, G.M., (2012)	$h = -74 \rightarrow 74$
$T_{min} = 0.868$, $T_{max} = 0.982$	$k = -16 \rightarrow 15$
55538 measured reflections	$l = -14 \rightarrow 14$

Refinement

Refinement on F^2	Secondary atom site location: difference Fourier map
Least-squares matrix: full	Hydrogen site location: inferred from neighbouring sites
$R[F^2 > 2\sigma(F^2)] = 0.044$	H-atom parameters constrained
$wR(F^2) = 0.111$	$w = 1/[\sigma^2(F_o^2) + (0.0613P)^2 + 5.682P]$ where $P = (F_o^2 + 2F_c^2)/3$
$S = 1.03$	$(\Delta/\sigma)_{max} = 0.003$
18180 reflections	$\Delta\rangle_{max} = 1.07$ e Å^{-3}
993 parameters	$\Delta\rangle_{min} = -1.32$ e Å^{-3}
129 restraints	Absolute structure: Flack x determined using 6998 quotients [(I+)-(I-)]/[(I+)+(I-)] (Parsons, Flack and Wagner, Acta Cryst. B69 (2013) 249-259).
Primary atom site location: iterative	Absolute structure parameter: -0.033 (14)

4.54

Crystal data

$C_{66}H_{74}Cl_2N_2O_4P_4Ru \cdot 0.5C_4H_{10}O \cdot 0.5C_4H_{10}O$	$F(000) = 2784$
$M_r = 1329.24$	$D_x = 1.366$ Mg m^{-3}
Monoclinic, $C2$	Mo $K\alpha$ radiation, $\lambda = 0.71073$ Å
$a = 27.4633$ (19) Å	Cell parameters from 12230 reflections
$b = 10.7473$ (8) Å	$\theta = 0.9–27.5°$
$c = 21.9392$ (15) Å	$\mu = 0.48$ mm^{-1}
$\beta = 93.7398$ (19)°	$T = 120$ K
$V = 6461.7$ (8) Å^3	Blade, brown
$Z = 4$	0.52 × 0.17 × 0.10 mm^3

Data collection

Rigaku RAXIS conversion diffractometer	14064 independent reflections
Radiation source: Sealed Tube	11049 reflections with $I > 2\sigma(I)$
Graphite Monochromator	$R_{int} = 0.046$
Detector resolution: 10.0000 pixels mm^{-1}	$\theta_{max} = 27.5°$, $\theta_{min} = 1.7°$
profile data from ω–scans	$h = -35 \rightarrow 28$
Absorption correction: multi-scan Rigaku *CrystalClear*-SM Expert 3.1 b27	$k = -13 \rightarrow 13$
$T_{min} = 0.657$, $T_{max} = 1.000$	$l = -28 \rightarrow 28$
22318 measured reflections	

Refinement

Refinement on F^2	Secondary atom site location: difference Fourier map
Least-squares matrix: full	Hydrogen site location: inferred from neighbouring sites
$R[F^2 > 2\sigma(F^2)] = 0.046$	H-atom parameters constrained
$wR(F^2) = 0.102$	$w = 1/[\sigma^2(F_o^2) + (0.0376P)^2 + 9.263P]$ where $P = (F_o^2 + 2F_c^2)/3$
$S = 1.01$	$(\Delta/\sigma)_{max} = 0.001$
14064 reflections	$\Delta\rangle_{max} = 0.77$ e Å^{-3}
766 parameters	$\Delta\rangle_{min} = -0.96$ e Å^{-3}
30 restraints	Absolute structure: Flack x determined using 4176 quotients [(I+)-(I-)]/[(I+)+(I-)] (Parsons, Flack and Wagner, Acta Cryst. B69 (2013) 249-259).
Primary atom site location: structure-invariant direct methods	Absolute structure parameter: 0.02 (2)

4.58

Crystal data

$C_{60}H_{60}CuN_4O_6P_4 \cdot BF_4 \cdot C_3H_7NO \cdot 0.5H_2O$	$Z = 2$
$M_r = 1289.45$	$F(000) = 1342$
Triclinic, $P\bar{1}$	$D_x = 1.373$ Mg m^{-3}
$a = 13.3453$ (5) Å	Mo $K\alpha$ radiation, $\lambda = 0.71073$ Å
$b = 13.6055$ (5) Å	Cell parameters from 12236 reflections
$c = 17.3545$ (6) Å	$\theta = 2.3$–$26.9°$
$\alpha = 94.5641$ (6)°	$\mu = 0.52$ mm^{-1}
$\beta = 90.8734$ (6)°	$T = 150$ K
$\gamma = 96.7969$ (6)°	Block, colourless
$V = 3118.0$ (2) Å^3	0.22 × 0.21 × 0.18 mm^3

Data collection

Bruker APEX 2 CCD area detector diffractometer	13801 independent reflections
Radiation source: fine-focus sealed tube	11162 reflections with $I > 2\sigma(I)$
Graphite monochromator	$R_{int} = 0.027$
ω rotation with narrow frames scans	$\theta_{max} = 27.2°$, $\theta_{min} = 1.5°$
Absorption correction: multi-scan *SADABS* v2012/1, Sheldrick, G.M., (2012)	$h = -17 \rightarrow 17$
$T_{min} = 0.894$, $T_{max} = 0.912$	$k = -17 \rightarrow 17$
40154 measured reflections	$l = -22 \rightarrow 22$

Refinement

Refinement on F^2	Primary atom site location: iterative
Least-squares matrix: full	Hydrogen site location: mixed
$R[F^2 > 2\sigma(F^2)] = 0.038$	H atoms treated by a mixture of independent and constrained refinement
$wR(F^2) = 0.102$	$w = 1/[\sigma^2(F_o^2) + (0.0478P)^2 + 1.4123P]$ where $P = (F_o^2 + 2F_c^2)/3$
$S = 1.03$	$(\Delta/\sigma)_{max} = 0.002$
13801 reflections	$\Delta\rangle_{max} = 0.49$ e Å^{-3}
807 parameters	$\Delta\rangle_{min} = -0.42$ e Å^{-3}
7 restraints	

4.63

Crystal data

$C_{58}H_{60}CuN_4O_4P_4 \cdot BF_4 \cdot C_4H_{10}O$	$F(000) = 2560$
$M_r = 1225.45$	$D_x = 1.346$ Mg m^{-3}
Monoclinic, $P2_1/n$	Mo $K\alpha$ radiation, $\lambda = 0.71073$ Å
$a = 14.4155$ (10) Å	Cell parameters from 64492 reflections
$b = 16.3974$ (11) Å	$\theta = 1.9$–$27.5°$
$c = 26.4465$ (19) Å	$\mu = 0.53$ mm^{-1}
$\beta = 104.6610$ (12)°	$T = 100$ K
$V = 6047.8$ (7) Å^3	Block, colourless
$Z = 4$	$0.21 \times 0.17 \times 0.14$ mm^3

Data collection

Rigaku Saturn724+ (2x2 bin mode) diffractometer	13818 independent reflections
Radiation source: Sealed Tube	12010 reflections with $I > 2\sigma(I)$
Graphite monochromator	$R_{int} = 0.061$
Detector resolution: 28.5714 pixels mm^{-1}	$\theta_{max} = 27.6°$, $\theta_{min} = 1.9°$
profile data from ω–scans	$h = -18 \rightarrow 17$
Absorption correction: multi-scan	$k = -21 \rightarrow 20$
$T_{min} = 0.706$, $T_{max} = 1.000$	$l = -34 \rightarrow 34$
68496 measured reflections	

Refinement

Refinement on F^2	Primary atom site location: iterative
Least-squares matrix: full	Secondary atom site location: difference Fourier map
$R[F^2 > 2\sigma(F^2)] = 0.039$	Hydrogen site location: mixed
$wR(F^2) = 0.111$	H atoms treated by a mixture of independent and constrained refinement
$S = 1.02$	$w = 1/[\sigma^2(F_o^2) + (0.0646P)^2 + 2.3873P]$ where $P = (F_o^2 + 2F_c^2)/3$
13818 reflections	$(\Delta/\sigma)_{max} = 0.002$
695 parameters	$\Delta\rangle_{max} = 0.75$ e Å^{-3}
0 restraints	$\Delta\rangle_{min} = -0.79$ e Å^{-3}

4.81

Crystal data

$C_{40}H_{35}CuN_3O_2P_2 \cdot BF_4 \cdot 2(C_4H_{10}O)$	D_x = 1.350 Mg m^{-3}
M_r = 950.24	Mo $K\alpha$ radiation, λ = 0.71073 Å
Orthorhombic, $Pna2_1$	Cell parameters from 42281 reflections
a = 12.9283 (11) Å	θ = 2.3–30.6°
b = 25.970 (2) Å	μ = 0.60 mm^{-1}
c = 13.9284 (11) Å	T = 150 K
V = 4676.4 (7) Å^3	Plate, green
Z = 4	0.45 × 0.25 × 0.04 mm^3
F(000) = 1984	

Data collection

Bruker APEX 2 CCD area detector diffractometer	9573 independent reflections
Radiation source: fine-focus sealed tube	7487 reflections with $I > 2\sigma(I)$
Graphite monochromator	R_{int} = 0.073
ω rotation with narrow frames scans	θ_{max} = 26.4°, θ_{min} = 1.6°
Absorption correction: multi-scan *SADABS* v2012/1, Sheldrick, G.M., (2012)	h = -16→16
T_{min} = 0.775, T_{max} = 0.976	k = -32→32
40758 measured reflections	l = -17→17

Refinement

Refinement on F^2	Secondary atom site location: difference Fourier map
Least-squares matrix: full	Hydrogen site location: mixed
$R[F^2 > 2\sigma(F^2)]$ = 0.047	H atoms treated by a mixture of independent and constrained refinement
$wR(F^2)$ = 0.111	$w = 1/[\sigma^2(F_o^2) + (0.0532P)^2]$ where $P = (F_o^2 + 2F_c^2)/3$
S = 1.02	$(\Delta/\sigma)_{max}$ = 0.001
9573 reflections	$\Delta\rangle_{max}$ = 0.46 e Å^{-3}
556 parameters	$\Delta\rangle_{min}$ = -0.54 e Å^{-3}
206 restraints	Absolute structure: Flack x determined using 2880 quotients [(I+)-(I-)]/[(I+)+(I-)] (Parsons, Flack and Wagner, Acta Cryst. B69 (2013) 249-259).
Primary atom site location: iterative	Absolute structure parameter: 0.034 (9)